

BEHAVIOR OF CONCRETE SLAB AND GIRDER BRIDGES

by

E. V. Leyendecker

and

J. E. Breen

Research Report Number 94-3F

Research Project Number 3-5-66-94

Structural Model Study of Concrete Slab and
Girder Spans

Conducted for

The Texas Highway Department

In Cooperation with the
U. S. Department of Transportation
Federal Highway Administration

by

CENTER FOR HIGHWAY RESEARCH
THE UNIVERSITY OF TEXAS AT AUSTIN

July 1969

The opinions, findings, and conclusions expressed in this publication are those of the authors and not necessarily those of the Federal Highway Administration.

P R E F A C E

This report is the final in a series which summarizes a detailed investigation of the behavior of pan-formed concrete slab and girder bridge systems, which are widely used by the Texas Highway Department. The initial report treated the detailed techniques developed for the utilization of reduced scale models and also reported on the degree of correlation between the model tests and the full-scale prototype testing. The second report treated the techniques employed and the results obtained in the field testing of the full scale prototype bridge.

This work is a part of Research Contract 3-5-66-94 entitled "Structural Model Study of Concrete Slab and Girder Spans." The studies described herein were conducted as a part of the overall research program at The University of Texas at Austin Center for Highway Research, under the administrative direction of Dean John J. McKetta. The work was sponsored jointly by the Texas Highway Department and the U.S. Bureau of Public Roads under an agreement between The University of Texas at Austin and the Texas Highway Department.

Liaison with the Texas Highway Department was maintained through the contact representatives, Mr. L. G. Walker and Mr. B. R. Winn; Mr. I. C. Daniel was the contact representative for the Bureau of Public Roads. Particular thanks are due all of these contact representatives as well as Mr. H. D. Butler, Design Engineer, Texas Highway Department, who rendered continued assistance during the life of the project.

This study was directed by John E. Breen, Professor of Civil Engineering. The model study phase was supervised by E. V. Leyendecker and the field study phase by T. A. Armstrong, both Research Engineers, Center for Highway Research.

This page replaces an intentionally blank page in the original.

-- CTR Library Digitization Team

A B S T R A C T

Detailed results of a research program to study the behavior of 40-ft. simple span pan-formed concrete slab and girder bridges are presented. The investigation was carried out using approximately 1/6-scale direct models of the bridges (including substructure); these model tests were supplemented by full-size field testing as well as analytical procedures. Four accurate models were tested at service loads, moderate overloads, and ultimate load levels in order to fully document the behavior of the structures for the full range of load conditions. Patterns of load distribution were obtained using both strain gages and deflection measurements. The main variables in the investigation were angle of skew, load level, and grade and quantity of reinforcement.

Comparisons are made with the service load AASHO load distribution factors for design of slab and stringer bridges, and with distribution factors computed from an orthotropic plate solution using a discrete element mathematical model. Design recommendations are made for computation of ultimate load capacity.

This page replaces an intentionally blank page in the original.

-- CTR Library Digitization Team

T A B L E O F C O N T E N T S

Chapter	Page
I. INTRODUCTION	1
1.1 General	1
1.2 Definition of Types of Plate Action	3
1.3 Methods of Analysis	3
1.3.1 Grillage Method	5
1.3.2 Primary and Secondary Members Method	5
1.3.3 Orthotropic Plate Method	6
1.3.4 Limitations	7
1.3.5 Design Requirements	7
1.4 Role of Mathematical and Structural Models	7
1.5 Prototype Bridge System	10
1.6 Object and Scope of Investigation	14
1.7 Program of Research	17
II. DIRECT MODEL SIMILITUDE	21
2.1 Introduction	21
2.2 Scale Relations	22
2.2.1 Materials	22
2.2.2 Loads	22
2.2.3 Geometrical Scale Factor	24
III. MODEL TECHNOLOGY	25
3.1 Introduction	25
3.2 Materials	25
3.2.1 Microconcrete	25
3.2.2 Reinforcement	26
3.3 Fabrication Techniques	28
3.4 Instrumentation	32
3.4.1 Load Control	32
3.4.2 Structural Response	32
3.5 Loading	33
3.5.1 Gravity Loads	33
3.5.2 Live Loads	33

Chapter	Page
IV. MODEL RELIABILITY	37
4.1 Introduction	37
4.2 Comparison at Service Load Levels	37
4.3 Ultimate Strength Reliability	40
V. MATHEMATICAL ANALYSIS	43
5.1 Introduction	43
5.2 Discrete Element Mathematical Model	43
5.3 Section Properties	44
VI. EXPERIMENTAL STUDY	47
6.1 Introduction	47
6.2 Section Details	47
6.2.1 Dimensions	47
6.2.2 Reinforcement	47
6.2.3 Microconcrete	51
6.3 Instrumentation	51
6.3.1 Grid System	51
6.3.2 Deflections	51
6.3.3 Strain Gages	72
VII. TEST RESULTS	75
7.1 Introduction	75
7.2 Dead Load	76
7.3 Distribution Factors	80
7.3.1 Introduction	80
7.3.2 Relationship between Distribution Factors	81
7.3.3 Data Comparisons	82
7.4 Service Loads	83
7.4.1 Influence Lines	83
7.4.2 Reciprocal Theorem	83
7.4.3 Wheel Loads	88
7.4.4 Single Truck Loads	94
7.4.5 Double Truck Loads	100
7.4.6 Triple Truck Loads	100
7.4.7 Effect of Skew	107
7.4.8 Effect of Longitudinal Reinforcement Percentage	114
7.4.9 Transverse Strains	123
7.5 Moderate Overloads	123
7.5.1 Deflection and Strain Distribution	123
7.5.2 Effect of Skew and Steel Percentage	127
7.5.3 Transverse Strains	130

Chapter	Page
7.6 Ultimate Load Behavior	130
7.6.1 Introduction	130
7.6.2 Factor of Safety	131
7.6.3 Model SG-1, 0° Skew	131
7.6.4 Model SG-2, 45° Skew	137
7.6.5 Model SG-3, 45° Skew	145
7.6.6 Model SG-4, 26° Skew	149
7.6.7 Deterioration of Deflection and Strain Distribution	159
7.6.8 Effect of Skew	159
7.6.9 Effect of Steel Percentage	160
7.6.10 Transverse Strains	160
7.7 Ultimate Load Calculations	160
7.7.1 Introduction	160
7.7.2 Basis for Hypothesis	161
7.7.3 Proposed Calculation Procedure	163
7.7.4 Application to this Study	167
(a) Model SG-1 (0° Skew)	167
(b) Model SG-2 (45° Skew), Ultimate No. 1	172
(c) Model SG-2 (45° Skew), Ultimate No. 2	175
(d) Model SG-3 (45° Skew), Ultimate No. 1	177
(e) Model SG-3 (45° Skew), Ultimate No. 2	179
(f) Model SG-4 (26° Skew)	181
7.7.5 Conclusions on Ultimate Load Calculations	184
7.7.6 Live Load Factors	184
7.7.7 Ultimate Load Distribution Factors	184
7.8 Secondary Tests	187
7.8.1 Punching Tests	187
7.8.2 Bent Cap Tests	189
VIII. CONCLUSIONS AND RECOMMENDATIONS	193
8.1 Summary of the Intestigation	193
8.2 Conclusions	193
8.3 Implementing Research Results into the Texas Highway Department Operations	196
8.3.1 AASHO Load Distribution Factors	196
8.3.2 Benefit from Implementation of Revised Load Distribution Factors	197
8.3.3 Substructure Design	197
APPENDIX A. PROTOTYPE BRIDGE PLANS	201
BIBLIOGRAPHY	211

This page replaces an intentionally blank page in the original.

-- CTR Library Digitization Team

L I S T O F F I G U R E S

Figure		Page
1.1	Load Distribution Behavior	2
1.2	Structural Orthotropic Elements	4
1.3	Typical CG Series Span, CG-0-35-40 (0° Skew Shown) . .	11
1.4	Prototype Reinforcement and Pan Forms	12
1.5	Pan Arrangements for Standard Skews	13
1.6	Pan Form Support Details	15
1.7	Bearing Support Details	16
2.1	General Stress-Strain Curve	23
3.1	Stress-Strain Curves for Microconcrete and Prototype Concrete	27
3.2	Typical Stress-Strain Curves for Main Flexural Reinforcement	29
3.3	Support Conditions	30
3.4	Models Ready for Casting	31
3.5	Live Load System	34
3.6	Relation between Full-Size and Model AASHO H20-S16 Truck	35
3.7	Relation between Full-Size and Model Overload Truck .	36
4.1	Comparison of AASHO H20 Design Vehicle and Vehicle Used for Tests	38
4.2	Strain Data for Two Trucks Spaced Apart	39
4.3	Summary of Model and Prototype Data with Regression Analysis	41
5.1	Discrete Element Model	44
6.1	Bridge Model Cross Sections (Prototype Dimensions in Parentheses)	47
6.2	Cross Section Reinforcement Details (Prototype Values in Parentheses)	48
6.3	SG-1 Grid System for Loading and Instrumentation . . .	51

Figure		Page
6.4	SG-2 and SG-3 Grid System for Loading and Instrumentation	52
6.5	SG-4 Grid System for Loading and Instrumentation . . .	53
6.6	Typical Strain Gage Locations	54
6.7	SG-1 Strain Gage Locations	56
6.8	SG-2 Strain Gage Locations	57
6.9	SG-3 Strain Gage Locations	58
6.10	SG-4 Strain Gage Locations	59
6.11	Bridge Loading Histories	60
6.12	Wheel, Axle, and Truck Loads (Prototype Values in Parentheses)	61
6.13	Designation of Wheel and Truck Loads Transversely . .	63
6.14	Orientation of Wheels and Truck Loads Longitudinally .	64
6.15	Theoretical Deflection Correction for the Case of Uniform Load	67
6.16	Correction Factor Application for Concentrated Load at Midspan	70
6.17	Interpolation for Strains in Girders G, J, and L in Bridge SG-1	73
7.1	Midspan Dead Load Deflections	76
7.2	Midspan Dead Load Strains	77
7.3	Dead Load Response	78
7.4	Influence Lines for Girder B for HS-20 Rear Wheel . .	83
7.5	Influence Lines for Girder E for HS-20 Rear Wheel . .	84
7.6	Deflection Profile for Girder B, Wheel Load at B-4 . .	85
7.7	Deflection Profile for Girder E, Wheel Load at E-4 . .	85
7.8	Deflection Profile for Girder B, Wheel Load at E-4 . .	86
7.9	Deflection Profile for Girder E, Wheel Load at B-4 . .	86
7.10	Midspan Distribution of Strains and Deflections for Wheel Load at A-4	88
7.11	Midspan Distribution of Strains and Deflections for Wheel Load at B-4	89
7.12	Midspan Distribution of Strains and Deflections for Wheel Load at C-4	90
7.13	Midspan Distribution of Strains and Deflections for Wheel Load at E-4	91

Figure		Page
7.14	Comparison between Experimental and Theoretical Distribution Factors with Varied Wheel Placement . . .	92
7.15	Midspan Distribution of Strains and Deflections for HS-20 Truck at A4-C4	94
7.16	Midspan Distribution of Strains and Deflections for HS-20 Truck at B4-D4	95
7.17	Midspan Distribution of Strains and Deflections for HS-20 Truck at E4-C4	96
7.18	Comparison between Experimental and Theoretical Distribution with Varied Single Truck Placement . . .	97
7.19	Midspan Distribution of Strains and Deflections for HS-20 Trucks at B4-D4 and G4-J4	100
7.20	Midspan Distribution of Strains and Deflections for HS-20 Trucks at B4-D4 and J4-L4	101
7.21	Midspan Distribution of Strains and Deflections for HS-20 Trucks at C4-E4 and H4-K4	102
7.22	Comparison between Experimental and Theoretical S t r a i n D i s t r i b u t i o n F a c t o r s f o r T w o H S - 2 0 T r u c k s with Varied Truck Placement	103
7.23	Comparison between Experimental and Theoretical Deflection Distribution Factors for Two HS-20 Trucks with Varied Truck Placement	104
7.24	Midspan Distribution Factors for Triple HS-20 Trucks .	105
7.25	Midspan Strains and Deflections for HS-20 Truck at A4-C4	107
7.26	Midspan Strains and Deflections for HS-20 Truck at E4-C4	108
7.27	Midspan Strains and Deflections for HS-20 Truck at B4-G4 and G4-J4	109
7.28	Midspan Strains and Deflections for HS-20 Trucks at C4-E4 and H4-K4	110
7.29	Midspan Deflections for Triple HS-20 Trucks	111
7.30	Midspan Strains for Triple HS-20 Trucks	112
7.31	Effect of Skew on Strains and Deflections	114
7.32	Effect of Steel Percentage for HS-20 Truck at A4-C4 on 45° Skew Bridges	116
7.33	Effect of Steel Percentage for HS-20 Truck at E4-G4 on 45° Skew Bridges	117
7.34	Effect of Steel Percentage for HS-20 Trucks at B4-D4 and G4-J4 on 45° Skew Bridges	118

Figure		Page
7.35	Effect of Steel Percentage for HS-20 Trucks at C4-E4 and H4-K4 on 45° Skew Bridges	119
7.36	Effect of Steel Percentage on Deflections for Triple HS-20 Trucks on 45° Skew Bridges	120
7.37	Effect of Steel Percentage on Strains for Triple HS-20 Trucks on 45° Skew Bridges	121
7.38	a. Magnitude of Transverse Strains under Service Loads	123
	b. Transverse Moments for One HS-20 Truck at B4-D4	124
7.39	Midspan Distribution of Strains and Deflections and Strains for 1.0 Overload Truck plus Impact	125
7.40	Deflections for 1.0 Overload Truck plus Impact at B4-D4	127
7.41	Strains for 1.0 Overload Truck plus Impact at B4-D4	128
7.42	Transverse Steel Strains for 1.0 Overload Truck plus Impact at B4-D4	131
7.43	Midspan Deflection for SG-1 during Ultimate Load Cycle	132
7.44	Midspan Strain for SG-4 during Ultimate Load Cycle	133
7.45	Longitudinal Crack between Girders D and E, Model SG-1	135
7.46	SG-1 Crack Pattern	137
7.47	Midspan Deflection for SG-2 during First Ultimate Load Cycle	138
7.48	Midspan Strain for SG-2 during First Ultimate Load Cycle	139
7.49	SG-2 Crack Pattern	141
7.50	Midspan Deflection for SG-2 during Second Ultimate Load Cycle	142
7.51	Midspan Strain for SG-2 during Second Ultimate Load Cycle	143
7.52	Midspan Deflection for SG-3 during First Ultimate Load Cycle	145
7.53	Midspan Strain for SG-3 during First Ultimate Load Cycle	146
7.54	SG-3 Crack Pattern	147
7.55	Midspan Deflection for SG-3 during Second Ultimate Load Cycle	149
7.56	Midspan Strain for SG-3 during Second Ultimate Load Cycle	150

Figure		Page
7.57	Midspan Deflection for SG-4 during Ultimate Load Cycle	151
7.58	Midspan Deflection for SG-4 during Ultimate Load Cycle (Reduced Scale)	152
7.59	a. Midspan Strain on Girders A through F for SG-4 during Ultimate Load Cycle	154
	b. Midspan Strain on Girders G through M for SG-4 during Ultimate Load Cycle	155
7.60	SG-4 Crack Pattern	156
7.61	SG-4 after Ultimate	157
7.62	Failure Concept	161
7.63	Shear Failure Zone and Shear Transfer Length	163
7.64	Proposed Calculation Procedure	165
7.65	Estimating Girders with Steel Yielding at Ultimate	168
7.66	Shear Transfer Lengths	169
7.67	Punching Tests	187
7.68	Bent Cap Tests	189
7.69	Comparison of Capacity of Bents with and without End Diaphragms in Place	190
A.1	Steel Forms for 40'-0" Slab and Girder Spans, Sheet 1 of 2	197
A.2	Steel Forms for 40'-0" Slab and Girder Spans, Sheet 2 of 2	198
A.3	Texas Highway Department Plan Sheet, CG-0-35-40	199
A.4	Texas Highway Department Plan Sheet, BCG-0-35-40	200
A.5	Texas Highway Department Plan Sheet, BCG-0-35-40 (45°-00')	201
A.6	Texas Highway Department Plan Sheet, CG-0-33-40	202
A.7	Texas Highway Department Plan Sheet, BCG-0-33-40 (26°-34')	203

This page replaces an intentionally blank page in the original.

-- CTR Library Digitization Team

N O T A T I O N

A_s	=	Area of tension reinforcement
C	=	Constant used in AASHO load distribution procedure
D	=	Reinforcement bar diameter
DL	=	Dead load
E	=	Modulus of elasticity
E_c	=	Modulus of elasticity of concrete
f	=	Stress
f_m	=	Model stress
f_p	=	Prototype stress
f_s	=	Tensile stress in reinforcement
f_y	=	Yield strength of reinforcement
f_u	=	Ultimate strength of reinforcement
f'_c	=	Compressive strength of concrete
$\sqrt{f'_c}$	=	Square root of compressive strength of concrete in psi
f'_t	=	Split cylinder tensile strength of concrete
FS	=	Factor of safety
I	=	Moment of inertia, Impact factor
i_m	=	Arbitrary point on the model material stress-strain curve
i_p	=	Arbitrary point on the prototype material stress-strain curve
k, k_A	=	Number of wheel loads = S/C
k_{GM}	=	Guyon-Massonnet longitudinal moment distribution factor
L	=	Span length
LL	=	Live load
l_m	=	Length dimension on model
l_p	=	Length dimension on prototype
M	=	Bending moment
M_{DL}	=	Dead load moment
M_x	=	Bending moment acting on a plate element in the x direction
M_y	=	Bending moment acting on a plate element in the y direction
M_Y	=	Yield moment
OL	=	Overload

xx

R	=	An error function
S	=	Average girder spacing in feet
S_{ϵ}	=	Strain scale factor, $S_{\epsilon} = \epsilon_p / \epsilon_m$
S_f	=	Stress scale factor, $S_f = f_p / f_m$
S_l	=	Geometric scale factor, $S_l = l_p / l_m$
SWG	=	Steel wire gage
t	=	Tangential deflection
UL	=	Ultimate load
v_u	=	Shear stress
W	=	Combined weight on first two axles of an AASHO H20-S16 truck
w	=	Weight of concrete, lb./cu. ft.
x,y,z	=	Cartesian coordinate system
x, x_0, x_1 x_2, x_n, x_s	=	Points of interpolation in Lagrangian Interpolation formula
y, y_0, y_1 y_2, y_n, y_s	=	Points of interpolation in Lagrangian Interpolation formula
ϵ	=	Strain
ϵ_m	=	Model strain
ϵ_p	=	Prototype strain
b_s	=	Shear transfer length
M_{SLL}	=	Service live load moment
M_{YLL}	=	Yield live load moment
M_{ULL}	=	Ultimate live load moment
P_R	=	Yield load of remaining girders outside yield zone
P_S	=	Service live load
P_T	=	Load transferred outside yield zone
P_Y	=	Yield load of yield zone girders
P_U	=	Ultimate load
t_c	=	Critical slab depth for shear transfer

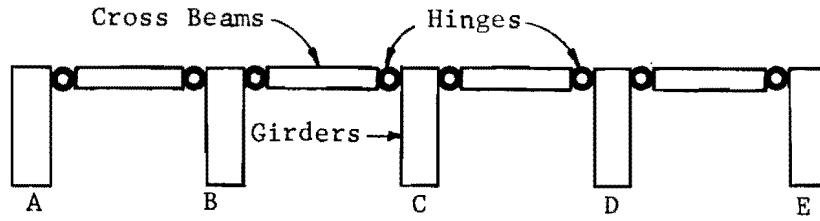
C H A P T E R I

INTRODUCTION

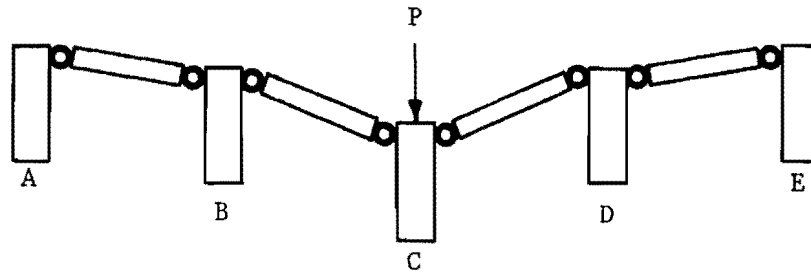
1.1 General

This report is the final in a series of reports on a research program entitled "Structural Model Studies of Concrete Slab and Girder Bridges." This report summarizes the important behavior of the bridge systems tested and the conclusions which can be found therefrom. Details of the model techniques used, the instrumentation procedures and the results from the full-scale bridge investigated, and the degree of corroboration between the model and full-scale testing have been outlined in the previous reports of the series.

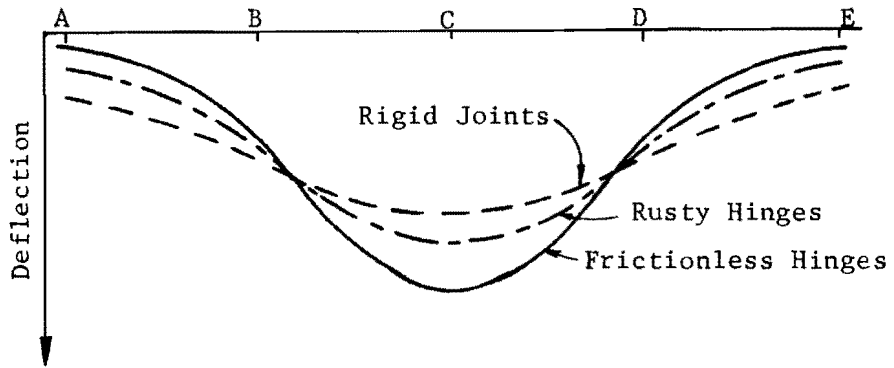
The manner in which a slab and girder bridge carries a load is dependent upon the stiffnesses and connections of the various bridge components. Consider the five girders interconnected by cross beams in Fig. 1.1a. The beam-to-girder connections are by frictionless hinges. A load P applied to girder C will result in a deflected shape similar to Fig. 1.1b. Girder C is restrained from deflecting by the hinged cross beams which exert an upward shear force. Shear forces exist at each hinge of the cross beams, with the differential shear acting on the adjacent longitudinal girder, causing it to deflect. Thus, each of the girders will carry a portion of the applied load. This deflection profile is shown in Fig. 1.1c (to a larger vertical scale) where it is labeled "frictionless hinges." If the hinges are allowed to "rust," they will be capable of transmitting a certain amount of moment. The ability to transfer moment as well as shear will reduce the deflection under the loaded girder C, while at the same time the other girders must deflect more than for the case with frictionless hinges. If the hinges are allowed to "rust" until they form



(a) Girders Connected by Hinged Cross Beams.



(b) Loaded System.



(c) Girder Deflection with Varying Hinge Restraints.

Fig. 1.1. Load Distribution Behavior.

a rigid connection between the girders and cross beams, then the unloaded girders will carry more load than for either the frictionless or rusty hinge case. These three cases are shown qualitatively in Fig. 1.1c.

This research program was concerned with evaluating the transverse load distribution characteristics of the pan-formed concrete bridge system described herein and with evaluating current design procedures. The primary research tool used was the structural model supplemented by a discrete element analytical method.

1.2 Definition of Types of Plate Action

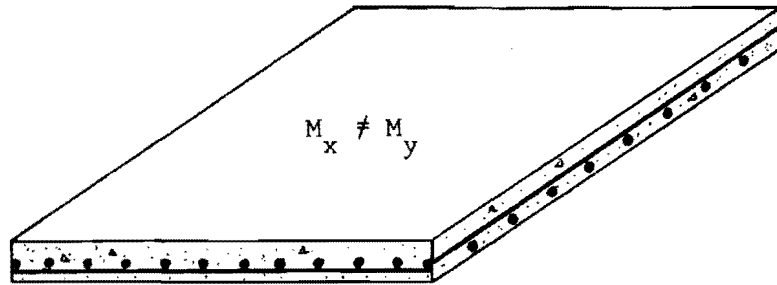
For ease in reference, the behavior of bridge plate systems can be classified as:

- (a) Isotropic Plate - A plate which shows identical elastic properties in all directions.
- (b) Anisotropic Plate - A plate which shows different elastic properties in different directions.
- (c) Orthogonally Anisotropic Plate - A plate which shows different elastic properties in two perpendicular directions. The term orthogonally anisotropic is frequently shortened to orthotropic.

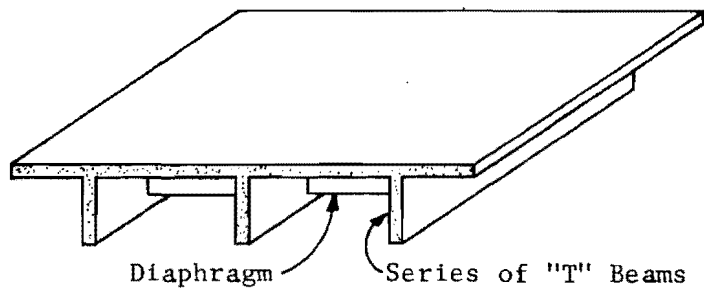
Strictly speaking, an orthotropic plate is one in which the physical properties of the plate material varies. They may be referred to as a "naturally orthotropic" plate. Another type of orthotropy occurs when a plate is stiffened with ribs. If the geometric arrangement of ribs differs in perpendicular directions, the plate may be referred to as "structurally orthotropic." Two types of "structural orthotropy" are illustrated in Fig. 1.2. Structural orthotropy exists in the case of Fig. 1.2a, due to different moment capacities in perpendicular directions. The structural orthotropy in Fig. 1.2b is due to different rib arrangements. Hereafter both "naturally orthotropic" and "structurally orthotropic" plates will simply be referred to as orthotropic plates.

1.3 Methods of Analysis

Analysis of slab and girder structures may be divided into three basic categories, which will be reviewed here. These categories are the



(a) Two-Way Reinforced Concrete Slab.



(b) "T" Beam Construction.

Fig. 1.2. Structural Orthotropic Elements.

grillage method, primary and secondary members method, and the orthotropic plate method. In addition, the design requirements of the American Association of State Highway Officials (AASHO), as set forth in the Standard Specifications for Highway Bridges,^{2*} will be reviewed.

1.3.1 Grillage Method. Lazarides¹² solved the slab and girder bridge by dividing the structure into a grillage of longitudinal and transverse members. Slope deflection equations were then set up for joint intersections of members, resulting in a set of simultaneous equations. Lightfoot and Sawko¹⁷ have shown that electronic computers may be used to deal with the abundance of arithmetic involved with this procedure.

1.3.2 Primary and Secondary Members Method. Another method of analysis separates the structure into primary longitudinal members and substitutes some form of secondary cross connection for the transverse members. This method has been used with the various assumptions listed below:

(a) Newmark²⁶ assumed the slab was an analogous continuous beam over any number of rigid or flexible girders extending between supports. Newmark's procedure was similar to the Hardy Cross method of moment distribution, involving flexural stiffnesses, carryover factors, and fixed end moments for the analogous slab. In certain cases the girder torsional restraint may be taken into account. Newmark and Siess used this method to study moments in I-beam bridges.^{27,30} The theoretical solution for rectangular slabs was confirmed by experimental results for right angle bridges. While skew slabs on I-beams were not solved theoretically, they were included in the experimental study.²⁹ The results of these investigations led to design recommendations for slab and stringer highway bridges.

(b) Hetenyi⁹ assumed no rotation of individual members at an intersection and used a sine series to represent the load and deflection of the system in the longitudinal direction.

(c) Pippard and de Waele³² assumed no rotation of longitudinal members and replaced the transverse members with a continuous medium.

*Superscript numbers refer to references in the Bibliography.

(d) Leonhardt¹⁴ assumed the transverse members could be replaced by a single member at midspan with no torsional stiffness.

(e) Hendry and Jaeger⁸ assumed the transverse members could be replaced by a continuous medium. The effects of rotation of longitudinal members may be included where necessary. The differential equation for the loading on each member is written using "harmonic analysis" to derive the deflections and bending moments on each longitudinal member.

1.3.3 Orthotropic Plate Method. The orthotropic plate approach replaces the actual bridge structure by an equivalent orthotropic plate which is then treated by classical theory.⁴⁵ This approach was first developed by Guyon for grillages with members of negligible torsional stiffness⁶ and later for isotropic slabs.⁷ Massonnet²⁰ extended this approach by including the effects of torsion. The combined work of Guyon and Massonnet is referred to as the Guyon-Massonnet load distribution theory.

Guyon and Massonnet's work has been extended by others^{22,23,25,35} and includes the development of a design procedure. An excellent presentation of the Guyon-Massonnet theory may be found in Rowe's book Concrete Bridge Design.⁴⁰ In the same book Rowe has summarized the results of numerous tests on model^{5,18 36,37} and full-size bridges^{24,38,39} that have been analyzed using the Guyon-Massonnet theory. Agreement between theoretical and experimental results were shown to be good. Mattock and Kaar²¹ have compared this theory with good results to an experimental study of a one-half scale continuous prestressed concrete bridge.

Orthotropic plate systems have also been solved by the use of discrete element mathematical models. Basically the method involves breaking a plate into a system of discrete parts, consisting of elastic blocks connected by rigid bars. The equations describing the discrete element system are obtained by free-body analysis of the model. Various discrete element models have been proposed, such as those described by Ang and Lopez⁴ and Hudson and Matlock.¹¹ The primary difference in the various models is the technique for modeling torsional stiffness. The value of a discrete element model lies in the ability to allow point-to-point variation of section properties. The true shape of a plate may be closely

approximated by the use of many discrete elements. In general, the smaller the elements the better the approximation.

1.3.4 Limitations. The problem of a skewed slab on girders or a skewed orthotropic plate has not been solved in a closed form. Hence, all of the methods discussed are limited to a rectangular system, with the possible exception of the discrete element techniques.

Furthermore, the methods discussed are limited to the linear elastic range of load response. This is a serious drawback in the case of reinforced concrete, which has a significant portion of its load-carrying capacity in the inelastic or nonlinear range.

1.3.5 Design Requirements. The Standard Specifications for Highway Bridges² contains an empirical method for determining the distribution of wheel loads to longitudinal girders. Each girder is designed to carry the fraction of a wheel load (both front and rear) determined by

$$k = \frac{S}{C} \quad (1.1)$$

where k = number of wheel loads
 S = average girder spacing in feet
 C = constant

The constant C depends on the type of slab and girder system and the number of traffic lanes. In the case of a concrete slab on concrete girders designed for one traffic lane, the constant is 6.0. The constant is 5.0 for two or three traffic lanes.

The specifications are based on Ref. 28 by Newmark and Siess. The procedures described in Ref. 28 were considered generally applicable for span lengths from 20 to 80 feet and girder spacings from 5 to 8 feet.

1.4 Role of Mathematical and Structural Models

In the analysis of the behavior of complex structures, the structural engineer has traditionally utilized a mathematical model for obtaining an understanding, or at least an insight, into the response of the structure to given sets of loadings. Due to the wide acceptance of the elastic

theory of analysis, the mathematical models developed tended to be linear, elastic formulations of the problems. As designers realized that the complexity of the problems was outstripping the methods of analysis available, a system of techniques for using linear, elastic, small-scale physical models of the prototype structure as analogue computers was developed. Usually the models were carefully fabricated from linear, elastic materials, such as plastics or light gage metals. Care was taken in loading to keep stresses within the proportional limits. Under these conditions the results of studies using structural models tended to confirm the results of elastic analyses. With the increased capability for handling large systems of simultaneous equations, through the use of high-speed digital computers, there was a decline in interest in the use of the elastic structural model, except in a few areas such as shell buckling.

However, developments in structural engineering in the past two decades have pointed out a growing awareness of some serious limitations of present methods of analysis. The development of plastic design concepts in structural steel, ultimate strength design concepts in reinforced concrete, as well as nonlinear analysis concepts, have created a demand for further observation of actual structural behavior to permit the accurate construction of new types of mathematical models for design tools. Further observations are required to correctly assess the limits of applicability of the design technique developed.

Needless to say, it would be impractical, and in some cases almost impossible, to gather all the required data from tests (including load tests to destruction) of prototype structures. To meet the needs for data describing basic cross-sectional capacities, tests have been run on individual structural members. In most cases the tests have been performed on reduced-scale structural models of the members manufactured from the same type materials as would be used in the prototype. Reduced-scale structural model tests of individual structural members have become a very accepted basis for structural research.

With the development of more accurate mathematical discrete element models for predicting the response of a member to a load stimulus, this study focuses attention on the adequacy of methods of structural analysis

to predict load distributions and overall structural behavior of pan-formed concrete slab and girder bridges subject to realistic loading. In particular, since most reinforced concrete structures are subject to localized cracking and inelastic stress distributions, the adequacy of linear methods of structural analysis must be examined. Since in beam and slab-type structures the moments developed in the slabs may be quite sensitive to beam deflections and the load distributed to the beam may be quite sensitive to slab stiffness, changes in flexural stiffness due to cracking or inelastic effects could greatly modify the results of convention methods of analysis.

Concurrent with the growing awareness of a need to reexamine design methods for complex structures, there has been the development of a system of "direct" structural model testing which emphasizes basic agreement between prototype and model physical characteristics. This is a welcome supplement to the indirect model which was simply an analogue computer representing the assumptions of the analysis rather than the properties of the structure. A great advantage of the detailed structural model is the ability to observe design omissions and detailing errors as well as design inconsistencies.

All of these points have been realized in this reinforced micro-concrete model study of concrete slab and girder bridge systems. Extensive developmental work has been completed to gain experience and confidence in microconcrete model techniques. Programs of investigation of material characteristics have developed microconcretes with typical values of f'_c and E_c as found in practice, as well as test equipment and methods suitable for reduced scale testing. Methods of fabrication have been developed for reinforcement cages and dimensional tolerances have been controlled to ensure repeatability. Complete loading and instrumentation systems have been developed to permit simulation and measurement of actual behavior at both service and ultimate loads. Comparisons with field measurements verified the accuracy.^{15,16}

In the same way, one of the most advanced methods of analysis of orthotropic plate systems was utilized to obtain a mathematical solution of the expected behavior of the bridge system. Utilizing programs developed

by Matlock et al.¹⁹ the results of a discrete element solution were compared to the measured behavior. By combining both the mathematical model and the structural model results it is felt that a significant insight has been obtained regarding the fundamental behavior of reinforced concrete pan-formed slab and girder systems.

1.5 Prototype Bridge System

The basic structural system investigated was the Texas Highway Department's widely used pan-formed slab and girder bridge system known as the CG Series. The basic structure is a monolithically cast pan-formed slab and girder unit, as shown in Fig. 1.3. It is designed as a simply supported span with a nominal span length of 40 ft.-0 in. for a right angle bridge. Standard designs are available for skew spans varying from 0° to 45° , with the angle of skew being the angle between the axis of the bent cap and a line perpendicular to the flow of traffic.

Figure 1.3 shows the transverse cross section, comprised of a series of semicircular arch units. This shape is obtained by casting on a series of standard semicircular pan forms. Detailed plans for these forms are given in Figs. A.1 and A.2 in Appendix A of this report. Typical girder and slab reinforcement, as well as a general view of the pan forms, is shown in Fig. 1.4.

The roadway width can be varied in three-foot increments by adding or subtracting the three-foot pan form units. The skew angle may be varied by sliding pans relative to one another until the desired skew is obtained. Skew angles are controlled by having a uniform hole spacing on the bottom connecting angles on each pan. Skew variations are obtained by slipping the pans one or more holes relative to the adjacent pans. Standard details are available for a one, two, three, or four-hole skew corresponding to skew angles as shown in Fig. 1.5. An increasing skew angle also slightly increases the span length. This is partially due to the greater width of the bent cap when measured on a skewed line. In addition, there is a need to increase the clear distance between bents to accommodate the standard square-end pans. The increase in clear distance is also indicated in Fig. 1.5(c).

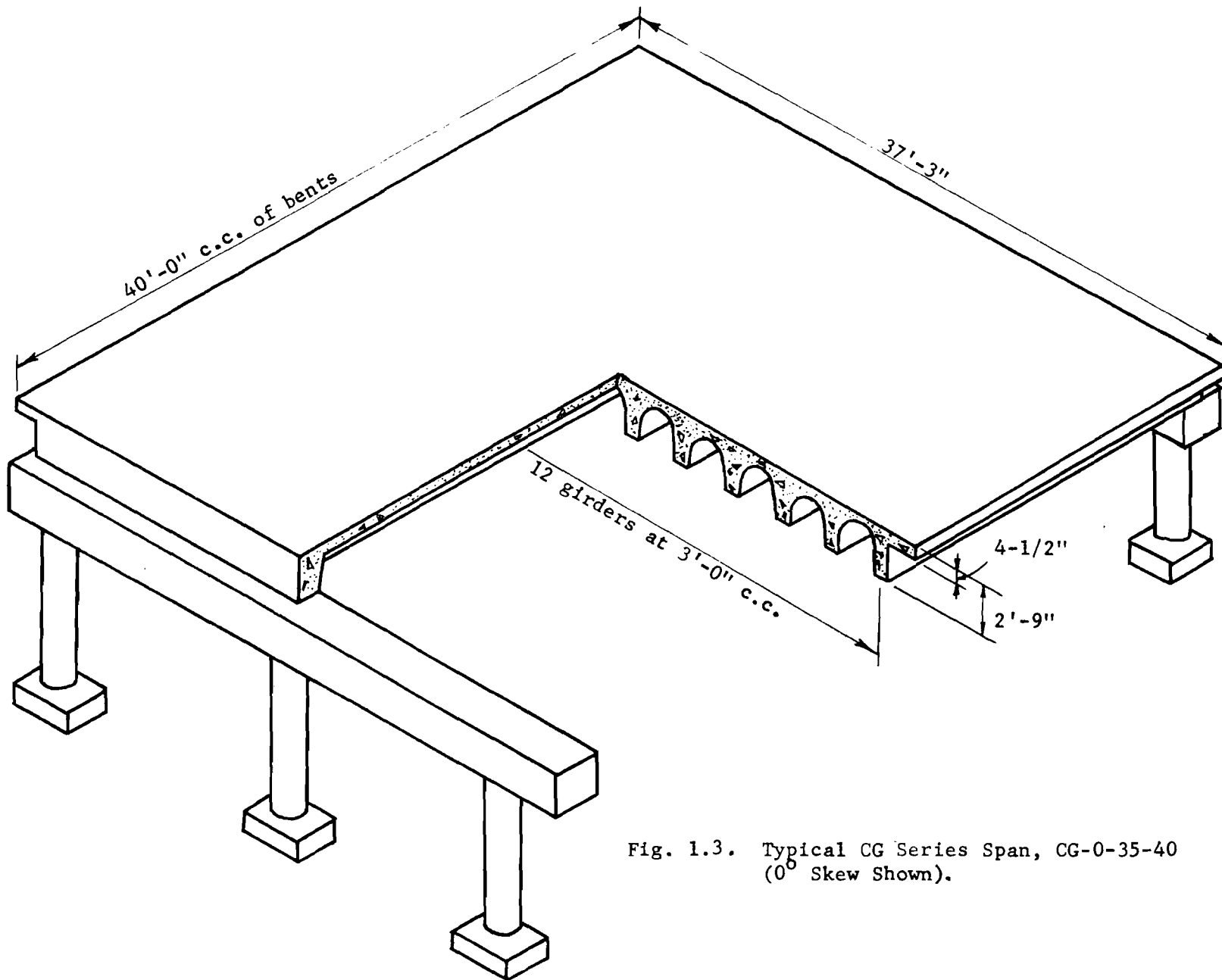
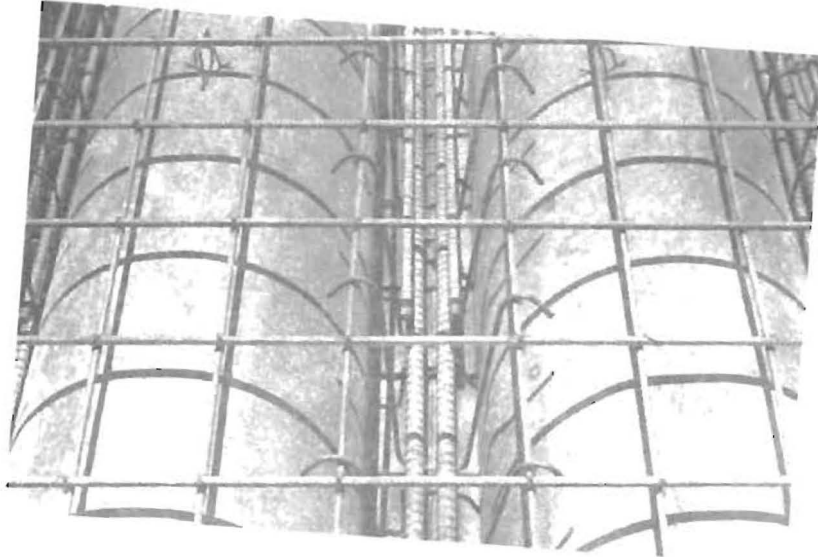
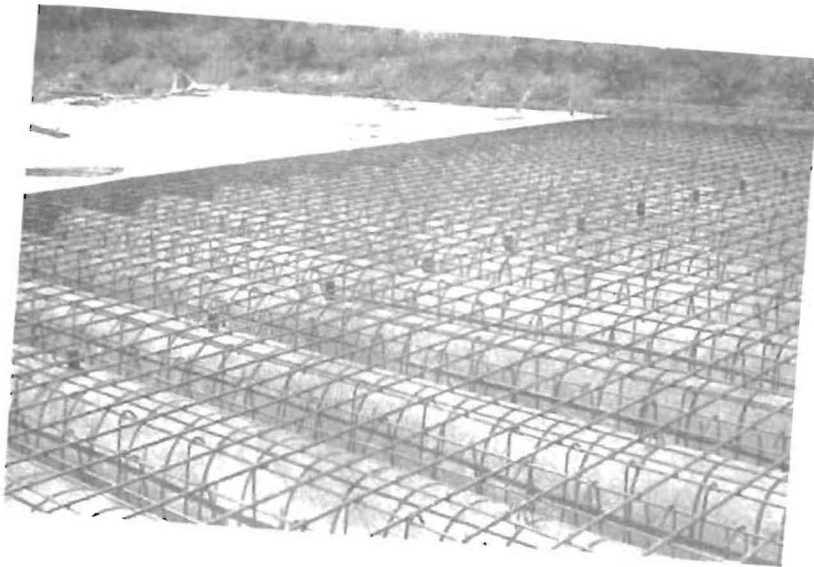


Fig. 1.3. Typical CG Series Span, CG-0-35-40
(0° Skew Shown).

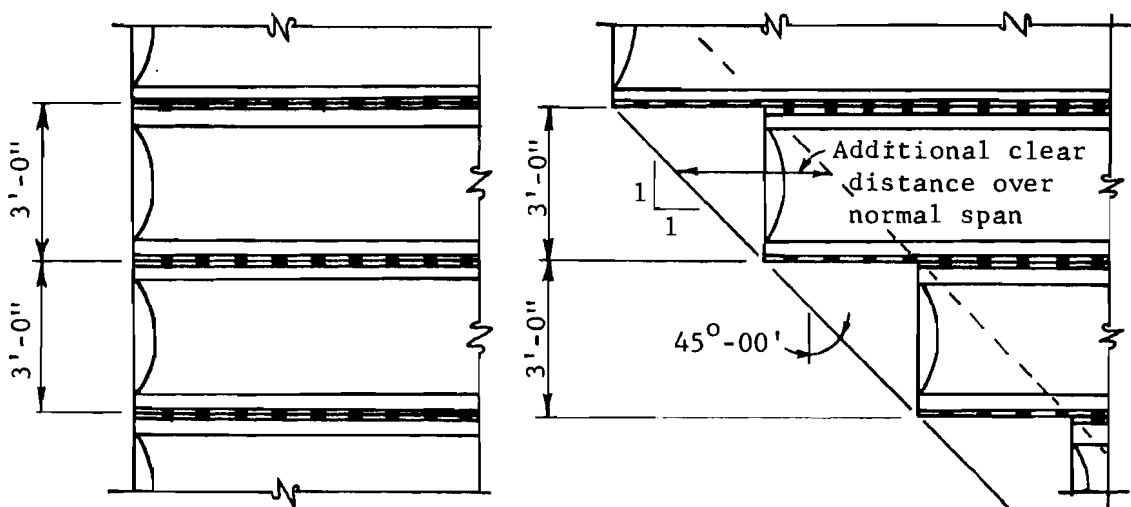


(a) Girder Steel.



(b) Slab Steel and View of Pan Forms.

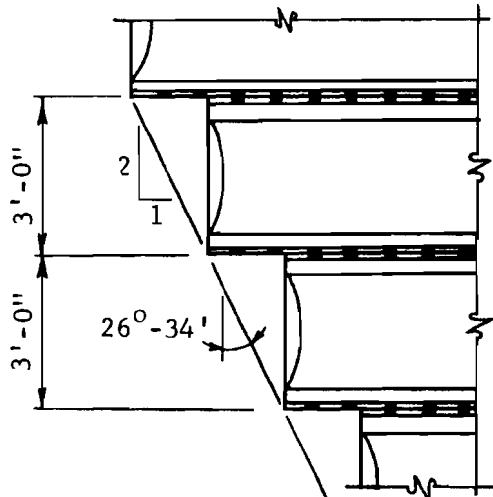
Fig. 1.4. Prototype Reinforcement and Pan Forms.



(a) Normal.

About 1/2" from and parallel to face of bent cap. Typical for all spans.

(c) Four Hole Skew.



(b) Two Hole Skew.

Not Shown
One Hole Skew
Three Hole Skew

Skew Angle	No. of holes Skew	Bevel	Span Length C. to C. of bents
Normal	None	None	40'-0"
14°-02'	1	1:4	40'-10"
26°-34'	2	1:2	41'-9"
36°-52'	3	3:4	42'-9"
45°-00'	4	1:1	43'-10"

Fig. 1.5. Pan Arrangement for Standard Skews.

Major economic benefits are realized by the design of the pan forms as structural units supported from the bent caps without interior falsework during construction. Pan support details vary according to the angle of skew, but basically the pans are supported from clips bolted to the faces of the bent caps. Typical pan supports are shown in Fig. 1.6 for a 26^o-34' skew. The triangular gap between the pan form and bent cap is usually formed with a piece of plywood.

The end diaphragms are cast directly on asphalt board lying on the top surface of the bent cap. The asphalt board is shown in place on the expansion end support in Fig. 1.6. Details for both supports are shown in Fig. 1.7.

The basic concrete cross section is used for several typical loadings (i.e., H15, H20, and H20-S16 AASHO trucks). Flexural capacity is varied by changing the quantity of flexural reinforcement provided. Shear capacity is varied by changing the stirrup size and spacing.

1.6 Object and Scope of Investigation

A detailed investigation was carried out on the CG Series of pan form slab and girder bridges, using approximately 1/6-scale "direct models" of the bridges (including substructure); these model tests were supplemented by full-size field testing, as well as analytical procedures. The overall objectives of the investigation were as follows:

- (a) To investigate the behavior at service loads, moderate overloads, and at ultimate loads of typical pan-formed concrete slab and girder bridge spans, using reinforced microconcrete structural models.
- (b) To confirm the observed behavior at service loads by full-scale testing of a prototype structure.
- (c) To evaluate the effectiveness of the end diaphragms in participating with the bent caps to carry slab loads.
- (d) To make recommendations regarding the adequacy of present design provisions based on these test results.

Objective (a) included an evaluation of "load distribution" patterns to the girders at various load levels. This was particularly desirable, since the curved cross section of the structure implies a higher transverse

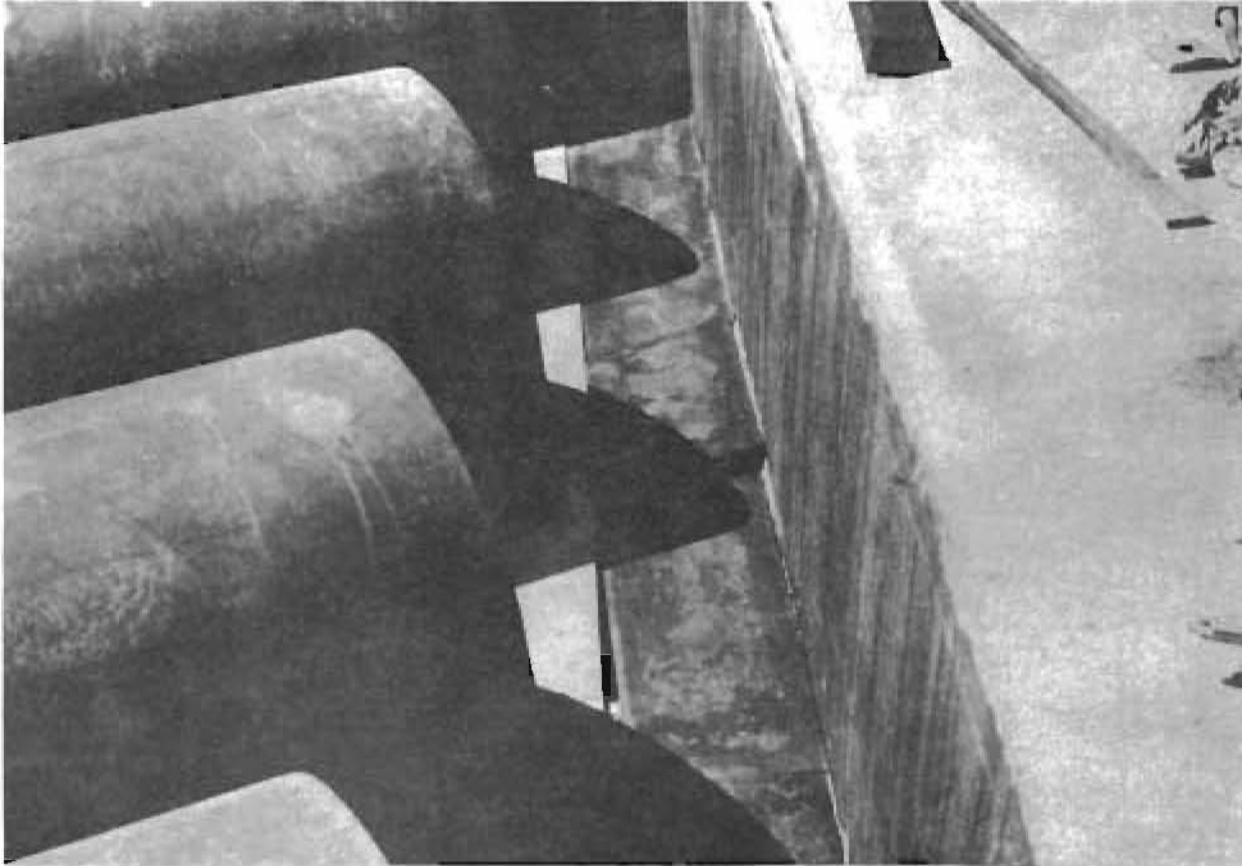


Fig. 1.6. Pan Form Support Details.

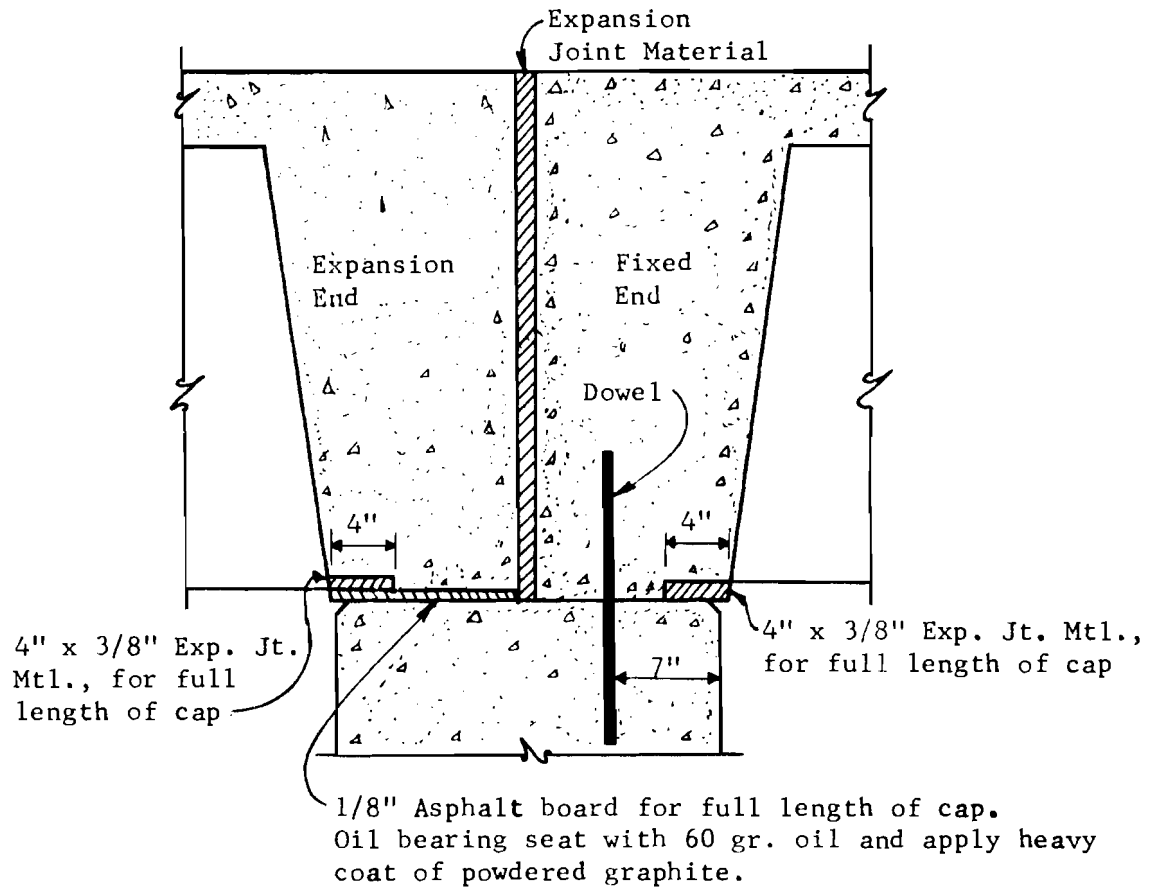


Fig. 1.7. Bearing Support Details.

rigidity than encountered in the usual slab and girder bridges having constant thickness slabs. This transverse rigidity caused some doubt over the accuracy of the usual AASHO slab and girder design procedures when applied to this type of bridge.

The desirability of testing at various levels of loading (some of which would cause cracking in the prototype) warranted the use of more complex microconcrete test specimens rather than an elastic test specimen.

1.7 Program of Research

The following criteria for the model study were adopted to meet the objectives of the investigation:

(a) Model materials must have properties closely resembling the prototype materials. While it is possible to utilize the mathematical theory of similitude to interpret and correlate the behavior of linear models with different material properties in the model and the prototype, no such procedure is valid in ultimate strength models. Since the failure mechanism in the prototype materials is not understood completely, it is felt essential to strive to utilize model materials with physical properties as identical as possible to those of the prototype to minimize variation in failure criteria.

(b) Boundary conditions must match the prototype as faithfully as possible. To carry this out it was considered essential to model a typical substructure unit in order to include typical support deflection and rotation effects. It was also felt necessary to include dead load effects from adjacent spans on these supports as well as typical joint details. While the span is idealized as having "simple supports," the actual details, as shown in Fig. 1.7, prevent both translation and rotation at one end and, hence, the span is "partially fixed." These support details were carefully modeled to assess this effect.

(c) Wherever possible independent checks of statically determinate subsystems must be utilized for verification of accuracy. Since inclusion of true boundary conditions makes theoretical analysis extremely difficult, all loading and measuring systems were verified in tests on simply supported

members with known behavior. In addition, backup check measurement systems were provided where possible. These precautions developed confidence in the techniques used with the indeterminate slab and girder system.

The overall study consisted of the following principal test specimens:

(a) Model SG-1. This is a 1/5.5-scale model of a 0° skew, 40-ft. span, CG Series bridge. Details are shown on the Texas Highway Department Plan Sheet CG-0-35-40 (Fig. A.3) in Appendix A. The model was cast in place on a model of the substructure design for the prototype span. Substructure details are shown on the Texas Highway Department Plan Sheet BCG-0-35-40 (Fig. A.4) in Appendix A.

(b) Model SG-2. This is a 1/5.5-scale model of a 45° skew, 40 ft.-10 in. span. Details are shown in Figs. A.3 and A.5.

(c) Model SG-3. This model duplicates SG-2 in all respects except for the main flexural reinforcement, where high strength steel ($f_y = 60$ ksi and $f_s = 24$ ksi) was substituted for intermediate grade steel ($f_y = 40$ ksi and $f_s = 20$ ksi). The area of steel provided was changed so that the total tensile force at allowable steel stress was maintained constant (i.e., $A_{sSG3} = \frac{20}{24} A_{sSG2}$). The model was cast in place on the same substructure used for Model SG-2.

(d) Model SG-4. This is a 1/5.5-scale model of a 26° -34' skew, 41 ft.-9 in. span. Details are shown on the Texas Highway Department Plan Sheet CG-0-33-40 (Fig. A.6) in Appendix A. The model was cast in place on a model of the substructure designed for the prototype span. Substructure details are shown on Texas Highway Department Plan Sheet BCG-0-33-40 (26° -34') (Fig. A.7) in Appendix A.

Model SG-4 (including substructure) is the reduced scale model of the full-size prototype bridge CG-1, which was tested at service load levels.

(e) Prototype CG-1. This is a full-size prototype bridge of a 26° -34' skew, 41 ft.-9 in. span, with the same details shown in Figs. A.6

and A.7 for Model SG-4. The bridge was part of a farm-to-market road near Belton, Texas.

Secondary tests were run on several models, as follows:

(a) Shear Tests. Model SG-2 was loaded for maximum moment and then reloaded with a maximum shear loading in order to determine which was more critical for design.

(b) Punching Tests. Punching tests to determine shear resistance to individual wheel loads were performed on an undamaged portion of the slab of model SG-3 after the bridge span had failed in flexure.

(c) Bent Cap Tests. The substructure for Model SG-4 was tested by loading the cap of one bent with a series of concentrated loads which were increased until failure occurred. The remaining bent was then loaded to failure by applying the same load configuration through the end diaphragms to determine the stiffening effect of these diaphragms.

Models SG-1, SG-2, SG-3, and SG-4, along with the auxiliary shear and punching tests, were tested in order to meet objective (a) in Section 1.6. Model SG-4 and Prototype CG-1 were tested in order to meet objective (b) in Section 1.6. The bent cap tests were performed in order to meet objective (c). Collectively, the results from all tests were designed to meet objective (d).

All of the details concerning similitude, model technology, and model reliability have been documented in a previous report in this series. In this report very detailed information concerning the materials used, fabrication technique, instrumentation systems, and loading procedures are given. In addition, a very detailed comparison is presented with the results of load distribution studies at service load levels between the models and prototype. The study indicates the credibility of the model results. Also, data are presented which establish the ultimate strength reliability of the structural model.

Physical tests can give definitive information only for the actual conditions existing in the specimens tested. Therefore, it is difficult to cover a wide range of variables using complex structural models such as

those of this investigation. For this reason it is desirable to have an accurate mathematical analysis which may be used for more rapid and economical study of many variables. Previous mathematical analyses were not felt sufficient to adequately describe the behavior of this type of concrete slab and girder bridge, because of limitations in representing transverse slab stiffness for the series of arches. Previous solutions were restricted to rectangular slabs, as well as the uncracked elastic range of loading.

In this investigation a discrete element mathematical model of an orthotropic plate was selected to obtain a theoretical solution, since properties may be varied from point to point.^{11,31} Both the theoretical solution and the experimental results are compared with each other as well as with current design practice, as reflected by the AASHO Standard Specifications for Highway Bridges.²

C H A P T E R I I

DIRECT MODEL SIMILITUDE

2.1 Introduction

Two very different types of structural models are available, i.e., "indirect models" or "direct models." These models have very different ranges of application and represent very different model technologies.

The indirect model is essentially an analogue computer for solution of idealized structural systems. The indirect model is usually fabricated from linearly elastic materials and is loaded so that stresses do not reach the proportional limit. Under those load conditions such models tend to confirm the results of mathematical analyses based on linear elastic assumptions.

Since it was evident from the outset that the present study had to consider structural behavior in both the uncracked and cracked section range, and since the fundamental relationships between factors such as flexural and torsional stiffness were not completely understood in both of these ranges, the indirect model was not used in this study.

The direct model is essentially an analogue computer for solution of the actual structural system with a minimum of "idealized" boundary conditions. The direct model emphasizes the agreement between prototype and model physical characteristics and boundary conditions. As such it does not satisfy erroneous analytical assumptions which distort the true nature of the structure.

The ideal direct model is a true-to-scale model, in which all details are linearly reproduced, although practicality requires that this type of model sometimes be simplified to omit minor details that should not significantly affect the structural behavior. The direct model is extremely

valuable in that it may be used to document elastic, inelastic, and ultimate load behavior. This use over the full range of loadings is valuable in determining the range of applicability of elastic theories for a prototype structure constructed from an inelastic material such as reinforced concrete.

2.2 Scale Relations

2.2.1 Materials. A generalized stress-strain curve illustrating idealized relations between the prototype and model materials is shown in Fig. 2.1. The factors S_f and S_ϵ are referred to as the stress and strain scale factors, respectively. The geometrical scale factor, S_L , relates the model and prototype dimensions (model length = $1/S_L$ x prototype length). Microconcrete may be designed with a resultant stress-strain diagram equal to that of the prototype, hence $S_f = S_\epsilon = \text{unity}$. With proper selection of model reinforcement, the same statement can apply to the reinforcing steel.

Where shear and torsional stresses may be important as well as with significant plate behavior, it is essential that Poisson's ratio for the model and prototype materials be equal. This requirement is readily achieved where the model materials are essentially the same as the prototype materials.¹

2.2.2 Loads. The "direct model" chosen utilizes the same material properties as the prototype, hence $S_\epsilon = S_f = 1$. Thus, the prototype and model loads are related only by the geometrical scaling factor. In this case the load relations become:¹⁶

1. Loads distributed over an area

$$\text{Model load per unit area} = \text{prototype load per unit area}$$

2. Loads distributed over a length

$$\text{Model load per unit length} = \frac{1}{S_L} \text{ prototype load per unit length}$$

3. Concentrated loads

$$\text{Model load} = \left(\frac{1}{S_L} \right)^2 \times \text{prototype load}$$

4. Gravity loads

$$\text{Model density} = S_L \times \text{prototype density}$$

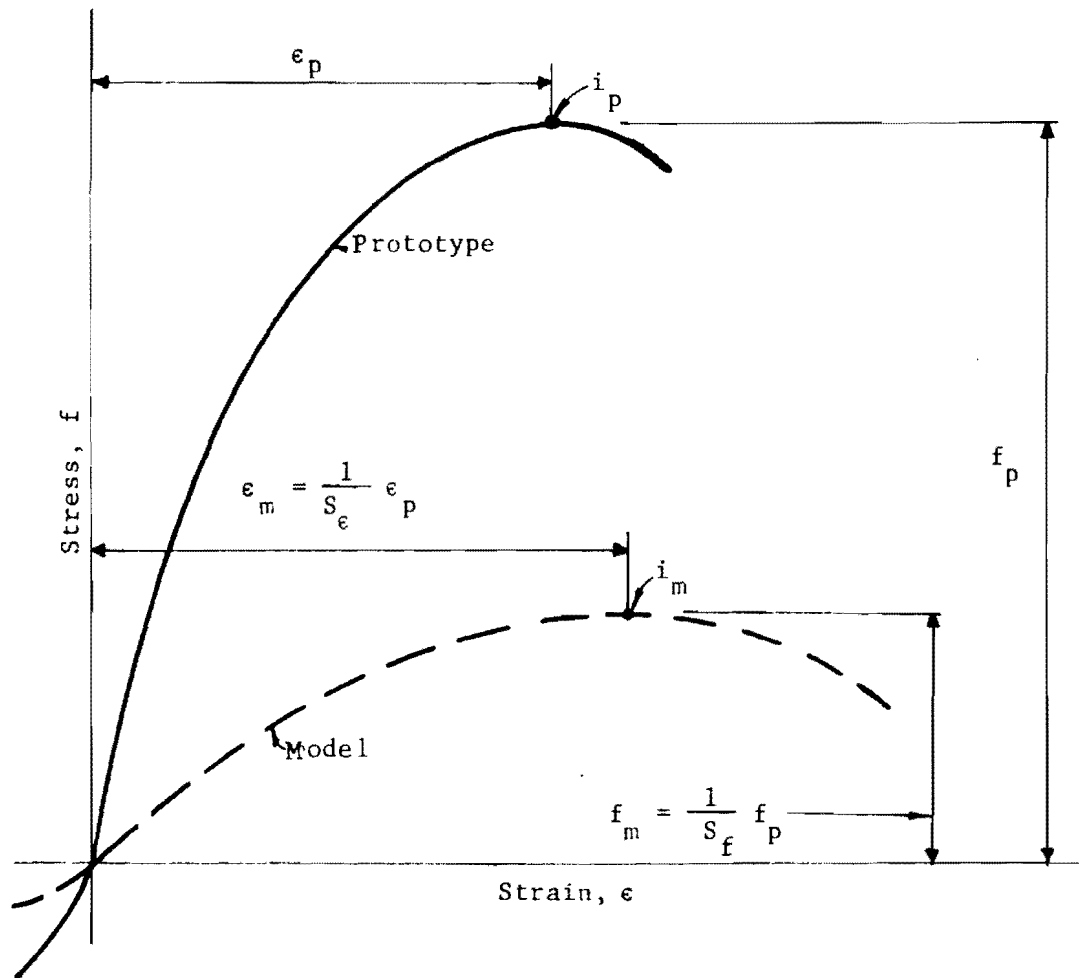


Fig. 2.1. General Stress-Strain Curve.

If the above requirements are met, then the measured strain in the model is equal to the prototype strain and the model deflections are $\frac{1}{S_d}$ times the prototype deflections.

The unrealistic requirement for substantially increased model density may be overcome by the application of external loads as discussed in a later section.

2.2.3 Geometrical Scale Factor. The geometric scale factor, $S_d = \frac{L_p}{L_m}$, is determined by economics, available materials, fabrication methods, and testing procedures. Frequently the major considerations are other than economic.¹⁶

At the beginning of this project a study was made of the factors affecting the fabrication and loading costs for these models for a number of scale factors. The total combined cost of fabrication and loading indicated a minimum cost at about 1/8 scale, with very little difference in costs in the range of 1/5 to 1/10 scales when compared to the cost of full-size testing (15 to 17 percent of prototype). In this study the main reinforcing steel in the prototype was a No. 11 bar; the availability of deformed No. 2 bars was a major consideration in the selection of the scale as $1/S_d = 2/11 = 1/5.5$.

CHAPTER III

MODEL TECHNOLOGY

3.1 Introduction

The basic goal in the direct modeling process is to obtain a realistic approximation of the behavior of the prototype over a complete spectrum of loads from dead load through service loads up to collapse loads. The detailed procedures developed in this study to obtain this realistic approximation have been given in detail in the previous report.¹⁶ The purpose of this chapter is to summarize the most important elements of this technology.

3.2 Materials

3.2.1 Microconcrete. The model concrete used in this investigation is referred to as microconcrete. It is designed based on geometric scaling of the aggregate gradation curve, using a typical Texas Highway Department mix design for superstructure concrete as a prototype. The model aggregate used the following combinations of aggregates:

TCM 1/8	26%
Ottawa Silica Bond Sand	30%
No. 1 Blast Sand	28%
No. 2 Blast Sand	8%
Colorado River Red Sand	8%

Final mix design was based on a trial batch basis until a workable concrete with stress-strain characteristics quite similar to the prototype concrete were obtained. A Texas Highway Department approved retarding agent "Airsene L" was used to delay initial set and improve workability. The final mix design used was:

Water-cement ratio by weight	0.687
Cement factor (sacks per cu. yd.)	5.0
Aggregate-cement ratio by weight	6.53
Retarding agent (fl. oz. per sack)	6.0

This microconcrete had an air content of 5-3/4 percent and a wet unit of 133 lbs. per cu. ft.

Stress-strain curves for both the microconcrete and the prototype concrete are shown in Fig. 3.1. The microconcrete of this investigation (shown as a solid curve with data points plotted) had an ultimate strength of 4530 psi, while the prototype concrete (shown as a dashed curve with data points plotted) had an ultimate strength of 4700 psi. The other curves (ultimate strengths on the order of 3000 psi) are taken from a study by Aldridge¹ and tend to verify the shape of the stress-strain curves for the prototype and microconcrete.

The computed moduli of elasticity shown are 3,410,000 psi and 3,950,000 psi for the microconcrete and prototype concrete, respectively. The values closely match the observed values for the secant modulus at $0.45 f'_c$ and shown that the difference between moduli is mostly a function of unit weight.

Split cylinder tensile strengths were obtained using cylinders from the same batches of microconcrete and prototype concrete. The microconcrete split cylinder strength was 555 psi, which is about $0.12 f'_c$ or $8.3 \sqrt{f'_c}$. The prototype concrete split cylinder strength was 480 psi, which is about $0.10 f'_c$ or $7.0 \sqrt{f'_c}$. The slightly increased tensile strength of the microconcrete should not greatly affect strength calculations but would lead to somewhat higher crack formation loads in microconcretes.

3.2.2 Reinforcement. In direct models it is essential that the steel used in the model and the prototype have virtually identical stress-strain curves, particularly with reference to sharpness of definition of yielding. The SWG wire initially obtained for this project exhibited a "round house" (i.e., no sharply defined yield plateau) stress-strain curve. Heat treatment was used to give the wire a desired "flat top" yield plateau, typical of intermediate grade reinforcement.

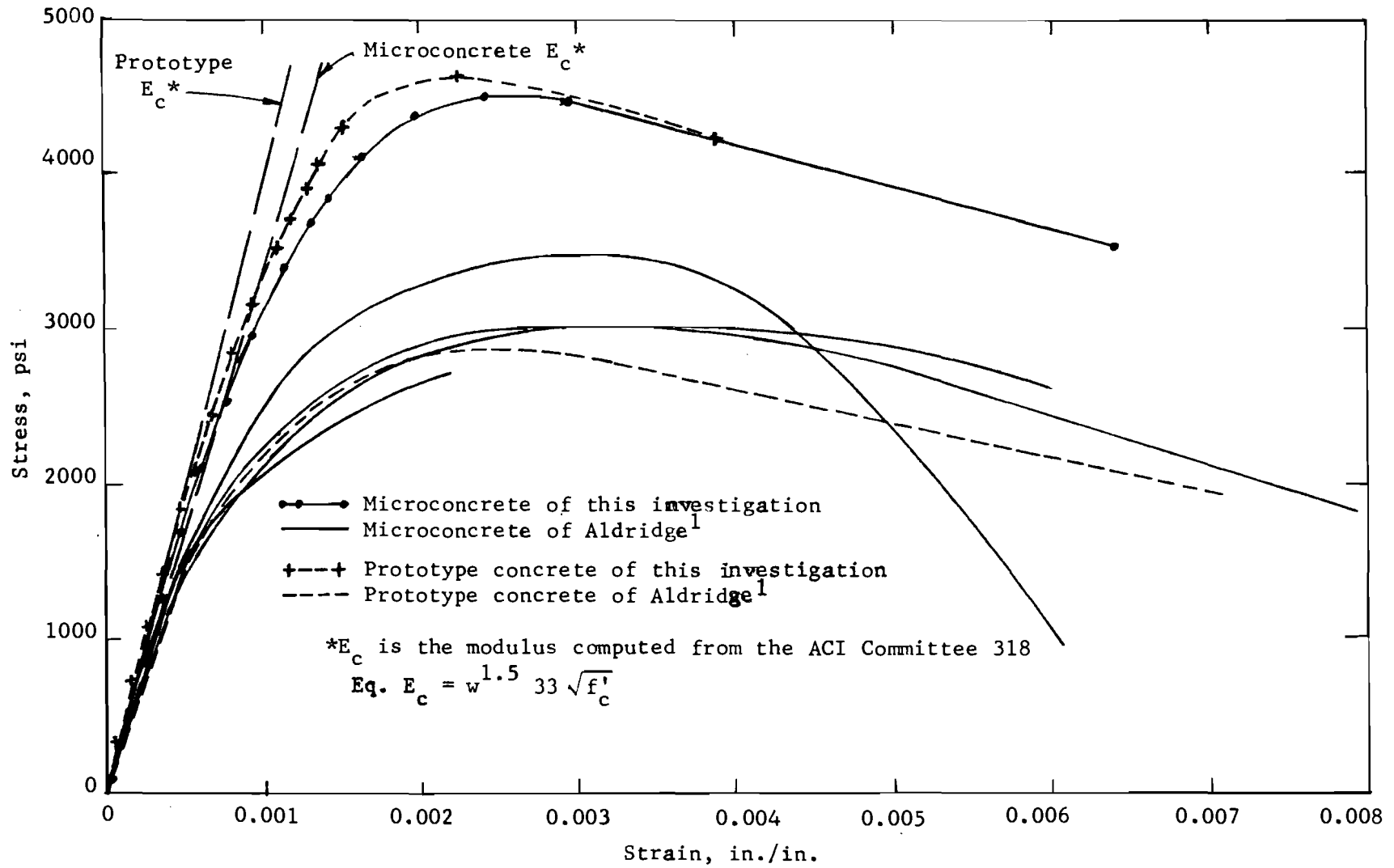


Fig. 3.1. Stress-Strain Curves for Microconcrete and Prototype Concrete.

Smooth (nondeformed) SWG wires and No. 2 bars do not function in bond in the same manner as deformed bars, hence their use is limited to studies where bond is not a major factor. The smooth wires used in this investigation were allowed to rust to improve bond properties. After two of the bridge models had been tested, a special supply of No. 2 deformed bars became available. Comparative tests using the No. 2 smooth and then the deformed bars as the main flexural reinforcement showed conclusively that the use of deformed bars resulted in more realistic crack patterns.¹⁶ Therefore, subsequent bridge models were reinforced with deformed No. 2 bars as the main flexural steel.

Typical stress-strain curves for the main reinforcement used in this investigation are shown in Fig. 3.2. Model SG-3 was identical to Model SG-2, except that high strength steel was used in the former and intermediate grade steel was used in the latter. The substitution was made by adjusting the areas so that the total bar force at design stress (24 ksi) for the high strength steel was equivalent to the total bar force at design stress (20 ksi) for intermediate grade steel.

3.3 Fabrication Techniques

In realistic modeling, fabrication tolerances must be reduced in proportion to the scale utilized. This requires careful consideration of forming and fabrication techniques. Carefully constructed Plexiglas forms were used. The transparent property of the Plexiglas forms greatly facilitated the placement of the large quantities of reinforcement to close tolerances. Detailed information on form manufacture and application is given in Ref. 16.

The substructure was detailed following Texas Highway Department Standard Plans, with each bridge model having the substructure which was usually designed for it. Bent caps were positioned in the test frame, the pan forms suspended from them and the slab cast in place. This procedure allowed modeling of the true support boundary conditions of the prototype as shown in Fig. 3.3. A 0° skew and a 45° skew model are shown ready for casting in Fig. 3.4(a) and (b).

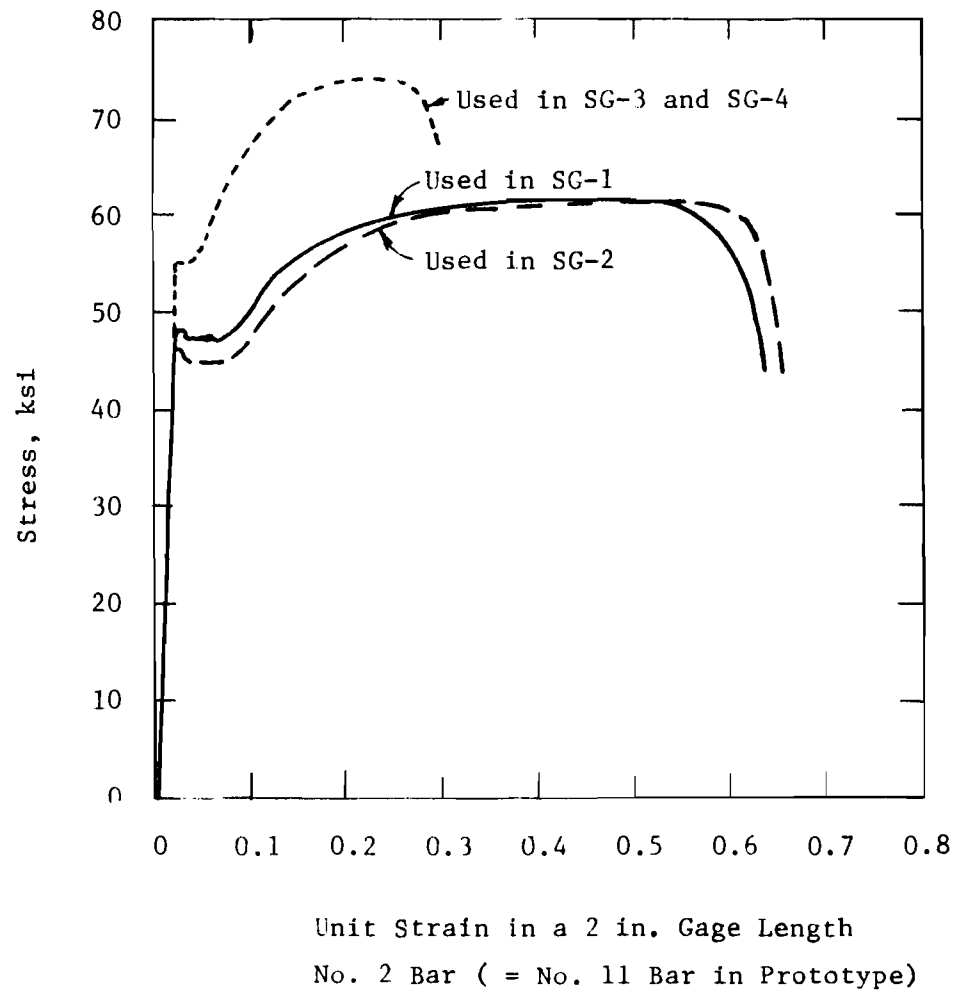
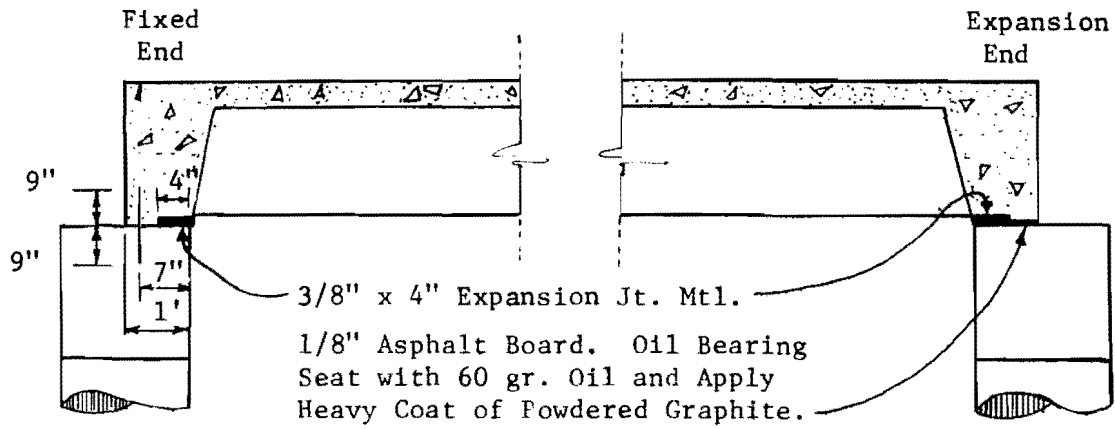
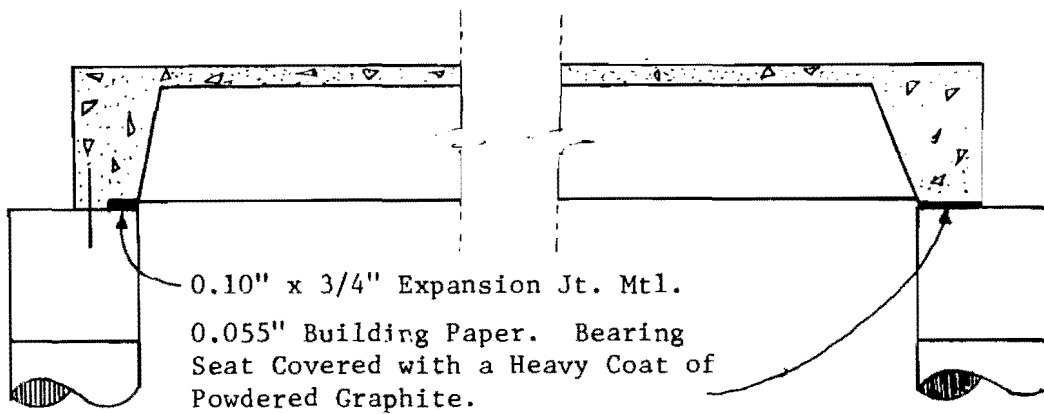


Fig. 3.2. Typical Stress-Strain Curves for Main Flexural Reinforcement.

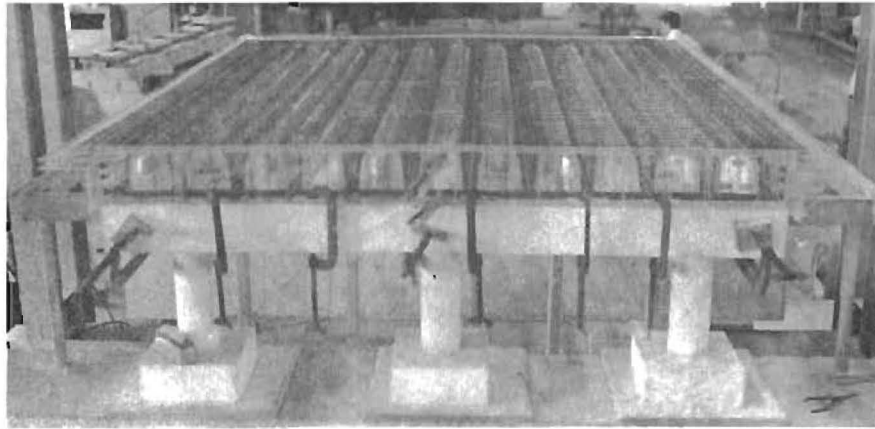


Prototype



Model
(Scale = 1/5.5)

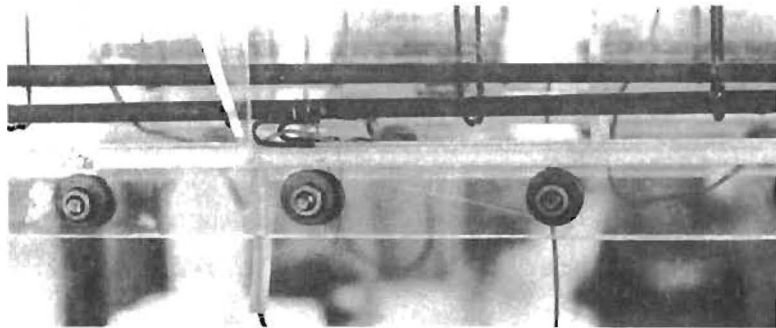
Fig. 3.3. Support Conditions.



(a) 0° Skew Bridge.



(b) 45° Skew Bridge.



(c) Location of Reinforcement.

Fig. 3.4. Models Ready for Casting.

Figure 3.4 also illustrates the ease with which steel placement may be checked when Plexiglas is used as a form material. The procedure for passing strain gage lead wires through the forms and in the wires used to support the dead load blocks are also shown.

Microconcrete was placed in uniform lifts and compacted with a standard laboratory immersion vibrator operating through a Variac. After casting, screeding, and troweling, the deck was sprayed with a membrane curing compound and covered with wet burlap. Forms were left in place as a moisture barrier for about three days, then stripped.

3.4 Instrumentation

3.4.1 Load Control. The loading system used was actuated by a hydraulic pressure system. However, since pressure gage readings are not reliable enough at low load levels, ram loads were controlled by the pancake-type electronic strain transducer load cell developed by Lee.¹³ This load cell has a sensitivity of about three pounds per microinch of strain, with a maximum working capacity of about 8000 pounds.

3.4.2 Structural Response. Concrete strains were measured with a Demec gage with a gage length of two inches. Due to the small amplitude of concrete strains, the number of these measurements taken was limited.

A wide variety of reinforcement steel strains were measured with electrical resistance strain gages attached to the reinforcement and waterproofed so that they could be immersed in the concrete. The main girder flexural steel had 1/4-in. gage length foil gages, while similar gages with a 1/8-in. gage length were applied to the smaller size transverse slab steel. Detailed locations of the gages are shown in Chapter VI.

Deflection measurements with reference to a movable gage base line system were taken using Federal dial gages with a least count of 0.001 in. with estimation to the nearest 0.0001 in. Deflections were taken at the ends, 1/8, 1/4, 3/8, and 1/2 spans over each girder for a maximum of 108 deflections per load. Frequently, only readings in the vicinity of the applied load were taken.

3.5 Loading

3.5.1 Gravity Loads. Prototype self-weight (dead load) stresses are difficult to reproduce in a model, since available model materials do not meet the density similitude requirements (model density = S_g x prototype density). With quasi-static loadings this was overcome by the application of compensating external uniform loads equal to $(S_g - 1)$ times the model weight (179 psf for these models).¹⁶ Closely spaced dead weights hung below the structure were used to simulate the basic moment envelope due to gravity load.

3.5.2 Live Loads. Live loading consisted of single wheel loads, axle loads, single truck loads, double truck loads, triple truck loads, a special overload vehicle, and ultimate loads. A versatile loading system was designed, as shown in Fig. 3.5 Using this system loads could be placed at any coordinate on the test slab. The two additional spans shown in Fig. 3.5 were used to simulate the boundary conditions of a typical interior span by balancing the dead load moment on the bent cap.

Truck loads were modeled from the AASHO design vehicles.² The relation between the full size H20-S16 truck and the model truck (with a scale factor of $S_g = 5.5$) is illustrated in Fig. 3.6. The dimensions of the loading pads (or "wheels") were determined by using an allowable tire pressure of 80 psi, the total load on the wheel, and a tire width based on the 1965 AASHO specifications.² A special vehicle, referred to as the overload truck, was used to apply moderate overloads. The prototype and model overload truck configuration is shown in Fig. 3.7. This truck was designated by the Texas Highway Department as the most severe vehicle which might be allowed on the bridge tested. A special permit is required to allow passage of this truck over the bridges tested. The vehicle is described in Ref. 44. Whenever multiple trucks were applied to the model bridge, all trucks were assumed to be heading in the same direction.

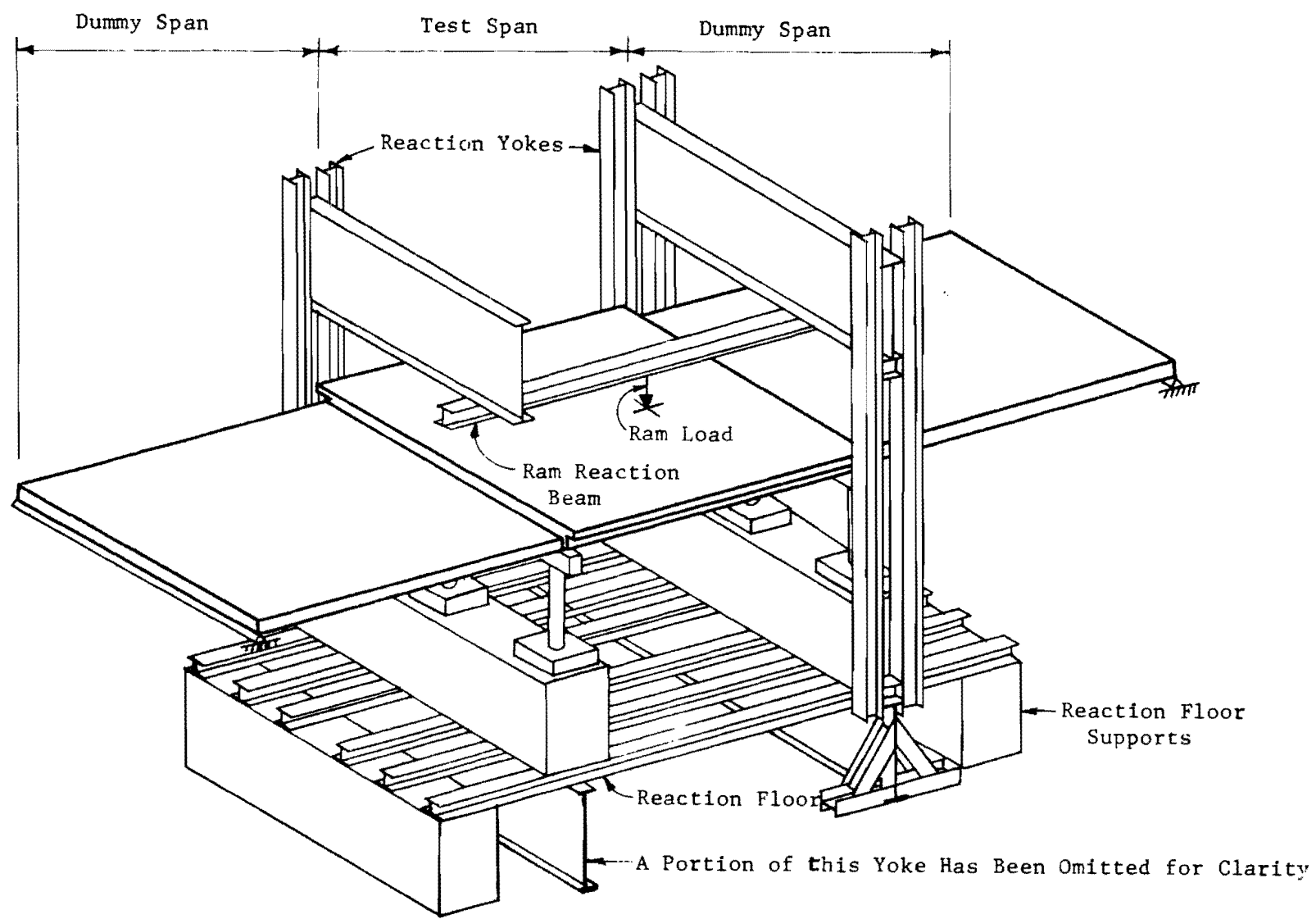
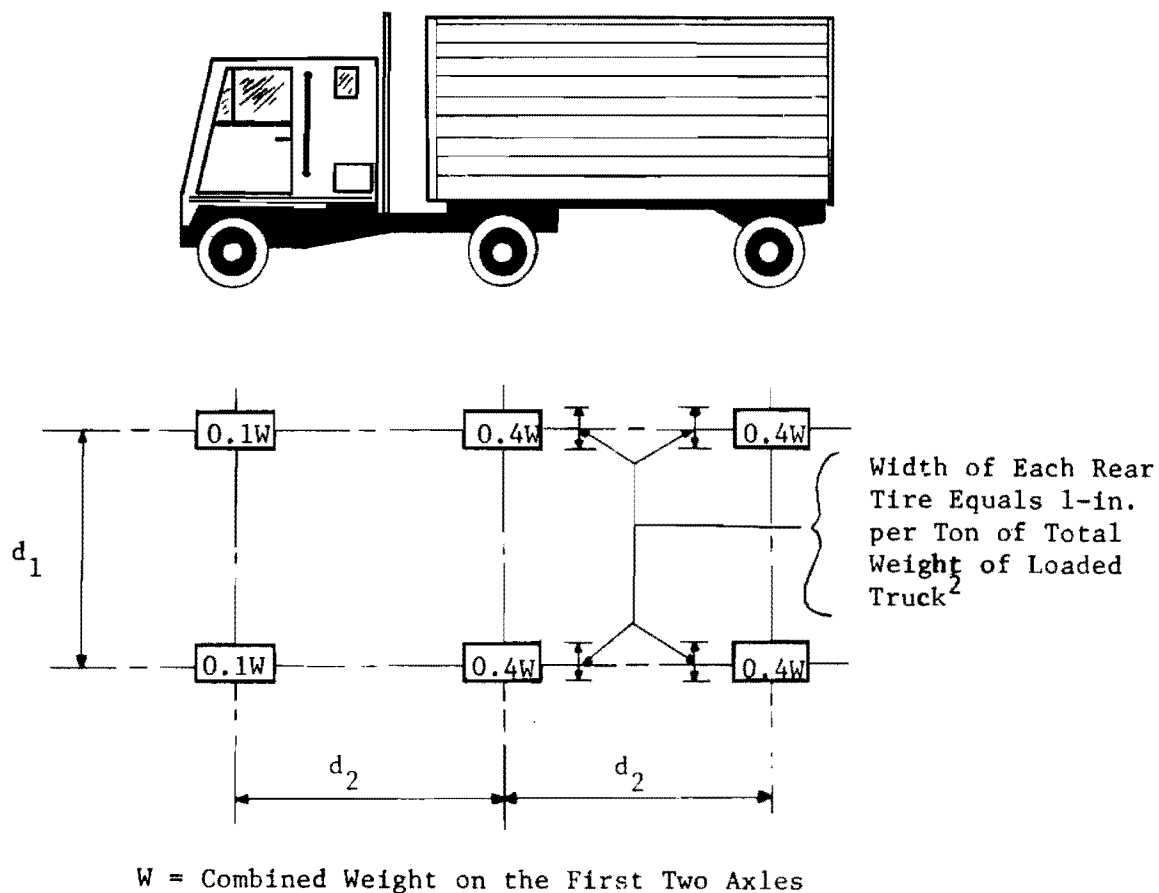
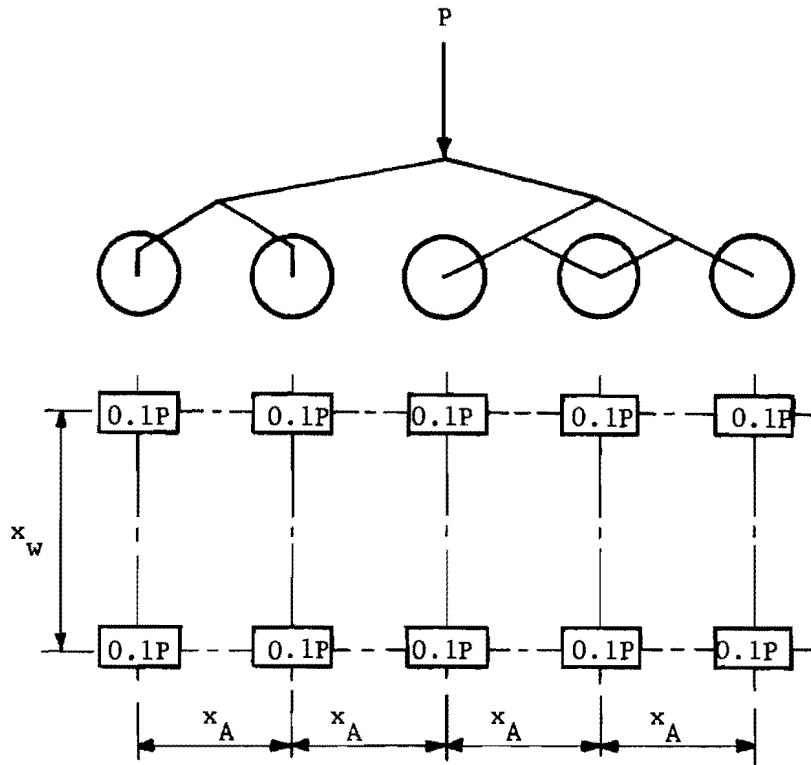


Fig. 3.5. Live Load System.



Item	Full Size Truck	Model Truck
Truck Type	H20-S16	H20-S16
W , lbs.	40,000	1,322.5
d_1 , ft.	6.0	1.091
d_2 , ft.	14.0	2.546

Fig. 3.6. Relation between Full Size and Model AASHO H20-S16 Truck.



P = Total Weight on Truck

Item	Full Size Truck	Model Truck
P , lbs.	81,400	2,690
x_w , ft.	6.0	1.091
x_A , ft.	4.0	0.727

Fig. 3.7. Relation between Full-Size and Model Overload Truck.

C H A P T E R I V

MODEL RELIABILITY

4.1 Introduction

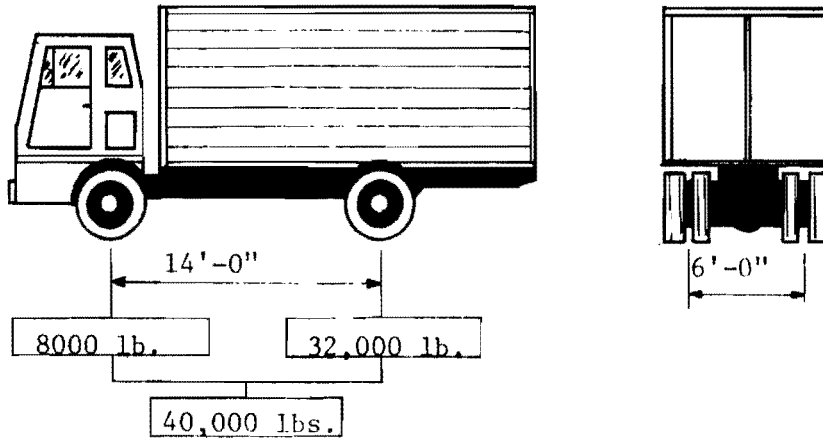
The main objective in the utilization of the direct structural model in this study was to establish the behavioral characteristics of the prototype structure over a wide range of loadings. In order to validate this technique for this type of structure, several studies were run to illustrate the credibility and reliability of the techniques utilized and reported in detail in Refs. 15 and 16 .

4.2 Comparison at Service Load Levels

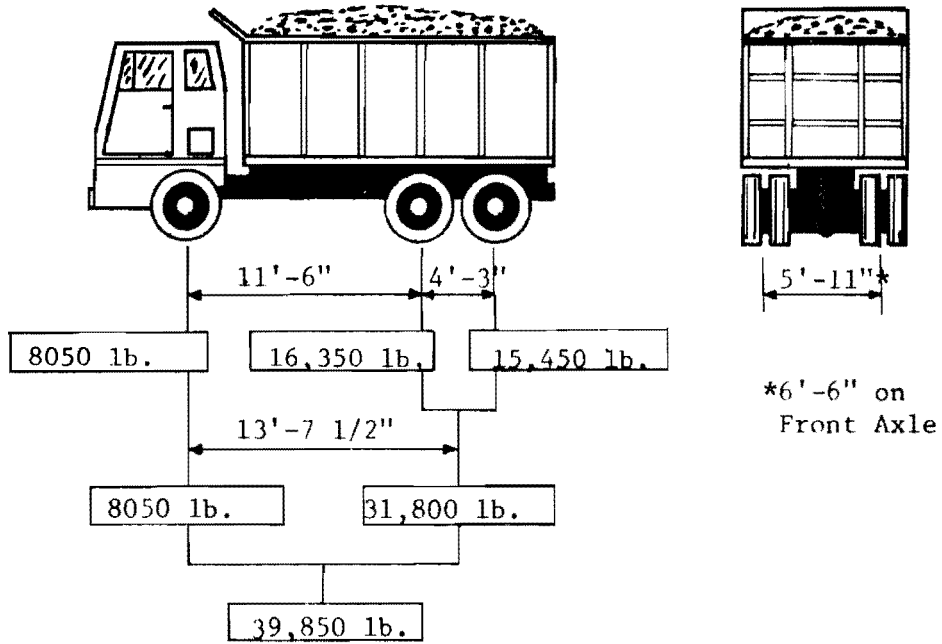
To assess the general relationship between response characteristics of the model and prototype at service load levels, a prototype bridge (CG-1) was instrumented and load-tested at service load levels. A corresponding model (SG-4) was constructed and loaded in the same fashion in the laboratory.

Loading consisted of single, double, and triple truck loads placed on the bridges. The prototype test vehicles were trucks loaded with sand until their total weight was equal to that of the standard AASHO H20 design truck. A slight difference between the design vehicle configuration and those actually used in both prototype and model tests was the distribution of the rear axle load, as shown in Fig. 4.1. The H20 design vehicle assumes a single rear axle, while the actual vehicle had two closely spaced rear axles.

A representative sample of typical midspan strain measurements is presented in Fig. 4.2. The lower plot shows the actual strains observed. The upper plot shows the strain distribution as a percent of the total midspan strain observed. Because of the relatively low magnitude of the strains, the latter is probably the better measure of the pattern of load distribution.



(a) AASHO H20 Design Vehicle.



(b) Typical Test Vehicle.

Fig. 4.1. Comparison of AASHO H20 Design Vehicle and Test Vehicle.

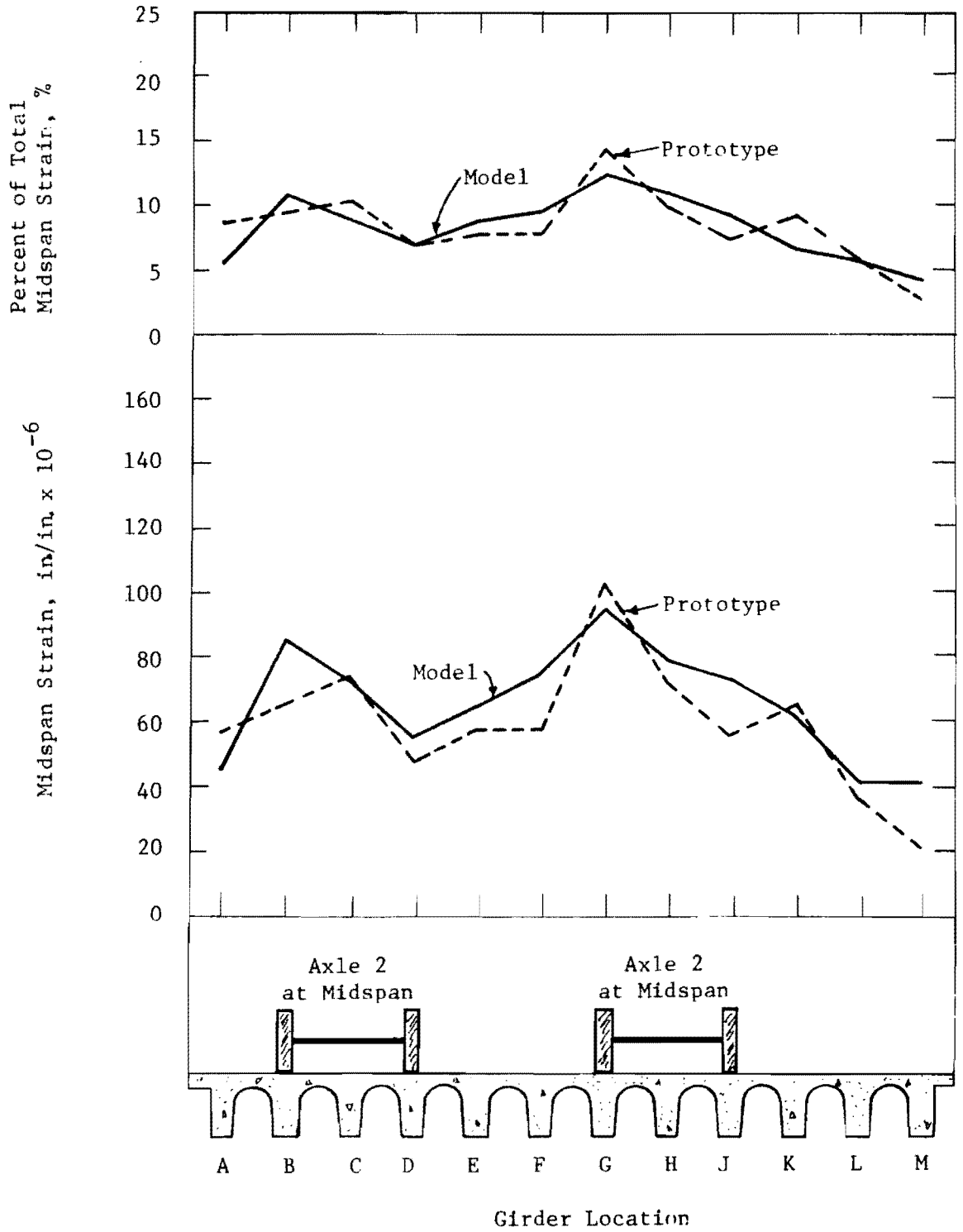


Fig. 4.2. Strain Data for Two Trucks Spaced Apart.

Midspan strain data have been plotted for twelve widely differing load cases in Fig. 4.3. Each datum point indicates the model and prototype strains for corresponding locations and loadings. Ideally, these should fall along the dashed 45° line. The regression equations shown were obtained as least squares curve fits. The equations and data show less than a perfect correlation between the two structures. The coefficient of linear correlation⁴² for the data shown is 0.90 and indicates relatively good linear correlation.

Overall examination of the results indicated that the model technique gave a very reasonable indication of the service load level participation of each girder and can be used to determine overall load participation in this type of a bridge system.¹⁶

4.3 Ultimate Strength Reliability

Since an ultimate load test of the prototype was not feasible, the accuracy of the model technique at ultimate load levels was established by testing statically determinate models of a reduced section of the bridge and then comparing the test results to accepted ultimate strength theory.

Two statically determinate models of reduced sections of the bridge, each consisting of two scaled girders, were tested to failure. Loading consisted of uniformly distributed blocks for dead load compensation, plus two equal concentrated loads at midspan.

Both specimens failed by first indicating yielding of the main flexural reinforcement, with concrete crushing after extensive deflection. Computed ultimate moments, based on conventional ultimate strength theory, indicated ratios of test to calculated ultimate moment of 0.998 and 0.985. The excellent agreement in these two tests established confidence in the loading system, instrumentation, and modeling techniques.¹⁶

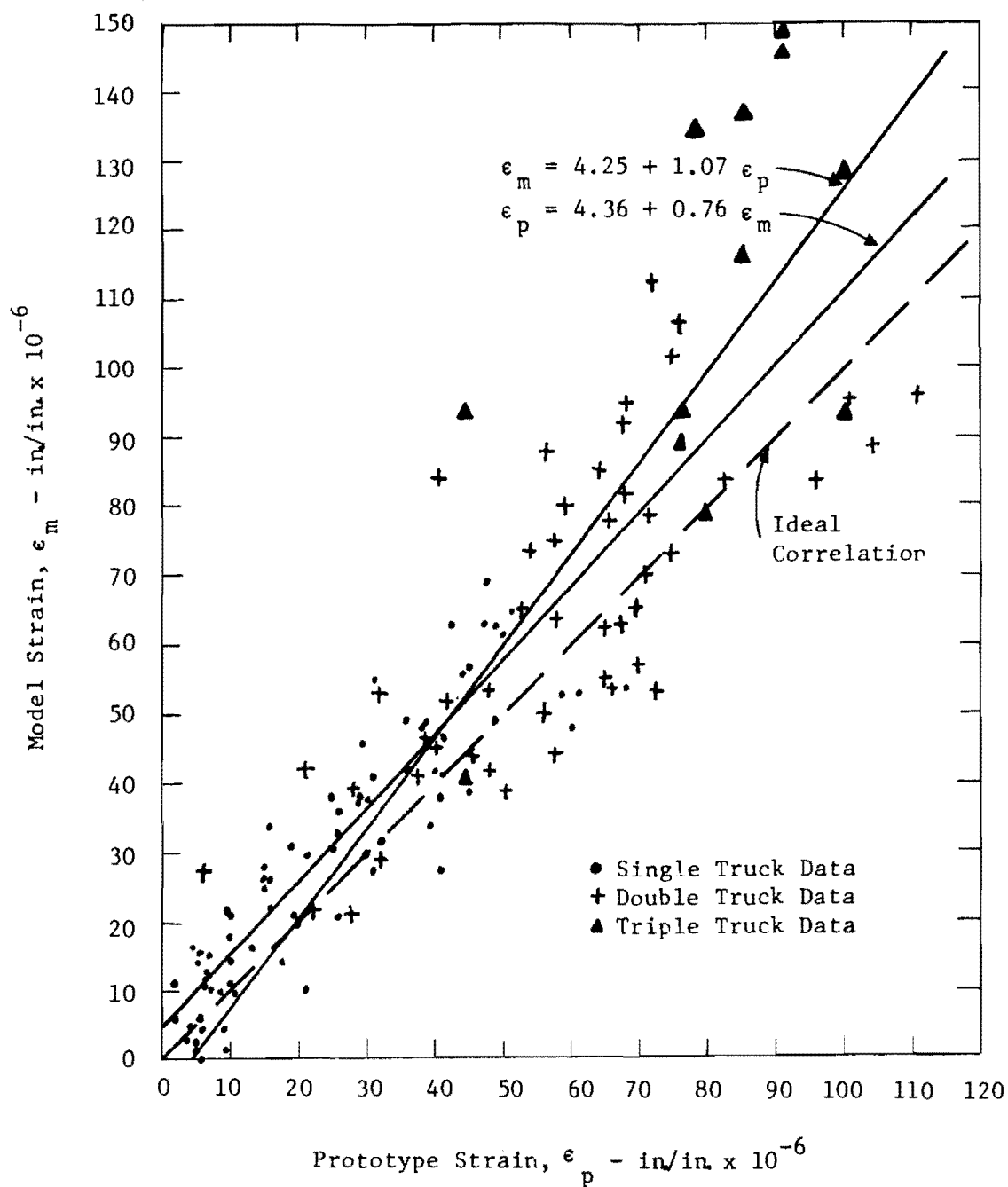


Fig. 4.3. Summary of Model and Prototype Data with Regression Analysis.

This page replaces an intentionally blank page in the original.

-- CTR Library Digitization Team

C H A P T E R V

MATHEMATICAL ANALYSIS

5.1 Introduction

Although not originally in the scope of this investigation, an analytic study under a parallel project was crosschecked with these test results. A brief introduction to the procedure utilized is presented in this chapter and some typical result curves are shown in subsequent chapters, since they greatly improve the overall application of the results. Complete descriptions of the procedures used will be presented in reports on Project 3-5-68-115 entitled "Experimental Verification of Computer Simulation for Slab and Girder Bridge Systems."

In view of the successful application of orthotropic plate theory to the analysis of slab and girder bridges,^{21,40} this concept was selected for the analytical approach. However, the Guyon-Massonnet procedures represent the longitudinal and transverse cross sections with a single parameter for each direction. While valid for constant thickness elastic slabs, it was not considered realistic to use a single stiffness value to describe the transverse arch system of the bridges tested. However, it was possible to use a discrete element mathematical model permitting point-to-point variation of longitudinal and transverse stiffnesses with a final solution based on the orthotropic plate equations for solutions to compare with the right angle bridge.

5.2 Discrete Element Mathematical Model

Hudson and Matlock^{10,11} developed a computer program for the solution of orthotropic plates using a discrete element physical model. The original program has been improved by Stelzer and Hudson⁴³ and Panak and Matlock³¹

but the original discrete element model has remained the same. This model represents the stiffness, geometry, and support conditions of the actual slab as shown in Fig. 5.1.

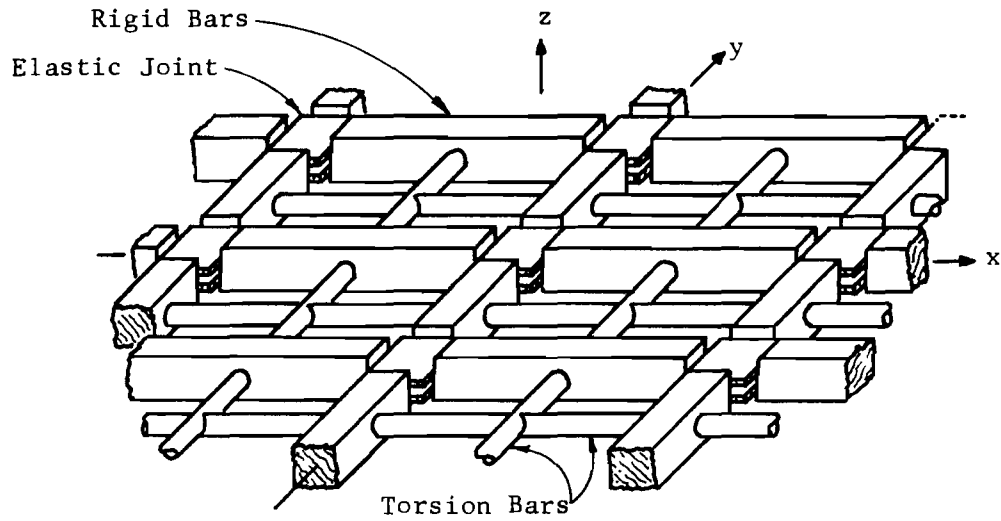
The discrete element model is solved by writing the equilibrium equations for each joint. The deflection at each joint is the unknown in the equilibrium equations which are applied at each joint. The procedure used for the solution of this system of equations is an implicit alternating-direction iterative process which is described in detail by Matlock,¹⁹ Stelzer,⁴³ and Hudson.¹¹ The computer program used is DSLAB 30 described by Panak and Matlock.³¹

5.4 Section Properties

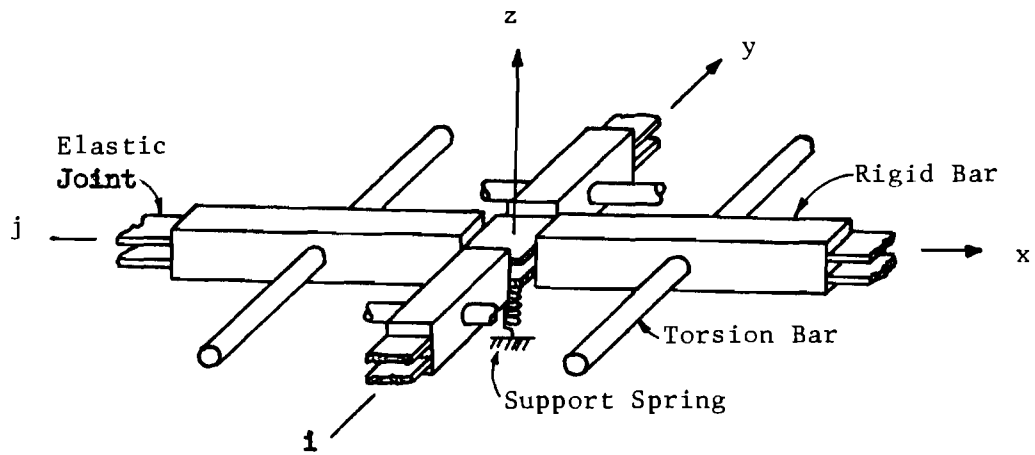
The Guyon-Massonnet procedure uses a single stiffness value in each direction to describe the equivalent slab system. In contrast, in the discrete element method the equilibrium equations are applied at each joint and each may have its own unique section properties. Thus, an irregular slab and girder bridge may be closely approximated by using a very fine grid system with varying stiffnesses.

The pan-formed concrete slab and girder bridge cross section was divided into fifty increments. The flexural and torsional stiffnesses used were varied in different runs of the program to check the effect of variation of stiffness of the structures. One series of data was based on the gross section properties, another series of data run was based on the gross-transformed section properties, and a final series of data runs was made using the crack section properties. In general it was found that the results using the gross section and the gross-transformed section properties agreed fairly well with the experimental data for service load levels, while the results of the cracked section properties were much closer to test results measured under high overloads and near ultimate loads. Details of these computations will be included in a forthcoming report on "Experimental Verification of Computer Simulation for Slab and Girder Bridge Systems."

Initial attempts to mathematically model the skew bridge structures utilizing the same program were unsuccessful. However, it appears that



(a) Discrete Element Model of a Plate or Slab.



(b) Typical Joint i, j Taken from Discrete Element Slab Model.

Fig. 5.1. Discrete Element Model. ^{10,11}

the major portion of the difficulty encountered was due to the use of an incorrect technique for inputting boundary conditions and it is anticipated that analytical comparisons with the skew model results will be available in the reports on Project 3-5-68-115.

CHAPTER VI

EXPERIMENTAL STUDY

6.1 Introduction

The procedures used in selecting materials and constructing the models of this investigation as well as scaling procedures have been described in Chapter III. Instrumentation and loading were described in general in the same chapter.

This chapter describes in detail specific dimensions and material properties of the test bridges. In addition, detailed instrumentation and loading are discussed.

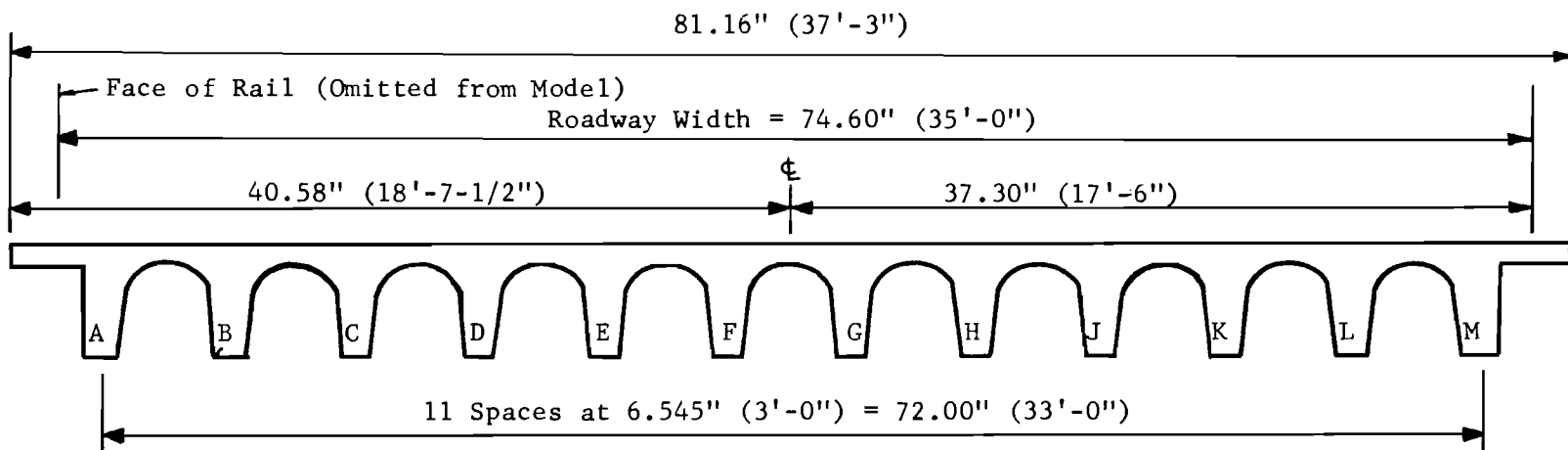
6.2 Section Details

6.2.1 Dimensions. Gross cross section dimensions are shown in Fig. 6.1. Concrete dimensions for SG-1, SG-2, and SG-3 (identical in cross section except for reinforcement) are shown in Fig. 6.1a. Dimensions for SG-4 are shown in Fig. 6.1b. The two basic cross sections differ only in the edge detail, with the slab overhang being 1'-0" shorter on the prototype for SG-4.

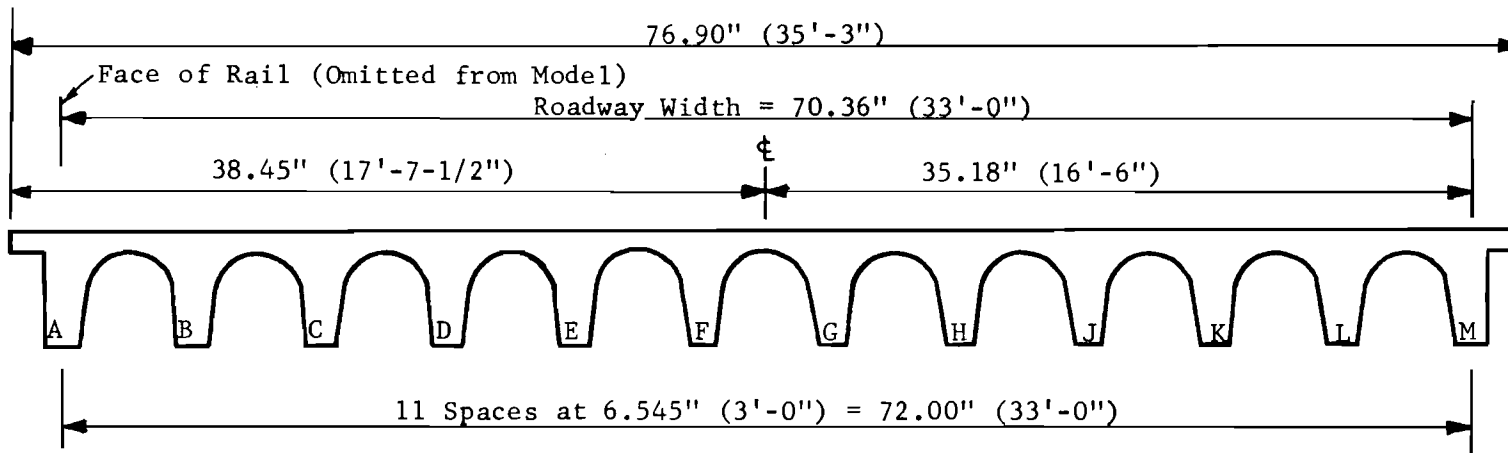
6.2.2 Reinforcement. Cross section reinforcement details are shown in Fig. 6.2 for the exterior girder and first interior girder (which are typical). The main longitudinal flexural reinforcement, which varies for each model, is provided by bars E, F, and Z. These bar sizes are shown in Table 6.1. Reinforcement properties are given in Table 6.2. Typical stress-strain curves are shown in Fig. 3.2.

TABLE 6.1 MODEL LONGITUDINAL TENSION REINFORCEMENT
(Prototype Values in Parenthesis)

Bridge	Bar E	Bar F	Bar Z
SG-1	No. 2 Smooth (No. 11)	No. 2 Smooth (No. 11)	None
SG-2	No. 2 Smooth (No. 11)	No. 2 Smooth (No. 11)	SWG 11 (No. 5)
SG-3	No. 2 Deformed (No. 11)	No. 2 Deformed (No. 11)	None
SG-4	No. 2 Deformed (No. 11)	SWG 4 (No. 10)	None



(a) Cross Section for SG-1, SG-2, and SG-3.



(b) Cross Section for SG-4.

Fig. 6.1. Bridge Model Cross Sections. (Prototype Dimensions in Parentheses.)

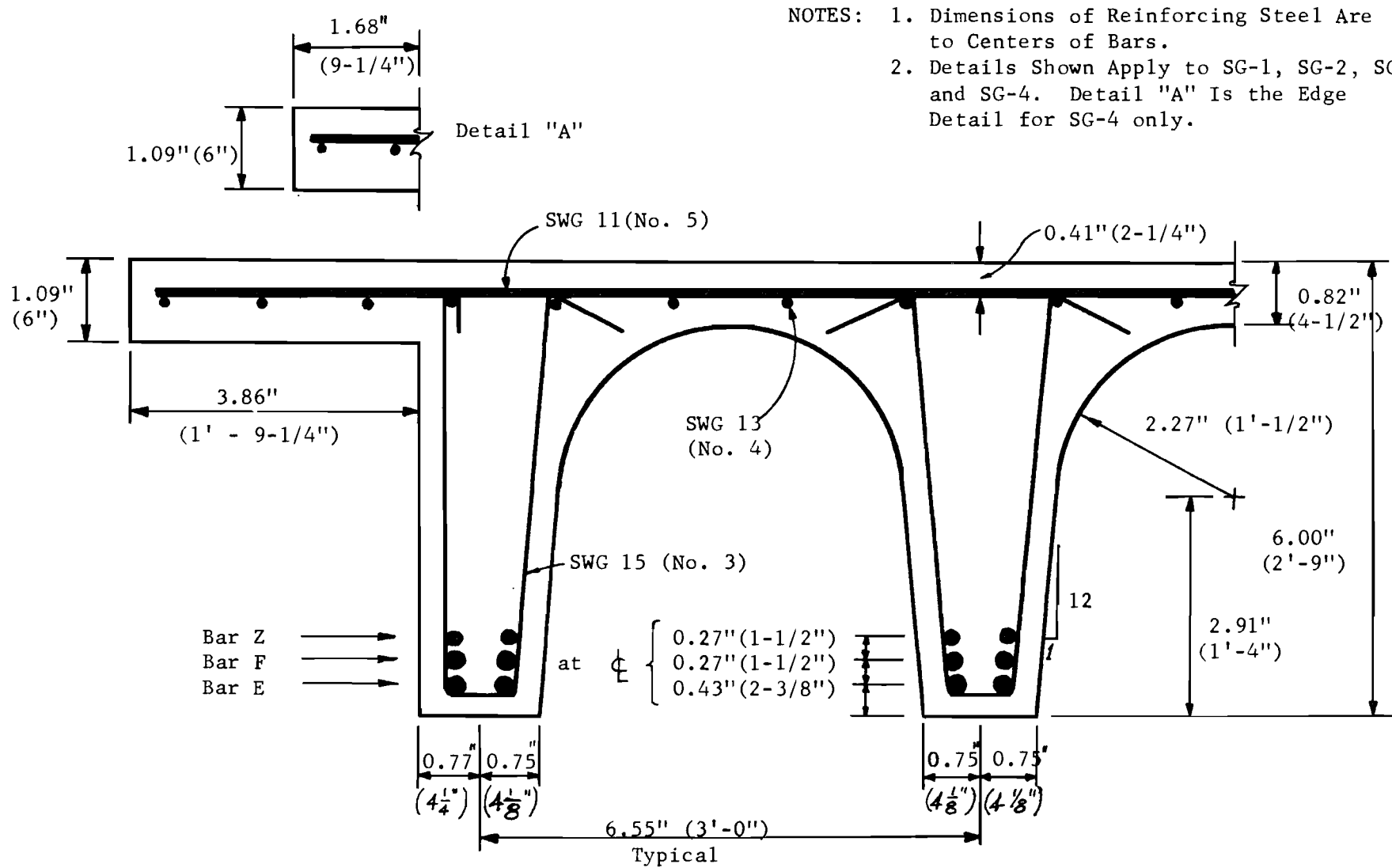


Fig. 6.2. Cross Section Reinforcement Details. (Prototype Values in Parentheses.)

TABLE 6.2 REINFORCEMENT PROPERTIES

(a) Reinforcement Common to All Bridges					
Prototype Reinforcement	Bar Size	D, in.	A_s , in. ²	f_y , ksi	f_u , ksi
No. 9	SWG 5	0.2056	0.0332	40.2	48.0
No. 8	SWG 6	0.1898	0.0283	31.8	45.7
No. 7	SWG 8	0.1609	0.0203	36.0	47.8
No. 6	SWG 10	0.1352	0.0144	44.5	52.9
No. 5	SWG 11	0.1194	0.0112	38.2	48.0
No. 4	SWG 13	0.0905	0.00642	35.8	47.1
No. 3	SWG 15	0.0722	0.00408	30.9	42.0
No. 2	SWG 18	0.0461	0.00167	31.3	45.6
(b) Special Reinforcement					
SG-1					
No. 11	No. 2, Smooth	0.2471	0.0480	46.6	64.5
SG-2					
No. 11	No. 2, Smooth	0.2477	0.0482	44.9	63.5
SG-3					
No. 11	No. 2, Deformed	0.250	0.0491	57.3	76.5
SG-4					
No. 11	No. 2, Deformed	0.250	0.0491	57.3	76.5
No. 10	SWG 4	0.2255	0.0400	35.9	40.7

6.2.3 Microconcrete. The results of compression tests and split cylinder tests based on 3-in. diameter cylinders are shown in Table 6.3. Although unintentional, the compressive strengths varied from 3770 psi to 4750 psi.

TABLE 6.3 MICROCONCRETE PROPERTIES

Bridge	f'_c , psi	f'_t , psi
SG-1	3770	450
SG-2	4040	-
SG-3	4320	530
SG-4	4750	550

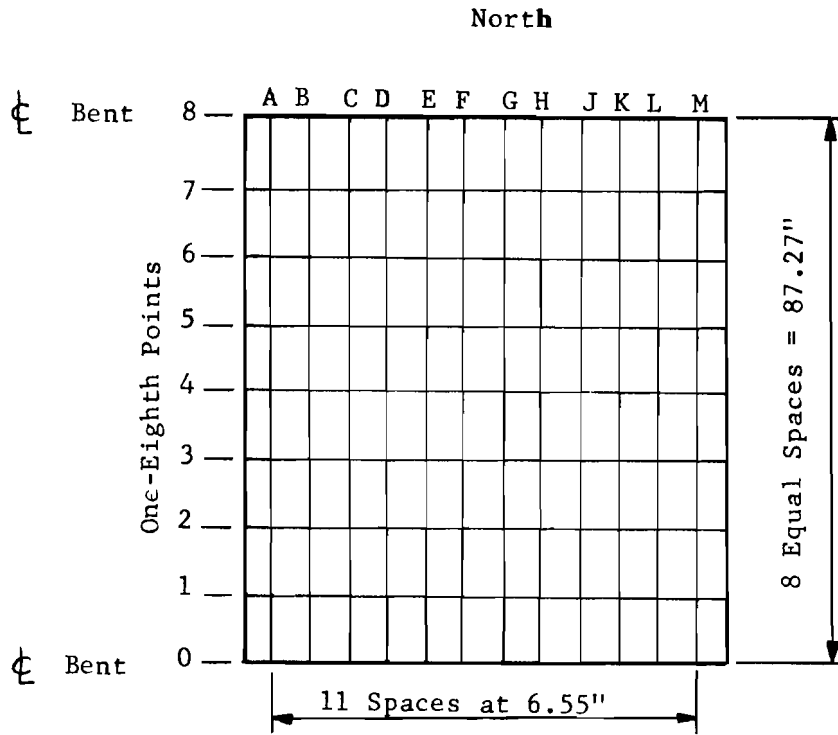
6.3 Instrumentation

6.3.1 Grid System. The model slab surfaces were divided into grid systems for controlling load locations. Each girder was identified by an alphabetical letter A through M (omitting the letter I). In the span direction the bridge was divided into 1/8 points. The grid systems for SG-1, SG-2 and SG-3, and SG-4 are shown in Figs. 6.3, 6.4, and 6.5, respectively.

6.3.2 Deflections. A portable dial system was used to measure deflections. Nine dial gages were mounted on a portable 2 in. x 2 in. aluminum box tubing ten feet long, which spanned between steel reference frames installed over each bent cap and supported independently of the test specimens. A system of guides was used to position the tubing above the centerline of each girder as desired, with deflection errors of less than 0.0005 in. Sheet metal pads glued to the deck at all dial gage points provided a smooth surface for the gage tips.

Since it was sometimes necessary to place loads over the supports, dial gages could not be placed exactly on support centerlines. Support deflections were obtained by slightly offsetting dial gages. The effect of this offset is discussed in Sec. 6.6.2.

6.3.3 Strain Gages. Longitudinal strain was measured with 1/4-in. gage length foil strain gages, located on No. 2 bars as shown in Fig. 6.6. Transverse strain was measured with 1/8-in. gage length foil strain gages located on SWG 11 gage wire, also shown in Fig. 6.6.



Plan View of Grid



Section at Midspan

Fig. 6.3. SG-1 Grid System for Loading and Instrumentation.

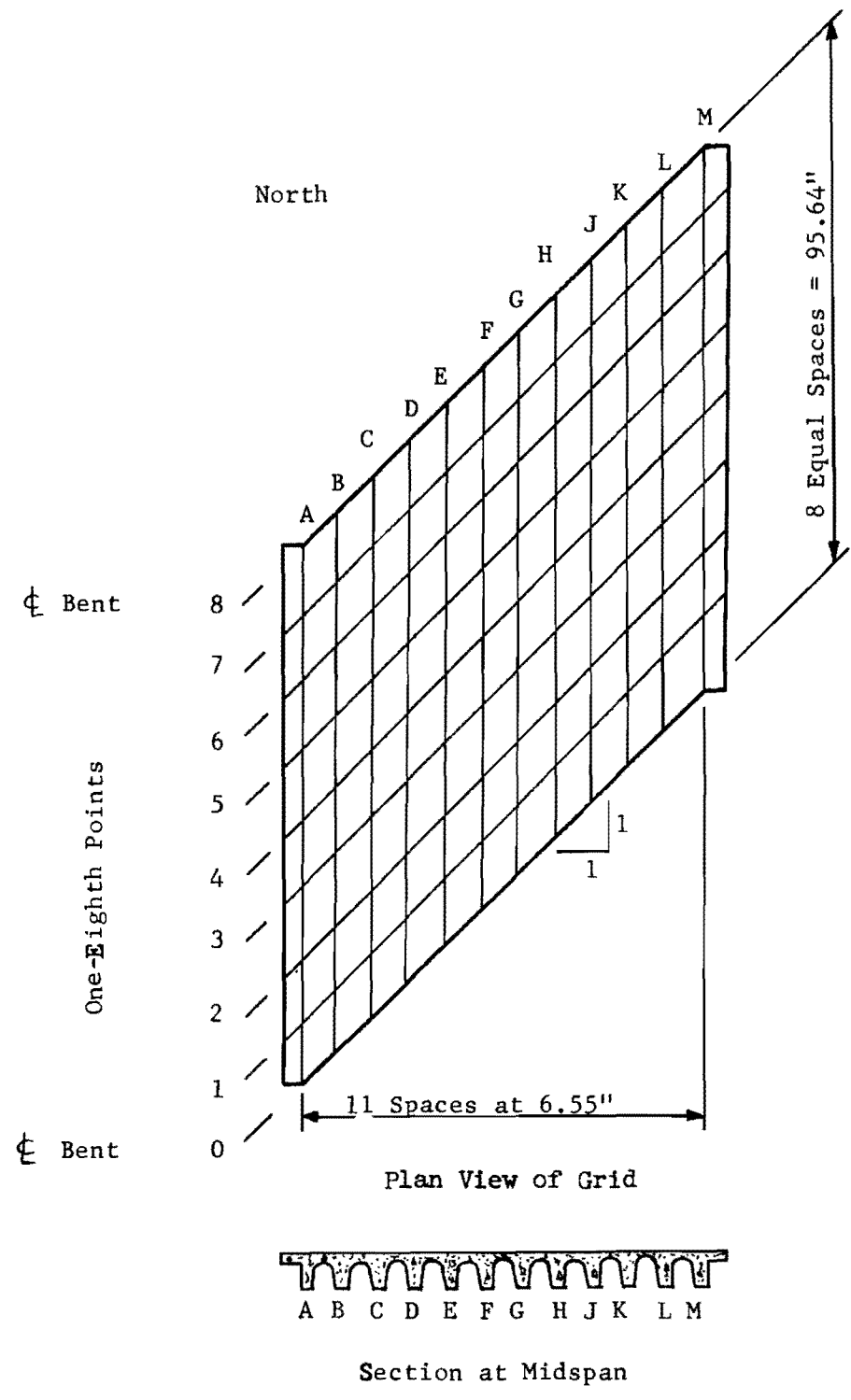
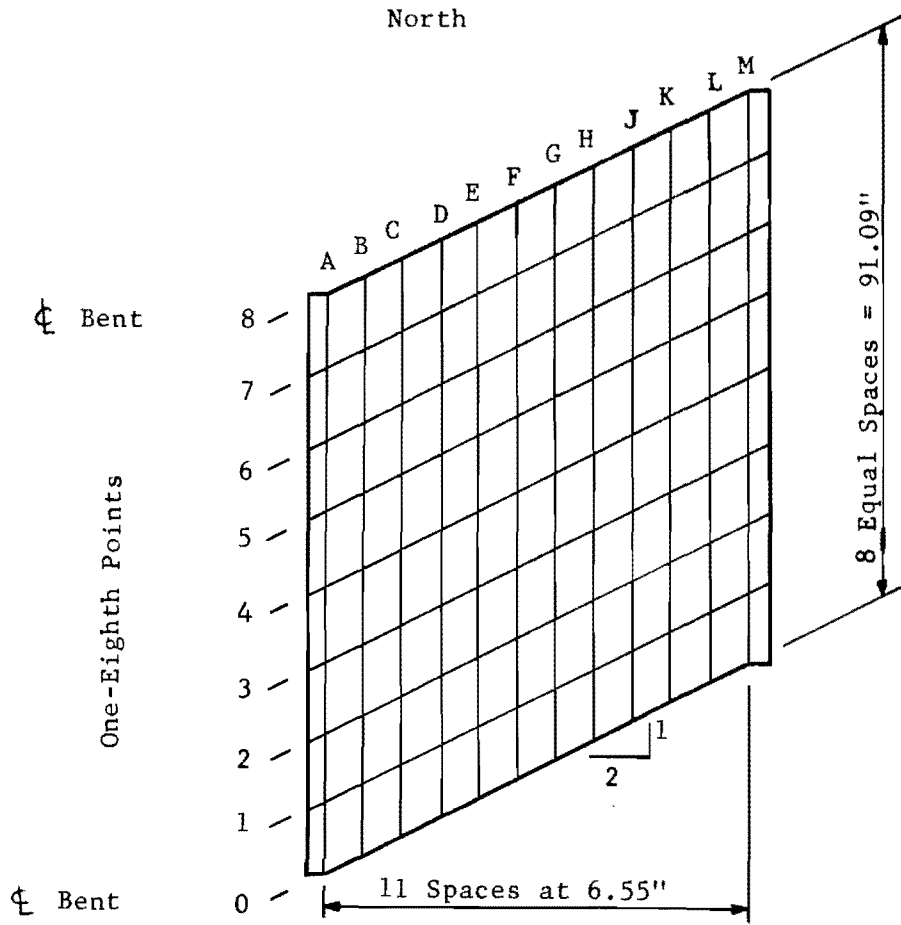


Fig. 6.4. SG-2 and SG-3 Grid System for Loading and Instrumentation.



Plan View of Grid



Section at Midspan

Fig. 6.5. SG-4 Grid System for Loading and Instrumentation.

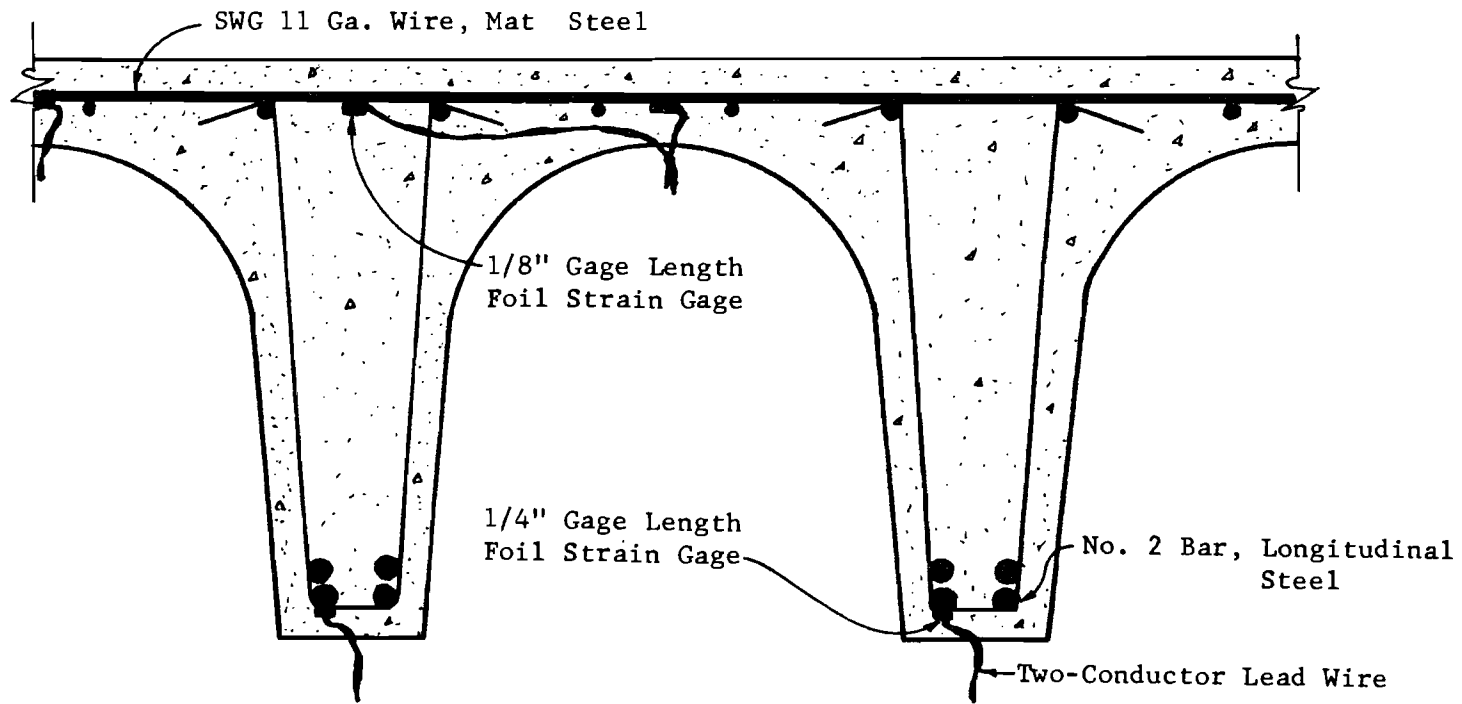


Fig. 6.6. Typical Strain Gage Locations.

Exact strain gage locations for bridges SG-1, SG-2, SG-3, and SG-4 are shown in Figs. 6.7, 6.8, 6.9, and 6.10, respectively. In these figures the longitudinal lines A through M locate the girder strain gages. The transverse lines are the mat bars on which transverse strain gages were installed.

6.4 Loading

All of the bridges tested had a similar loading history, which is summarized in Fig. 6.11 and described below.

(a) Dead Load Application. Supplementary dead load was applied to bring the model weight per square foot up to the same weight per square foot as the prototype structure. Adjacent dummy span loads were also applied at this time.

(b) Single Wheel Loads. Single wheel loads were scaled from the rear wheel of an AASHO H20-S16 truck. The wheel load and loading area are shown in Fig. 6.12a.

(c) Single Axle Loads. Single axle loads were scaled from the rear axle of an AASHO H20-S16 truck. The axle load and configuration are shown in Fig. 6.12b.

(d) Single Truck Loads. Single truck loads were scaled from an AASHO H20-S16 truck, which is the design vehicle for SG-1, SG-2, and SG-3. Truck axle loads and spacings are shown in Fig. 6.12c. In the case of SG-4 the design vehicle is an AASHO H20 truck; hence both H20 and H20-S16 loadings were applied to SG-4.

(e) Double Truck Loads. Double truck loads consisted of two scaled H20-S16 trucks; in addition, H20 truck loads were applied to SG-4.

(f) Triple Truck Loads. Triple truck loads consisted of three scaled H20-S16 trucks; in addition H20 truck loads were applied to SG-4.

(g) Overload Truck. The overload truck was a vehicle designated by the Texas Highway Department as the most severe loading allowed on the type of bridge tested. The axle loads and spacings are shown in Fig. 6.12d.

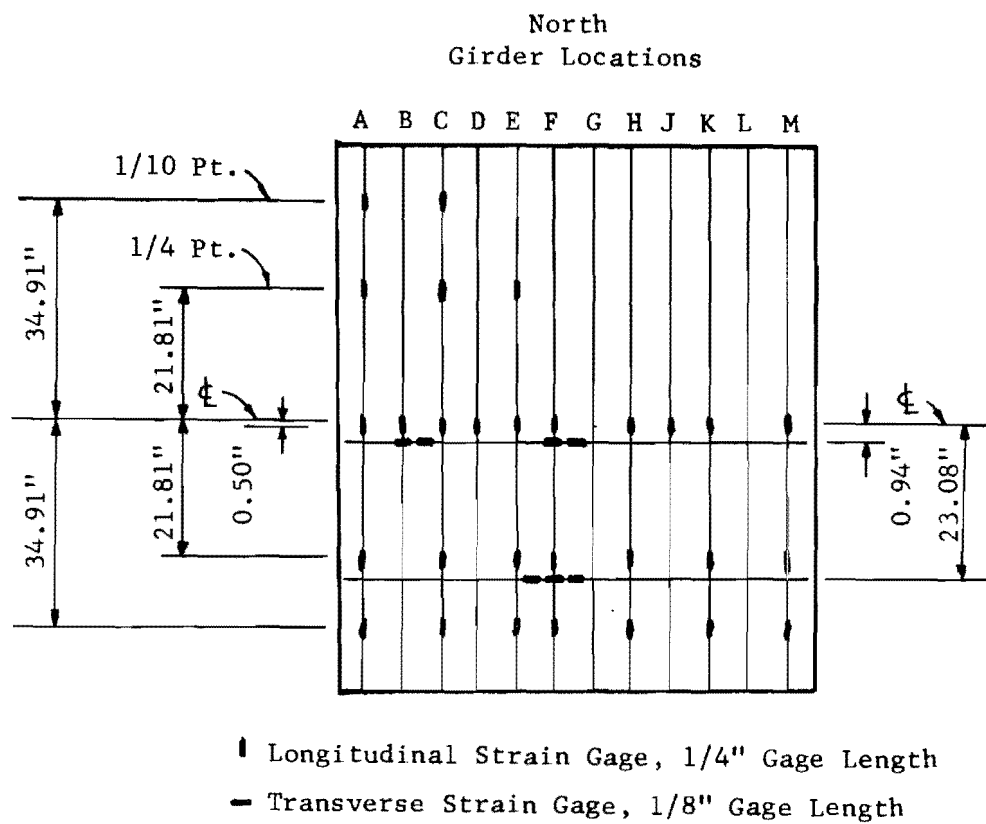


Fig. 6.7. SG-1 Strain Gage Locations.

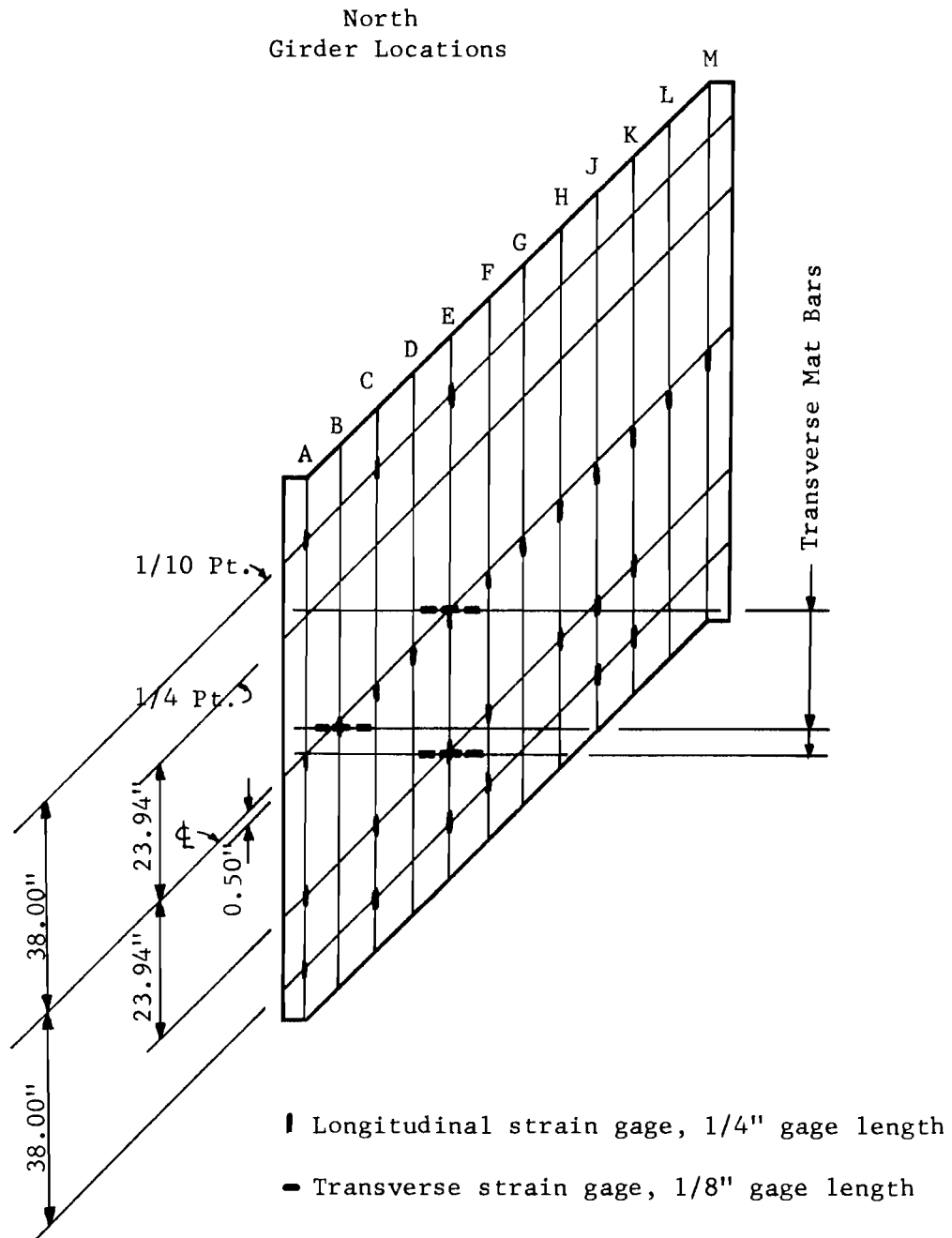


Fig. 6.8. SG-2 Strain Gage Locations.

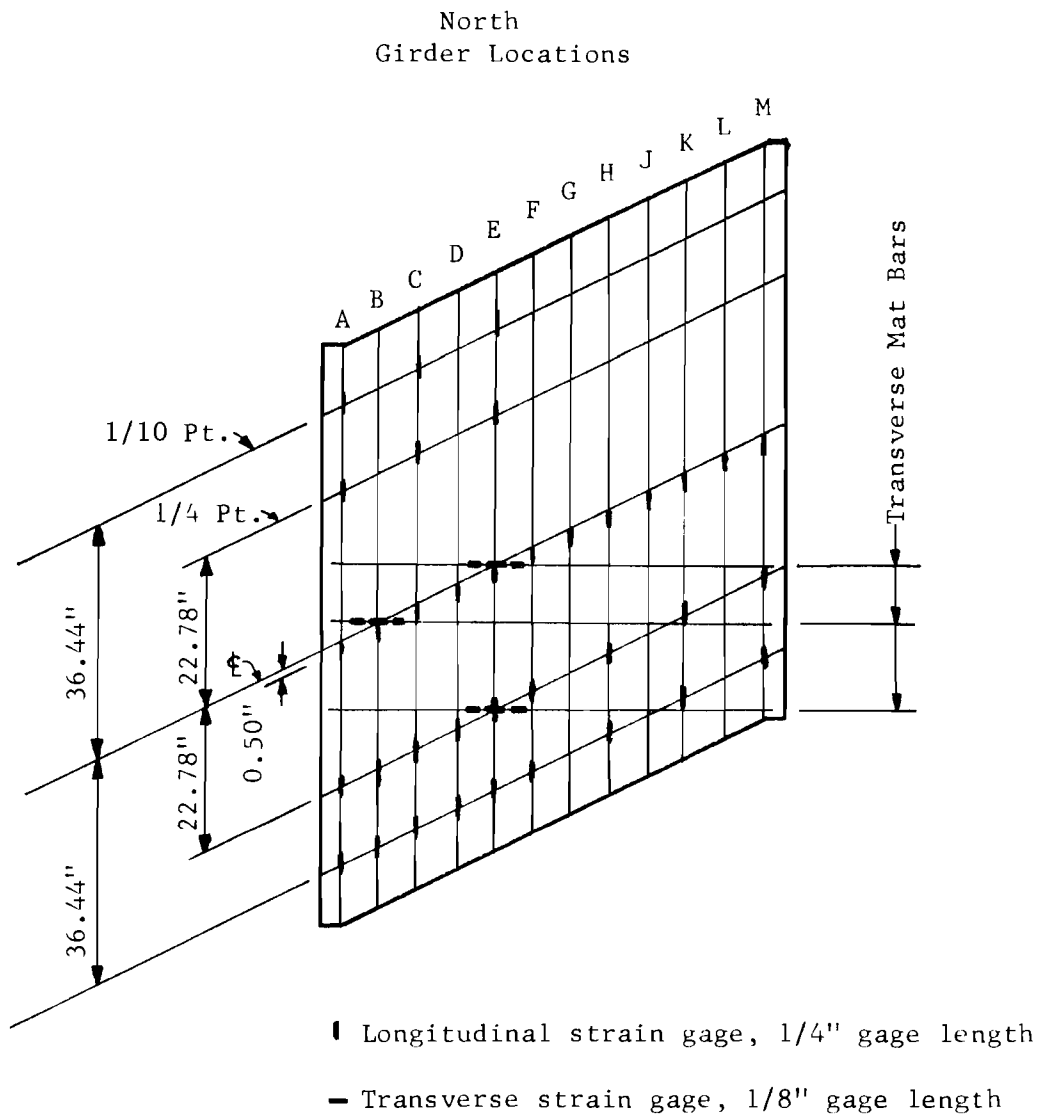


Fig. 6.10. SG-4 Strain Gage Locations.

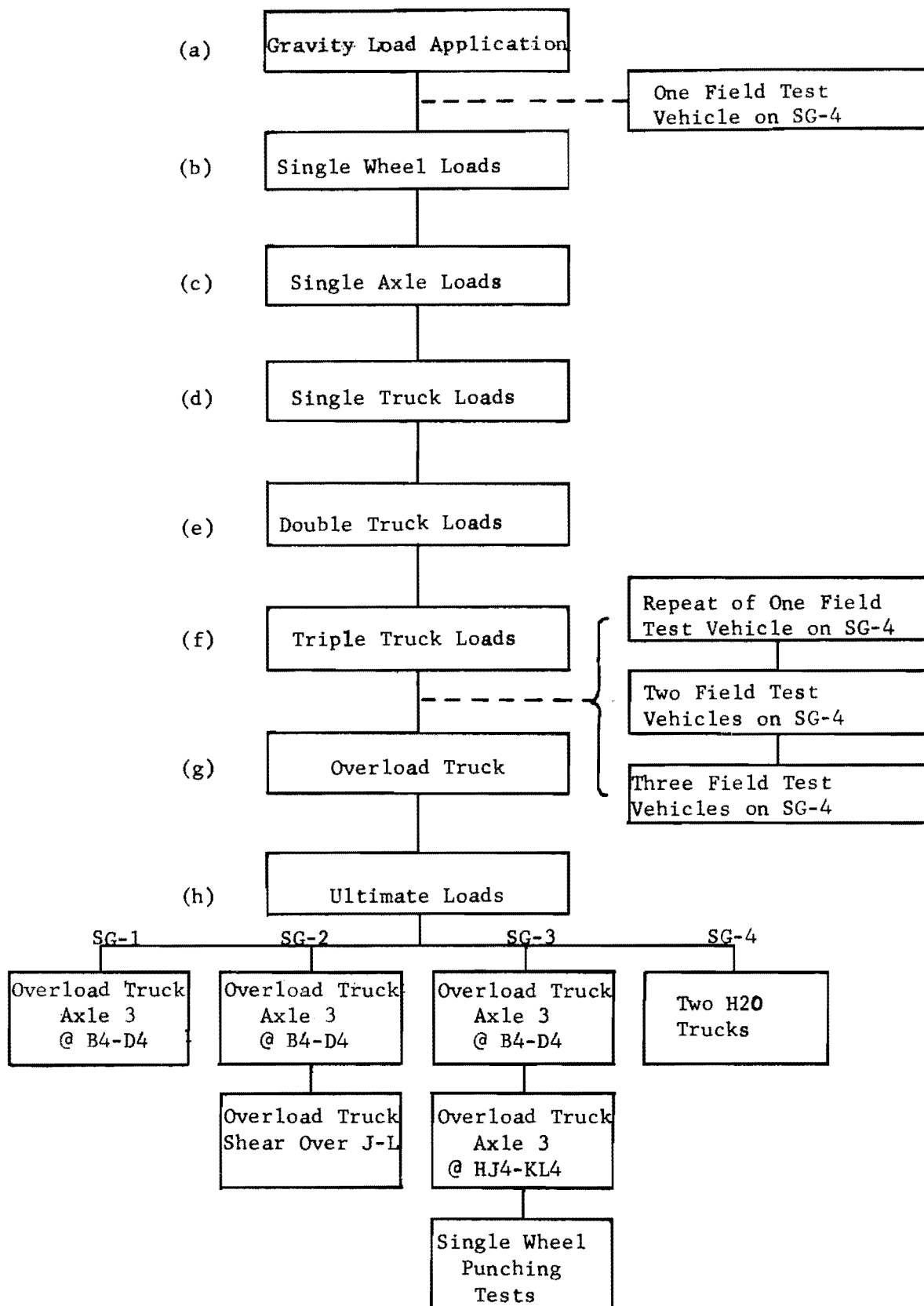
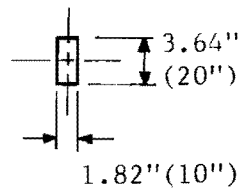


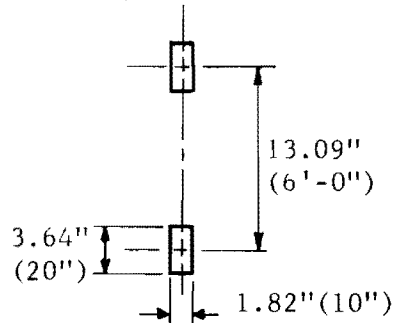
Fig. 6.11. Bridge Loading Histories.

Wheel Load
529 lb
(16,000 lb)

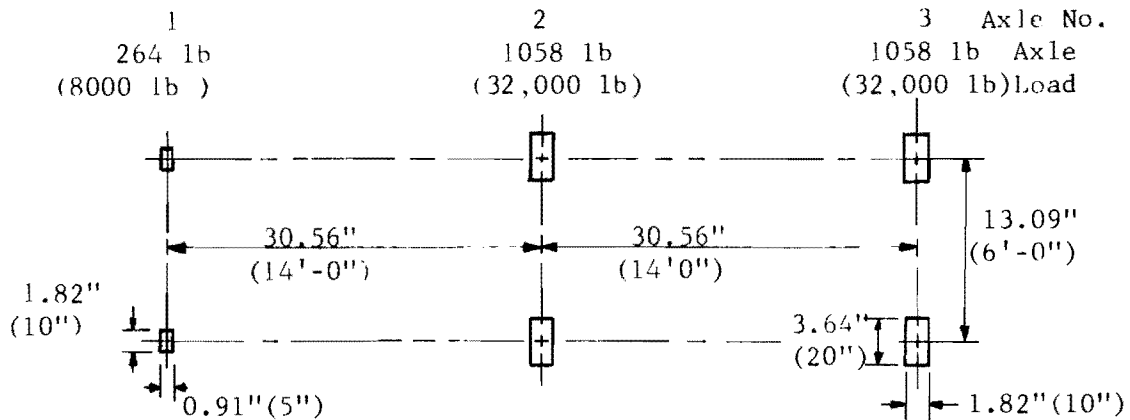


(a) Wheel Load.

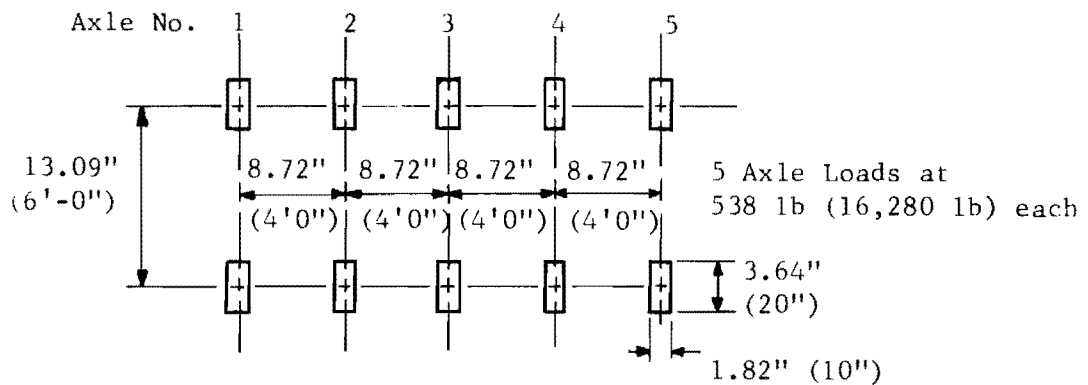
Axle Load
1058 lb
(32,000 lb)



(b) Axle Load.



(c) HS-20 Truck (Omit Axle 3 for H-20 Truck).



(d) Overload Truck.

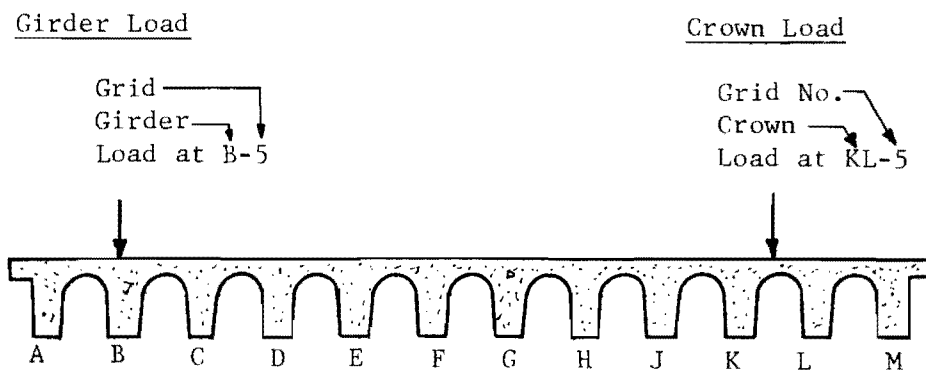
Fig. 6.12. Wheel, Axle, and Truck Loads.
(Prototype Values in Parentheses.)

(h) Ultimate Loads. Ultimate load tests varied for the different bridges tested, hence they will be discussed in the test results for the various bridges.

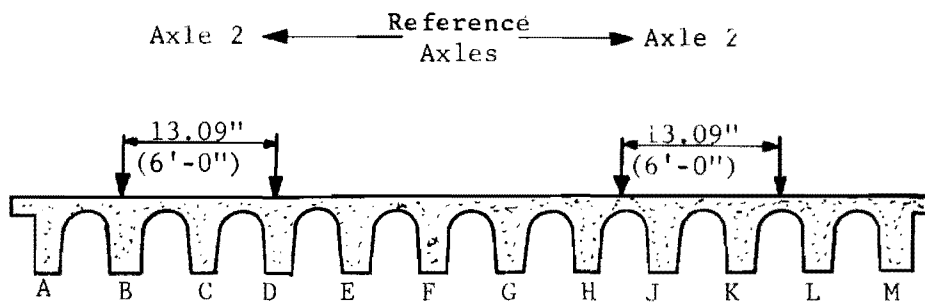
Load placement was referenced to the previously described grid systems (Sec. 6.3.1). Transverse load placement was referred to girders or crowns. Longitudinal placement was designated by the adjacent grid line (and a particular axle in the case of a truck). Transverse placement for wheel loads is shown in Fig. 6.13a. The wheel load at B-5 means the wheel is located over girder B at grid line 5 (this is 5/8 of the span from grid line 0). On the other hand, the designation KL-5 means the wheel is located on the crown midway between girders K and L on grid line 5. The orientation of the wheel pad with respect to the grid system is shown in Fig. 6.14. Note that in Fig. 6.14b the loading pad is oriented in the direction of traffic flow. Placement of trucks is similar to the designation for wheel loads. For example, referring to Fig. 6.13b, one truck is designated as Axle 2 at B3-D3. This means that Axle 2 of the truck loading (the middle axle in the case of an HS loading) is located with its wheels at grids B-2 and D-3. The other axles fall at their proper spacing from Axle 2 but still on grid lines B and D. It should be pointed out that the girder spacing is at 3'-0" centers (on the prototype), and thus, if one wheel of an axle falls over a girder, then the other wheel must be two girders away. Orientation of the reference axle is shown in Fig. 6.14 (only the reference axle is shown). Note that for the skew bridge in Fig. 6.14b the axle orientation is in the direction of traffic flow (as are the girders). In the case of skew the wheel designation is nominal. For instance the axle designated at B3-D3 actually has the centroid of load at C-3 with the axle oriented in the direction of traffic flow.

The exact number and location of loads placed on each bridge varied slightly but was approximately as follows:

(a) Single Wheel Loads (75 load positions)--Wheel loads were placed on each grid line for typical exterior and interior girders and crowns. In this manner bridge behavior could be studied as a wheel moved along a girder or crown.

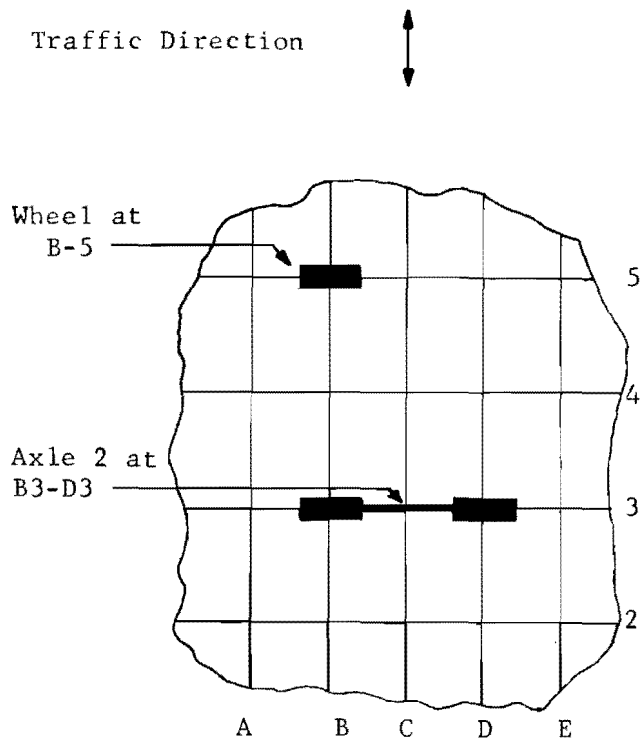


(a) Designation of Wheel Loads.

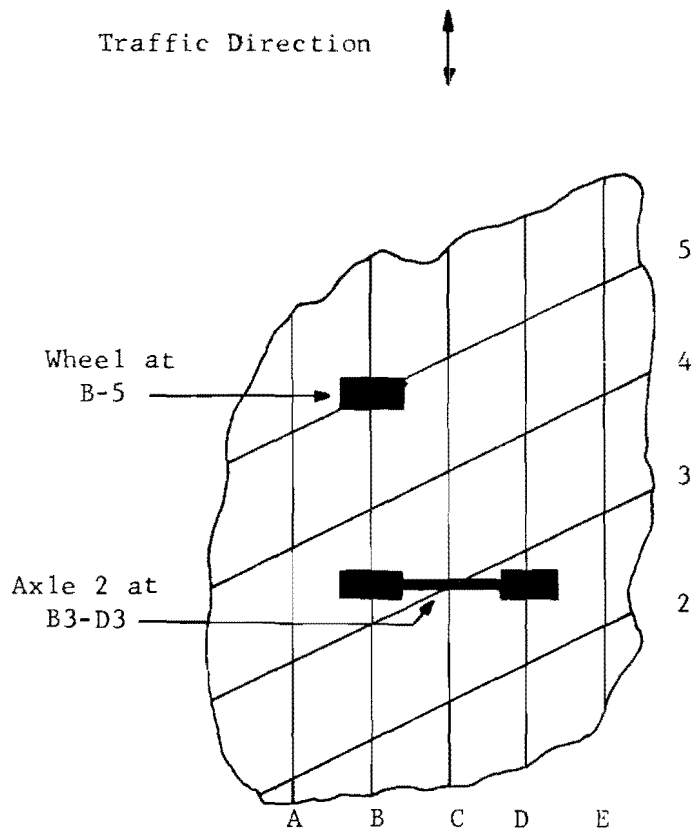


(b) Designation of Truck Loads.

Fig. 6.13. Designation of Wheel and Truck Loads Transversely.



(a) No Skew Bridge.



(b) Skew Bridge.

Fig. 6.14. Orientation of Wheels and Truck Loads Longitudinally.

(b) Single Axle Loads (25 load positions)--Single axles of the HS-20 truck were placed at the 1/8, 1/4, 3/8, and 1/2 points over girders and crowns near the edge and middle of the bridges studied.

(c) Single HS-20 Trucks (20 load positions)--Truck loads were concentrated at midspan with locations varying transversely. Some loads were placed at the 1/8, 1/4, and 3/8 points. In the case of SG-4 the H-20 design truck was placed on the bridge in addition to the HS-20 truck.

(d) Double HS-20 Trucks (4 load positions)--Trucks were positioned with Axle 2 at midspan and varied in location transversely. In the case of SG-4 the H-20 design trucks were also placed on the bridge in addition to the HS-20 trucks.

(e) Triple HS-20 Trucks (3 load positions)--Three trucks were spaced almost equally across the bridge width with Axle 2 at midspan. Data were taken for different directions of truck travel. In the case of SG-4 the H-20 design trucks were placed on the bridge in addition to the HS-20 trucks.

(f) Overload Truck (3 load positions)--The truck was positioned with Axle 3 at midspan and the location varied transversely near the edge and middle of the bridges.

(g) Ultimate Loads--The number of ultimate loads as well as the location and type of truck varied for each bridge. These are discussed in Chapter VII.

6.5 Test Procedure

The same test procedure was used for all models. Deflection dial and strain gage readings were taken before the addition of auxiliary dead load. Gage readings were taken at various intervals and upon completion of the supplementary dead load phase of loading. Thereafter, for each location of wheel, axle, and truck load gage readings were taken before and after the application of each load. In this manner zero drift due to temperature change was minimized for the live load readings.

Loadings were divided into three classes, as follows:

(a) Class 1 - Read all strain gages and dial gages.

(b) Class 2 - Read all strain gages and dial gages in the vicinity of the load.

(c) Class 3 - Read all strain gages only.

6.6 Data Reduction and Processing

6.6.1 General. All data were reduced on a CDC 6600 computer at The University of Texas at Austin Computation Center. Computer programs were written to reduce strain gage and deflection dial readings into true strains and deflections. Two values of output were obtained from the programs. Changes due to live load only and total absolute changes due to both live load and dead load were obtained. In computing both of these values, account was taken of instrument zero drift and zero drift due to temperature.

6.6.2 Deflections. In measuring deflections account was taken of support settlement by dial gages placed near but not on the centerline of the supports. This offset requires a theoretical correction to the measured deflections (corrected for support settlement). The procedure used is shown in Fig. 6.15 using the method of area moments. The case of uniform load is used as an example.

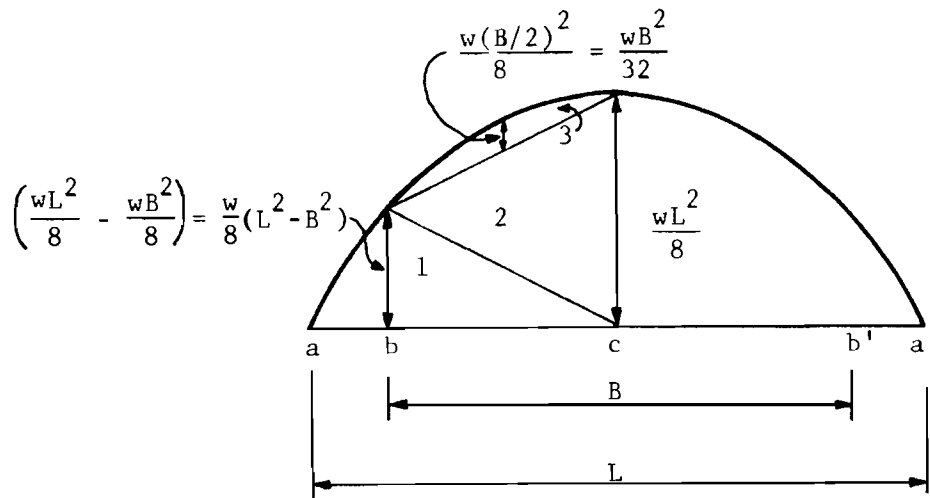
From symmetry, the elastic deflection curve is horizontal at midspan. A reference tangent through point c deflects but does not rotate. Hence, since a and a' do not deflect, the tangential deviation of a with respect to c, t_{ac} , may be used to find the deflection at c, y_c . Assuming constant EI

$$\begin{aligned} t_{ac} &= \frac{1}{EI} \text{ (Moment about a of M diagram from a to c)} \\ &= \frac{1}{EI} (5/8 \times L/2 \times 2/3 \times wL^2/8 \times L/2) \\ &= \frac{5}{384} \frac{wL^4}{EI} = \left(\frac{5w}{384 EI} \right) L^4 \end{aligned}$$

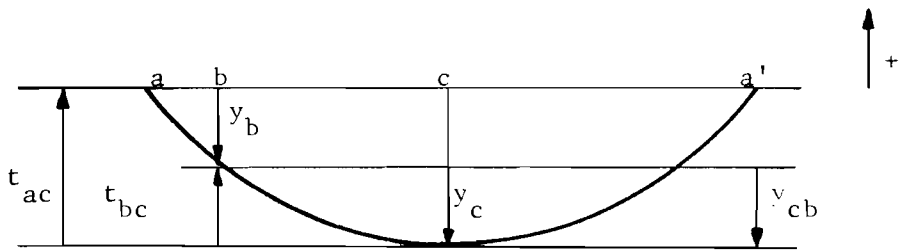
In the case illustrated point "a" lies the amount t_{ac} above the reference tangent, hence the tangent deflected downwards. Thus

$$y_c = - t_{ac}$$

Similarly t_{bc} may be computed assuming constant EI.



(a) Moment Diagram and Subdivisions for Area Moments.



Ref. tang. through c

(b) Deflection Curve Showing True Deflections and Tangential Deviations.

Not to Scale

Fig. 6.15. Theoretical Deflection Correction for the Case of Uniform Load.

$$t_{bc} = \frac{1}{EI} [1/3 \times B/2 \times 1/2 \times B/2 \times w/8(L^2 - B^2) + 2/3 \times B/2 \times 1/2 \times B/2 \times wL^2/8 + 1/2 \times B/2 \times 2/3 \times B/2 \times WB^2/32]$$

After reduction

$$t_{bc} = \left(\frac{5wL^4}{384 EI} \right) \left[\frac{6}{5} \left(\frac{B}{L} \right)^2 - \frac{1}{5} \left(\frac{B}{L} \right)^4 \right]$$

From Fig. 6.15b

$$y_b = y_c + t_{bc} = -t_{ac} + t_{bc}$$

The actual measured deflection, y_{cb} , is the deflection of point c with respect to b. Thus the true deflection y_c consists of two parts.

$$y_c = y_b + y_{cb}$$

However, from Fig. 7.1b

$$y_{cb} = -t_{bc}$$

Hence

$$y_c = y_{cb} \times \frac{t_{ac}}{t_{bc}}$$

where

$$\frac{t_{ac}}{t_{bc}} = \frac{5}{6(B/L)^2 - (B/L)^4} \quad (6.1)$$

The correction factor t_{ac}/t_{bc} for uniform load depends only on the ratio B/L if EI is constant. Each type of loading requires a different correction factor.

The validity of the deflection correction factor was confirmed experimentally by testing a statically determinate beam, MSG-3. This beam was obtained by cutting an undamaged section two girders wide from bridge model SG-1 after it had been loaded to failure. A section consisting of girders K and L (refer to Fig. 6.1) was obtained by cutting down the center-line of the crowns between girders J and K and girders L and M. MSG-3 was loaded with uniform load and midspan concentrated loads. The span length L

was 86.25 in. and the distance B was 76.0 in. Dial gages were placed at points a, b, c, b', and a' (refer to Fig. 6.15). Using these dial gages the true centerline deflection was measured, as well as the centerline deflection relative to bb'.

Using Eq. 6.1 the deflection correction factor is 1.17 for the case of uniform load. Applying this correction factor to the full uniform load deflection of 0.0247 in. relative to bb', a corrected centerline deflection of 0.0290 in. was obtained. This compares excellently with the true measured deflection of 0.0291 in. The full uniform load deflection was 0.0294 in. (average of 12 girders) for the model SG-1 from which MSG-3 was cut.

The range of application of the correction factor was checked by loading beam MSG-3 to flexural ultimate with a concentrated load at midspan. The correction factor for a midspan concentrated load derived from area moment principles may be obtained from Eq. 6.2

$$\text{Correction factor} = \frac{2}{3(B/L)^2 - (B/L)^3} \quad (6.2)$$

which gives 1.215 for the case being investigated. The corrected centerline deflections and the measured centerline deflections for the concentrated load are compared for beam MSG-3 in Fig. 6.16. If the correction factor is valid the deflections should fall along the 45° line. This is the case even for the deflection taken at ultimate load. Deflections taken after the flexural ultimate capacity was reached deviate only slightly from the line of equality. This is to be expected, since the correction factors were derived assuming constant EI. This is not the case, particularly near the ultimate load.

TABLE 6.4 B AND L DIAL GAGE DISTANCES

Bridge Model	L in.	B in.	B/L
SG-1	87.27	76.25	0.874
SG-2	95.64	84.25	0.881
SG-3	95.64	84.25	0.881
SG-4	91.09	79.97	0.877

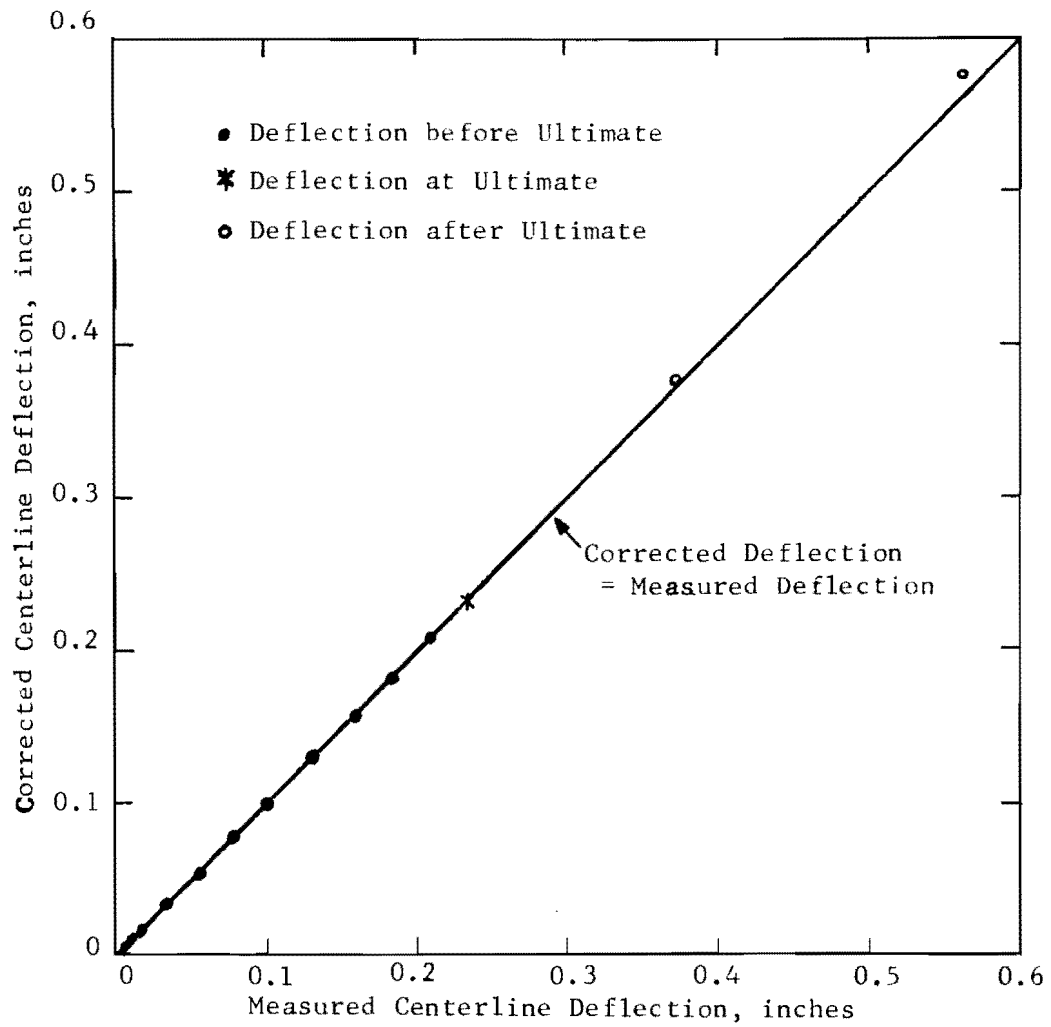


Fig. 6.16. Correction Factor Application for Concentrated Load at Midspan.

6.6.3 Strain Gages. For each location of load complete strain readings were taken at the locations indicated in Sec. 6.6.3. Gage zero readings were taken before and after applying each load. In this manner zero drift was minimized in computing live load strains. Total strain due to dead weight, creep, and live load was computed for each load by assuming that the change due to zero drift was the same as the change in similar unloaded strain gages. The unloaded gages were read along with the gages on the test specimen. The drift correction gages were the same type of strain gage used on the test specimens. Concrete cover on the correction gage and loaded gages was similar.

It was desirable for later interpretation of data to have strain readings on the tensile steel for each girder at midspan. In model SG-1 the steel on girders G, J, and L was not instrumented with strain gages at midspan (all subsequent models had midspan strain gages on all girders). In the case of SG-1 strains on girders G, J, and L were obtained by the use of a Lagrangian interpolation formula.⁴¹

If the points of interpolation are x_0, x, x_1, \dots, x_n , then

$$y = \sum_{s=0}^n A_s(x) y_s + R \quad (6.3)$$

where

$$A_s(x) = \frac{(x-x_0)(x-x_1) \dots (x-x_{s-1})(x-x_{s+1}) \dots (x-x_n)}{(x_s-x_0)(x_s-x_1) \dots (x_s-x_{s-1})(x_s-x_{s+1}) \dots (x_s-x_n)} \quad (6.4)$$

R represents the error function

$$R = \frac{1}{(n+1)!} (x-x_0)(x-x_1) \dots (x-x_n) \bar{Y}^{(n+1)} \quad (6.5)$$

where $\bar{Y}^{(n+1)}$ is the maximum value of the (n+1)th derivative of y with respect to x.

For the case of three-point interpolation used here, Eq. 6.3 may be written as

$$y = \frac{(x-x_1)(x-x_2)}{(x_0-x_1)(x_0-x_2)} y_0 + \frac{(x-x_0)(x-x_2)}{(x_1-x_0)(x_1-x_2)} y_1 + \frac{(x-x_0)(x-x_1)}{(x_2-x_0)(x_2-x_1)} y_2 \quad (6.6)$$

where

y = unknown value at x

y_0, y_1, y_2 = known values at points $x_0, x_1,$ and $x_2,$ respectively.

The procedure used was to number each midspan strain gage from 1 to 12 and use these as the known x values. Measured strains were then used as the y values. The actual strain gages used for interpolation of each unknown strain are shown in Fig. 6.17. The validity of this procedure was checked by applying the interpolation procedure to one of the bridges that was completely instrumented at midspan. Computed strains agreed quite well with measured strains, except for the case of a single point load directly over the strain gage in question.

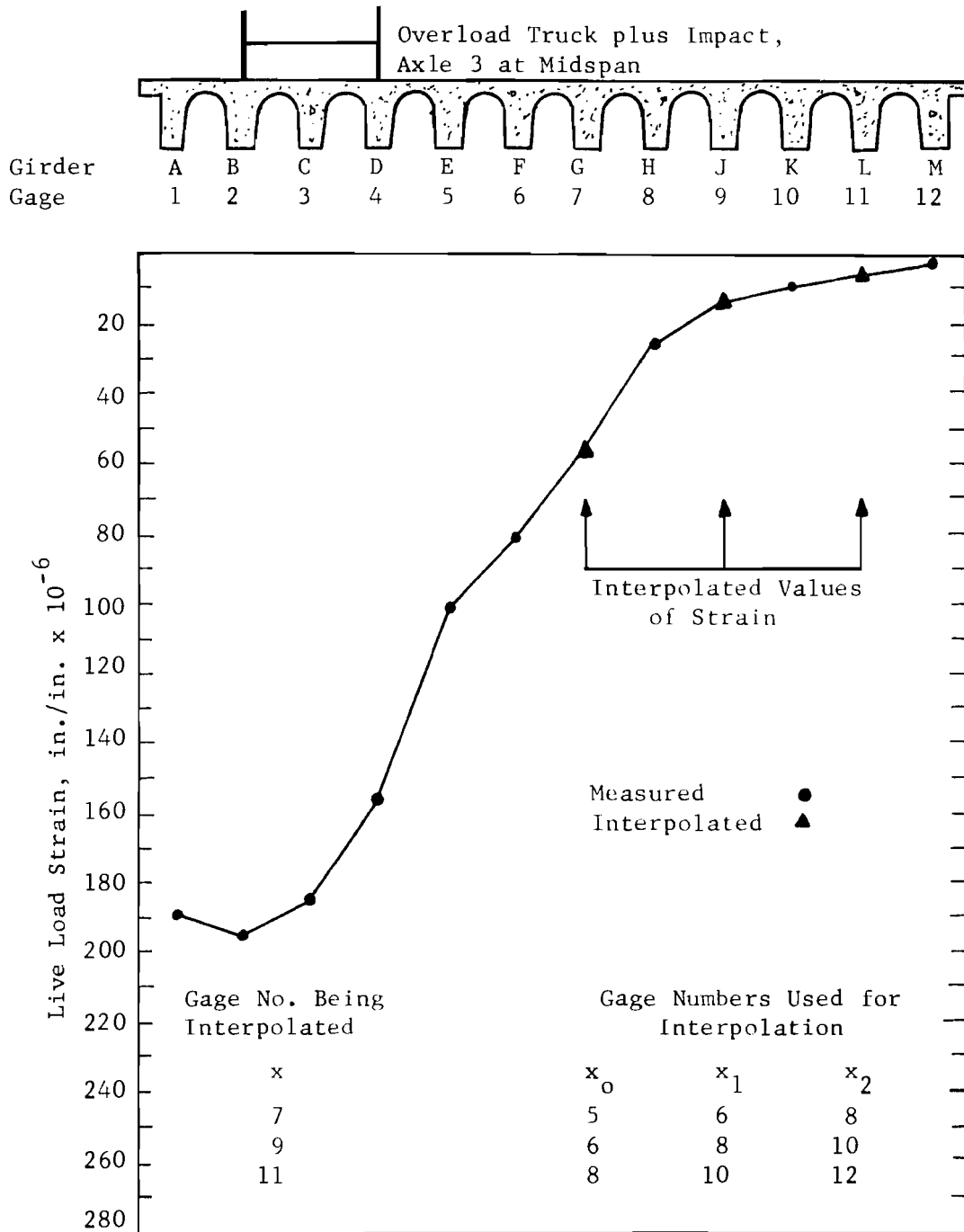


Fig. 6.17. Interpolation for Strains in Girders G, J, and L in Bridge SG-1.

CHAPTER VII

TEST RESULTS

7.1 Introduction

The overall objectives of this investigation were as follows:

- (a) To investigate the behavior at service loads, moderate overloads, and at ultimate loads of typical pan-formed concrete slab and girder bridge spans, using reinforced microconcrete structural models.
- (b) To confirm the observed behavior at service loads by full-scale testing of a prototype structure.
- (c) To evaluate the effectiveness of the end diaphragms in participating with the bent caps to carry slab loads.
- (d) To make recommendations regarding the adequacy of present design provisions based on these test results.

Objectives (a), (c), and (d) will be covered in this chapter. Objective (b) has been covered elsewhere¹⁶ and briefly reviewed in Chapter IV.

The span data, material properties, and design trucks are summarized in Table 7.1. For simplicity, model SG-4 will be referred to as a 26^o skew

TABLE 7.1 BRIDGE MODEL SUMMARY

Model	Skew	Span		Longitudinal Tension Reinforcement		Model	Model	Design Truck
		Model	Prototype	Model	Prototype	f'_c psi	f_y psi	
SG-1	0 ^o -00'	87.27"	40'-00"	4-No. 2	4-No. 11	3770	46.6	HS-20
SG-2	45 ^o -00'	95.64"	43'-10"	4-No. 2	4-No. 11	4040	44.9	HS-20
				2-SWG 5	2-No. 5		40.2	
SG-3	45 ^o -00'	95.64"	43'-10"	4-No. 2	4-No. 11	4320	57.3	HS-20
SG-4	26 ^o -34'	91.09	41'- 9"	2-No. 2	2-No. 11	4750	57.3	H-20
				2-SWG 4	2-No. 10		35.9	

bridge in the test and figures. The steel area, A_s , used for identification in tables and figures is the longitudinal tensile flexural reinforcement in each girder. The yield point in figures and tables other than Table 7.1 is for the No. 2 bars on which strain gages are mounted.

7.2 Dead Load

The dead load deflections and strains for the four models tested are shown in Figs. 7.1 and 7.2, respectively. Each datum point represents the average of the deflection or strain measured in three girders (A, F, and M). Measured data do not include the effect of model self-weight, which varies slightly for the different skew models. The applied load is the ratio 4.5/5.5 multiplied by the total dead load. Total dead load deflections and strains are found by extrapolating backward to the zero load axis the measured initial linear portions of the deflections and strains. These values are then added to the measured quantities to obtain total dead load deflections and strains.

The deflection measurements in Fig. 7.1 indicate that cracking occurred between 80 percent and 100 percent of full dead load for all models. Cracking is slight in models SG-1 (0° skew), SG-2 (45° skew), and SG-4 (26° skew). Model SG-3 (45° skew, high strength steel) shows more cracking effects than its companion model SG-2, which had intermediate grade steel and hence a higher steel area.

Midspan strain measurements are much more sensitive to behavior at the highest stressed section than are deflection measurements. The strain readings shown in Fig. 7.2 indicate that models SG-1 and SG-3 cracked at a slightly lower load level than indicated by deflection data.

Average total midspan strains and deflections are shown in Fig. 7.3a and 7.3b, respectively. Each value is the average of the data for three girders. Theoretical strains and deflections computed using the discrete element model for SG-1 with both the gross and gross-transformed sections are also shown.

The ratio of dead load deflection-to-span is shown in Table 7.2. The ratios should be valid for both the model and the prototype. The

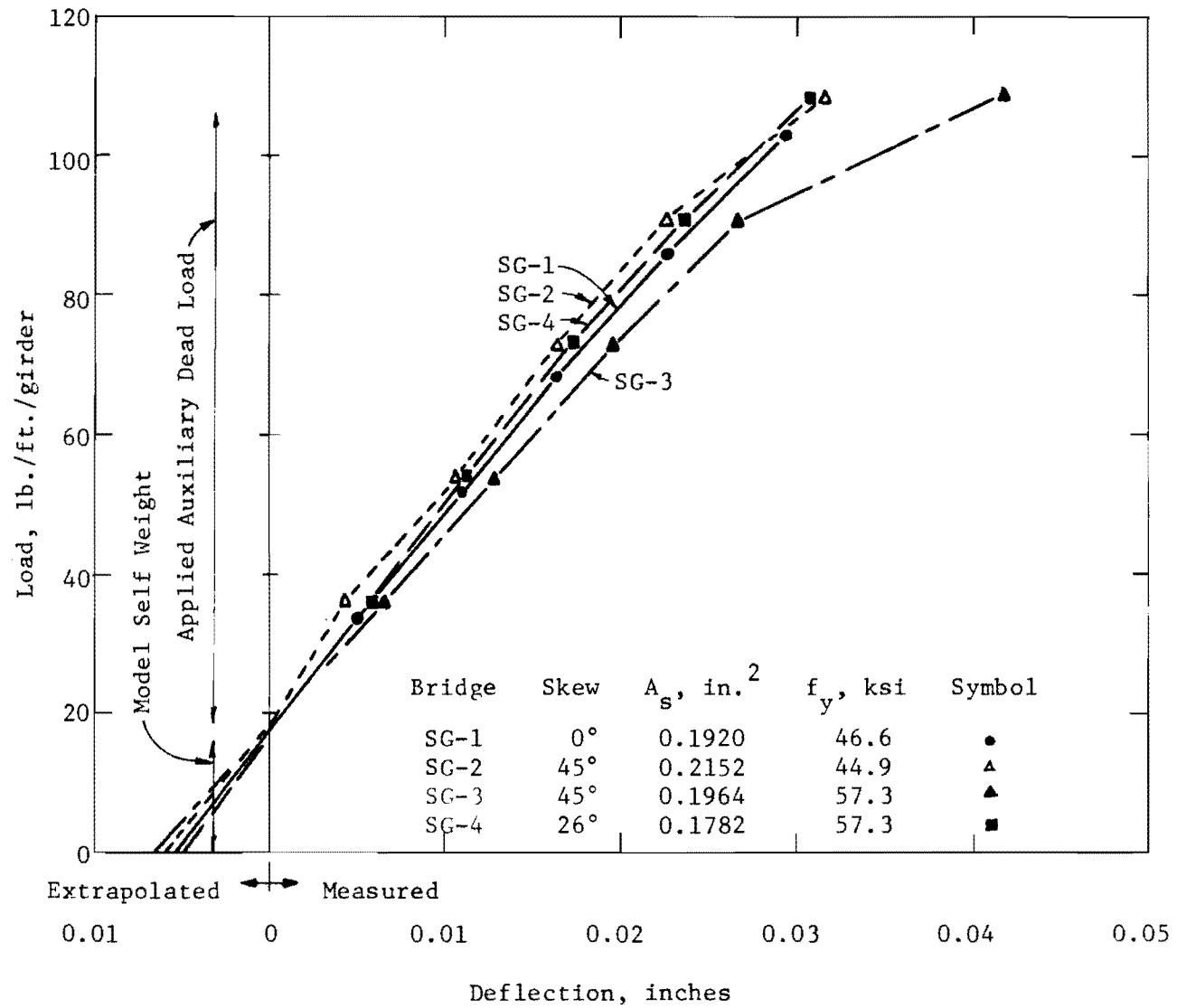


Fig. 7.1. Midspan Dead Load Deflections.

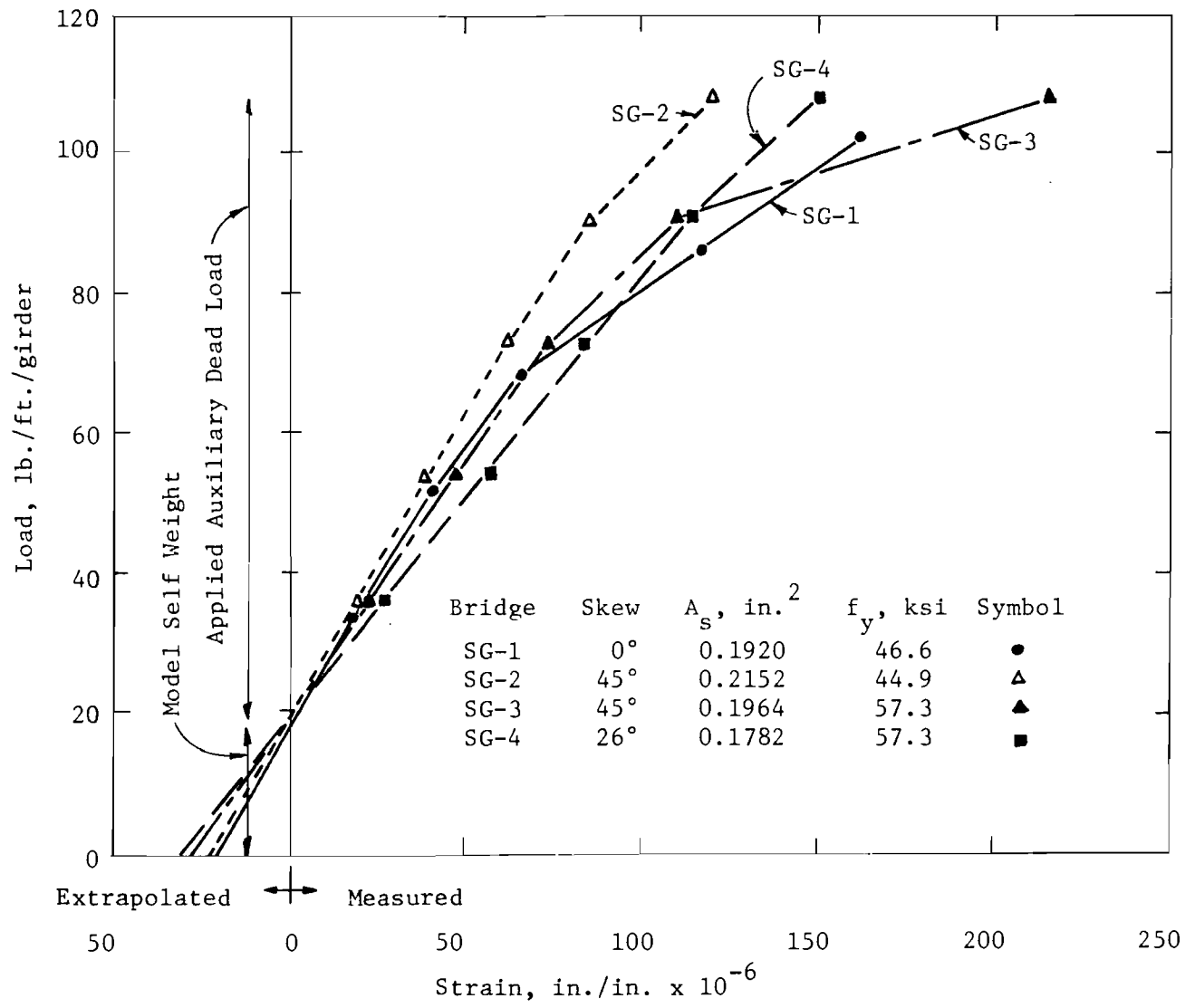
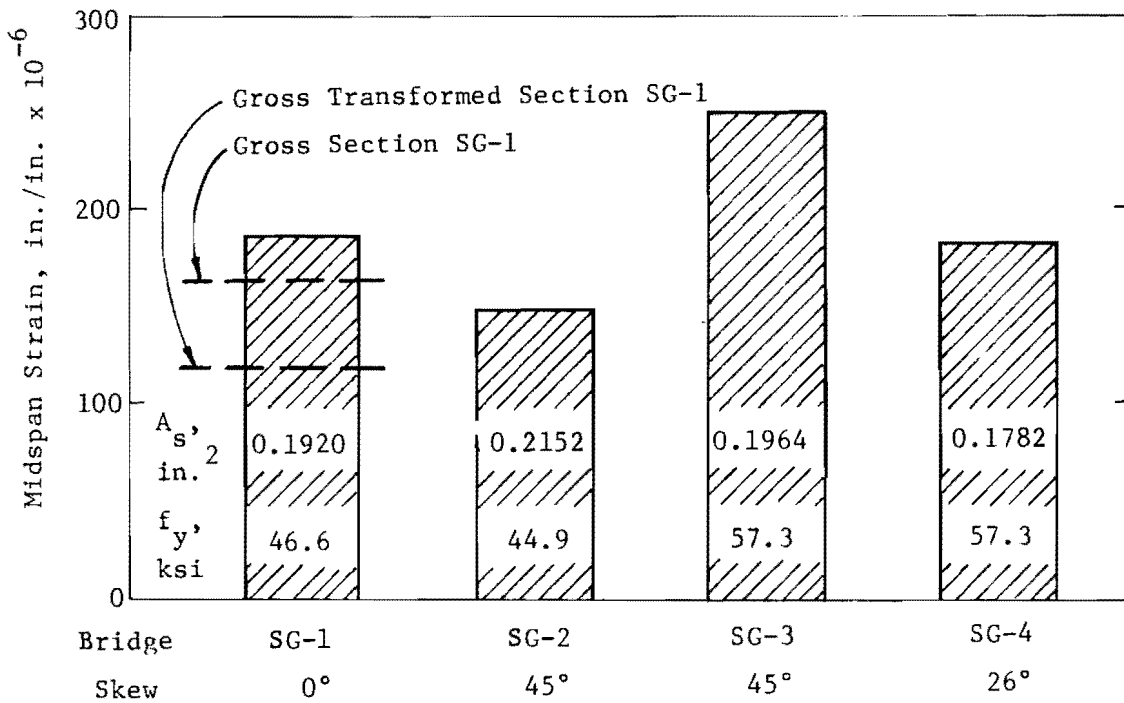
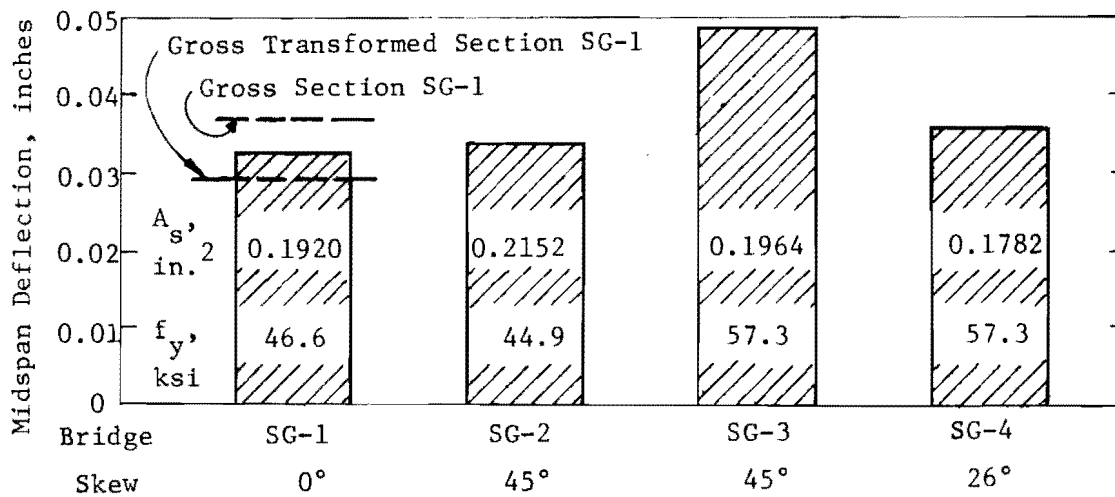


Fig. 7.2. Midspan Dead Load Strains.



(a) Total Dead Load Strain.



(b) Total Dead Load Deflection.

Fig. 7.3. Dead Load Response.

TABLE 7.2 DEFLECTION-TO-SPAN RATIOS

Bridge	Skew	A_s in. ²	f_y ksi	Instantaneous Δ	Sustained
				Span	Load Δ Span
SG-1	0°	0.1920	46.6	1/2690	1/896
SG-2	45°	0.2152	44.9	1/2820	1/940
SG-3	45°	0.1964	57.3	1/1970	1/656
SG-4	26°	0.1782	57.3	1/2540	1/856

observed deflections include the effect of self-weight by using the previously described extrapolation technique. A factor of 3.0 was assumed for computing the sustained load deflection-to-span ratios in Table 7.2, in accordance with AASHTO Specifications² recommendation that the concrete sustained load modulus of elasticity be assumed as 1/30 of that of steel. A factor of 3.0³ is also in agreement with the procedure recommended by the ACI Building Code.

The long-time deflection-to-span ratios agree well with the AASHTO recommendation of L/800 for the live load, except for the case of SG-3. The sustained load deflections (prototype values) for SG-1, SG-2, SG-3, and SG-4 are 0.535 in., 0.560 in., 0.803 in., and 0.585 in., respectively. These values justify the 3/4 in. camber built into the prototype bridges.

7.3 Distribution Factors

7.3.1 Introduction. The AASHTO load distribution factor, k_A , specifies the fraction of a wheel load carried by a girder. This factor has been discussed in Sec. 1.3.5. The design criterion may be stated as

$$k_A = \frac{S}{C} \quad (1.1)$$

where

- k_A = number of wheel loads carried by a girder
- S = average girder spacing in feet
- C = constant

The constant C depends on the type of slab and girder system and the number of traffic lanes. In the case of a concrete slab on girders designed for one traffic lane, the constant is 6.0. The constant is 5.0 for two or three traffic lanes. The factor k_A is varied according to the number of wheel lines on the bridge by adjusting C in Eq. 1.1.

The Guyon-Massonnet type longitudinal moment distribution factor, k_{GM} , for a girder may be stated as

$$k_{GM} = \frac{M}{M_A} \quad (7.1)$$

where

- M = longitudinal moment in a specific girder
- M_A = average longitudinal moment in all girders = M_T/N_G
- M_T = total longitudinal moment on all girders
- N_G = number of longitudinal girders

The Guyon-Massonnet type factor may be determined from measured test results or from an accurate analytical solution. The AASHTO factor is a design criterion based on an extensive test program of slab and girder bridges. The relationship between these two factors is derived in Sec. 7.3.2.

7.3.2 Relationship between Distribution Factors. Let M_1 be the maximum longitudinal moment due to one longitudinal line of wheels. The AASHTO design moment, M_D , per girder is

$$M_D = k_A M_1 \quad (7.2)$$

Using Eq. 7.1, the actual girder moment, M, may be written as

$$M = k_{GM} M_A \quad (7.3)$$

If the moment, M, is referred to as the design moment, M_D , Eq. 7.3 becomes

$$M_D = k_{GM} M_A \quad (7.4)$$

Equating Eqs. 7.2 and 7.4

$$k_A = k_{GM} \frac{M_A}{M_1} \quad (7.5)$$

The average moment, M_A , is

$$M_A = \frac{M_T}{N_G} \quad (7.6)$$

The total moment, M_T , for the case of N_W equal wheel lines may be written as

$$M_T = N_W M_1 \quad (7.7)$$

Combining Eqs. 7.6 and 7.7, the average moment is

$$M_A = \frac{M_1 N_W}{N_G} \quad (7.8)$$

Substituting Eq. 7.8 into Eq. 7.5,

$$k_A = k_{GM} \frac{N_W}{N_G} \quad (7.9)$$

The constant, C , in Eq. 1.1 may be evaluated, since

$$k_A = \frac{S}{C} = k_{GM} \frac{N_W}{N_G} \quad (7.10)$$

or,

$$C = \frac{S}{k_{GM}} \frac{N_G}{N_W} \quad (7.11)$$

where S is the prototype girder spacing in feet.

Comparisons between the test results and the AASHO design factors, k_A and C , can be made using Eqs. 7.10 or 7.11.

7.3.3 Data Comparisons. Comparisons among the data may be made on the basis of dimensionless data ratios or may use absolute magnitudes of data. The deflection distribution factor may be defined for a particular loading as the ratio of the deflection of an individual girder to the average deflection of all girders. The definition of the longitudinal moment distribution factor is similar. Theoretical curves for the distribution of longitudinal moment are constructed by dividing the moment computed or measured as acting on a girder by the average moment per girder obtained by determining the total moment acting across the entire section and dividing this value by the number of girders. With relatively constant lever arms and steel areas in each girder, the strain distribution may be assumed equal to the longitudinal moment distribution.

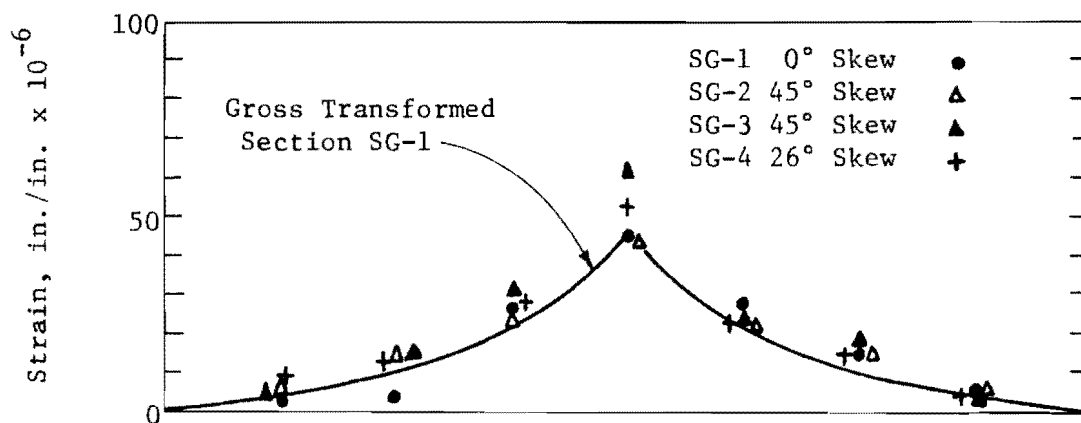
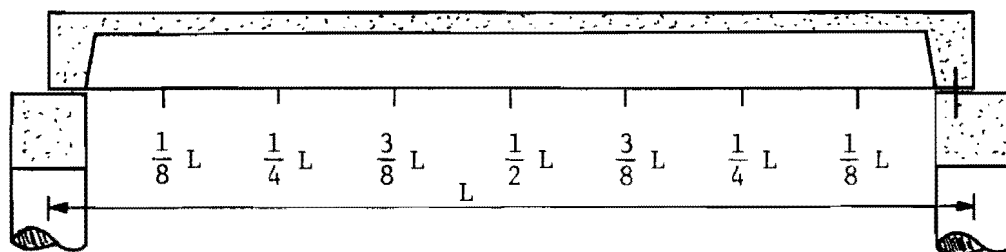
7.4 Service Loads

7.4.1 Influence Lines. Computed influence lines for midspan deflection and longitudinal tensile steel strain on girders B and E are shown in Figs. 7.4 and 7.5, respectively. These are influence lines for one HS-20 rear wheel passing directly over an exterior (B) and an interior (E) girder. The agreement of the observed data and the discrete element theoretical solution for SG-1 is considered good. Data for all models agree reasonably well with the theoretical solutions for SG-1 based on the gross-transformed section.

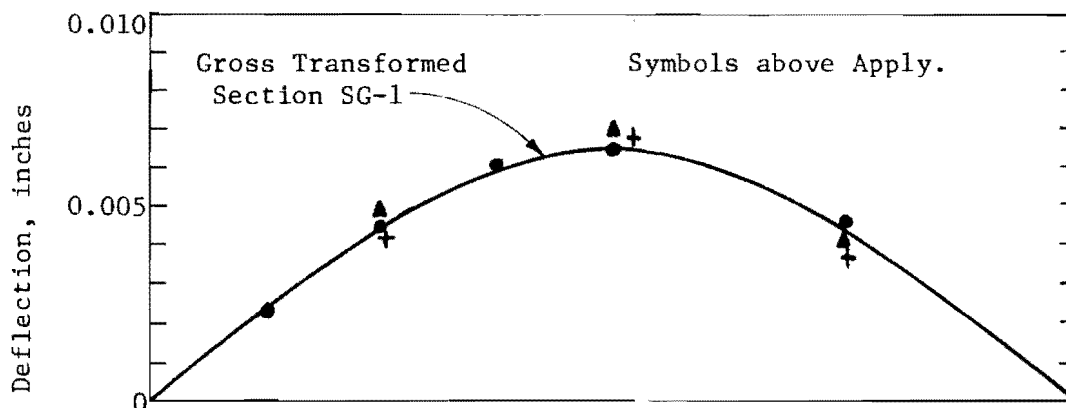
Figs. 7.4 and 7.5 indicate that discrete element solution influence lines can be used in designing the various girders. However, the experimental data were obtained for the lowest level of total stress, i.e., dead load plus one AASHO wheel.

The influence line for strain for a simply supported constant section beam reflects the shape of the moment diagram. Thus the influence line at midspan for strain for a simply supported beam is a triangle with the maximum ordinate at midspan. When a wheel moves along a slab the wheel deflects the slab locally into a depression similar to a saucer-like pattern. The local depression moves with the wheel along the slab. A similar slab effect occurs on a slab and girder bridge. It is this local effect which causes the influence line for strain to be curved. The shape shown in Figs. 7.4a and 7.5a is typical for the midspan influence line for strain on a loaded girder. The influence line for midspan strain on an unloaded girder (that is not loaded directly by the wheel load) is curved similar to the shape of a parabola. The sum of the influence lines for midspan strain on each girder as a load moves along one particular girder is a triangle.

7.4.2 Reciprocal Theorem. Deflection profiles are shown in Figs. 7.6, 7.7, 7.8, and 7.9. Deflection profiles for girder B are shown in Fig. 7.6 for a load at B-4, and Fig. 7.8 for a load at E-4. Deflection profiles for girder E are shown in Fig. 7.7 for a load at E-4, and Fig. 7.9 for a load at B-4. Experimental data as well as a discrete element solution using the gross-transformed section are shown in each figure.

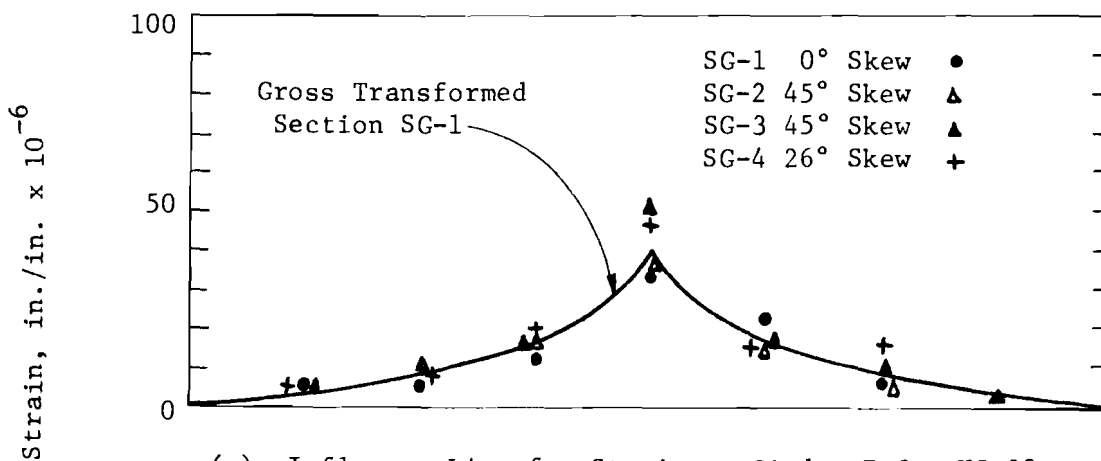
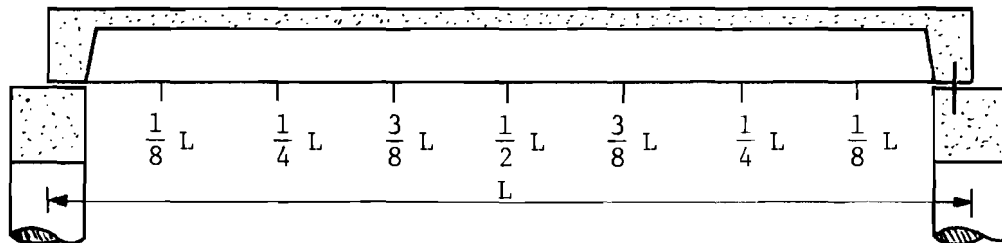


(a) Influence Line for Strain on Girder B for HS-20 Rear Wheel Moving along Girder B.

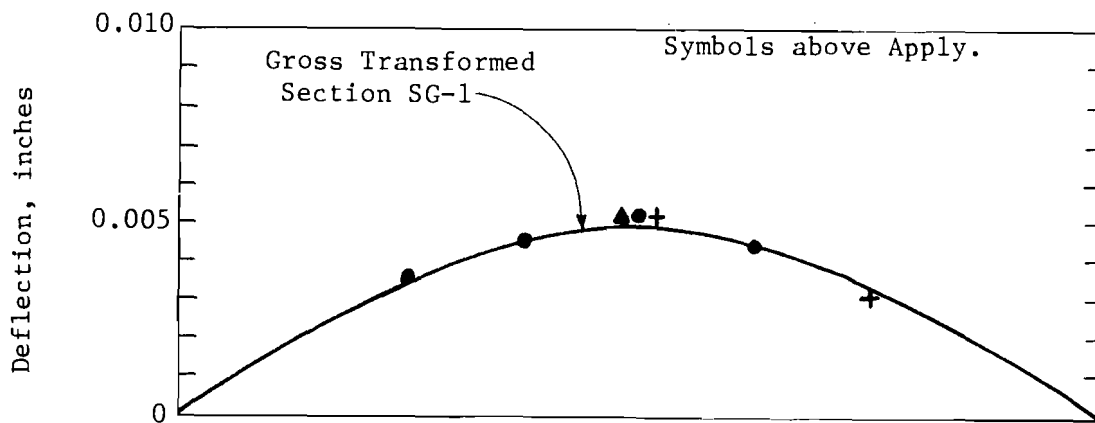


(b) Influence Line for Deflection on Girder B for HS-20 Rear Wheel Moving along Girder B.

Fig. 7.4. Influence Lines for Girder B for HS-20 Rear Wheel.



(a) Influence Line for Strain on Girder E for HS-20 Rear Wheel Moving along Girder E.



(b) Influence Line for Deflection on Girder E for HS-20 Rear Wheel Moving along Girder E.

Fig. 7.5. Influence Lines for Girder E for HS-20 Rear Wheel.

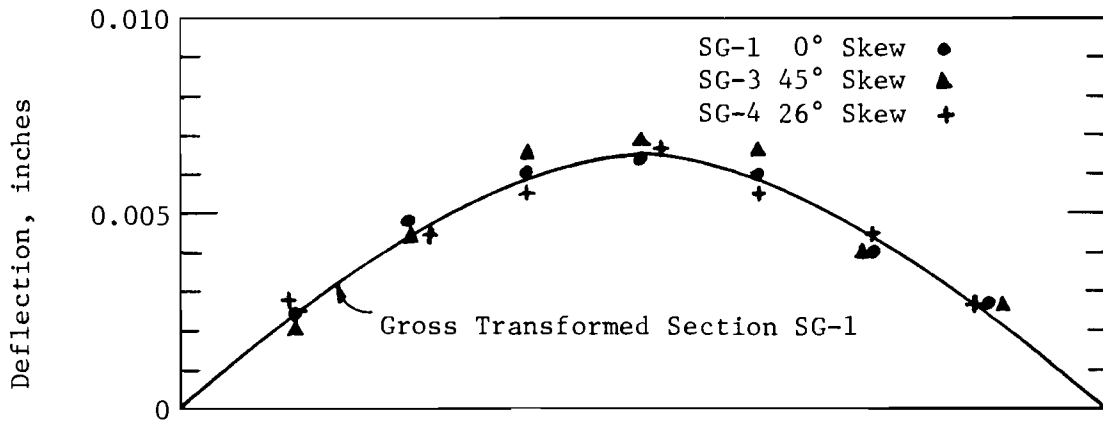
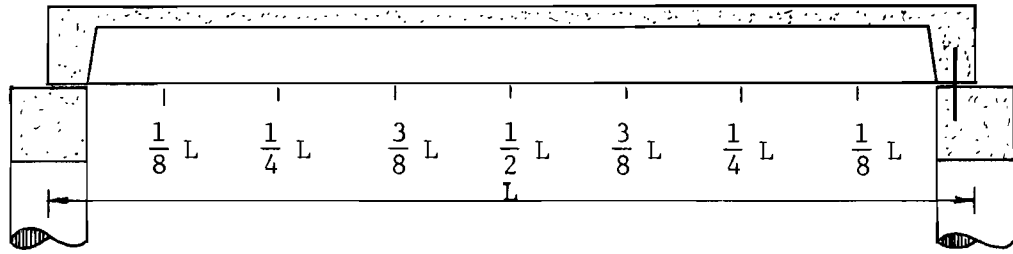


Fig. 7.6. Deflection Profile for Girder B, Wheel Load at B-4.

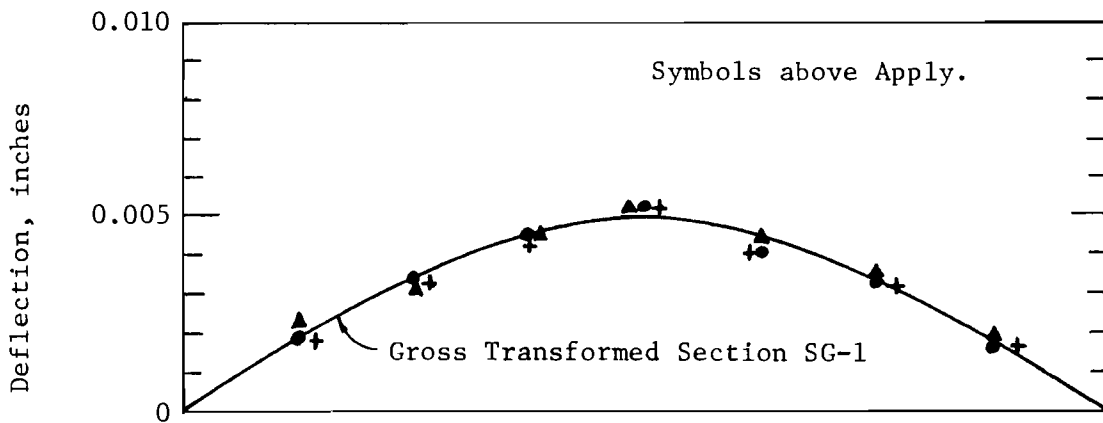


Fig. 7.7. Deflection Profile for Girder E, Wheel Load at E-4.

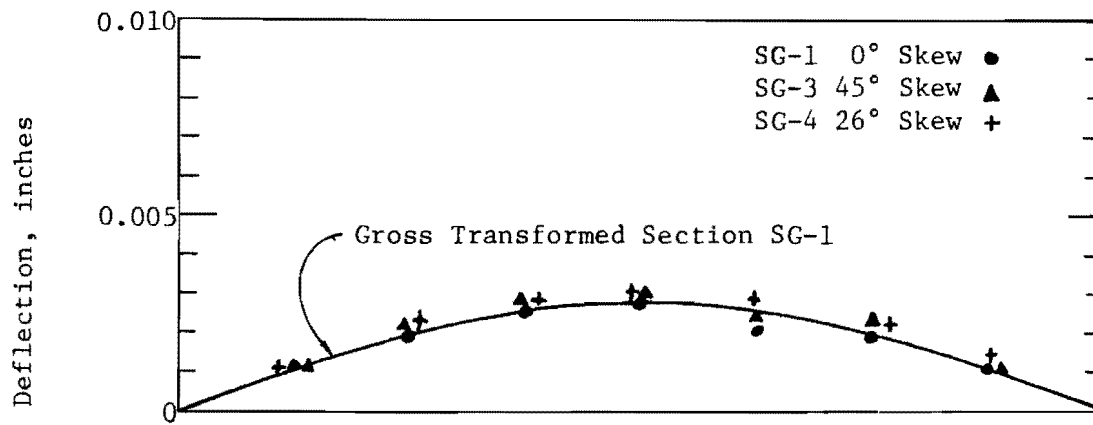
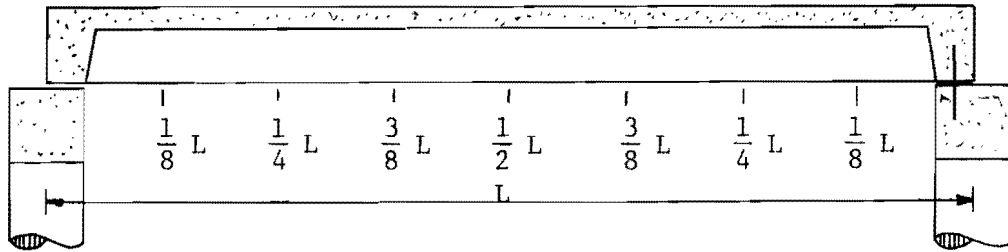


Fig. 7.8. Deflection Profile for Girder B, Wheel Load at E-4.

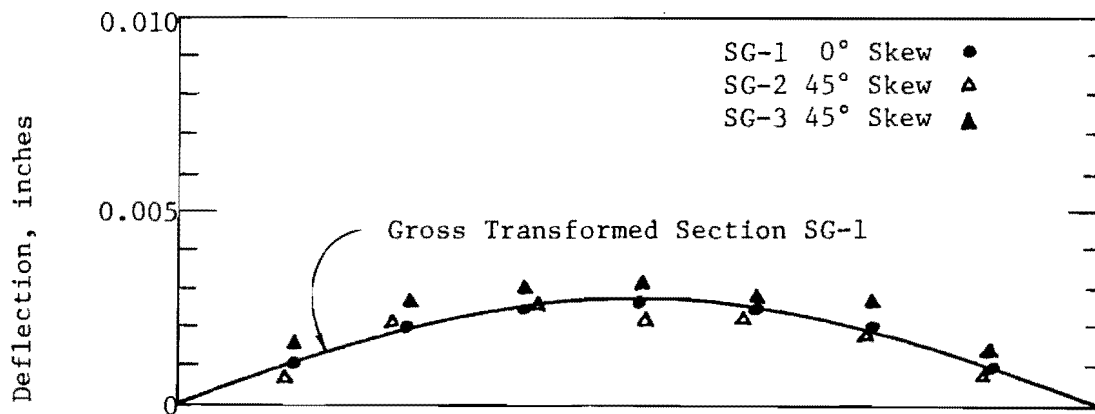


Fig. 7.9. Deflection Profile for Girder E, Wheel Load at B-4.

Figures 7.8 and 7.9 are important when thought of in terms of Maxwell's "Reciprocal Theorem" for elastic structures. This theorem states that the deflection at point Y due to a load at point X is equal to the deflection at point X due to the same load at point Y. Thus the deflection profiles in Figs. 7.8 and 7.9 should be the same. As may be seen in the figures, the experimental data are essentially the same.

These data indicate that the reciprocal theorem is valid for these low stress levels of dead load plus one wheel load.

7.4.3 Wheel Loads. Variations in midspan strain and deflection distribution factors for a wheel in various transverse locations on the bridge may be seen by comparing Figs. 7.10, 7.11, 7.12, and 7.13. Distributions are shown for placement of wheel loads over girders A, B, C, and E, respectively. Experimental datum points are shown for all four bridges tested. Two theoretical curves obtained from the discrete element mathematical model are shown. The solid curves were obtained using the gross-transformed section properties. The dashed curves were obtained using gross section properties. Only the solid curve is shown when the two solutions coincide. Both theoretical curves are for the right angle bridge SG-1.

The gross-transformed section theoretical curve predicts the shape of the deflection distribution with the wheel at A-4 in Fig. 7.10. The theoretical solution underestimates the actual strain distribution directly under the point of application of the wheel load. The larger actual strain may be due to a small flexural crack passing over or near the strain gage. Such a crack would cause stress formerly carried by the uncracked concrete to be transferred to the tensile steel. This would result in an increased steel strain. Figures 7.10 through 7.13 indicate the same trends as in Fig. 7.10. In all cases the gross-transformed section gives a reasonable prediction of strain and deflection distribution within experimental error, except under the point of load application.

The experimental strain and deflection distribution factors under the load points A, B, C, and E (Figs. 7.10 through 7.13, respectively) are compared in Fig. 7.14. The theoretical solution for SG-1 is shown for reference.

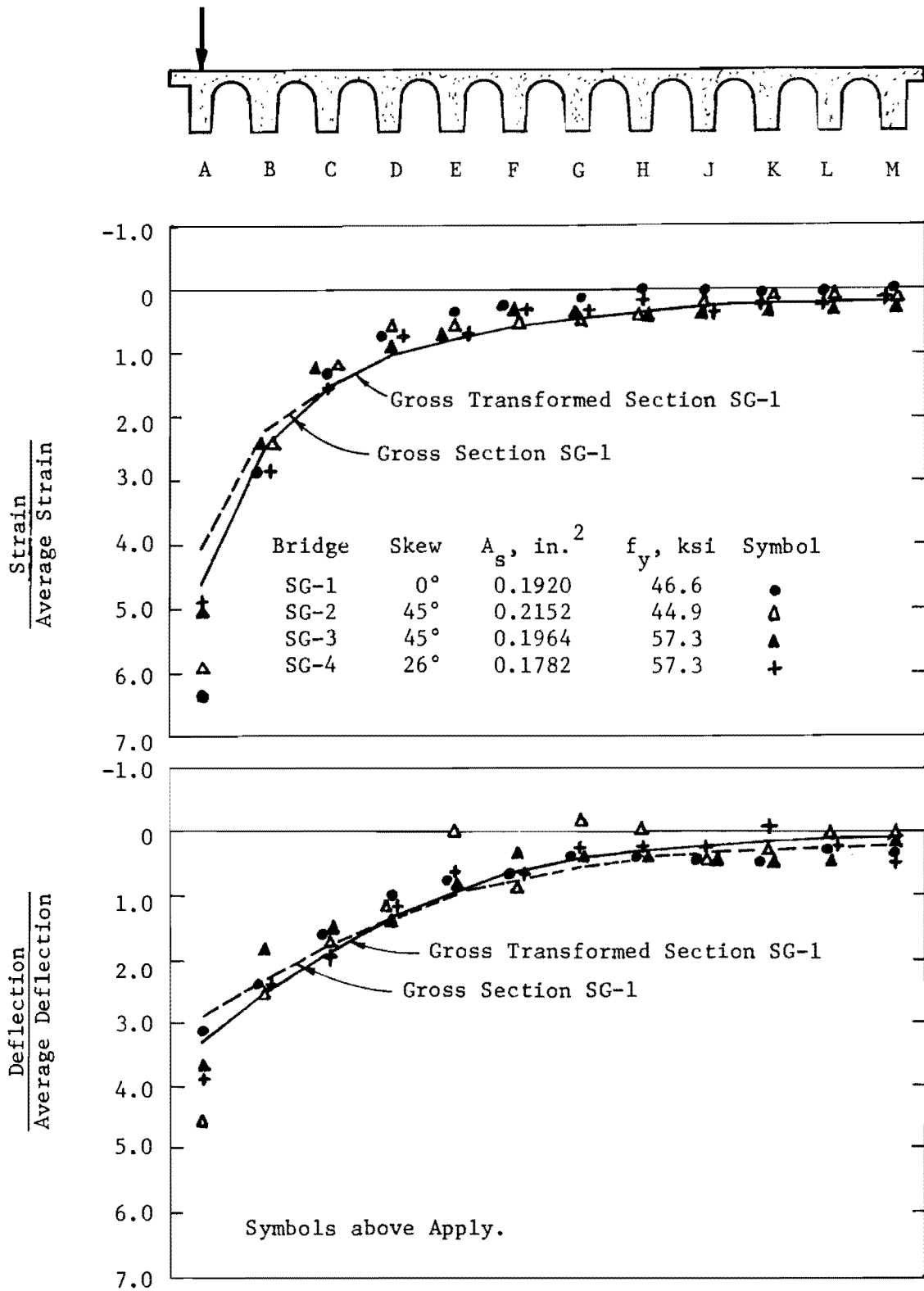


Fig. 7.10. Midspan Distribution of Strains and Deflections for Wheel Load at A-4.

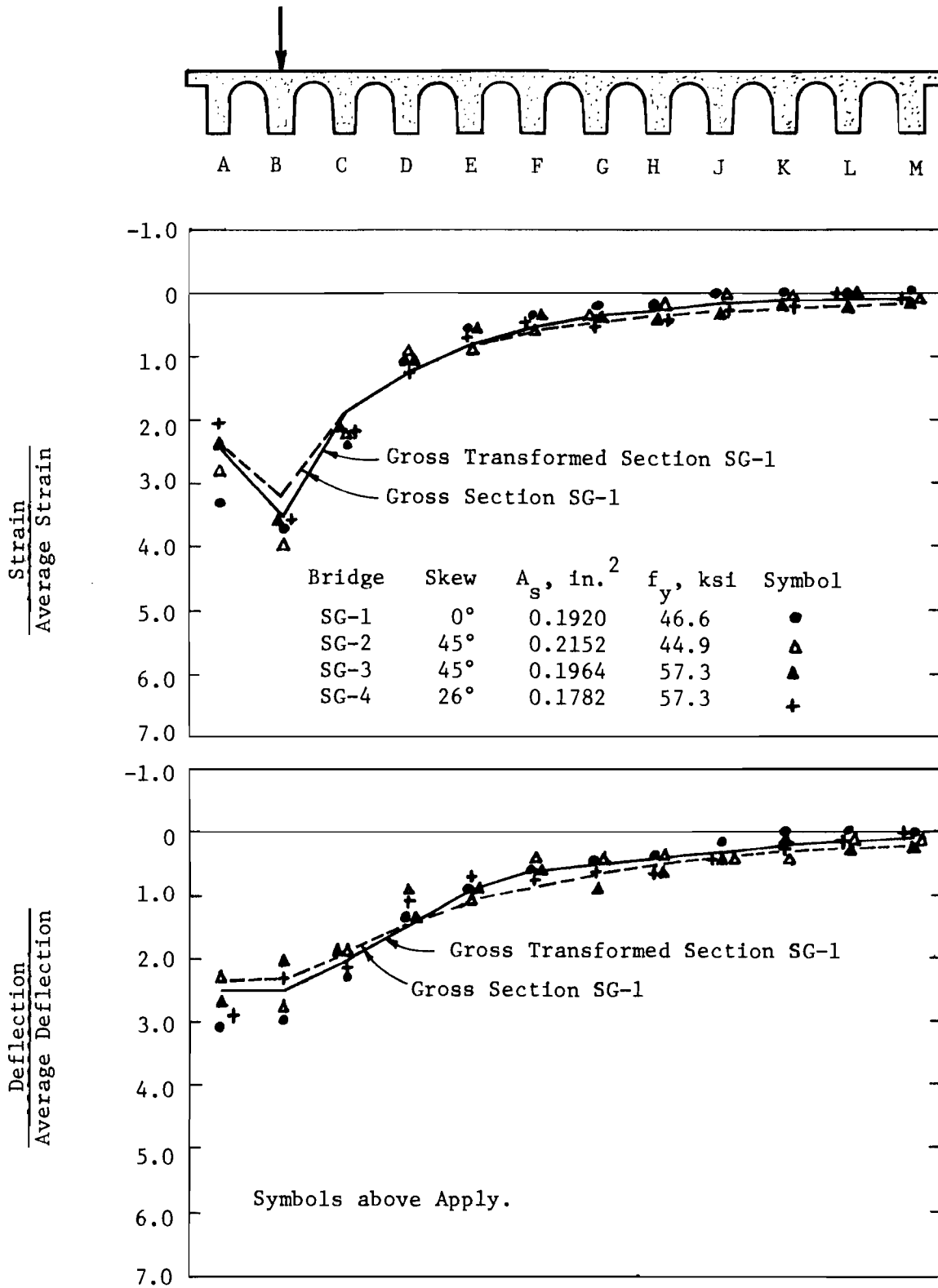


Fig. 7.11. Midspan Distribution of Strains and Deflections for Wheel Load at B-4.

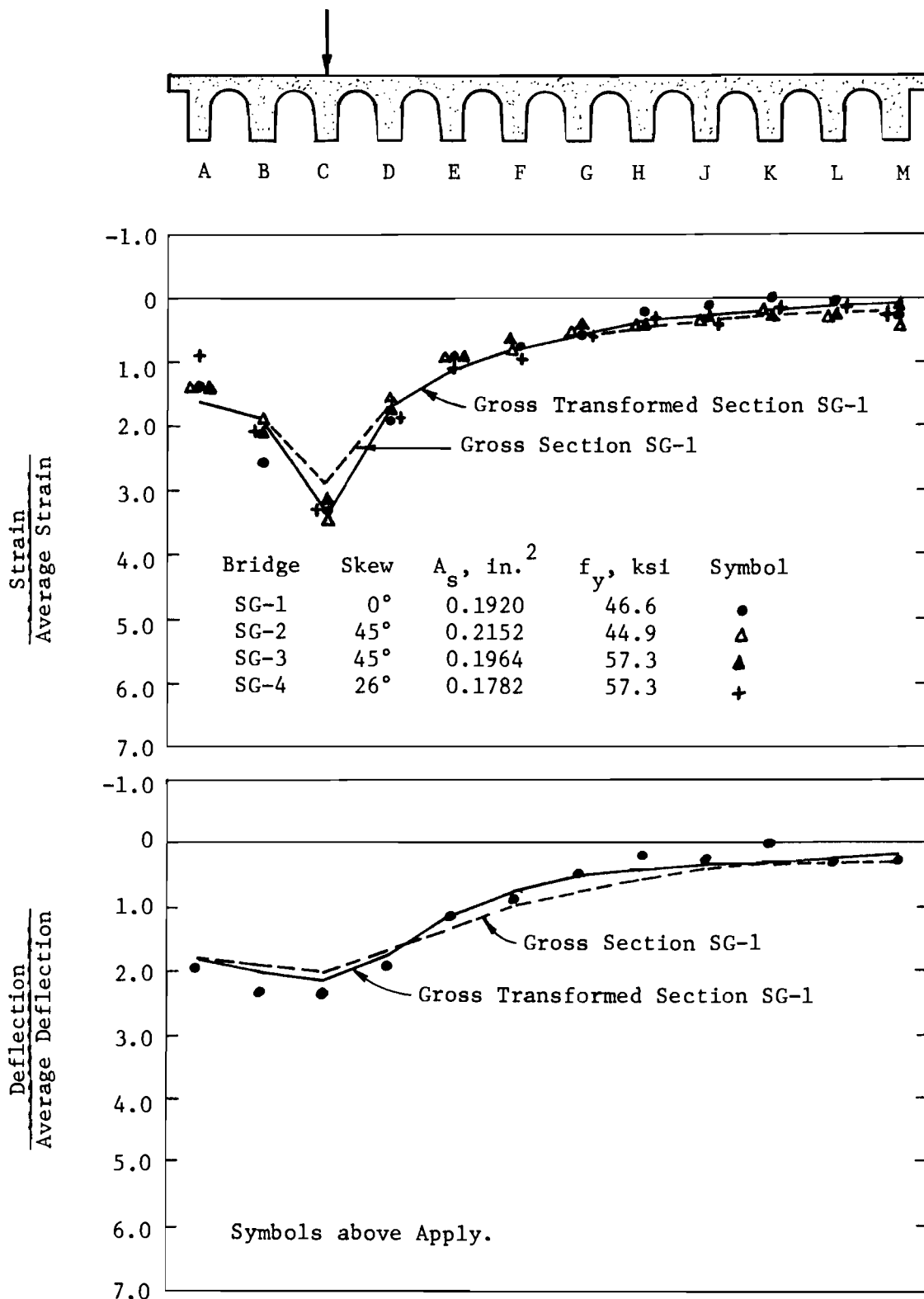


Fig. 7.12. Midspan Distribution of Strains and Deflections for Wheel Load at C-4.

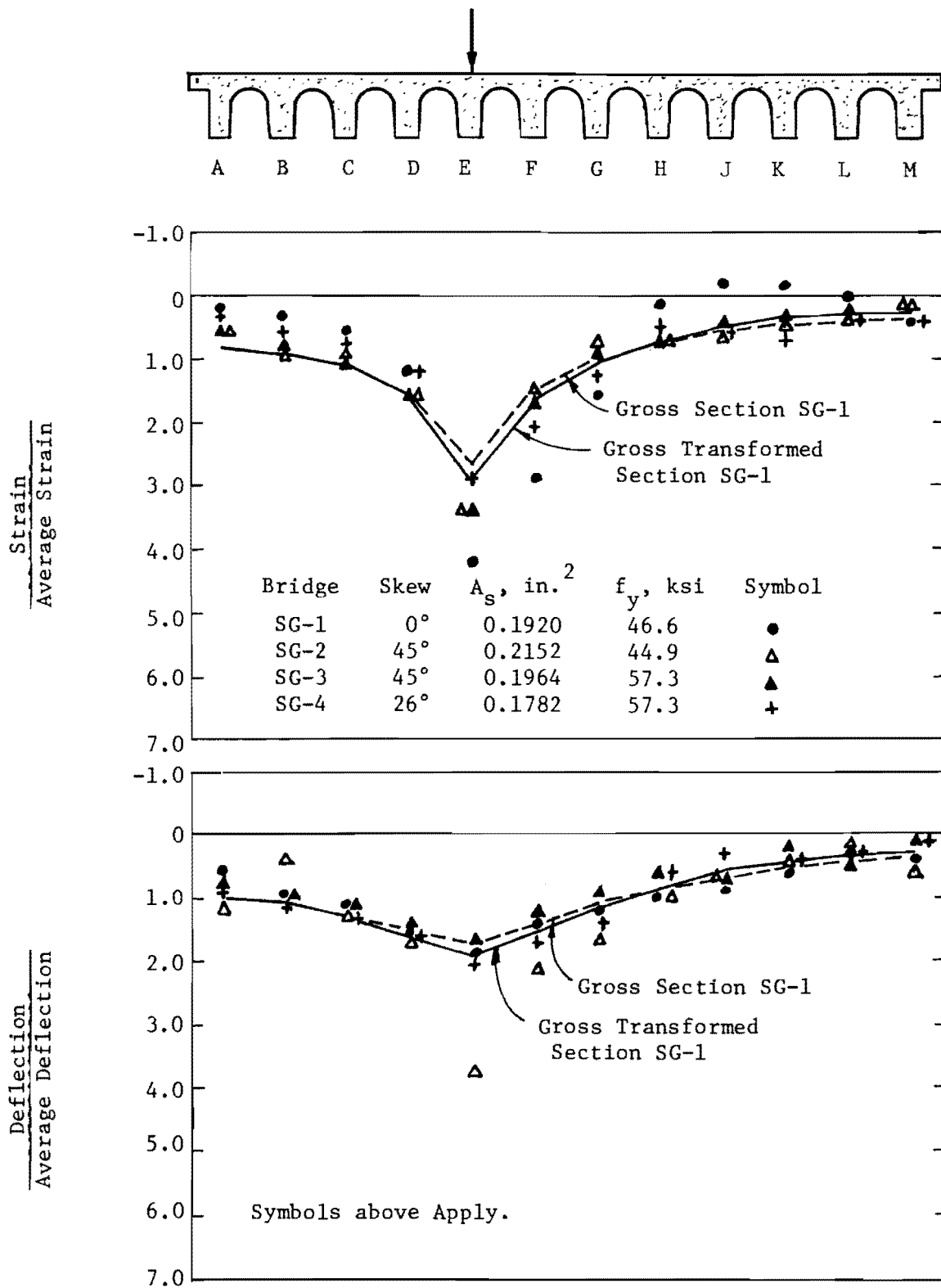
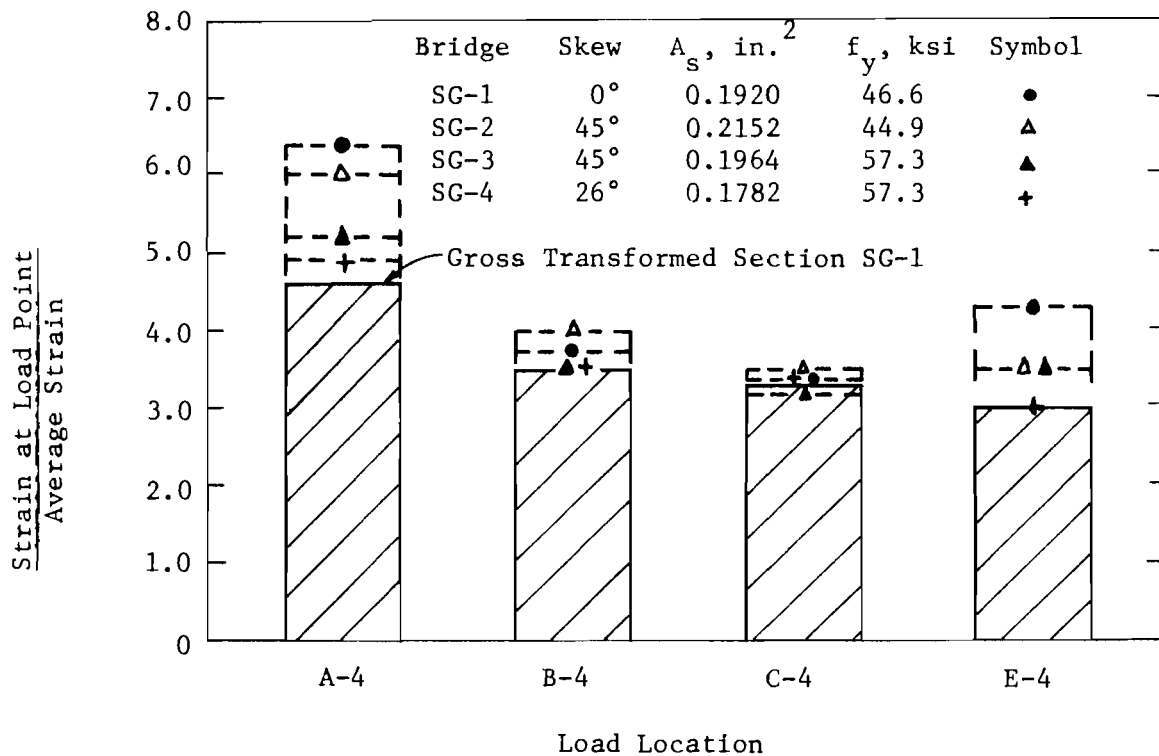
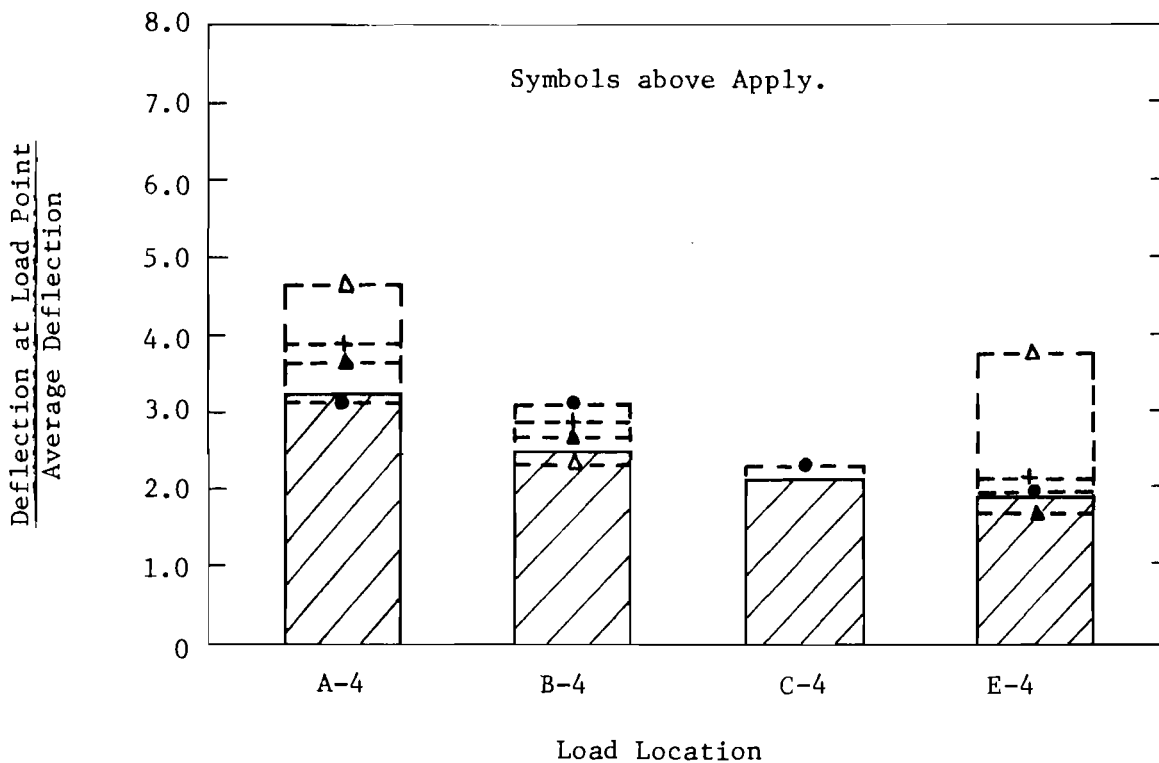


Fig. 7.13. Midspan Distribution of Strains and Deflections for Wheel Load at E-4.



(a) Strain Distribution.



(b) Deflection Distribution.

Fig. 7.14. Comparison between Experimental and Theoretical Distribution Factors with Varied Wheel Load Placement.

There is no apparent pattern evident in Fig. 7.14 showing the effect of skew or quantity of longitudinal tensile steel. Since no pattern is evident, the maximum measured strain distribution factor is used for the value of k_{GM} in discussing design criteria. The AASHO type load distribution factor, $k_A = S/C$ (Eq. 1.1), is used for a design criterion. The value of $C = 36/k_{GM}$ is found for the prototype using Eq. 7.11.

TABLE 7.3 SERVICE LOAD SINGLE WHEEL DESIGN CRITERIA

Load Location	Girder	k_{GM}	Prototype k_A	AASHO Recommendation
A-4	A	6.35	S/5.66	None
B-4	B	4.03	S/8.93	None
C-4	C	3.47	S/10.38	None
E-4	E	4.22	S/8.54	None

There are no AASHO service load design recommendations in terms of $k_A = S/C$ for a single wheel. The service load data in Table 7.3 suggest using a factor of S/5.5 in designing the exterior girder and a factor of S/9.0 in designing girder B. Girders more than two spaces away from the edge could be designed using a factor of S/10.0. The data for girder E of bridge SG-1 indicate a more severe ratio of S/C than girder C, but the preponderance of data (as well as the theoretical solution) indicate S/C ratios for interior girders varying from S/12 to S/10.3.

7.4.4 Single Truck Loads. Midspan strain distribution factors for an AASHO HS-20 truck in various transverse positions are shown in Figs. 7.15 through 7.17. Theoretical deflection distribution curves are also shown, although no experimental data are plotted. Deflection measurements were taken for girders in the vicinity of the applied load. These data are not sufficient for plotting distributions, since data from all girders are required for this type of curve. Magnitudes of the measured deflections are shown in Sec. 7.4.7 and Sec. 7.4.8.

The loadings represented in Figs. 7.15, 7.16, and 7.17 are for trucks at the edge (A4-C4), near the edge (B4-D4), and near the middle (E4-G4) of

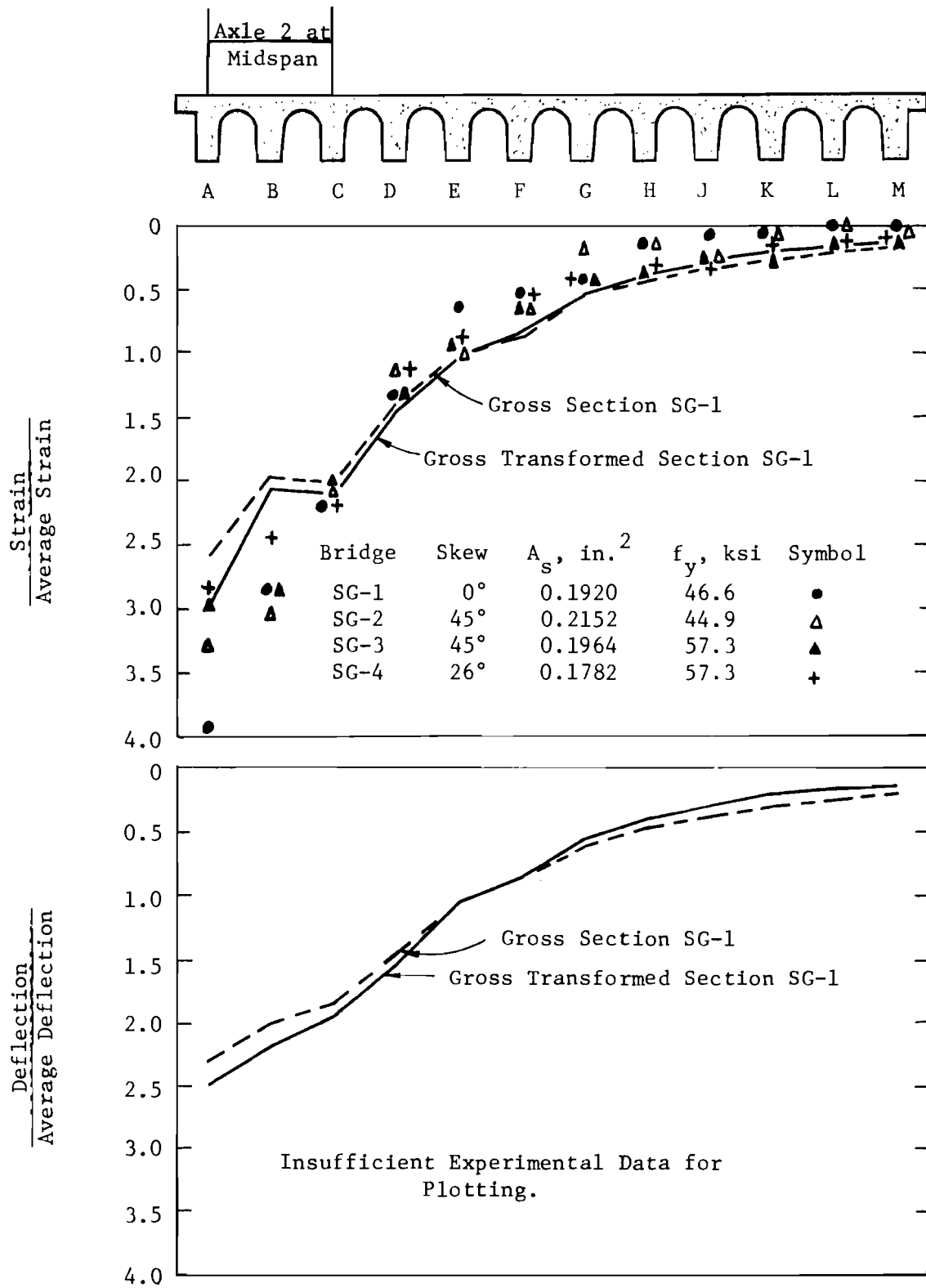


Fig. 7.15. Midspan Distribution of Strains and Deflections for HS-20 Truck at A4-C4.

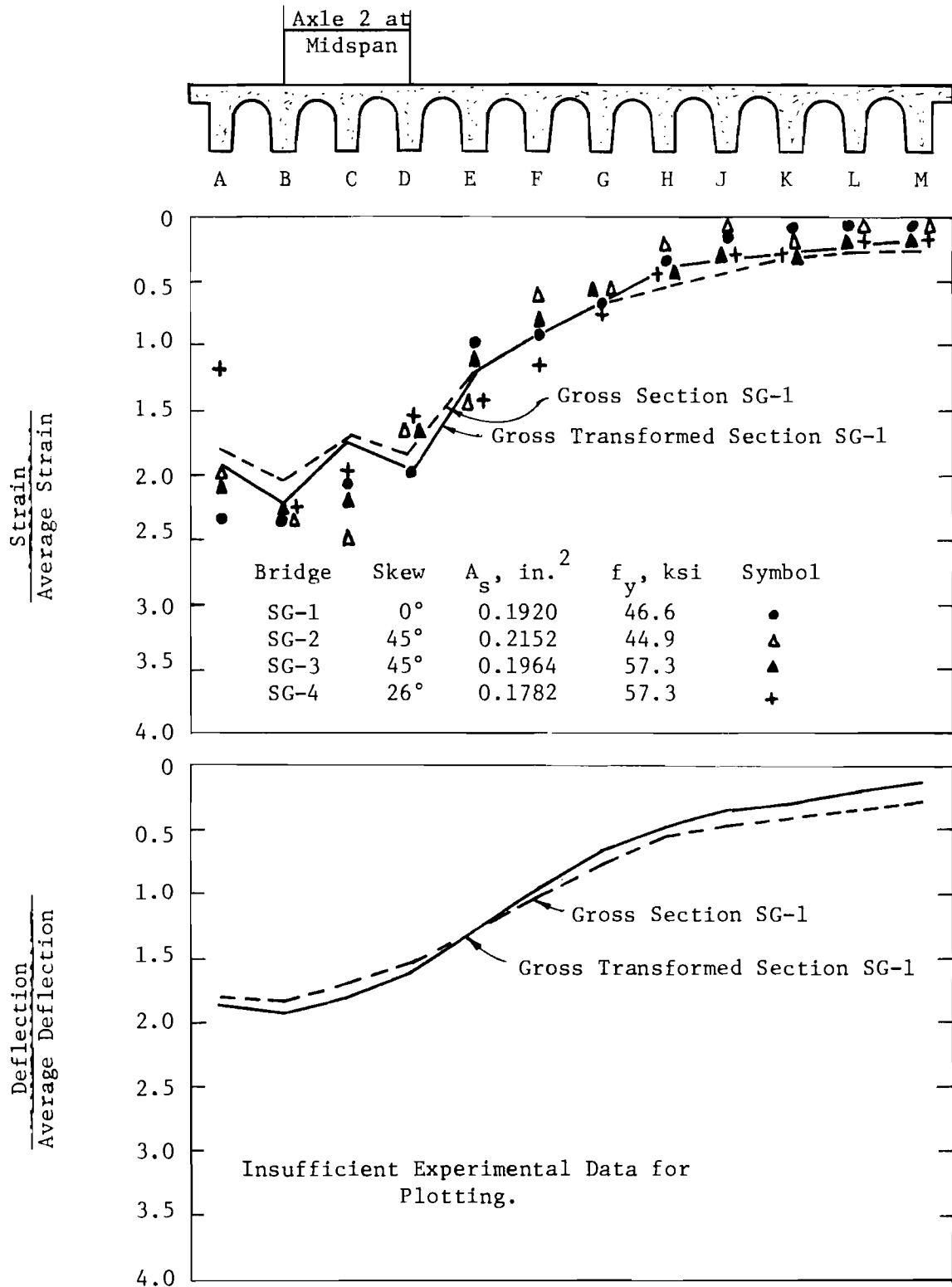


Fig. 7.16. Midspan Distribution of Strains and Deflections for HS-20 Truck at B4-D4.

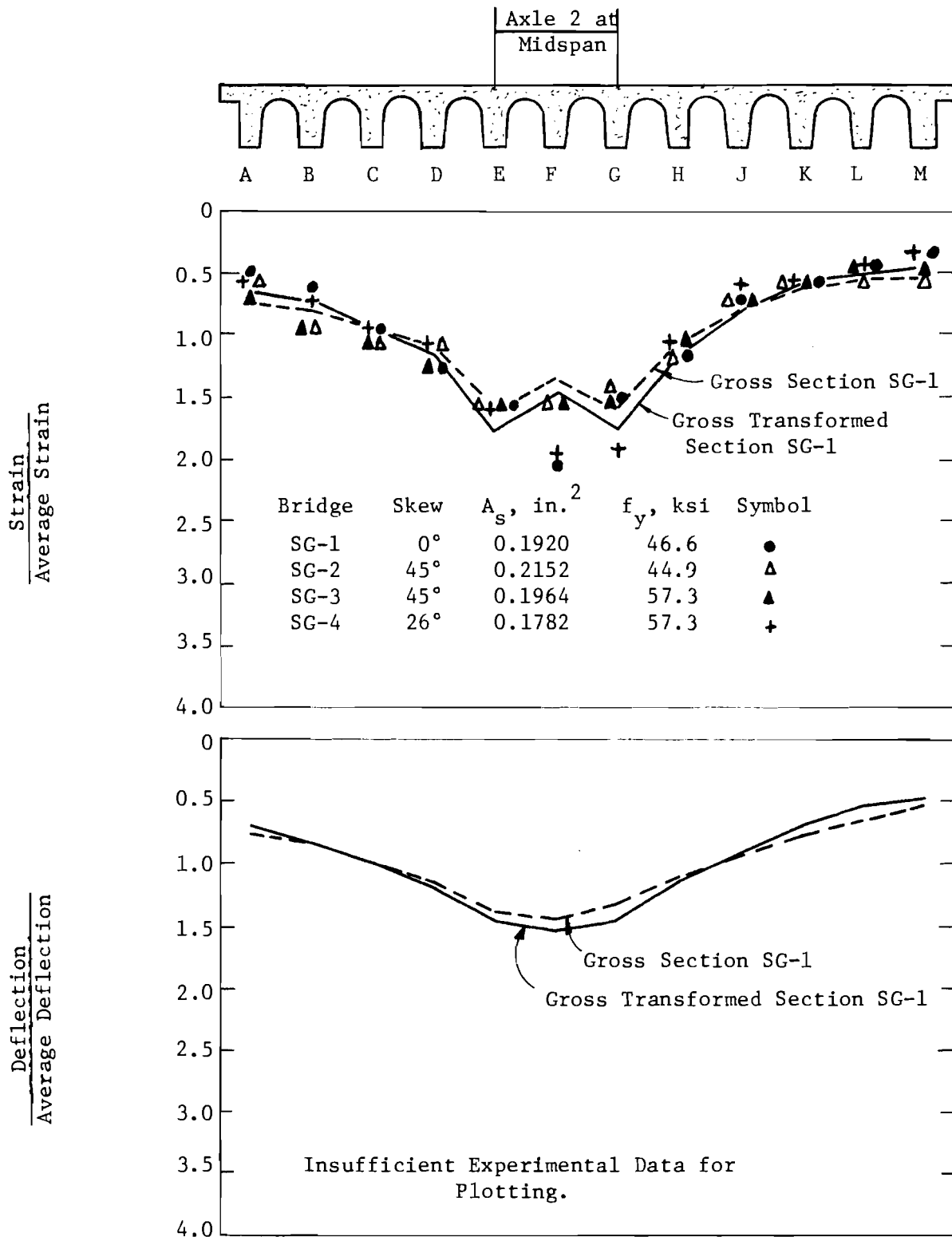


Fig. 7.17. Midspan Distribution of Strains and Deflections for HS-20 Truck at E4-G4.

the bridge cross section, respectively. The gross-transformed section discrete element solution predicts the shape of the strain distributions except for the point midway between the wheels. The accuracy of the predicted strain distributions improves as the truck is moved away from the edge position. This was also the case for the single wheel loading.

The theoretical and experimental strain distribution factors are summarized in Fig. 7.18 for the same three loadings shown in Figs. 7.15 through 7.17. Only the factors for the girders beneath each truck are shown in Fig. 7.18.

There is no apparent pattern of an effect of skew in the distribution factors summarized in Fig. 7.18. Since no pattern is evident, the maximum strain distribution factor over each girder will be used in discussing a design criterion. The AASHO load distribution factor, $k_A = S/C$ (Eq. 1.1), is used for a design criterion. The value of $C = 18/k_{GM}$ for use in the ratio S/C in the prototype is found using Eq. 7.11.

The current AASHO design recommendation for a single truck load is $S/C = S/6.0$. The factor k_A for the data in Fig. 7.18 is given in Table 7.4. The largest value for each girder is shown, regardless of skew angle.

TABLE 7.4 SERVICE LOAD SINGLE AASHO TRUCK DESIGN CRITERIA

Load Location	Girder	k_{GM}	Prototype k_A	AASHO Recommendation
A4-C4	A	3.91	S/4.5	Special Case*
	B	3.01	S/5.98	S/6.0
	C	2.28	S/7.9	S/6.0
B4-D4	B	2.38	S/7.55	S/6.0
	C	2.49	S/7.22	S/6.0
	D	2.00	S/9.00	S/6.0
E4-G4	E	1.56	S/11.55	S/6.0
	F	2.07	S/8.6	S/6.0
	G	1.83	S/9.85	S/6.0

*The exterior girder is designed by applying to the girder the reaction of the wheel load obtained by assuming the flooring to act as a simple beam between girders. The fraction of a wheel load shall not be less than $S/5.5$, where S is 6.0 ft. or less.

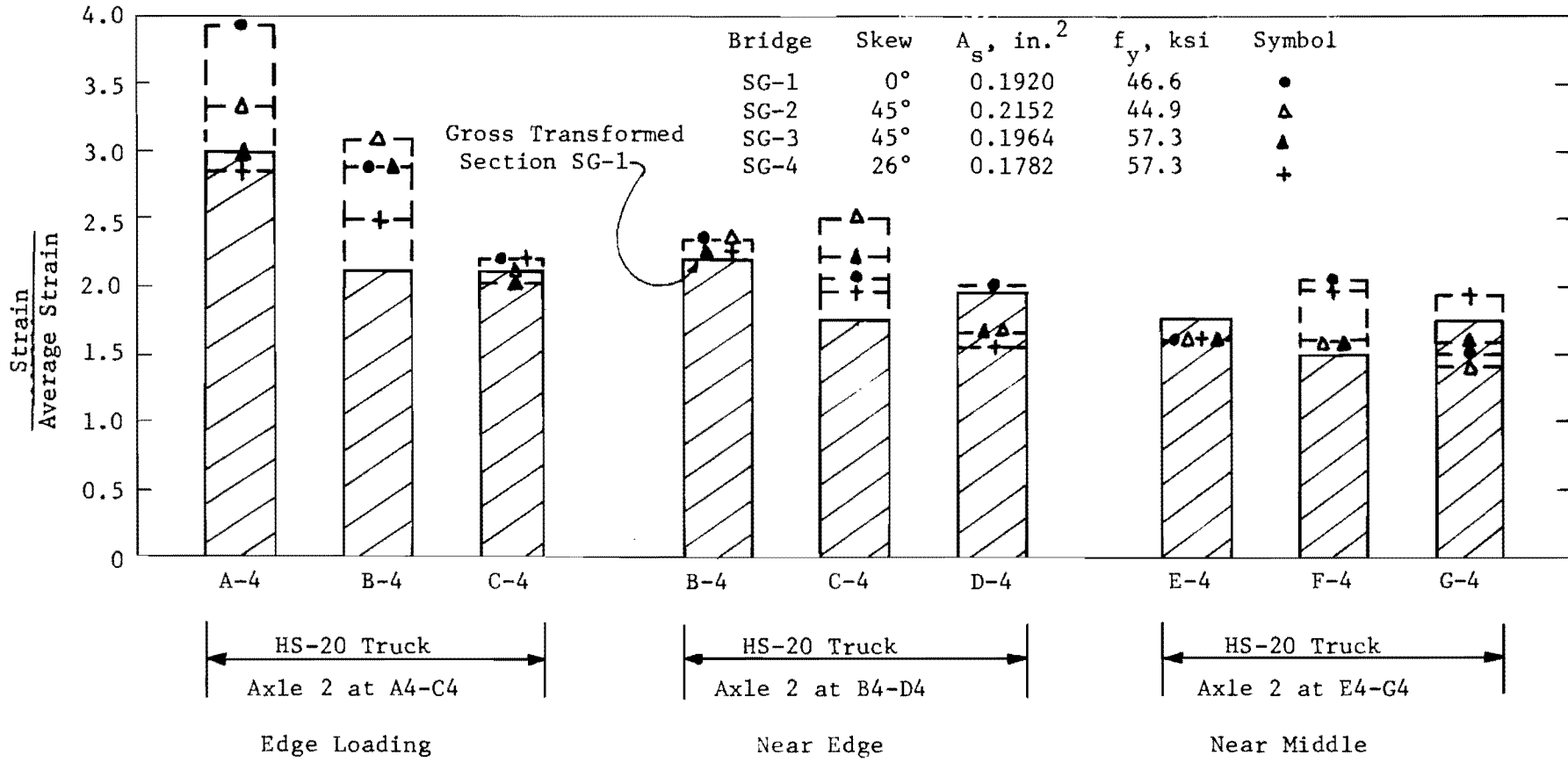


Fig. 7.18. Comparison between Experimental and Theoretical Distribution Factors with Varied Single Truck Placement.

The data in Table 7.4 indicate that the AASHO design criterion of $S/6.0$ is in excellent agreement with the experimental factor $S/5.98$ for girder B under the A4-C4 loading. The loading over B4-D4 results in a ratio of $S/C = S/7.22$ for girder C. The loading E4-G4 results in a ratio of $S/8.6$ for girder F. These factors indicate that, with the exception of the two edge girders, the AASHO factor is 20 percent to 43 percent conservative and could be greatly relaxed for design of these interior girders.

7.4.5 Double Truck Loads. Midspan strain and deflection distribution factors for two HS-20 trucks in various transverse positions on the bridge are shown in Figs. 7.19 through 7.21. The theoretical solutions for the gross and gross-transformed solutions coincide for all practical purposes at the scale used.

The theoretical solution for the right angle bridge agrees well with the experimental data for the right angle bridge. The predicted deflection distribution is in better agreement with the test results than the strain distributions. The distribution factors for the three loading cases in Figs. 7.19 through 7.21 are summarized in Figs. 7.22 and 7.23 for strain and deflection, respectively. In each of these two figures only the data under the truck with the largest distributions factors from each loading are shown.

The AASHO distribution factor for the double truck loading is $S/5.0$. The value of the factor $C = 9/k_{GM}$ (Eq. 7.11) is used in determining an experimental ratio for S/C . The strain distributions indicate that $k_{GM} = 1.37$ is appropriate for use with any of the loading combinations shown. The resulting S/C ratio is $S/6.56$. The AASHO distribution factor is about 30 percent conservative for this type of bridge with double HS-20 truck loading.

The bridges tested in this study were designed for two traffic lanes.

7.4.6 Triple Truck Loads. Midspan strain and deflection distributions for three HS-20 trucks are shown in Fig. 7.24. Deflections are essentially constant across the bridge cross section. Strain distributions indicate a factor $k_{GM} = 1.21$ should be used for design. This is an AASHO type factor of $S/C = S/4.96$. The AASHO specifications use a value of $S/C = S/5.0$ for two or more truck loads. These are in excellent agreement.

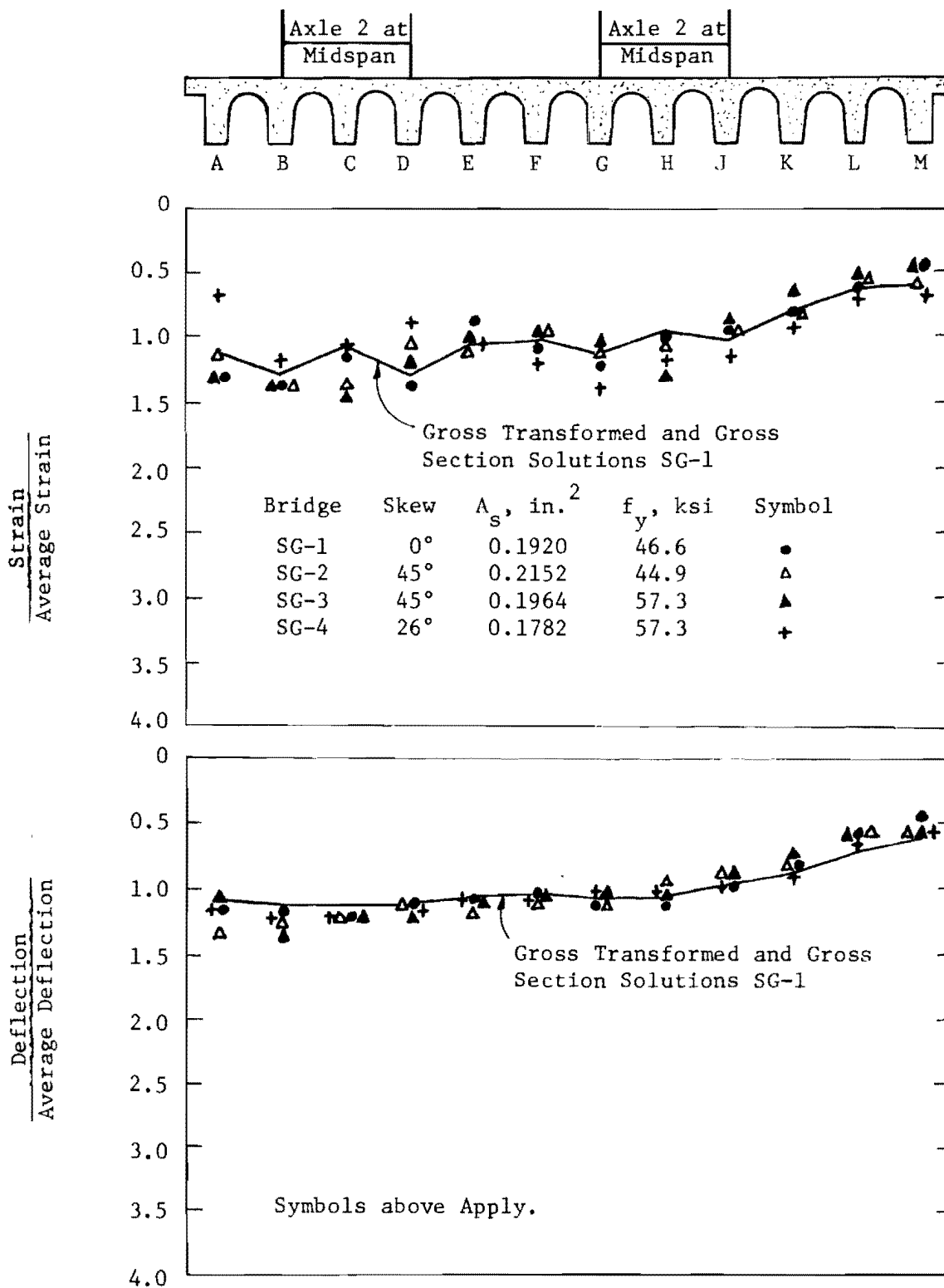


Fig. 7.19. Midspan Distribution of Strains and Deflections for HS-20 Trucks at B4-D4 and G4-J4.

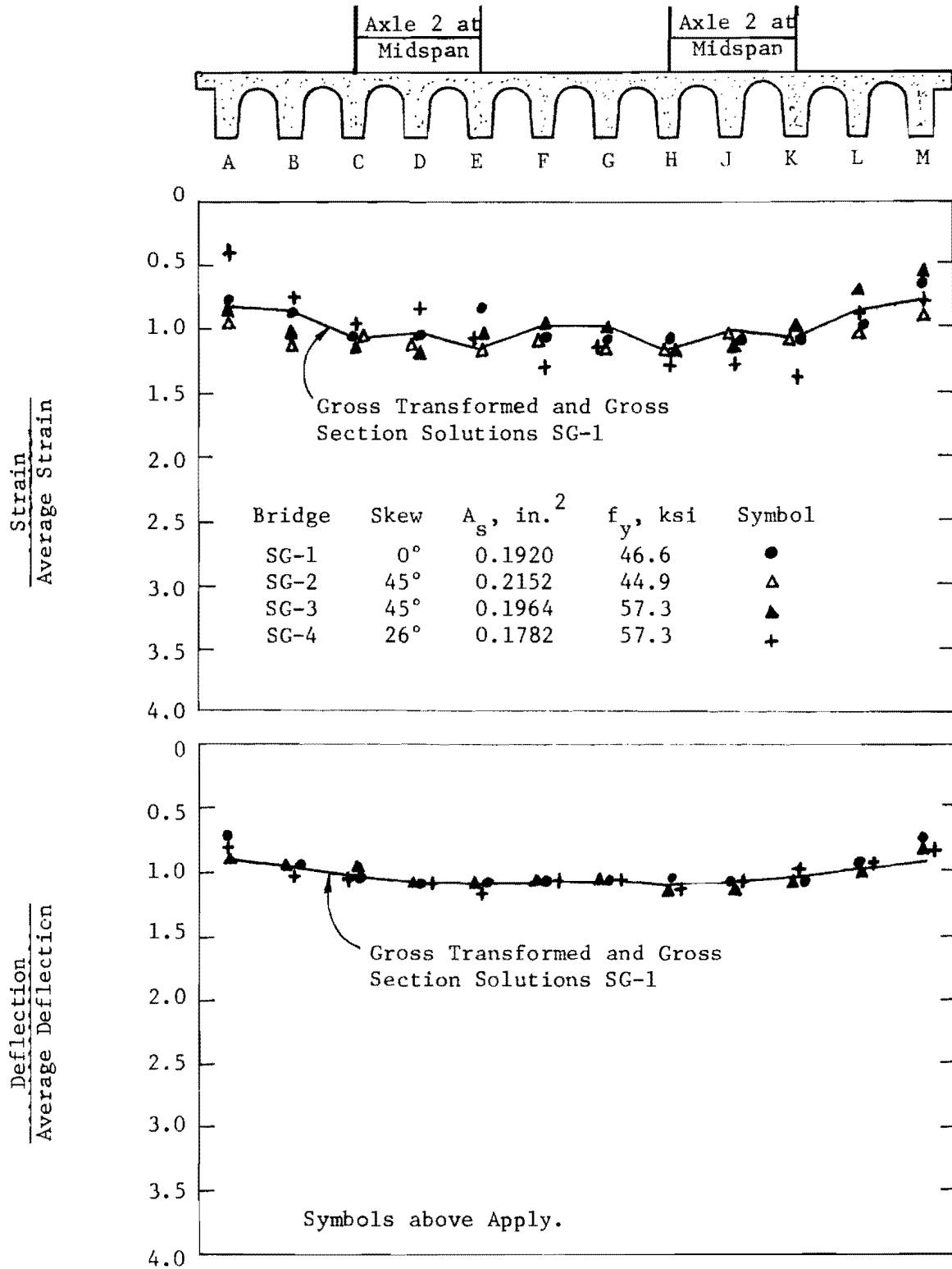


Fig. 7.21. Distribution of Strains and Deflections for HS-20 Trucks at C4-E4 and H4-K4.

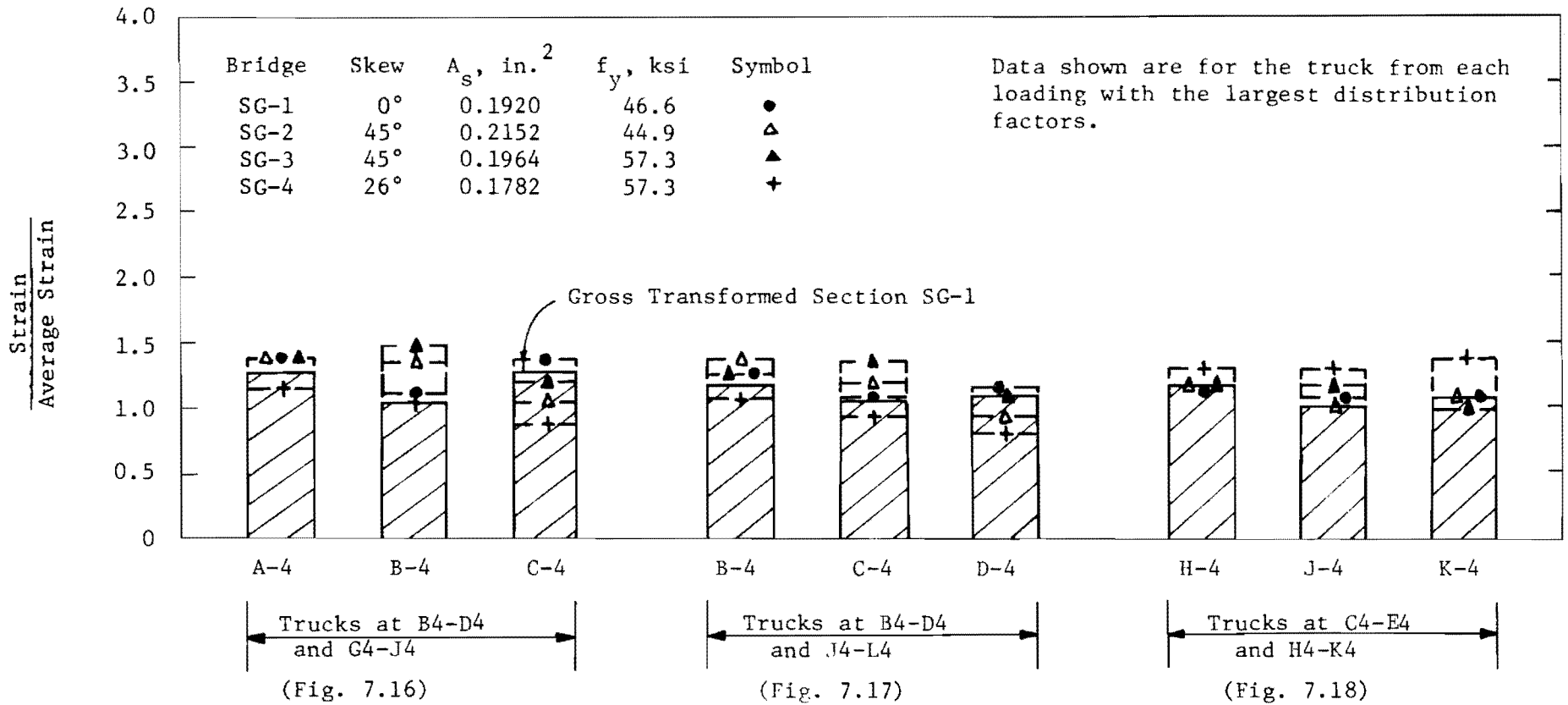


Fig. 7.22. Comparison between Experimental and Theoretical Strain Distribution Factors for Two HS-20 Trucks with Varied Truck Placement.

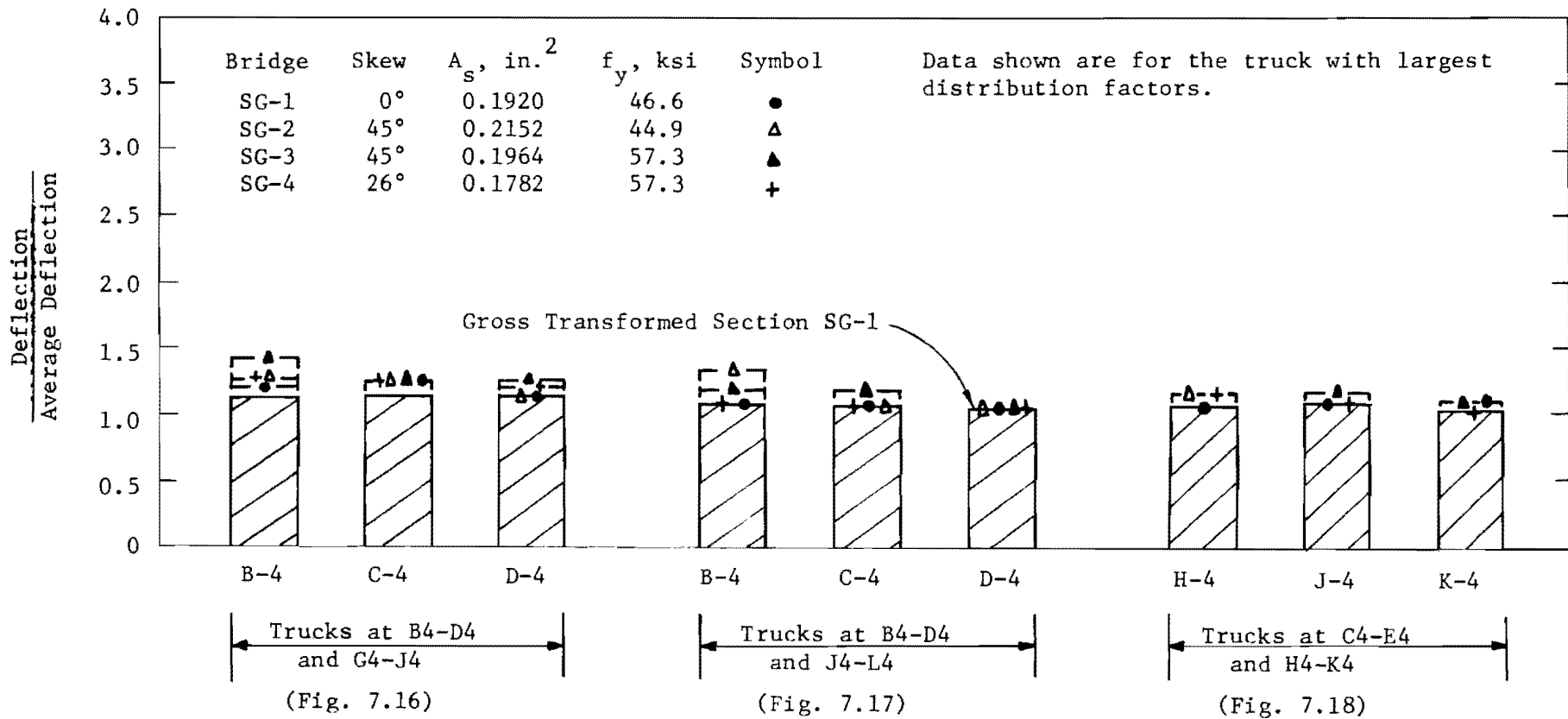


Fig. 7.23. Comparison between Experimental and Theoretical Deflection Distribution Factors for Two HS-20 Trucks with Varied Truck Placement.

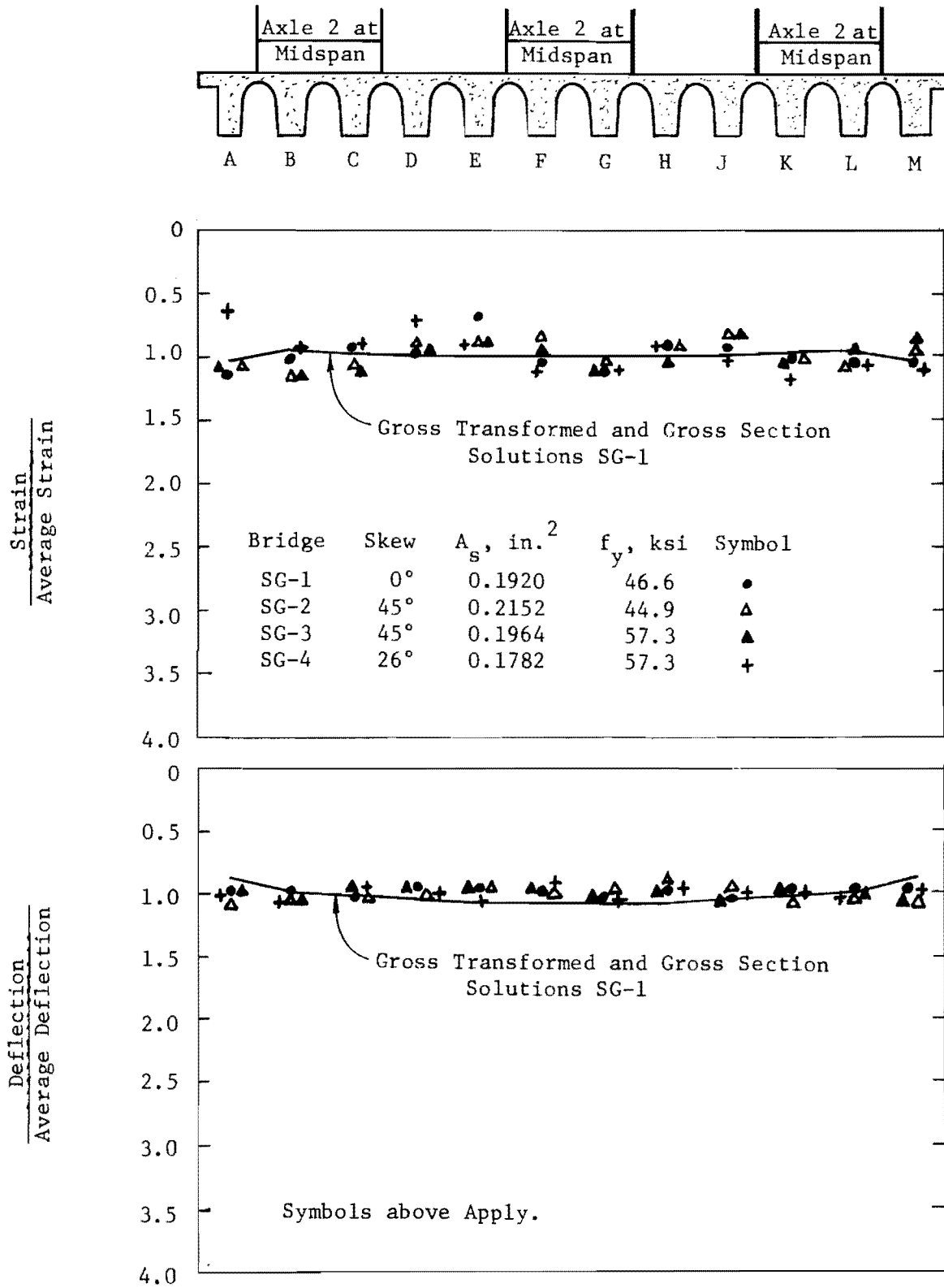


Fig. 7.24. Midspan Distribution Factors for Triple HS-20 Trucks.

7.4.7 Effect of Skew. The data in Sec. 7.4.3 through 7.4.6 indicate that the midspan strain and deflection distributions are not critically dependent on the angle of skew or steel percentage for the type of bridge tested. This cannot be stated conclusively, due to scatter in test data. It was felt that the effect of variation in skew would be more apparent if actual absolute magnitudes of strains and deflections were compared. Three similarly reinforced bridges were selected for comparison. Data for the three bridges are shown in Table 7.5. Model SG-4 has less reinforcement than SG-1 and SG-3, but was the only model available with an intermediate skew.

TABLE 7.5 BRIDGE DATA FOR SKEW COMPARISONS

Bridge	Skew	Model Span in.	A_s in. ²	f_y ksi	f'_c psi
SG-1	0°	87.27	0.1920	46.6	3770
SG-3	45°	95.64	0.1964	57.3	4320
SG-4	26°	91.09	0.1782	57.3	4750

Five typical loading cases are shown in Figs. 7.25 through 7.30. Data points shown are for measured midspan strains and deflections. Theoretical curves for the 0° skew bridge based on the discrete element solutions using both the gross and gross-transformed sections are also shown for comparison.

For these five loading cases the 0° skew bridge deflections are closely predicted by the gross-transformed section theoretical curve. Strain data are more erratic than deflection data, but generally fall between the two theoretical curves.

Strains on the right angle bridge near the load are always near or above the gross section solution while they are nearer the gross-transformed solution values away from the load. This indicates the local cracking effects near the load which are reflected in the strain measurements.

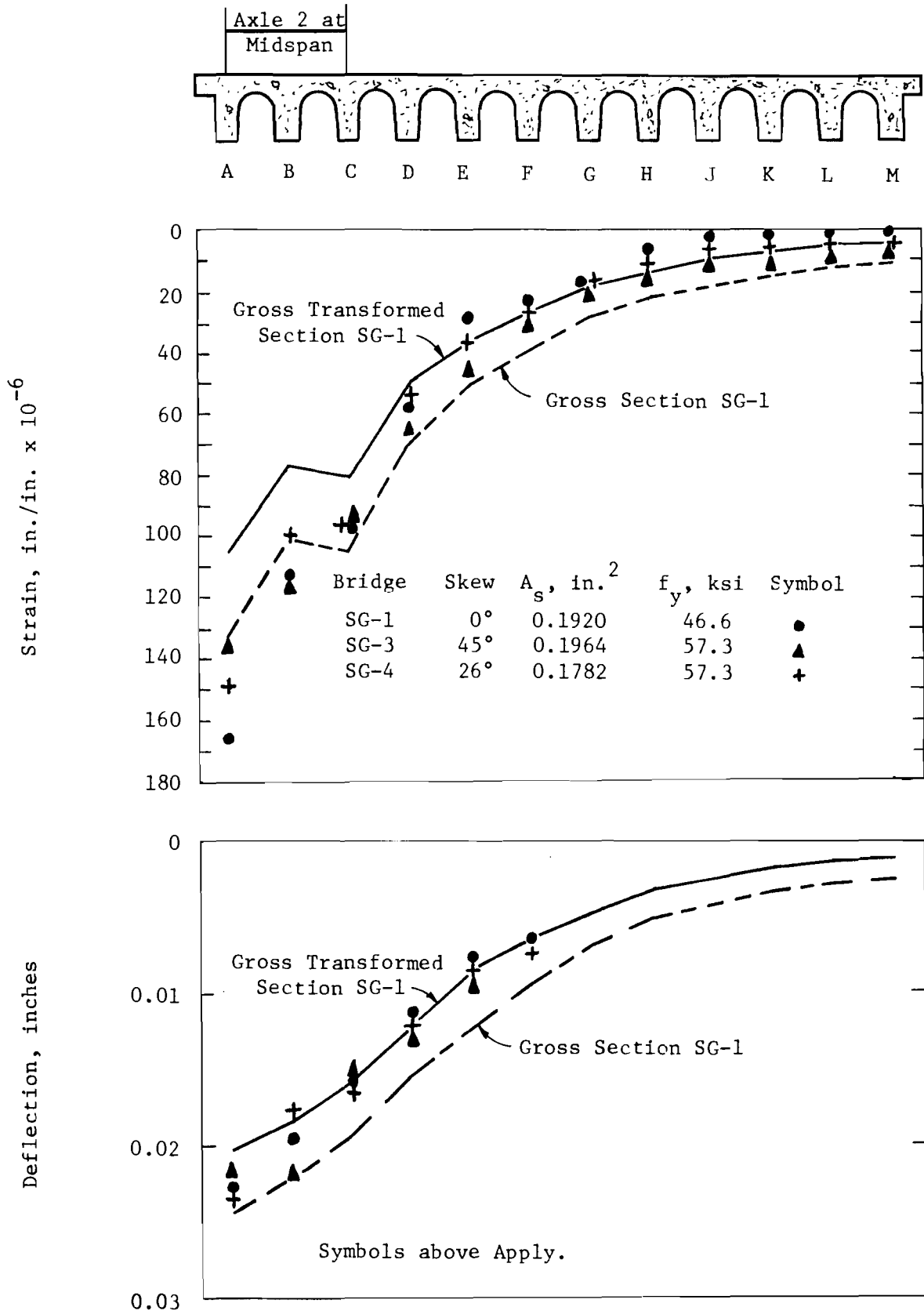


Fig. 7.25. Midspan Strains and Deflections for HS-20 Truck at A4-C4.

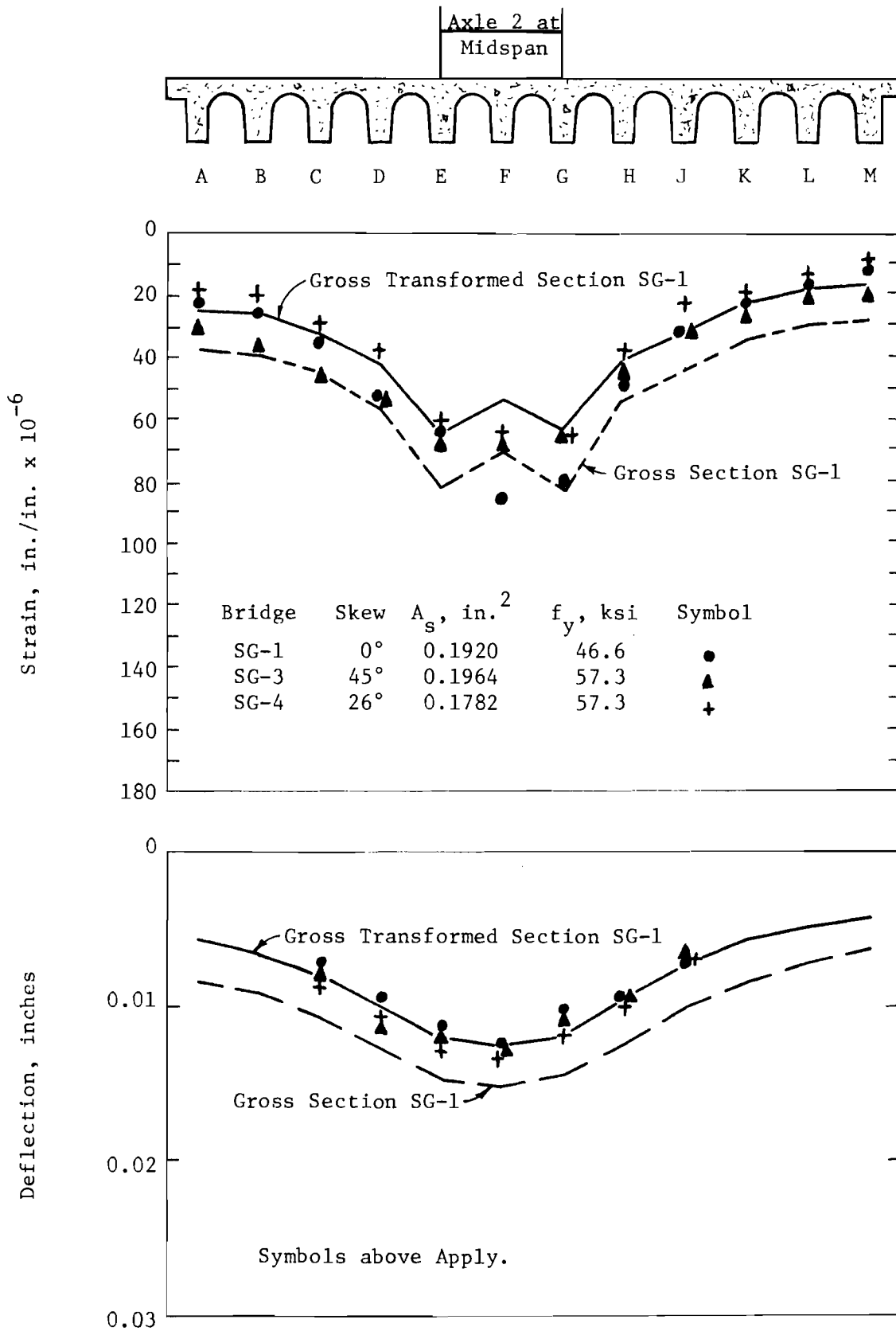


Fig. 7.26. Midspan Strains and Deflections for HS-20 Truck at E4-G4.

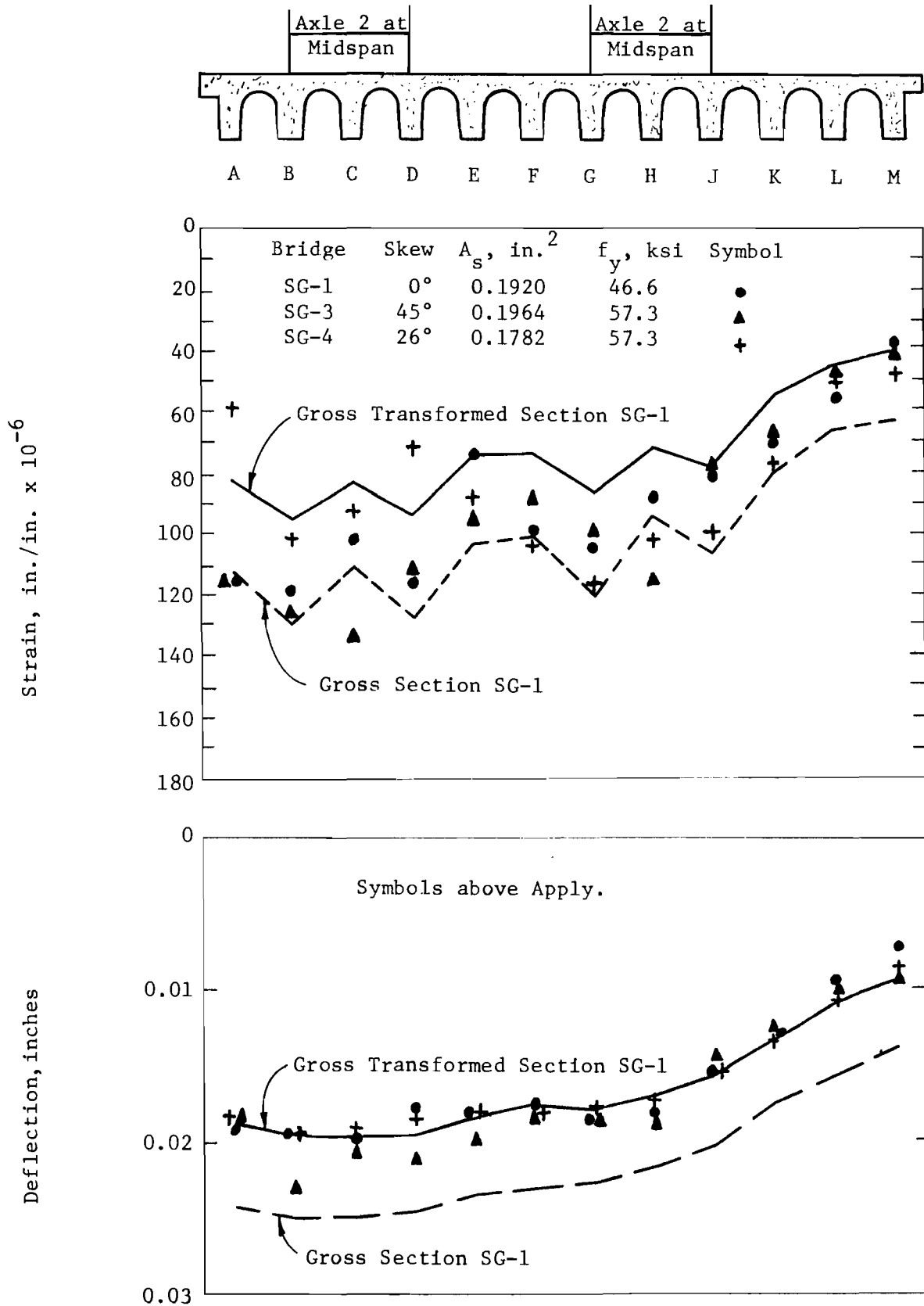


Fig. 7.27. Midspan Strains and Deflections for HS-20 Trucks at B4-D4 and G4-J4.

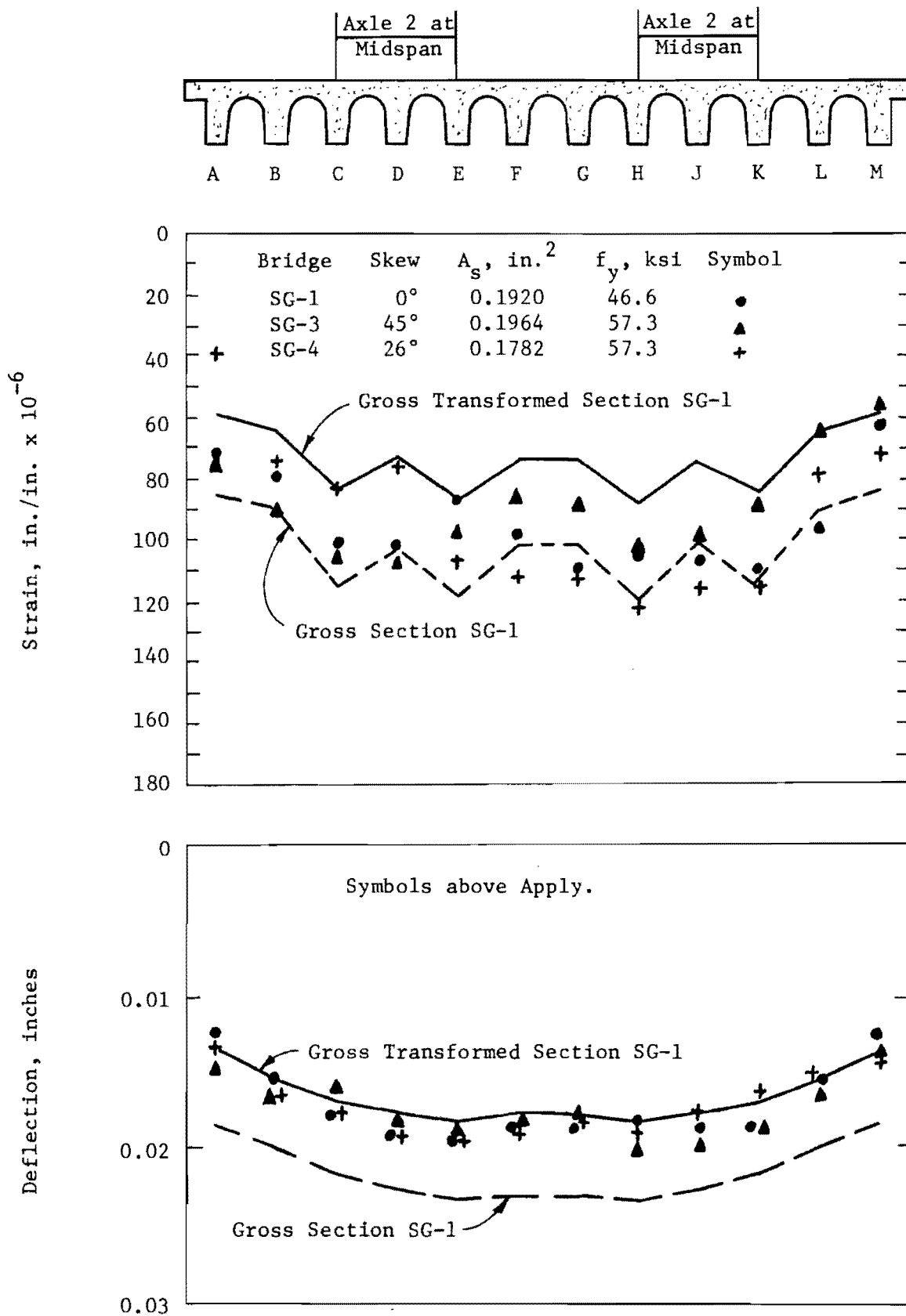


Fig. 7.28. Midspan Strains and Deflections for HS-20 Trucks at C4-E4 and H4-K4.

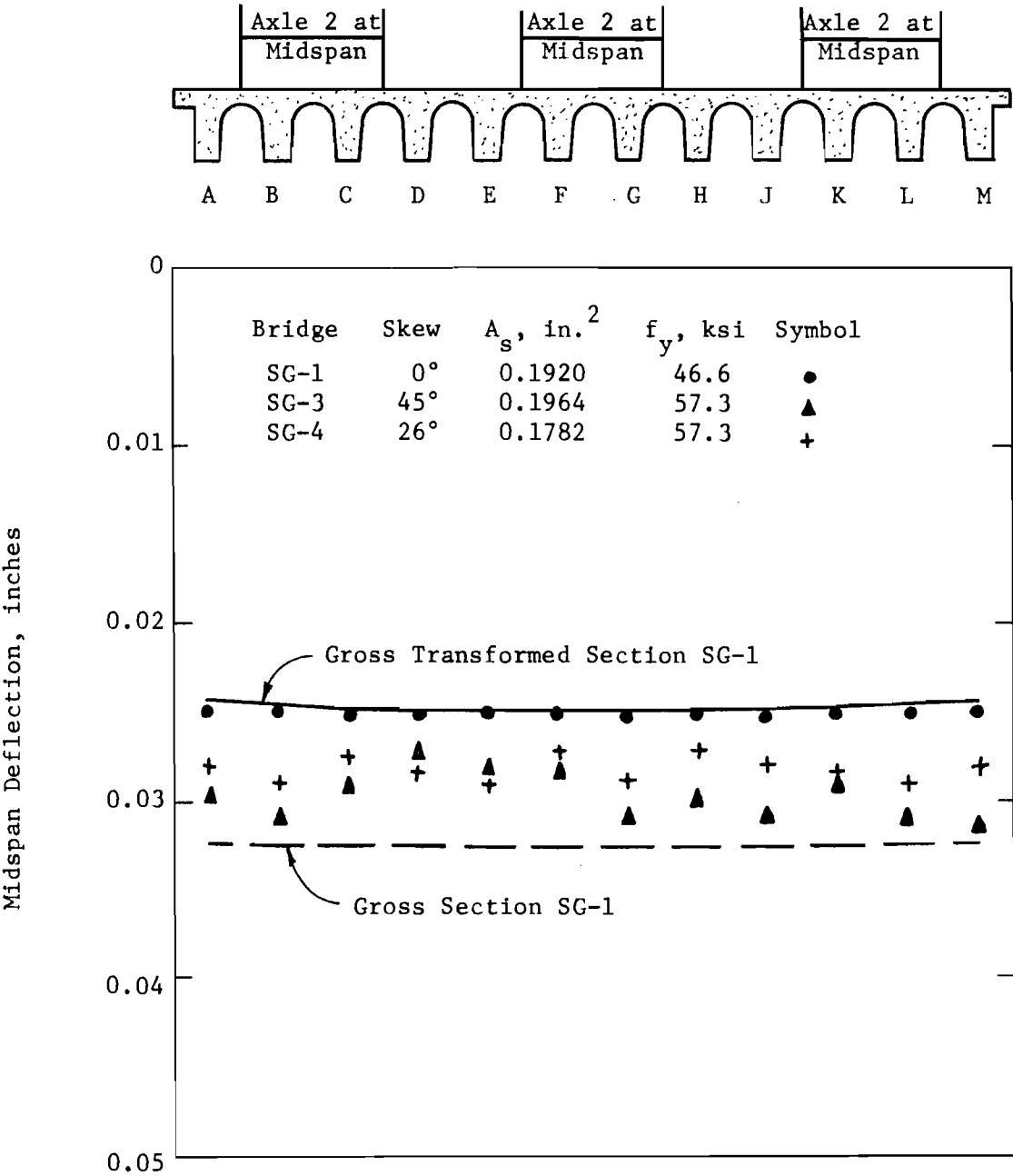


Fig. 7.29. Midspan Deflections for Triple HS-20 Trucks.

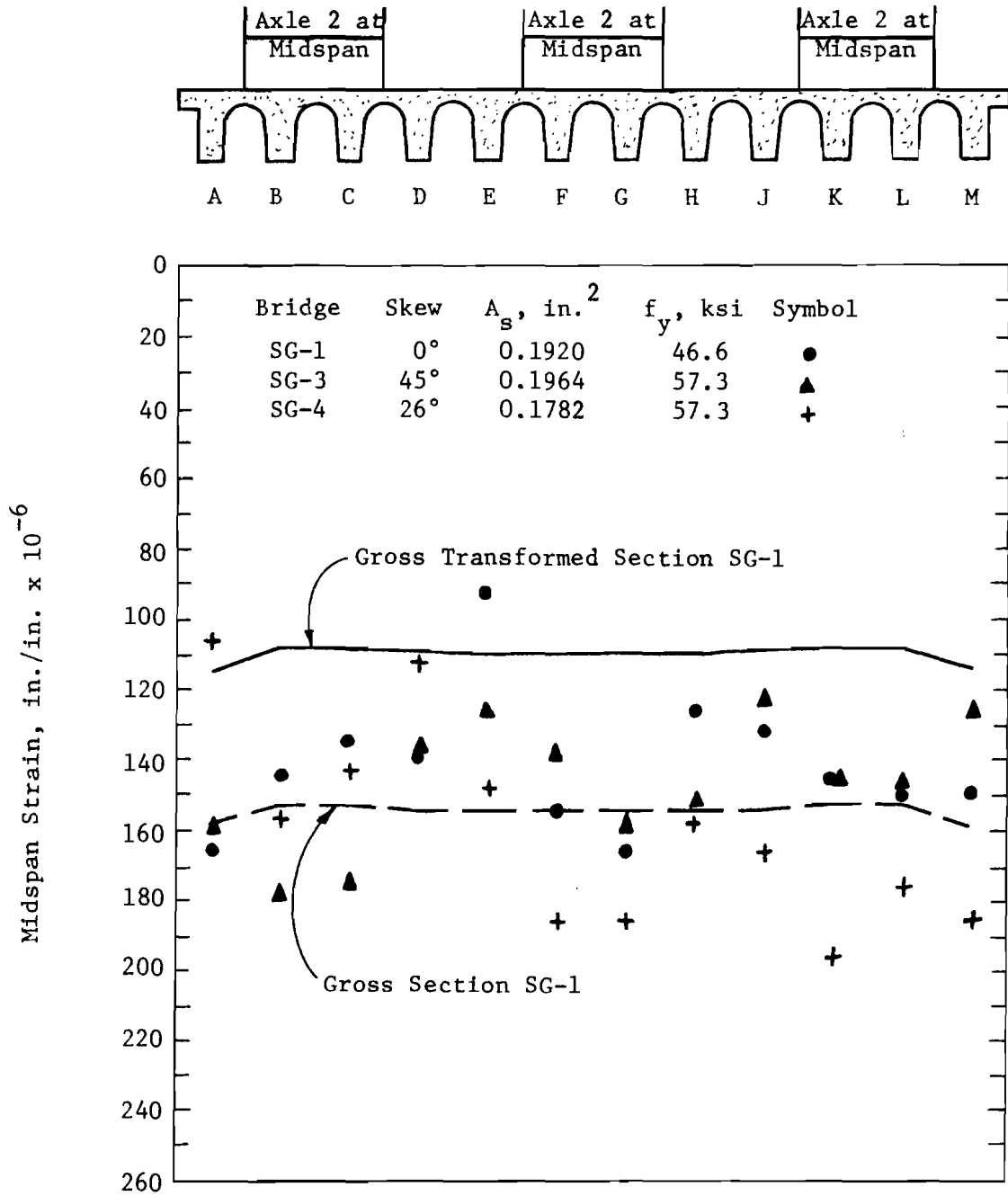


Fig. 7.30. Midspan Strains for Triple HS-20 Trucks.

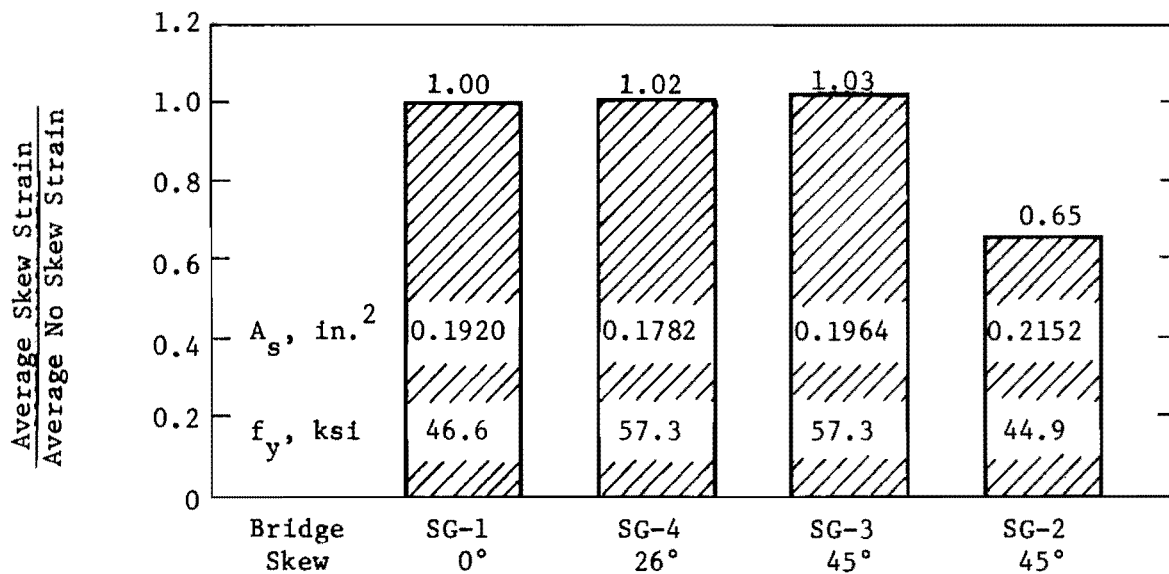
The local cracking does not significantly affect midspan deflections. Midspan deflections are affected by the state of cracking along the entire length of the span.

No consistent effect of skew is apparent in Figs. 7.25 through 7.30. While considerable scatter is evident it seems largely independent of skew. The possibility of a skew effect is investigated further in Fig. 7.31. In constructing Fig. 7.31 the average strain and deflection for all five loading cases in Figs. 7.25 through 7.30 were found for each bridge. Then, using the no-skew bridge as a basis of comparison, the relative average strains and deflections for the skew bridges were computed. The data for bridge SG-2 were not included in Figs. 7.25 through 7.30 because of the large difference in absolute values. However, the averaged results for this model are shown in Fig. 7.31.

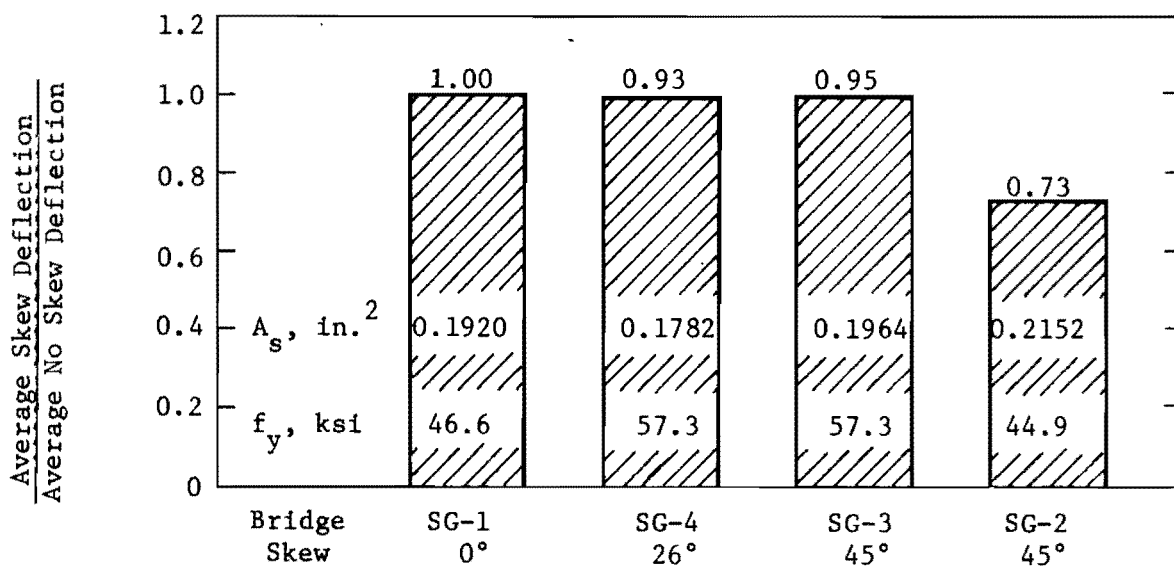
Both deflection and strain data indicate no appreciable difference among the similarly reinforced bridges. The difference in strains and deflections between SG-1 (0° skew) and SG-2 (45° skew) are significant. On the average the deflection for SG-2 (45° skew) was 73 percent of the 0° skew deflections.

The comparisons among the four bridges cannot be used to arrive at a definite conclusion of any skew effect. It is possible that the true measure of skew effect may be obscured by different states of cracking among the models.

7.4.8 Effect of Longitudinal Reinforcement Percentage. The effect of varying longitudinal reinforcement percentage was investigated by testing two 45° skew bridges SG-2 and SG-3. SG-2 was reinforced with four No. 2 bars and two SWG No. 11 wire (four No. 11 and two No. 5 bars in the prototype) of intermediate grade steel. SG-3 was reinforced with No. 2 bars (four No. 11 bars in the prototype) of A-432 grade steel. The ratios of steel areas should be 1.2, since the general design procedure would call for the steel in SG-3 to be reduced by the ratio of the allowable steel stresses (24 ksi/20 ksi). The actual ratio used was 1.1, since four No. 11 bars were assumed in the prototype rather than the more accurate reduced quantity of two No. 11 bars and two No. 10 bars. The decision to use four



(a) Effect on Strains.



(b) Effect on Deflections.

Fig. 7.31. Effect of Skew on Strains and Deflections.

No. 2 bars in the model was based on the desire to use available No. 2 deformed bars for the main flexural reinforcement.

Five loading cases are shown in Figs. 7.32 through 7.37. These are the same loading cases used in considering the effect of skew. Since both strain and deflection should be generally proportional to steel stress and since the steel stress is usually thought of as directly related to steel area, the strains and deflections in SG-3 might be expected to be 1.1 times as large as those measured in SG-2. However, as shown in Fig. 7.31, the average strain in SG-3 is 1.58 times the average strain in SG-2. This is probably due to somewhat more cracking in SG-3.

Referring to Fig. 7.2, the full dead load moment brought SG-3 to a marked cracking stage, while SG-2 was barely showing cracking effects. The ratio of $(DL + LL)/DL$ is 1.29 for one AASHO truck and 1.57 for two AASHO trucks. Since the ratio of steel areas is 1.1, model SG-2 should also display marked cracking effects under these loads but will always be stiffer than SG-3.

The observed deflection data for one AASHO truck in Figs. 7.32 and 7.33 do not show much difference between SG-2 and SG-3, although SG-3 (less A_s) shows somewhat larger deflections. The data for double trucks (Figs. 7.33 and 7.34) indicate a larger difference in deflections. The triple truck loading in Fig. 7.37 shows still larger deflections for SG-3. The strain data in Figs. 7.32 through 7.37 show the same trend.

Again, in Fig. 7.31 the average deflection for SG-3 is 1.3 times the average for SG-2. This confirms the effect of cracking on the higher stressed SG-3.

Model SG-2 (45° skew) shows a pronounced skew effect in Fig. 7.31 which reduced strains and deflections when compared to model SG-1 (no-skew). Model SG-3, which differed from SG-2 only by having 8.5 percent less steel area, does not show any significant skew effect at service loads. It was suggested in Sec. 7.4.7 that the effect of skew was obscured by different states of cracking among the models. The data in this section comparing models SG-2 and SG-3 (Figs. 7.32 through 7.37) support this idea, although no quantitative conclusion can be reached.

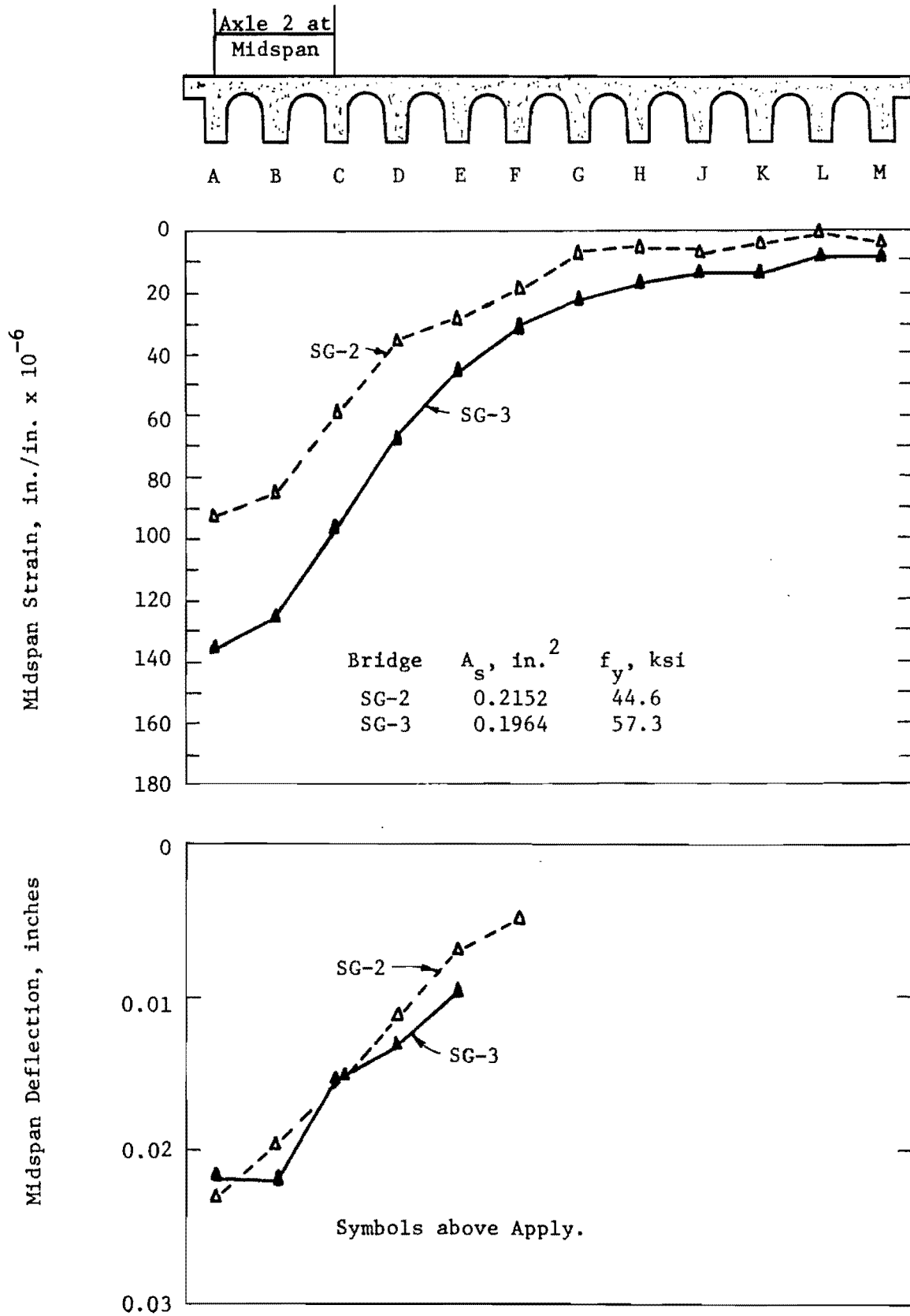


Fig. 7.32. Effect of Steel Percentage for HS-20 Truck at A4-C4 on 45° Skew Bridges.

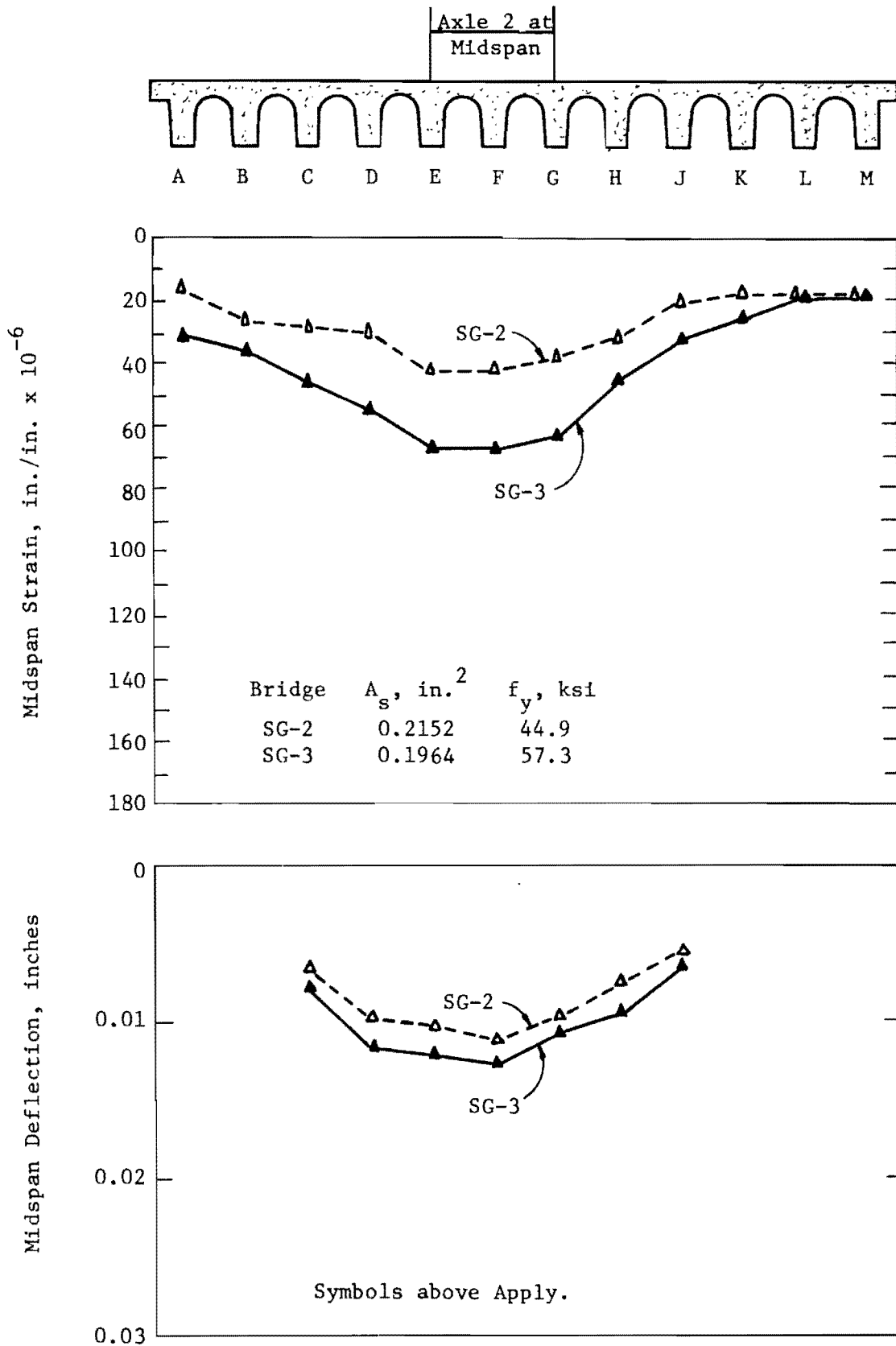


Fig. 7.33. Effect of Steel Percentage for HS-20 Truck at E4-G4 on 45° Skew Bridges.

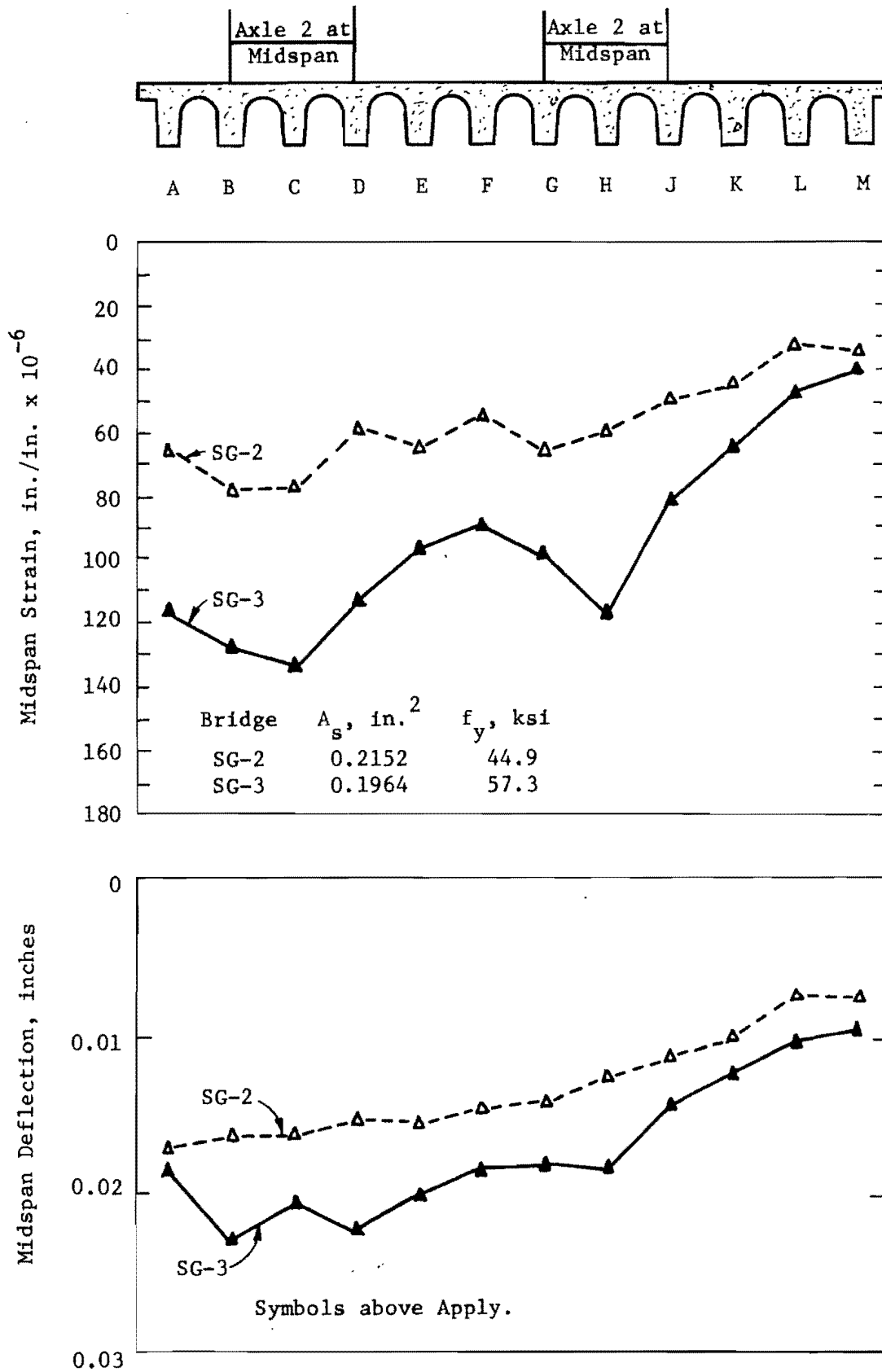


Fig. 7.34. Effect of Steel Percentage for HS-20 Trucks at B4-D4 and G4-J4 on 45° Skew Bridges.

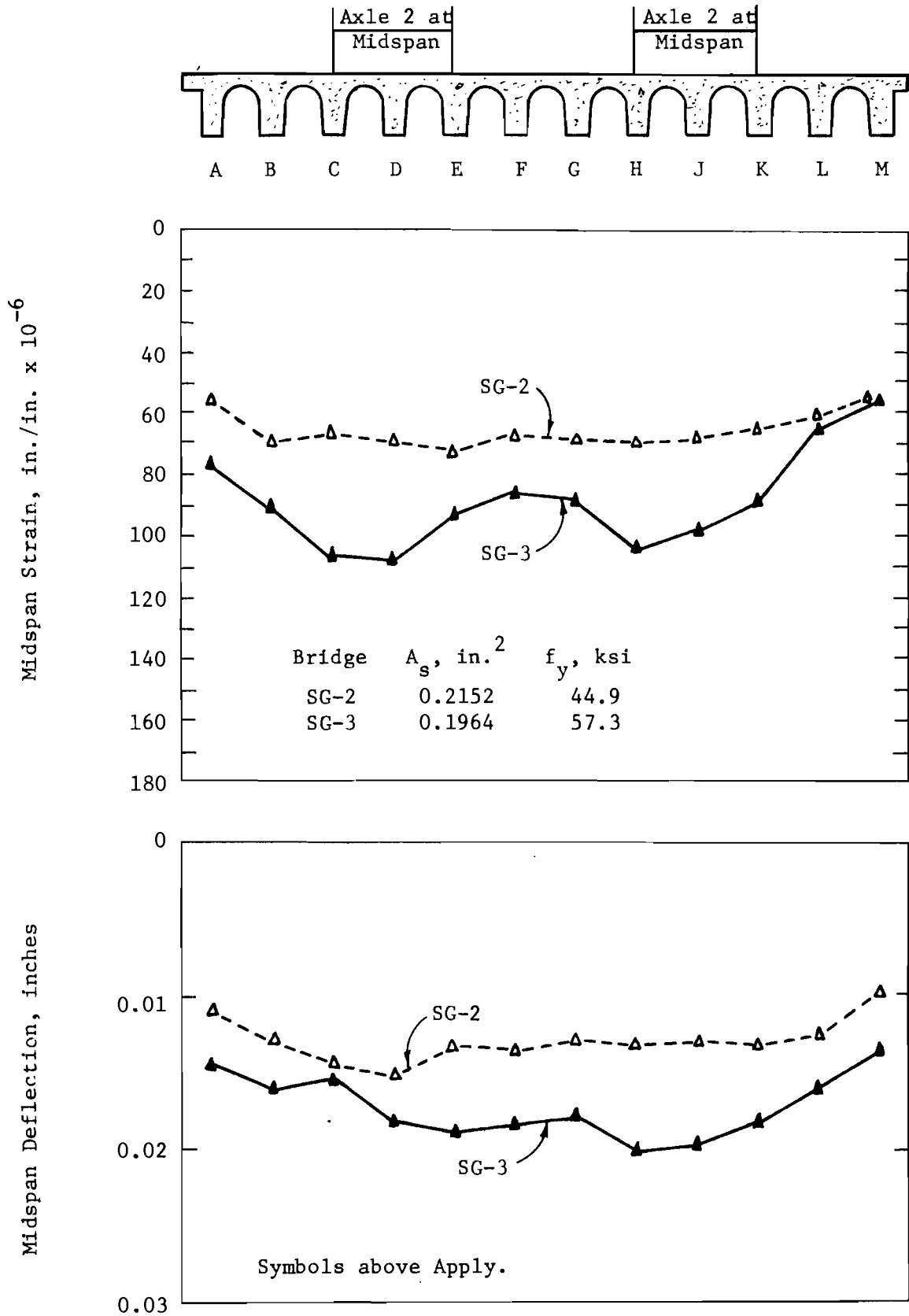


Fig. 7.35. Effect of Steel Percentage for HS-20 Trucks at C4-E4 and H4-K4 on 45° Skew Bridges.

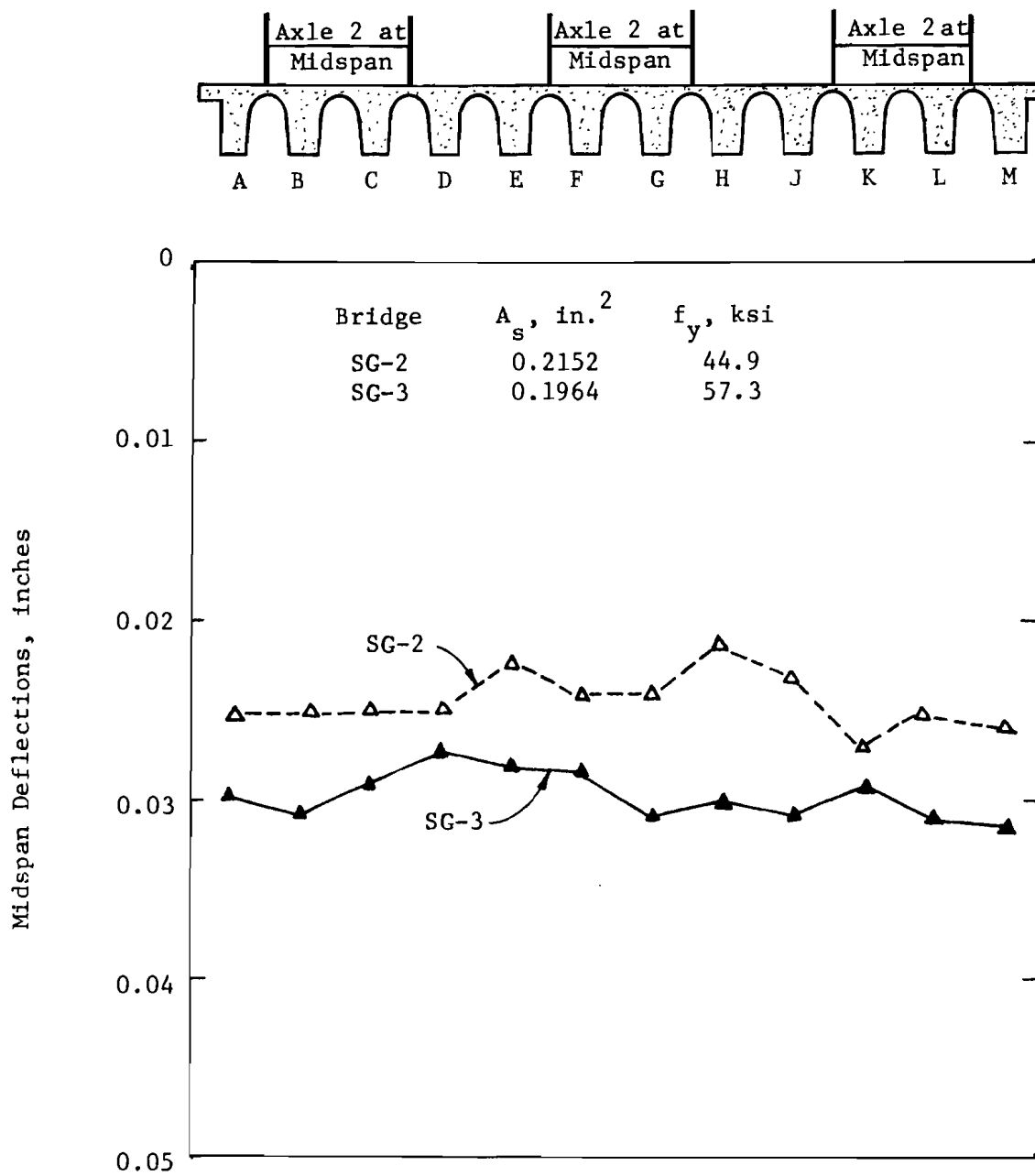


Fig. 7.36. Effect of Steel Percentage on Deflections for Triple HS-20 Trucks on 45° Skew Bridges.

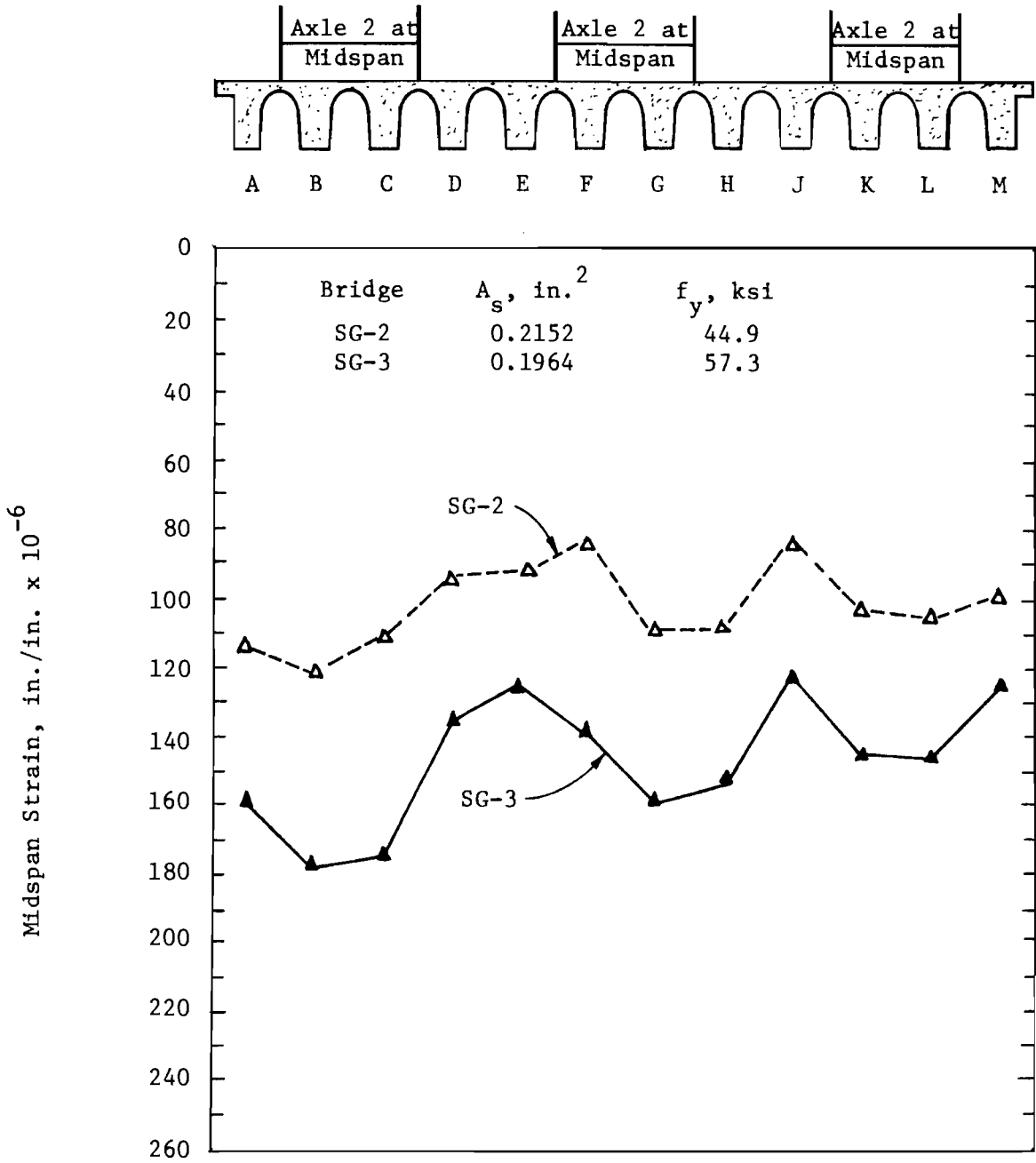


Fig. 7.37. Effect of Steel Percentage on Strains for Triple HS-20 Trucks on 45° Skew Bridges.

7.4.9 Transverse Strains. Magnitudes of transverse strains measured on the transverse mat reinforcement were small at service loads. An indication of the magnitudes of these strains is shown in Fig. 7.38a for an AASHO HS-20 truck at B4-D4. The transverse reinforcement size was the same for the four bridges tested (SWG No. 11).

At service loads, regardless of loading, the mat steel strain never exceeded a measured value of 30×10^{-6} in./in. This is a stress of 870 psi which indicates that the mat steel stress is so small that it is insignificant. This is reasonable if the concrete is uncracked, since the steel is at the midheight or neutral axis (in the transverse direction) at the thinnest portion of the slab.

The transverse midspan moments obtained from the discrete element solution are shown in Fig. 7.38b for an AASHO truck at B4-D4. The cracking moment for the transverse concrete slab system is also shown in Fig. 7.38b. The cracking moment was obtained by multiplying the split cylinder tensile strength by the section modulus for each discrete element slab segment. The comparison of the discrete element moments and the cracking moments indicates that the slab system is uncracked. This indicates that transverse moments are not critical in design criteria for this particular type of bridge and level of load.

7.5 Moderate Overloads

The overload truck described in Sec. 3.5.2 is the most severe loading allowed on the type of bridge tested and it is allowed only with special permits. Only one vehicle at a time is permitted on the bridge. Data are presented for a level of 1.0 overload plus impact. This is a load of 350 lb. per wheel on the model (10,582 lb./wheel on the prototype). The wheel lines are positioned over girders B and D.

7.5.1 Deflection and Strain Distribution. Deflection and strain distributions are shown in Fig. 7.39. The theoretical and experimental results are in about the same agreement as for the AASHO loadings. The experimental results do not show any clearly defined effect of skew angle.

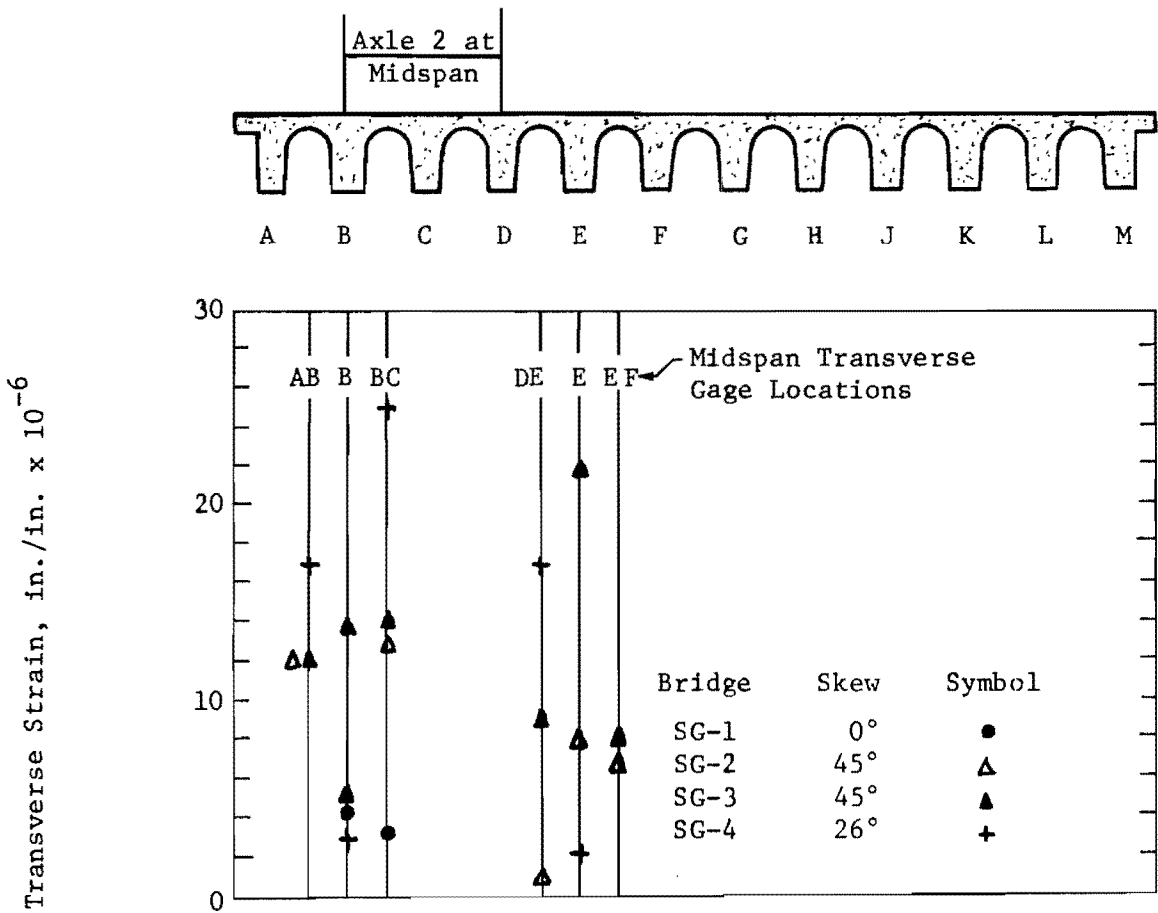


Fig. 7.38a. Magnitude of Transverse Strains under Service Loads.

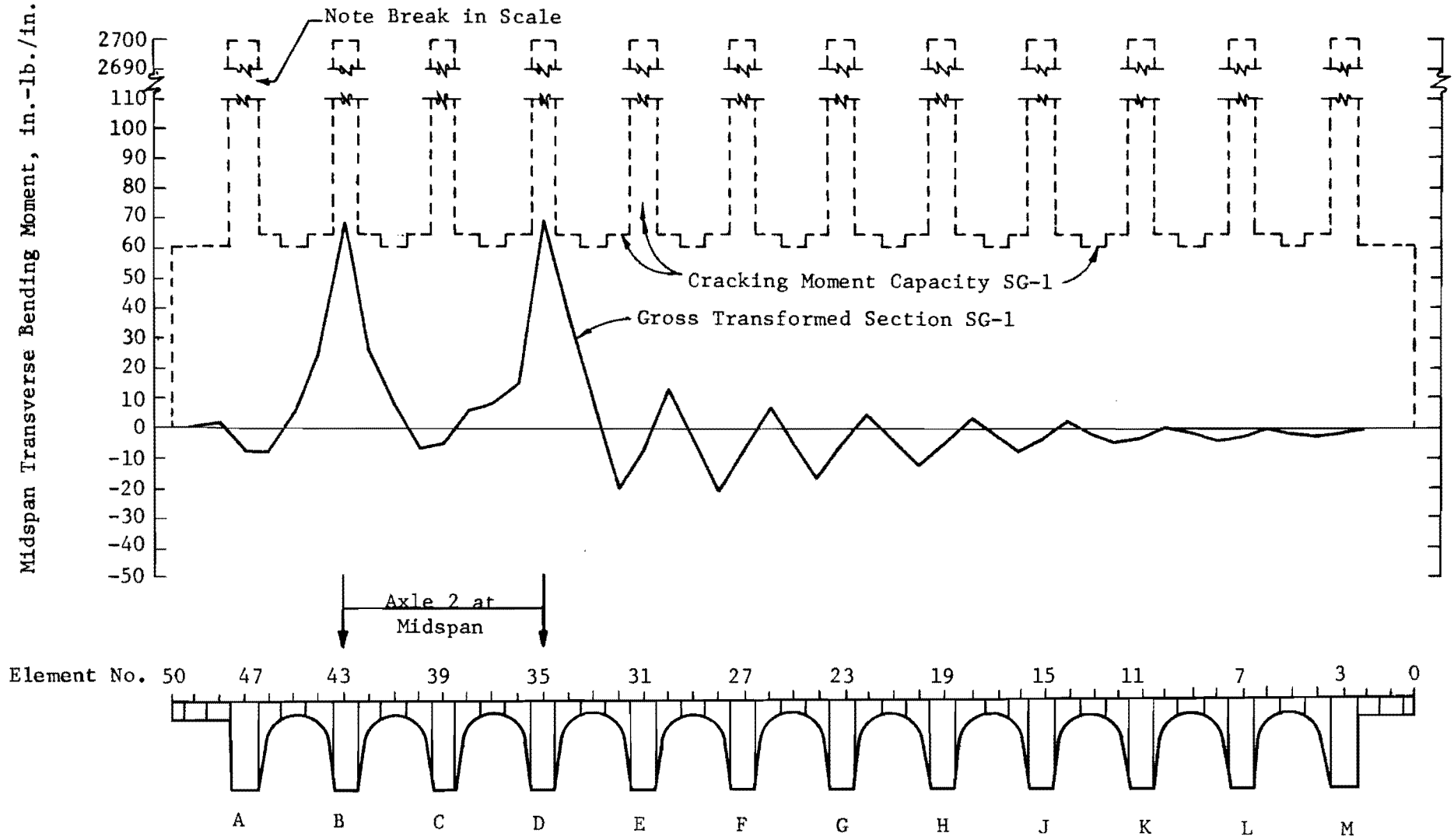


Fig. 7.38b. Transverse Bending Moments for One HS-20 Truck at B4-D4.

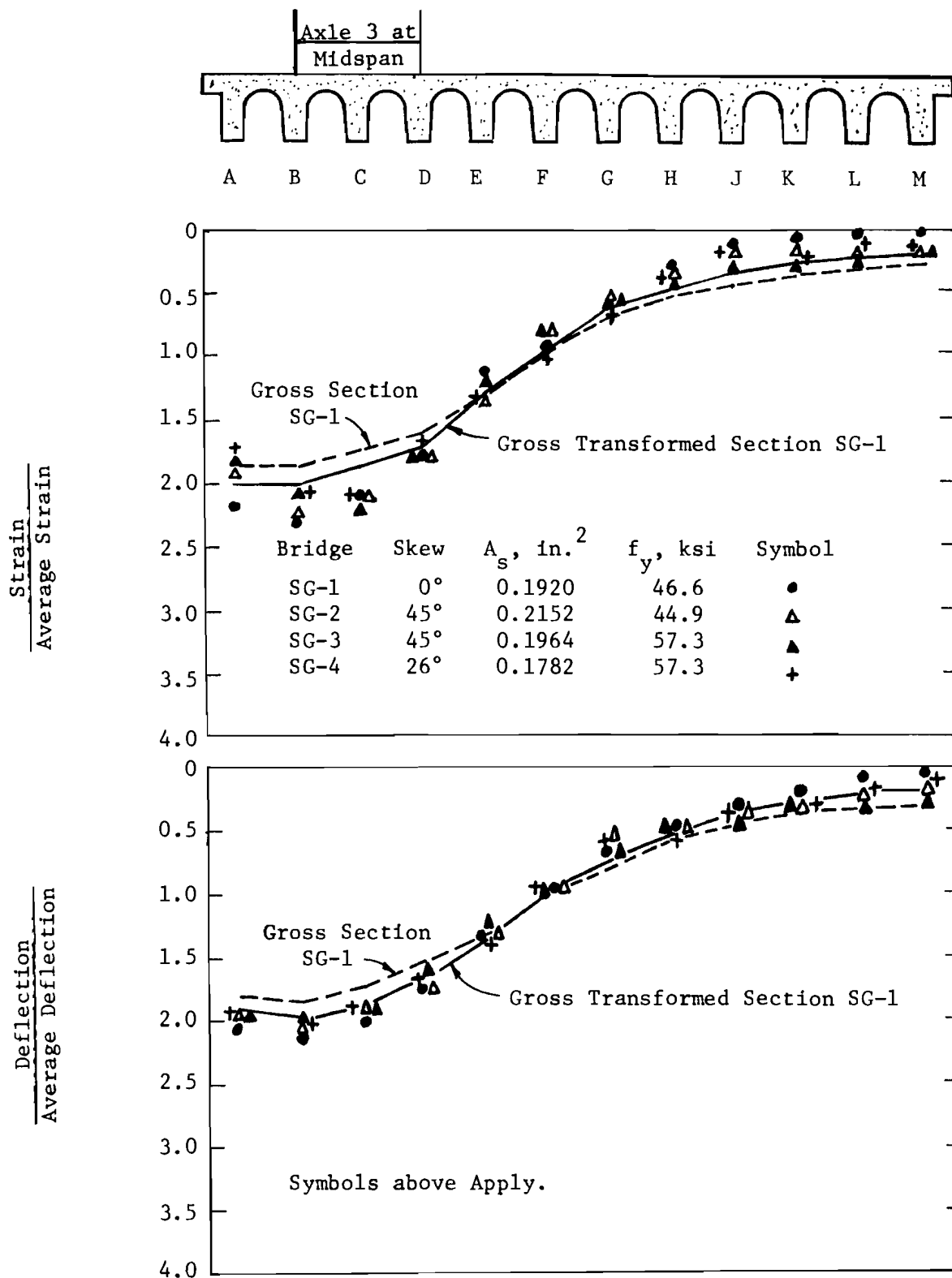


Fig. 7.39. Midspan Distribution of Strains and Deflections for 1.0 Overload Truck Plus Impact.

The strain distributions indicate that the three exterior girders may be designed using a load distribution factor $S/C = S/7.85$. This is a somewhat more favorable design factor than the $S/7.2$ obtained for an HS-20 truck similarly located (Fig. 7.16) and a substantial improvement over the AASHO design criterion of $S/6.0$.

The theoretical strain distributions for the HS truck (Fig. 7.16) and the overload truck (Fig. 7.39) differ markedly in the area of the wheel loads. In particular the overload truck does not exhibit the double peaks under the wheels indicated for the HS loading. This is apparently due to the interaction of the five closely spaced axles of the overload truck.

7.5.2 Effect of Skew and Steel Percentage. The actual magnitudes of deflections and strains are shown in Figs. 7.40 and 7.41, respectively. Theoretical curves are shown for the right angle bridge for comparison, using the gross-transformed and gross section properties.

Deflections in Fig. 7.40 are predicted accurately by the discrete element solution, using the gross-transformed section in the vicinity of the load for the right angle bridge. This same theoretical solution also is a good indicator of the deflection for SG-2 and SG-4. However, the deflections for the 45° skew bridge with low steel percentage exceed those of the right angle bridge SG-1. These deflections were about the same for the AASHO loadings.

Steel strains in the right angle bridge, SG-1, are of about the same magnitude as the theoretical solution using the gross section. This indicates increased cracking at midspan when compared to the AASHO HS-20 truck stress levels.

No clearly defined effect of skew may be observed in the strain or deflection data. Two changes are evident over the AASHO loadings. Bridges SG-1 and SG-4 still have about the same magnitudes of strain and deflection. However, SG-2 now has strains and deflections that are much closer to SG-1 than for the AASHO loadings. Deflections are now almost the same (previously 73 percent) and strains are about 85 percent of the right angle bridge strains compared to a previous average value of about 65 percent. On the other hand, the data for the more highly cracked model SG-3, which were about the same as for SG-1, are now about 30 percent greater in the area of the load.

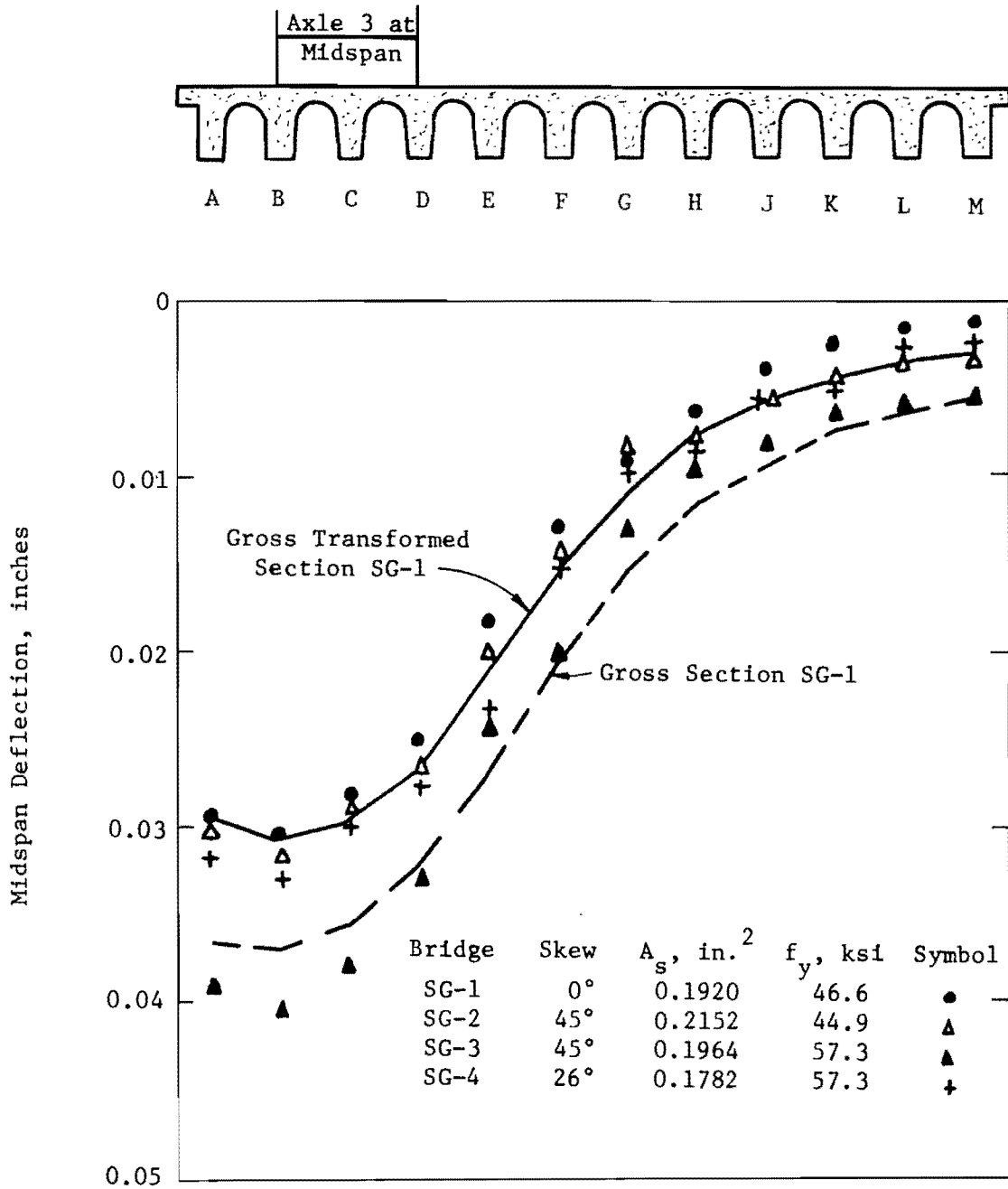


Fig. 7.40. Deflections for 1.0 Overload Truck Plus Impact at B4-D4.

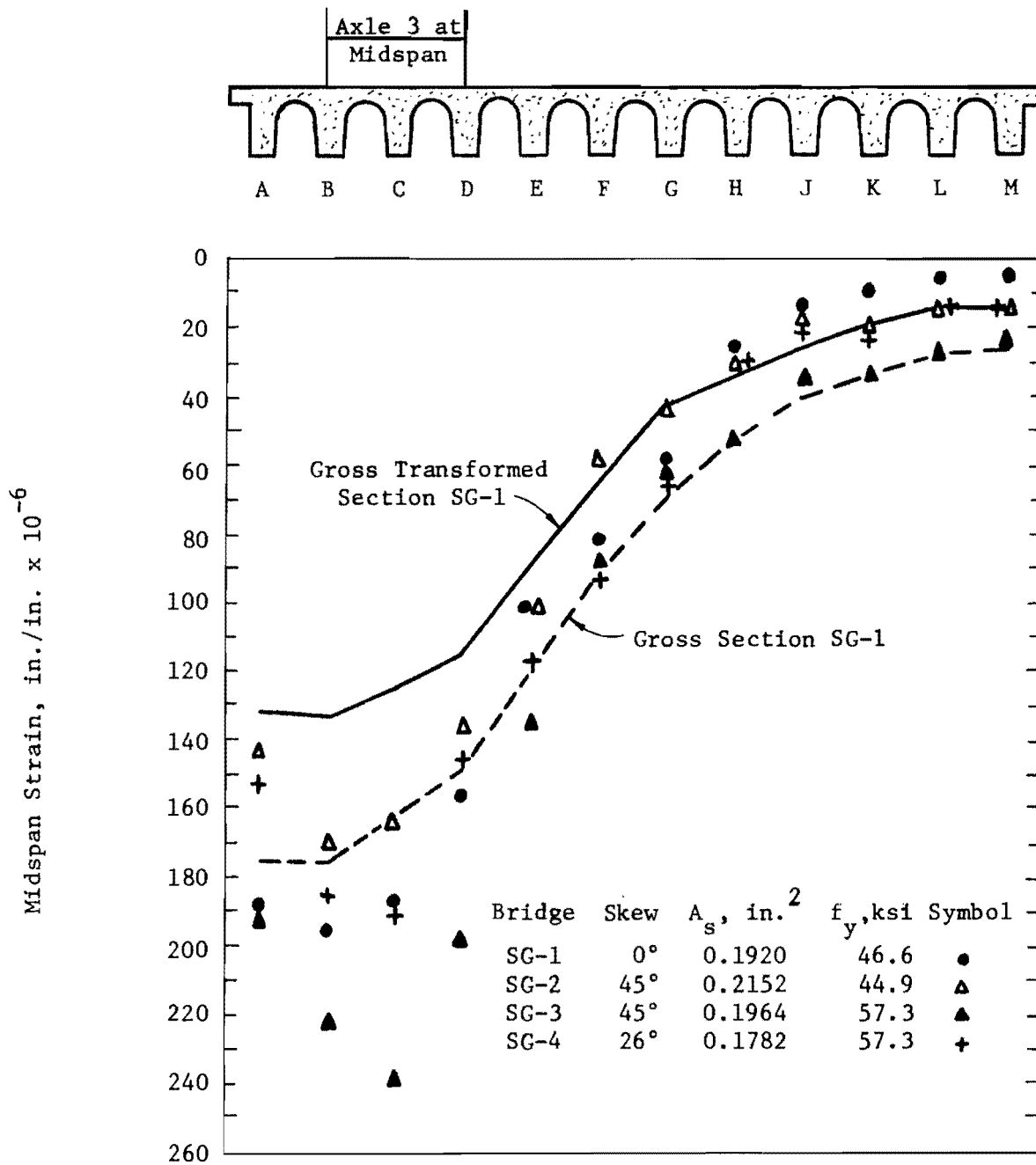


Fig. 7.41. Strains for 1.0 Overload Truck Plus Impact at B4-D4.

The two 45° skew bridges with different amounts of longitudinal reinforcement behave about the same as under the AASHO loadings. No significant differences are readily apparent.

7.5.3 Transverse Strains. Measured transverse strains were small with the overload truck in the position shown in Fig. 7.42. The maximum strain observed was on model SG-4 on crown BC. The observed strain was 45×10^{-6} in./in. or a stress of 1300 psi. This indicates that the transverse steel stress is not a design problem at this load level.

7.6 Ultimate Load Behavior

7.6.1 Introduction. The closely spaced multiple axle overload vehicle was used in the ultimate load tests for bridges SG-1, SG-2, and SG-3. The use of this loading in the ultimate tests was recommended by the Texas Highway Department, since it is the most severe loading allowed on this type bridge, even though a special permit is required.

The primary ultimate load position selected for SG-1, SG-2, and SG-3 was with axle 3 at B4-D4. Service load data indicate that an edge loading is the most severe transverse truck position. Clearance requirements from the face of the rail would make it very difficult to position the vehicle over A4-C4. A truck position over AB4-CD4 is just possible, but it was felt that the driver of such a heavy vehicle would drive nearer the center of the bridge. The position B4-D4 was a compromise between the most severe edge loading and the feeling that the truck driver would tend to stay away from the edge.

Load placement for secondary tests on SG-2 and SG-3 was selected based on an evaluation of the remaining structure following the failures during the primary ultimate load tests.

The ultimate loading selected for SG-4 was two H-20 trucks, the design vehicle for that bridge. It was felt that no significant additional information would be obtained by using the overload vehicle on this last model tested. The load positions selected were based on trucks traveling in two lanes. The intent was to obtain data on whether or not all girders could be yielded with more than one truck on the bridge.

7.6.2 Factor of Safety. The overall factor of safety, FS, for each of the bridges is computed from

$$FS = \frac{UL}{DL + (LL + I)} \quad (7.12)$$

where

UL = ultimate load = DL + X(LL + I)

DL = dead load

X = number of (LL + I) units

LL = live load

I = impact load = 0.30 LL

In view of the generally low LL/DL ratios used and the relative certainty of dead load calculations, the live load plus impact factor of safety, X, should be of substantial interest as the primary measure of overload capacity.

7.6.3 Model SG-1, 0° Skew. Model SG-1 was tested to failure using the wheel pattern of the overload truck. Axle 3 of the test vehicle was placed at midspan with the wheel lines over girders B and D as indicated in the top of Fig. 7.43. Wheel loads were increased monotonically until failure occurred. The load increments were multiples of 350 pounds per wheel, representing 1.0 overload truck plus impact of 30 percent, 1.0(OL + I).^{*} Readings were taken of all strain gages and both midspan and support dial gages after each load increment. In addition, dial gages located at the quarter points were read every other load increment.

Midspan live load deflections are shown in Fig. 7.43 at intervals of 1.0(OL + I)(350 lb./wheel) until failure. Data taken between these intervals are not shown. Girder deflection data are shown with a solid circle before yield of the longitudinal tensile steel.

Midspan strains observed during the test are shown in Fig. 7.44. The strains at zero live load are dead load strains immediately before starting the ultimate load cycle.

^{*}OL + I = overload truck plus impact.

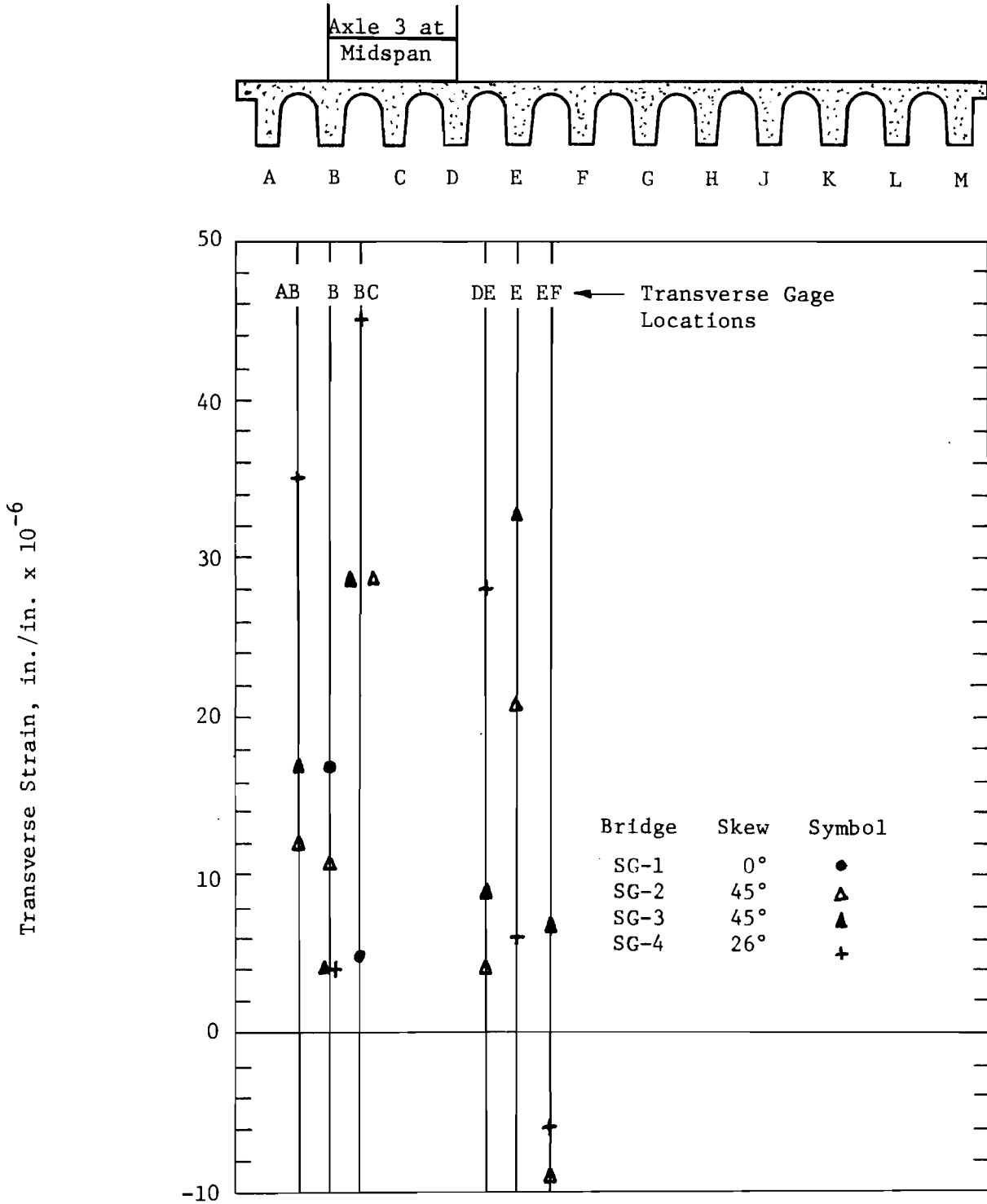


Fig. 7.42. Transverse Steel Strains for 1.0 Overload Truck Plus Impact.

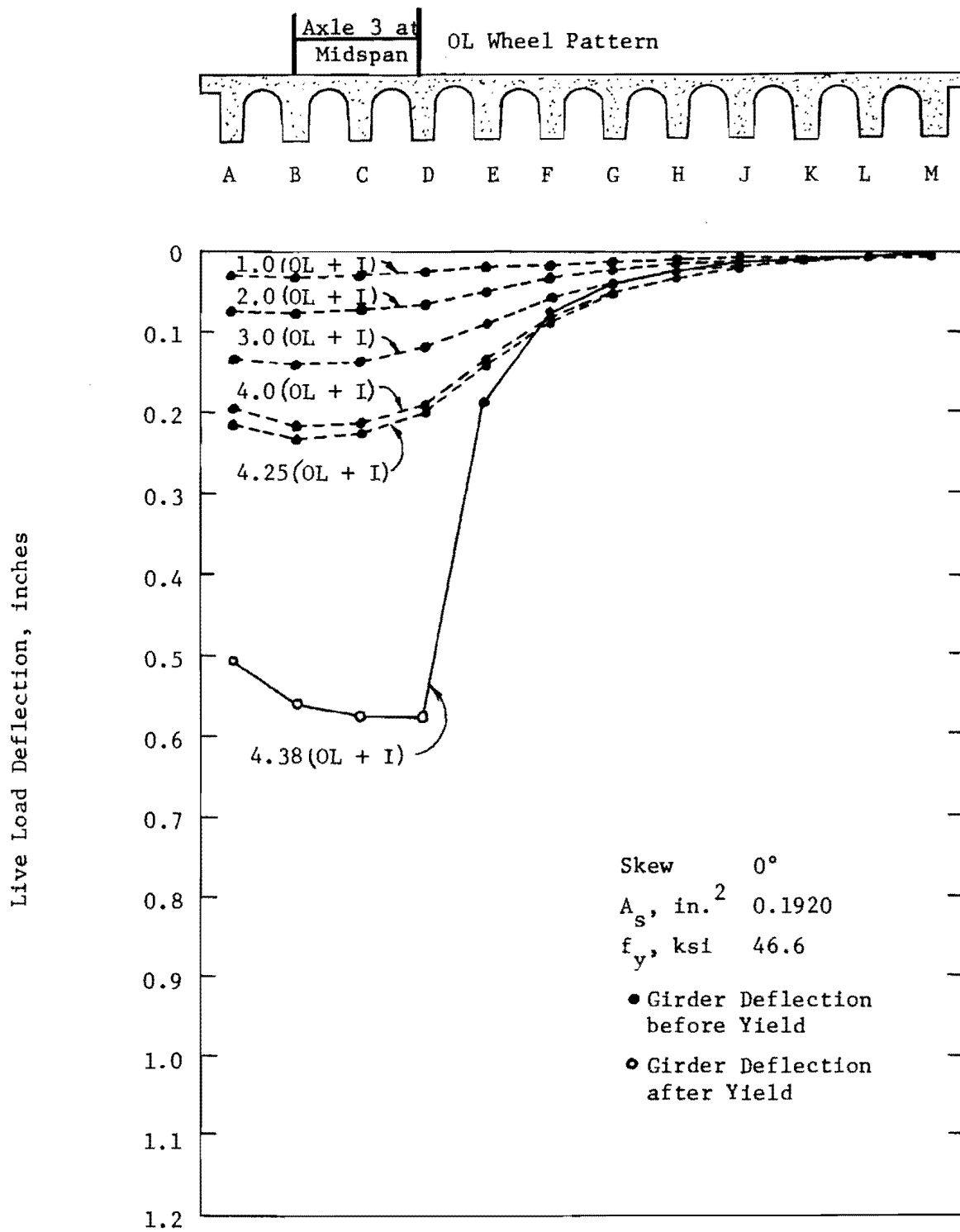


Fig. 7.43. Midspan Deflection for SG-1 during Ultimate Load Cycle.

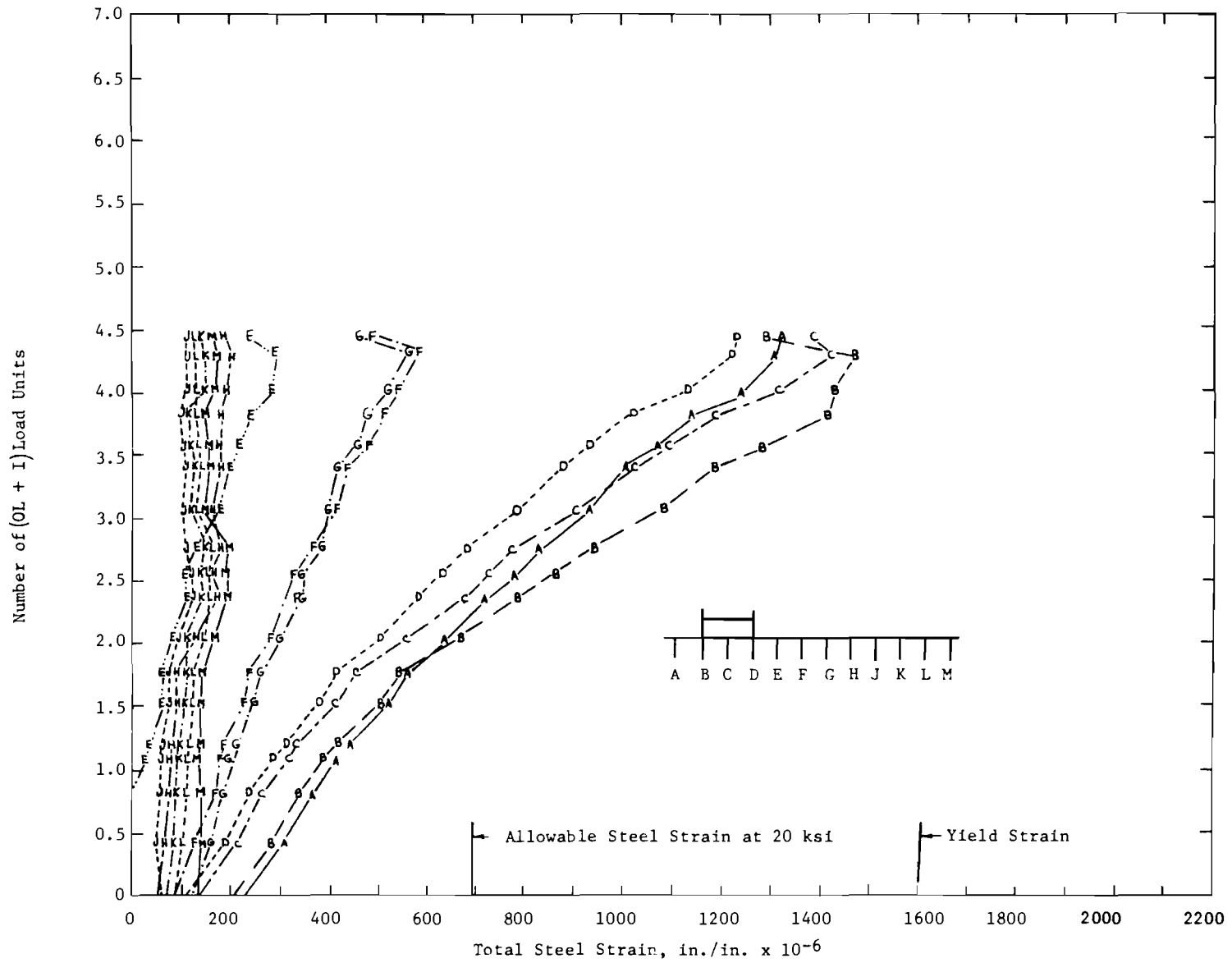


Fig. 7.44. Midspan Strain for SQ-1 during Ultimate Load Cycle.

The allowable steel stress in this model was 20.0 ksi. At a load of $2.0(OL + I)$ the total stress (including that due to dead load) in girder B at midspan was 19.6 ksi. At $2.3(OL + I)$ the steel stress in girders A, B, and C had exceeded the allowable steel stress. The steel in girder D exceeded the design stress at $2.7(OL + I)$. Only the steel in these four girders yielded at ultimate load.

The dead load strain on gage E was subject to significant drift during the course of the test. This gage indicated a compressive strain at the start of the ultimate loading and probably should be discarded. The actual dead load strain should be much nearer that of girder F.

Deflections increased rapidly when the steel yielded in girders A, B, C and D. The deflection increase may be observed in Fig. 7.43 by comparing data taken at $4.38(OL + I)$ with data taken at $4.25(OL + I)$, the preceding load level. Strain gage readings do not clearly indicate yield of steel, although it was determined that yield had occurred by observation of crack widths. A massive longitudinal break through the slab, progressing from quarter-point to quarter-point, occurred between girders D and E at $4.38(OL + I)$. This crack is shown in Fig. 7.45. The formation of this crack prevented the further transfer of any significant load to other girders. Close examination of this longitudinal break indicates that it is predominantly due to shear-diagonal tension rather than torsion or transverse bending. The formation of this crack or break occurs as a secondary failure in the general mode of failure.

The formation of the slab break between girders D and E caused a sudden drop in applied load. In order to obtain meaningful deflection data the load was allowed to drop slightly rather than maintaining load. This is probably the reason the strain in girders A through D do not show clear yielding of longitudinal steel, since they were taken while the load was dropping.

An investigation of strain data in the girder steel indicated that gage E registered unusually low strains, even when considering a shift in dead load strain. If the curve for gage E is moved to have the same starting point as gage F, then the strains are about the same as for gage F. It is felt that the true strain should lie between girders D and F. If E is

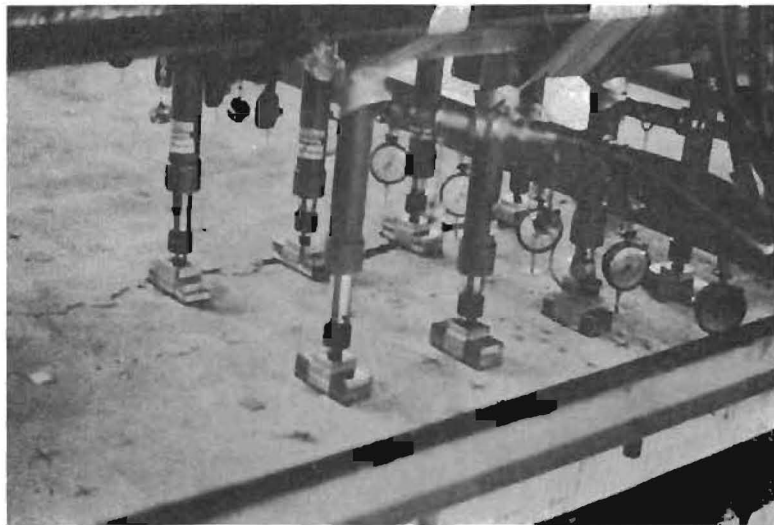


Fig. 7.45. Longitudinal Crack between
Girders D and E, Model SG-1.

assumed midway between D and F, then the tensile steel in girder E reached 70 to 80 percent of the yield strain. This is thought to be closer to the actual case.

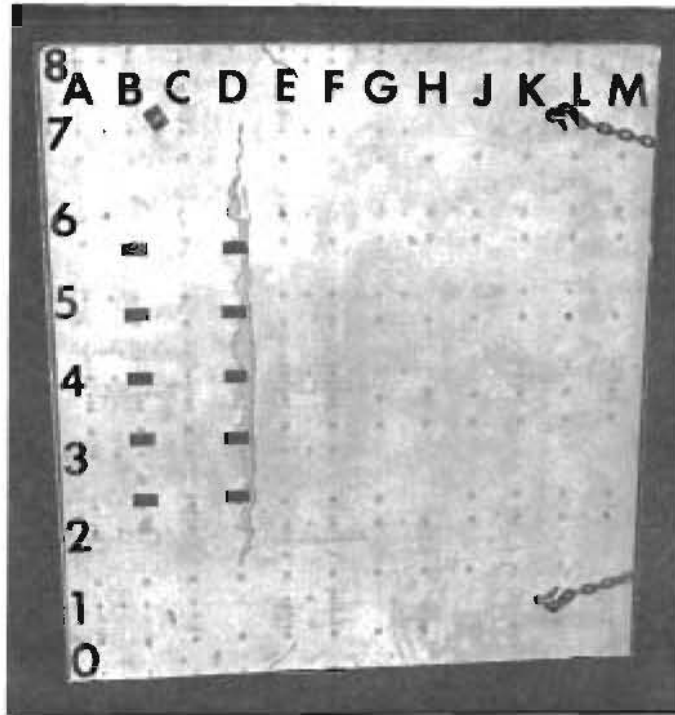
The complete crack patterns for the top and bottom of the bridge are shown in Fig. 7.46. The ten small rectangles are the load connections near midspan of the highly loaded girders rather than being more uniformly spaced over the girder length. This is considered to be the result of using smooth bars for the main flexural reinforcement in this bridge.

The measured total factor of safety against failure at $4.38(OL + I)$ is 2.25 for this bridge and loading.

7.6.4 Model SG-2, 45° Skew. Model SG-2 was tested to failure under two loading conditions, both using the wheel pattern of the overload truck. In the first test Axle 3 was placed at midspan over girders B and D for a flexural test. The second test was conducted with the truck placed near the support for a shear test with the wheels over girder J and L on the relatively undamaged side. In both tests wheel loads were increased monotonically until failure occurred. The load increments were multiples of 350 lb./wheel representing $1.0(OL + I)$. After each increment of load was added, readings were taken of all strain gages and both midspan and support dial gages. Dial gages located at the quarter-points were read every other load increment.

Midspan deflections for live load are shown in Fig. 7.47 for the first ultimate load test. Deflections plotted with an open circle indicate that the steel in that location has yielded.

Midspan strains observed during the test are shown in Fig. 7.48. The strains at zero live load are dead load strains immediately before starting the ultimate load cycle. The allowable steel stress in this model was 20.0 ksi. This stress was exceeded in girders B and C at a load of $2.0(OL + I)$. At a load of $2.5(OL + I)$ the design stress was exceeded in girders A, B, C, and D. Girder E exceeded the design stress at $3.0(OL + I)$. The steel in girders A, B, C, and D yielded at failure, while the steel in girder E reached 93.5 percent of yield.



Top View

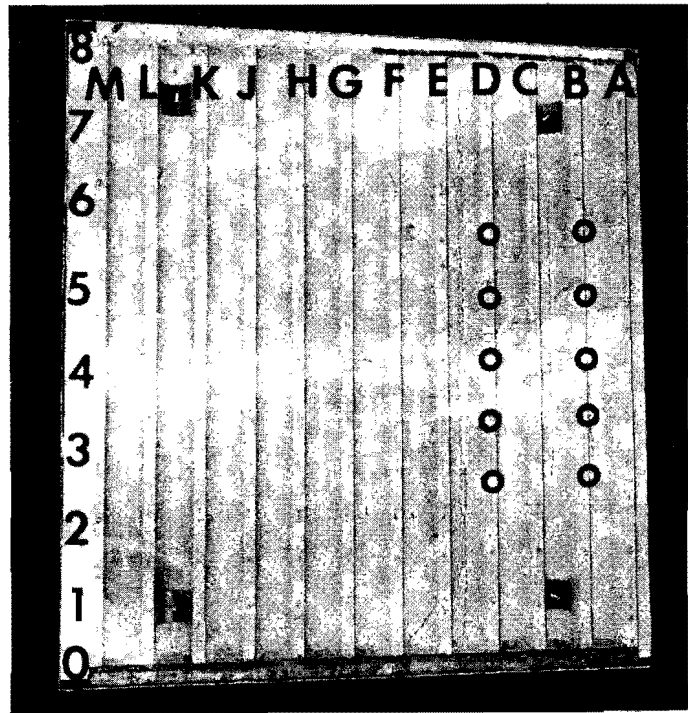


Bottom View

Fig. 7.46. SG-1 Crack Pattern.



Top View



Bottom View

Fig. 7.46. SG-1 Crack Pattern.

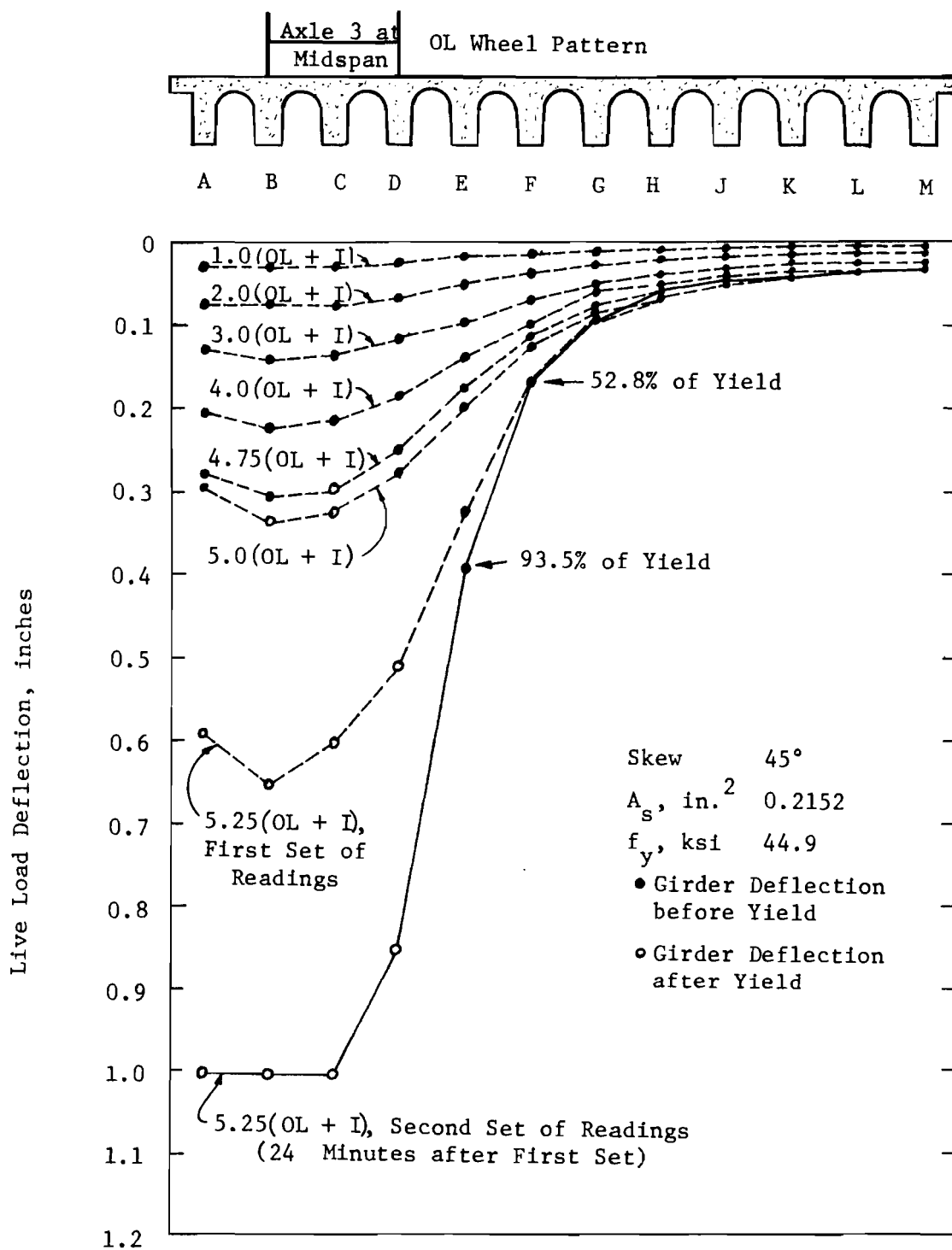


Fig. 7.47. Midspan Deflection for SG-2 during First Ultimate Load Cycle.

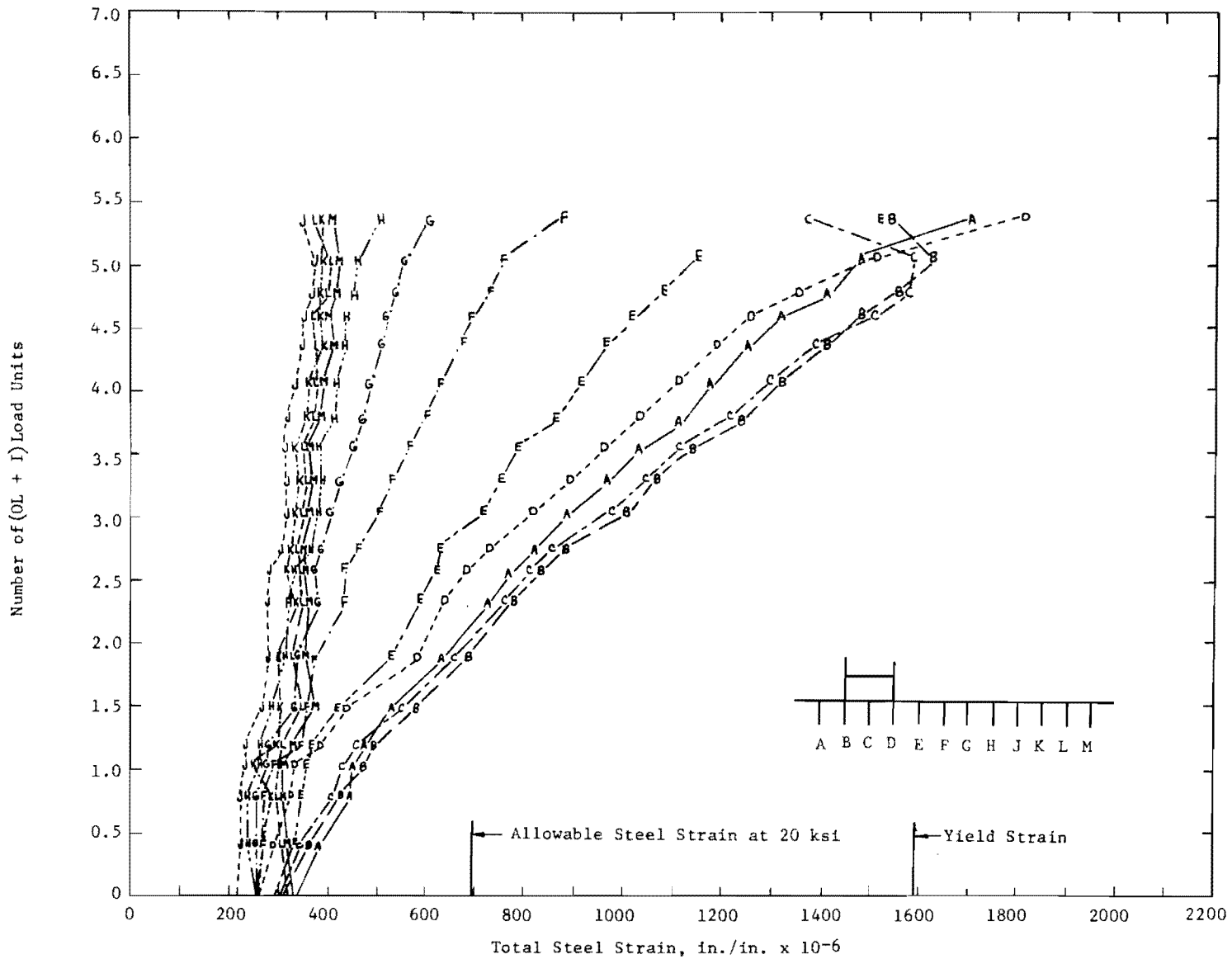


Fig. 7.48. Midspan Strain for SG-2 during First Ultimate Load Cycle.

The first yield of steel occurred at a load level of $4.75(OL + I)$ in girder C. Referring to the crack pattern in Fig. 7.49, the cracks in the bottom of the crown between A and B and B and C were formed at the same time. The cracks from A to F were formed by the first ultimate test, while the cracks from G to H were formed by the second ultimate test. The crack between F and G was a combination of both tests.

As indicated in Fig. 7.47, the yielding in this bridge was more gradual than the yielding in model SG-1. Numerous cracks began to form in the top of the slab at $5.25(OL + I)$. Instrumentation indicated that failure was close, so a second set of readings was taken. Both sets of data are shown in Fig. 7.47.

A massive longitudinal break formed in the slab between girders D and E at $5.25(OL + I)$ preventing further transfer of load to other girders. This was similar to the break in model SG-1. Girders A, B, C, and D yielded at failure. A fifth girder E was at 93.5 percent of yield. The factor of safety against failure was 2.42.

The complete crack pattern is shown in Fig. 7.49.

The second ultimate test was intended to represent maximum shear loading and was conducted with the wheels of the overload truck located as shown in Fig. 7.49 with the wheels as close to the support as possible while still having all wheels on the bridge. The maximum moment due to live load occurs under the fourth axle from grid line zero. General yielding between grid lines three and four was indicated by flexural cracking. Midspan deflections and strains are shown in Figs. 7.50 and 7.51, respectively.

The failure was a flexural type with the steel yielding in girders H through M. The sequence of yielding is not known, since the strain gages at midspan were not at the position of maximum moment. They were the nearest gages to the points of maximum moment. An ultimate load of $6.25(OL + I)$ was reached in this test. This load was not maintained long enough for deflection and strain readings to be obtained. The overall factor of safety was 2.63.

The purpose of this test was to see if shear in the girders was a design problem. Except for being closer to the support, this test was

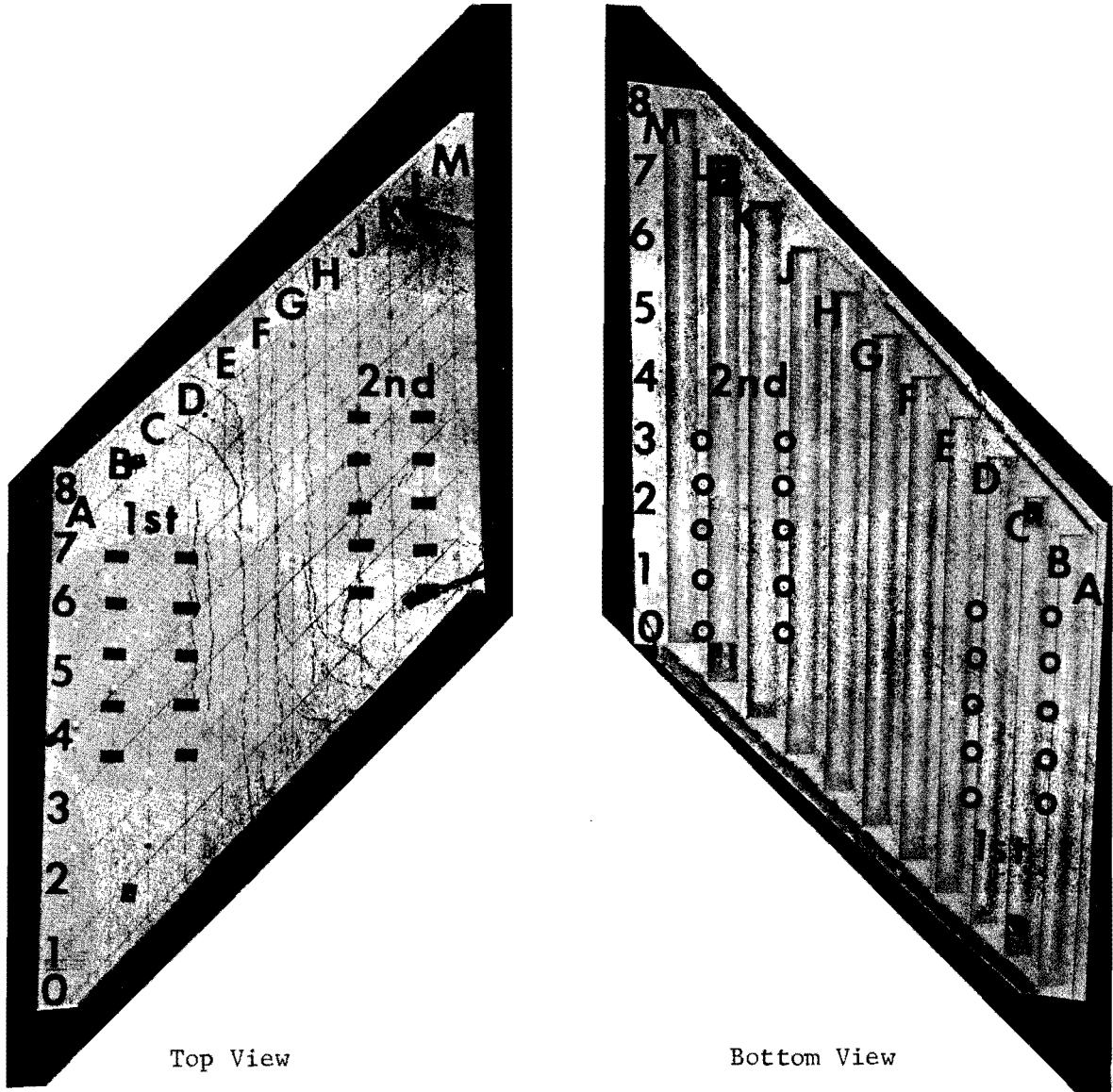


Fig. 7.49. SG-2 Crack Pattern.

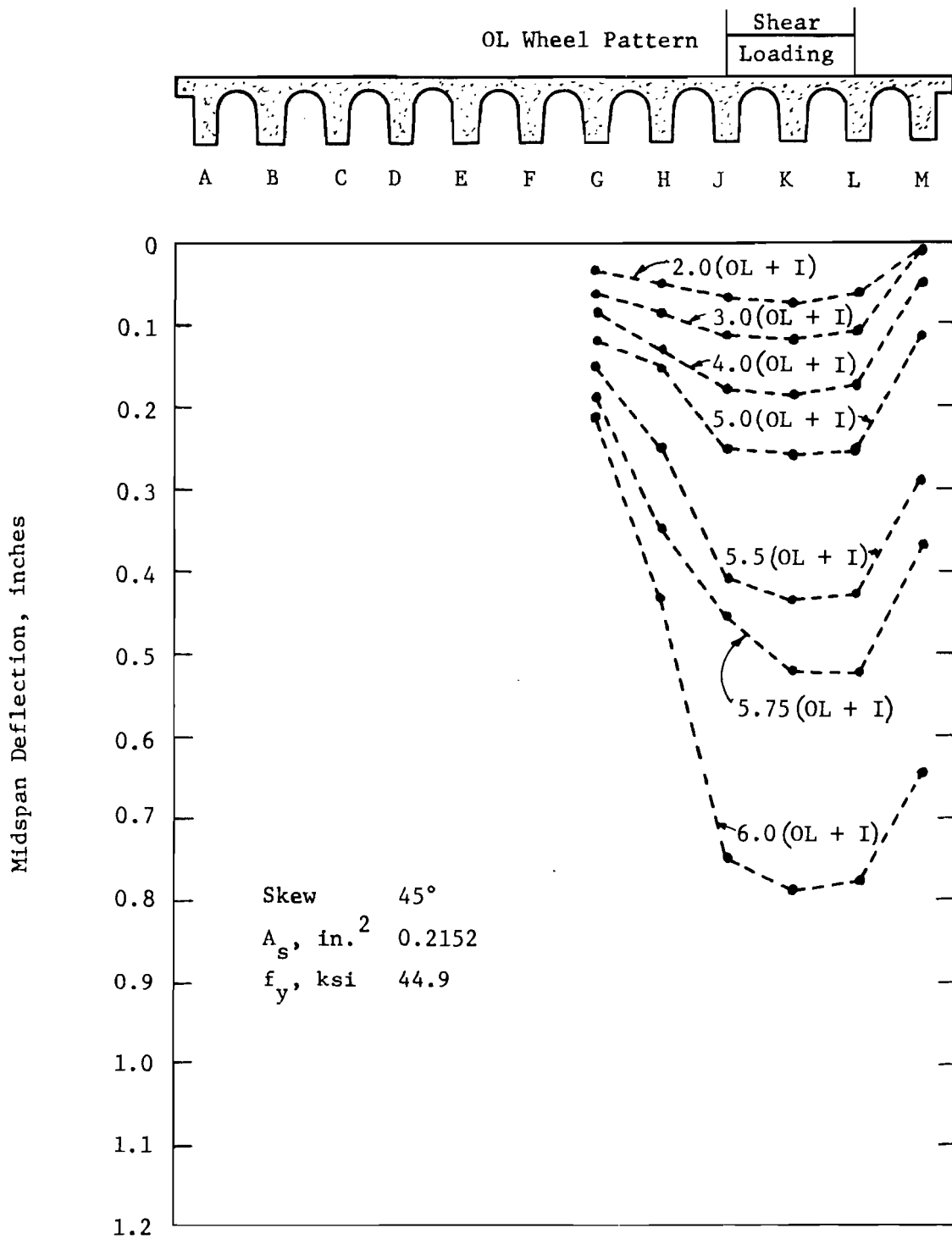


Fig. 7.50. Midspan Deflection for SG-2 during Second Ultimate Load Cycle.

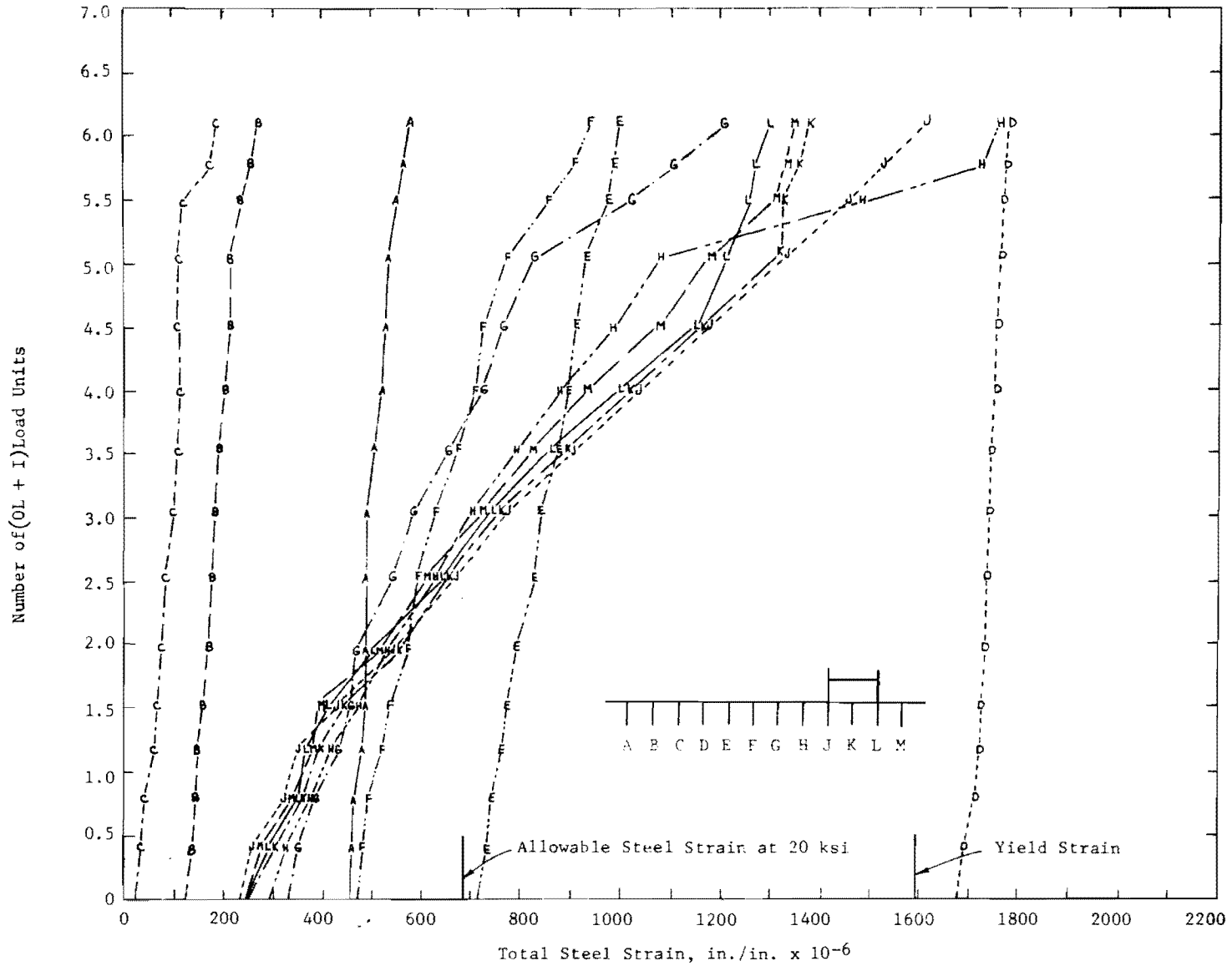


Fig. 7.51. Midspan Steel Strain for SG-2 during Second Ultimate Load Cycle.

similar to the ultimate load test with the truck placed over girders B and D. Based on the results of this test, it was concluded that if punching did not occur the bridge would not fail in shear before failing in flexure.

7.6.5 Model SG-3, 45° Skew. Model SG-3 was tested to failure under two loading conditions, both using the overload truck wheel pattern. Axle 3 was placed at midspan with the location varying transversely. Load increments and recorded data were as described in Sec. 7.6.4.

Midspan deflections for live load are shown in Fig. 7.52 for the first ultimate load test with wheel lines directly over the centerlines of B and D. Strains are shown in Fig. 7.53.

The allowable stress in this model was 24.0 ksi. This stress was exceeded in girders A, B, C, and E at a load level of $1.5(OL + I)$. The companion bridge SG-2 with more steel (allowable $f_s = 20$ ksi) did not exceed the allowable stress until $2.0(OL + I)$ under identical loading. This is probably due to the advanced state of cracking in model SG-3 as observed, even at service loads, by larger strains and deflections in SG-3. Under $1.0(OL + I)$ the observed strains for SG-3 were about 1.3 times those for SG-2. The load level $2.0(OL + I)/1.3$ is $1.54(OL + I)$. This is felt to account for the somewhat earlier excess over design stress in SG-3.

The steel in girders A, B, C, D, and E yielded at ultimate load. The steel in girders F, G, and H exceeded the design stress but did not yield at ultimate load.

First yield of steel occurred at a load level of $4.25(OL + I)$ in girder C. The steel in girder C also yielded first in model SG-2. Referring to the final crack patterns in Fig. 7.54, the crack in the top of the slab between E and F also formed at $4.5(OL + I)$. The cracks from A to F were formed by the first ultimate load test, while the cracks from G to M were formed by the second ultimate test. The crack between F and G was a combination of both tests. A crack was noticed in the bottom of the crown between A and B at $5.0(OL + I)$. The steel in girders A through E yielded at $5.5(OL + I)$. As the load was increased to $6.0(OL + I)$ deflections increased rapidly with the remaining cracks in Fig. 7.54 forming at that time. The last crack to form was the typical diagonal crack observed in previous tests to the right

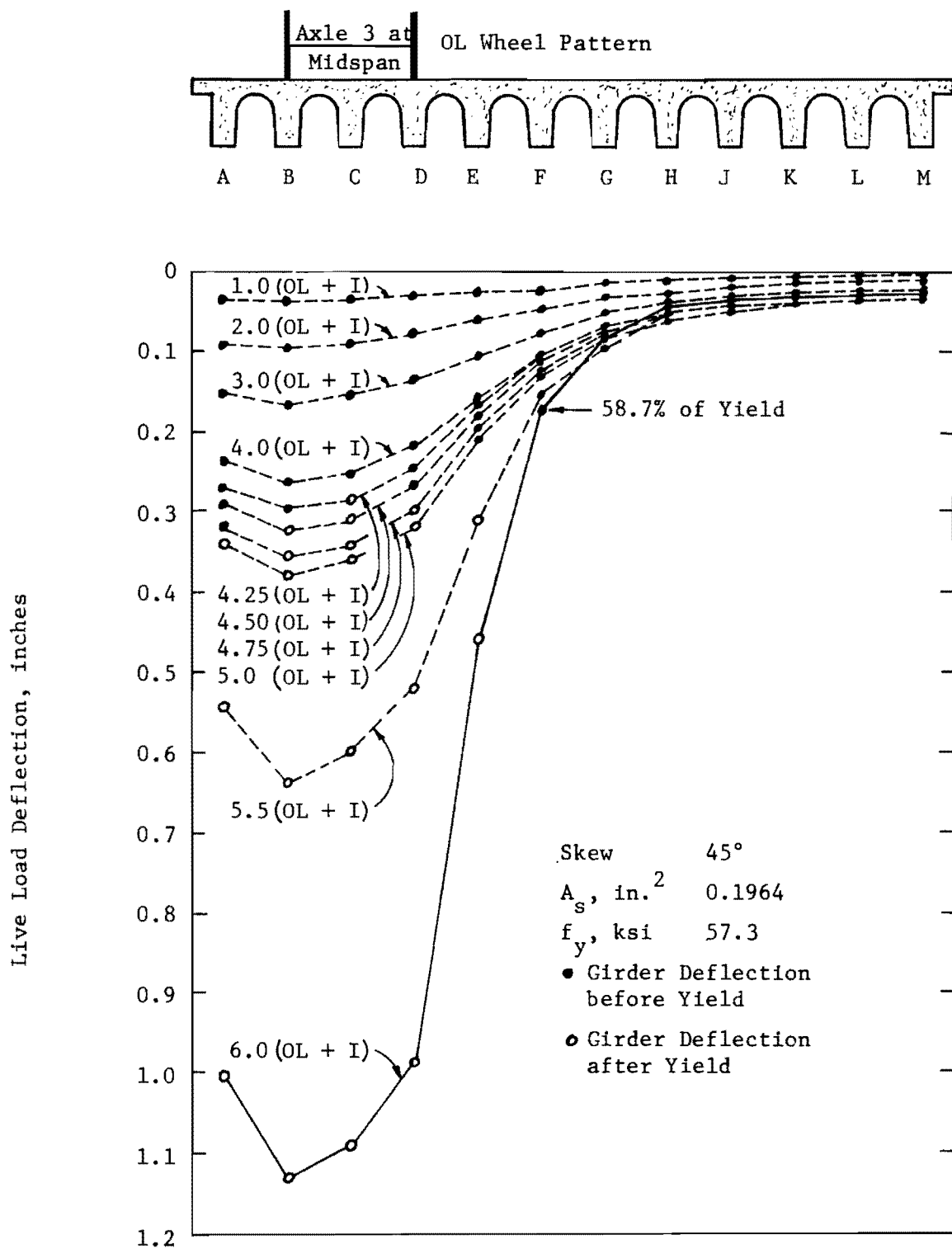


Fig. 7.52. Midspan Deflection for SG-3 during First Ultimate Load Cycle.

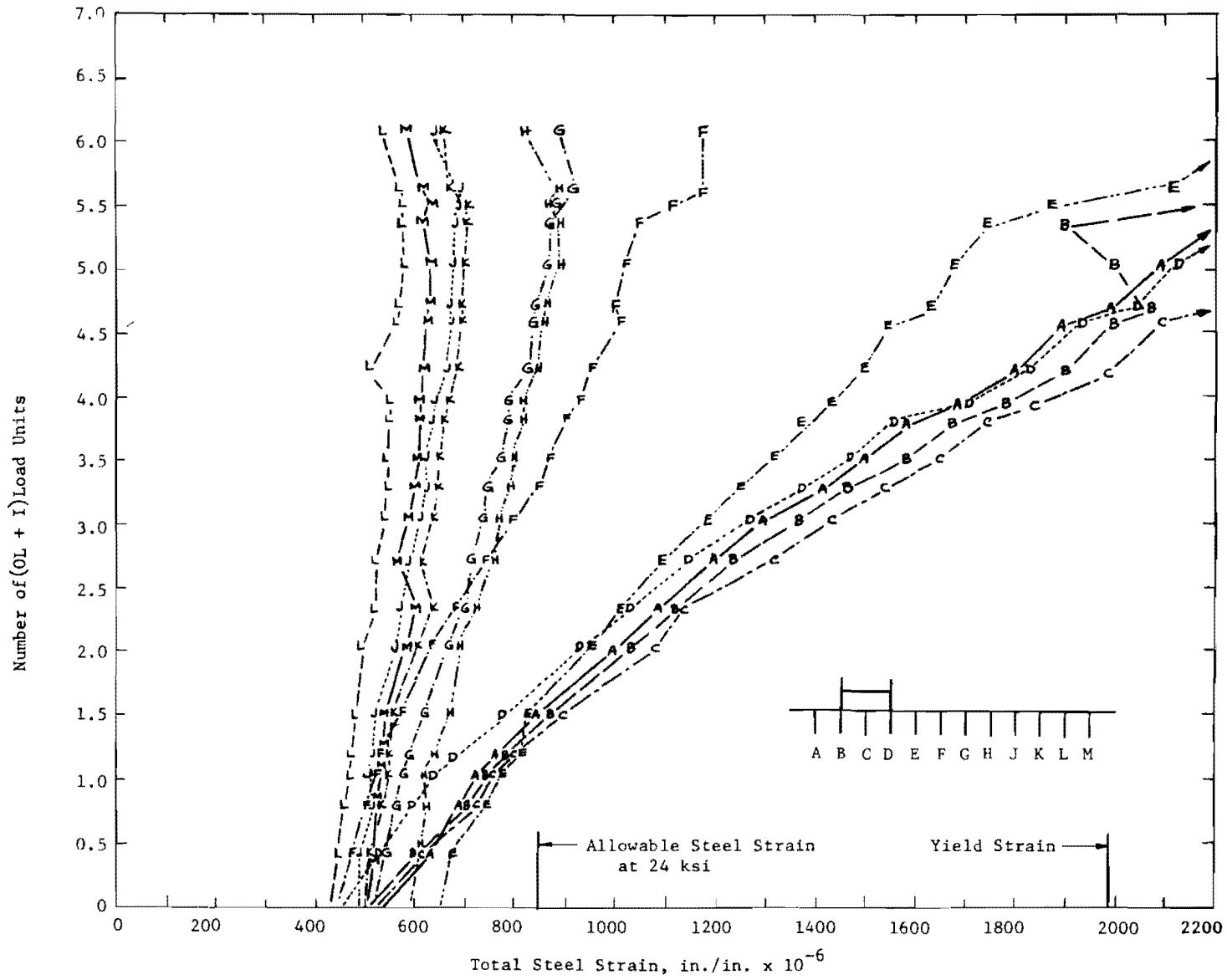


Fig. 7.53. Midspan Strain for SG-3 during First Ultimate Load Cycle.

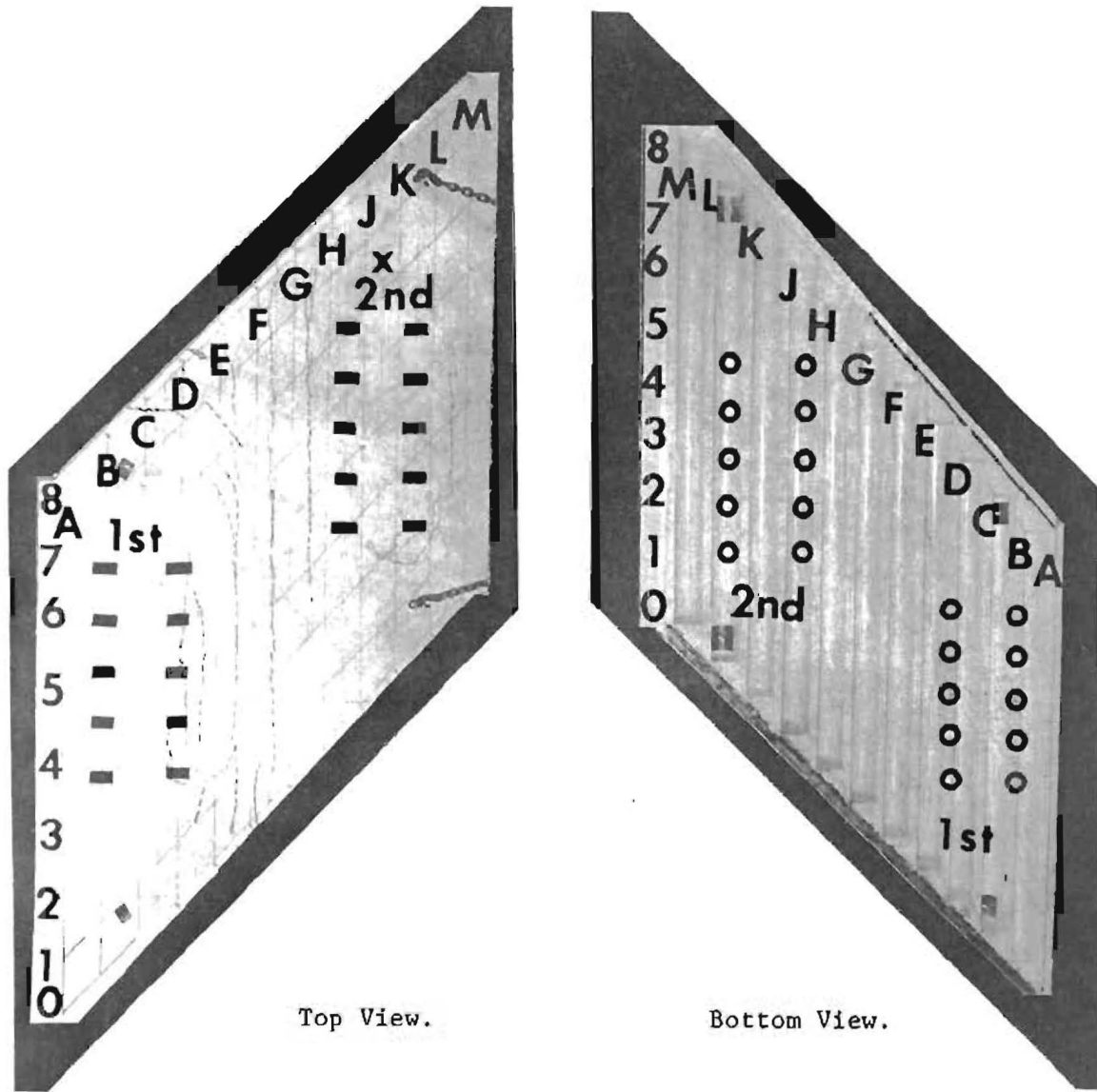


Fig. 7.54. SG-3 Crack Pattern.

of the line of wheels over girder D. At this point the load could not be maintained so the test was discontinued.

The factor of safety at the ultimate load of $6.0(OL + I)$ was 2.69.

The second ultimate load test was performed by locating the wheel lines of the overload truck pattern over crowns HJ and KL as shown in the top of Fig. 7.55. Dial gages were read only for girders G through M. Other data were recorded as described previously. Observed deflections are shown in Fig. 7.55 and strains are shown in Fig. 7.56.

For this loading the design stress was exceeded in girders H and K at a load of $1.5(OL + I)$. At a load of $2.0(OL + I)$ the design stress was exceeded in girders H, J, K, L, and M. First yield of flexural steel occurred in girders J and K at a load of $4.5(OL + I)$. At ultimate load the steel had yielded in girders H through M. The crack in the top of the slab (Fig. 7.54) between G and H occurred at a load of $5.0(OL + I)$, as did the crack in the bottom of the slab between K and L. The remaining cracks formed at failure. At a load of $5.5(OL + I)$ girders H through M had yielded. At a load of $6.0(OL + I)$ girders H through L failed in shear. The shearing crack shows through the deck in Fig. 7.54 as the crack near the quarter-point and extends around the wheels continuing down the crown LM. The factor of safety at the ultimate load of $6.0(OL + I)$ was 2.69.

7.6.6 Model SG-4, 26° Skew. Model SG-4 was tested to failure using the wheel pattern of the H20 design truck. Two H20 trucks were placed on the bridge as shown at the top of Fig. 7.57, with Axle 2 at midspan. Actual wheel locations are shown in Fig. 7.60. Wheel loads were increased monotonically in the proportions for an H20 truck until failure occurred. Load increments were in multiples of 689 lbs./wheel of Axle 2, representing the load on one rear wheel of each H20 truck plus 30 percent impact. This is abbreviated as $1.0(H20 + I)$. Strain gages and both midspan and support dial gages were read after each load increment. In addition, dial gages located at the quarter-points were read every other load increment.

Midspan deflections for live load are shown in Fig. 7.57 and Fig. 7.58 to a smaller scale. Data for deflections in a girder are shown with a solid

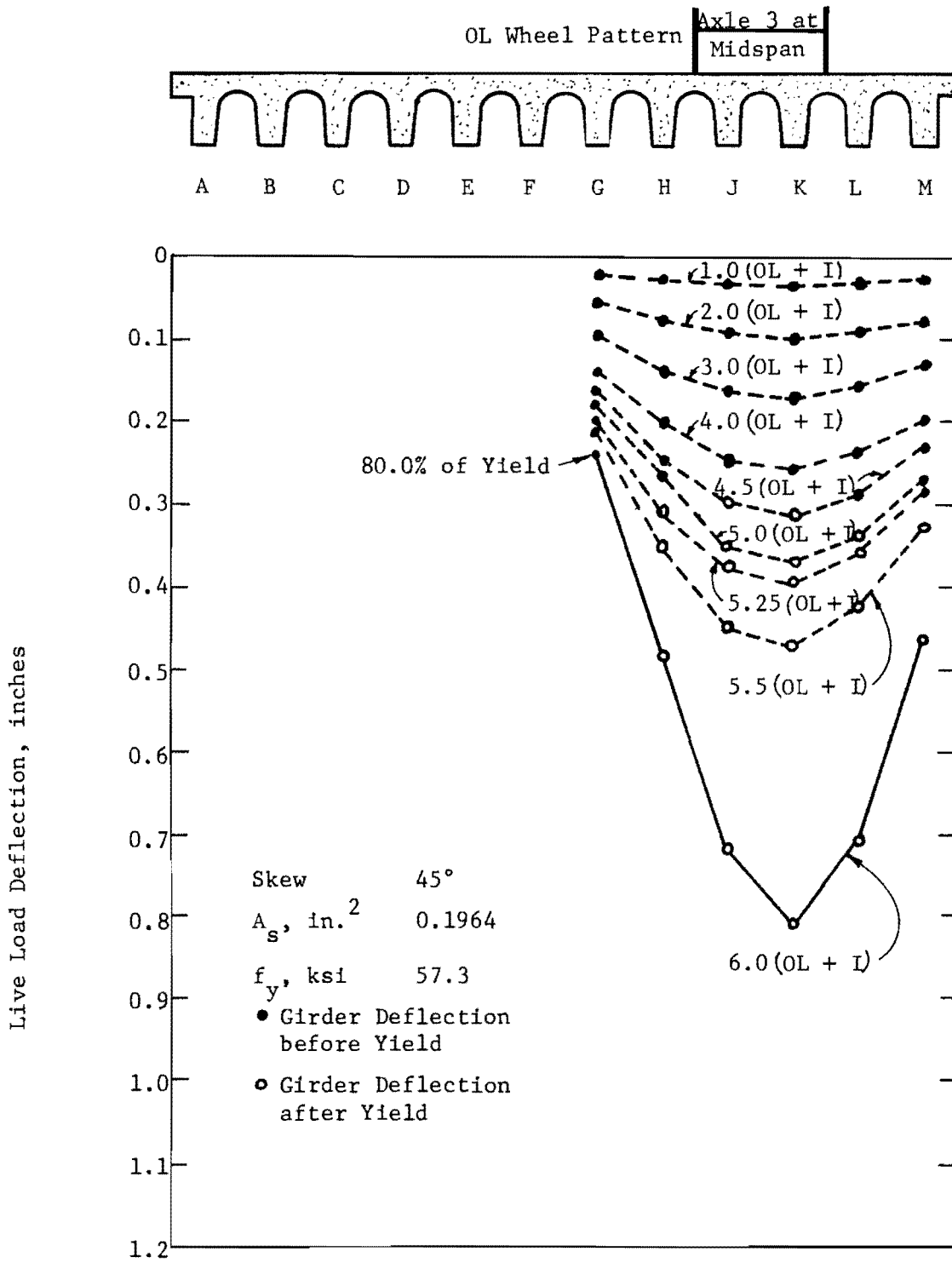


Fig. 7.55. Midspan Deflection for SG-3 during Second Ultimate Load Cycle.

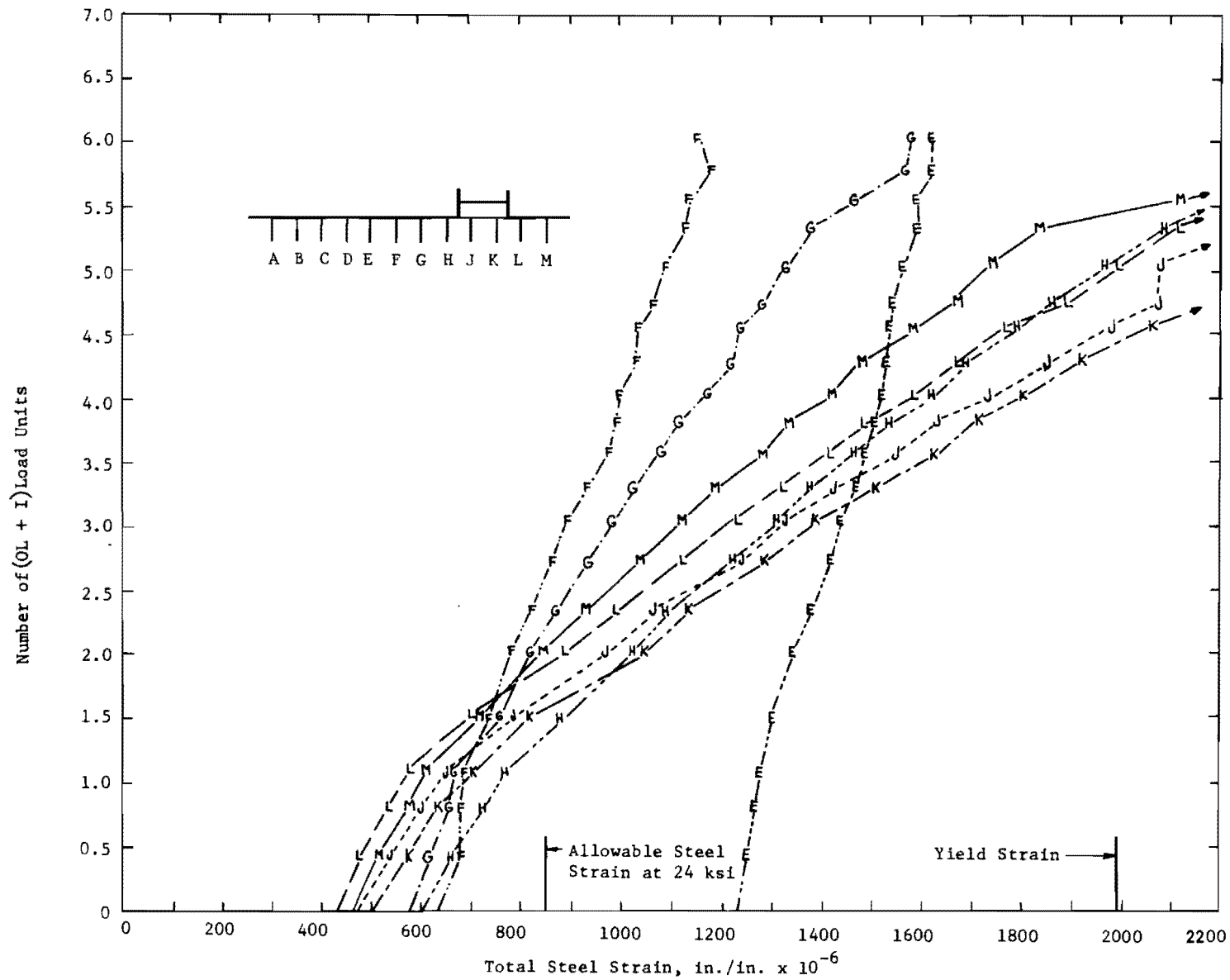


Fig. 7.56. Midspan Strain for SG-3 during Second Ultimate Load Cycle.

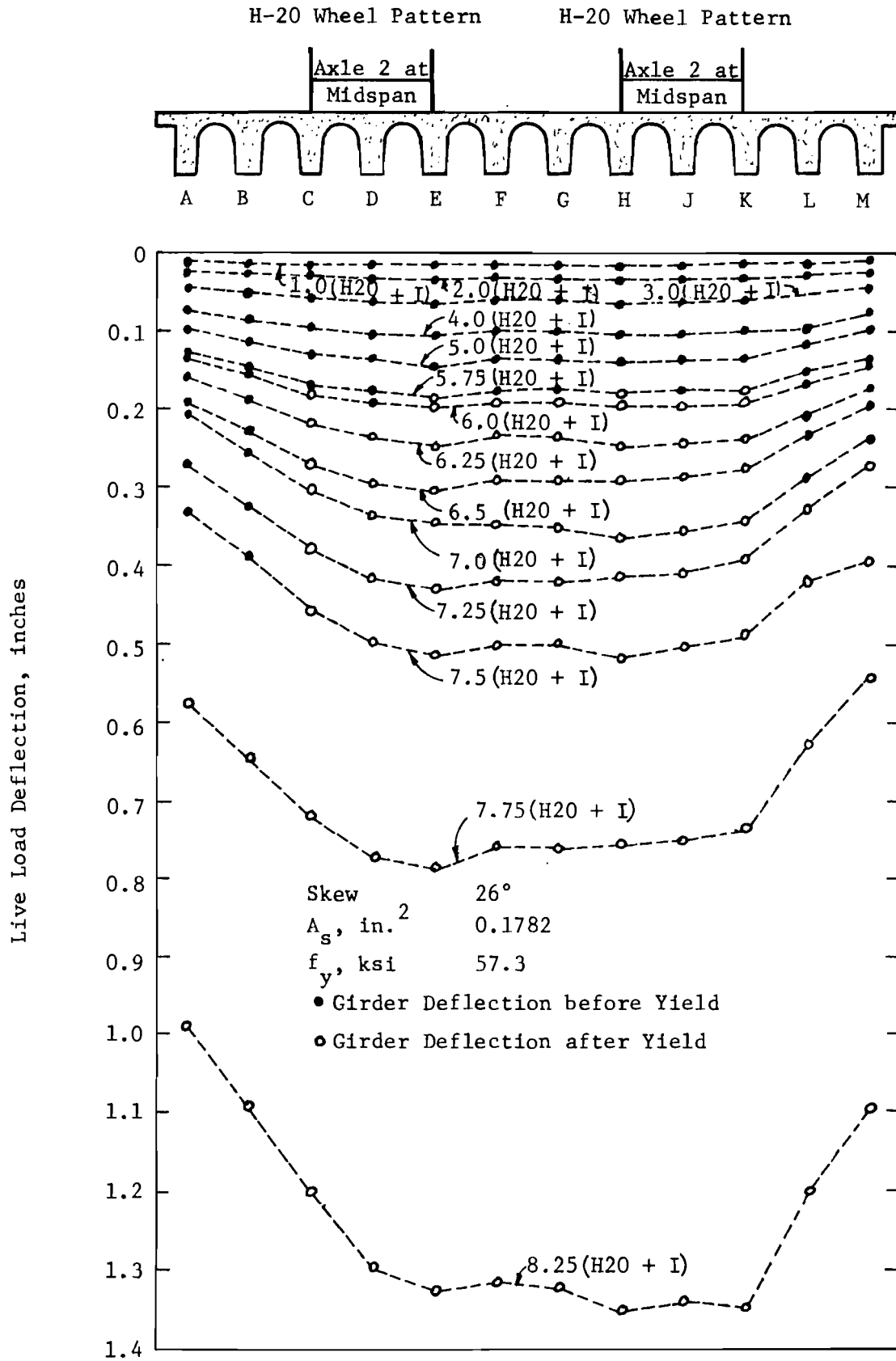


Fig. 7.57. Midspan Deflection for SG-4 during Ultimate Load Cycle.

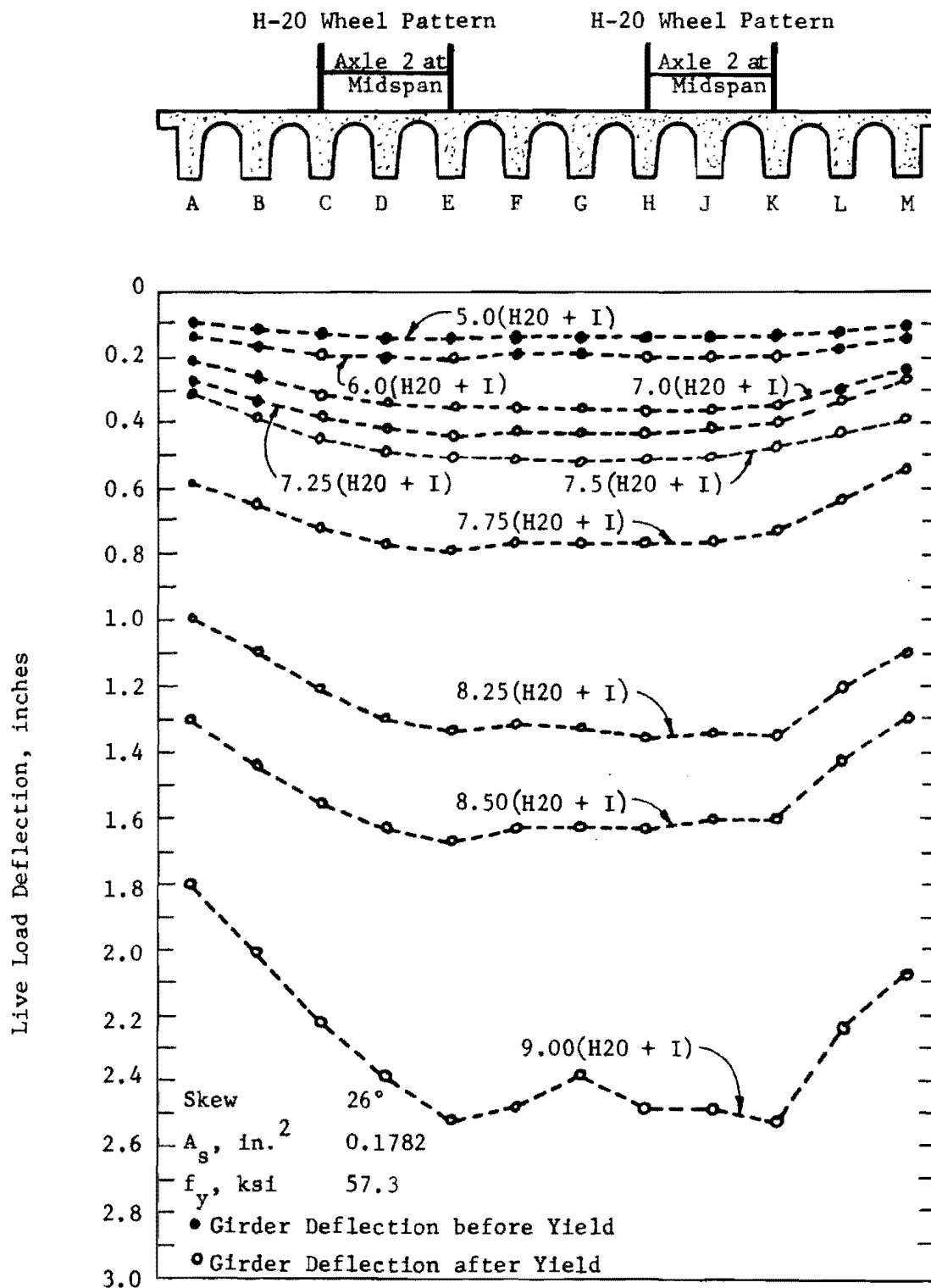


Fig. 7.58. Midspan Deflections for SG-4 during Ultimate Load Cycle (Reduced Scale).

circle before yield of flexural steel and with an open circle after yield. Strain data for girders A through F are shown in Fig. 7.59a and in Fig. 7.59b for girders G through M.

The allowable stress in this model was 20.0 ksi. At a load of $2.0(H_{20} + I)^*$ the steel in girder K slightly exceeded this value. At a load of $3.0(H_{20} + I)$ the steel in girders C, E through K, and M exceeded the design stress.

Before discussing yield of steel and ultimate load data, attention should be called to the type of steel used in this bridge. The design criteria called for two No. 11 and two No. 10 bars of intermediate grade steel in the prototype. This amounts to two No. 2 bars and two SWG No. 4 wire in the model. No. 2 deformed bars with a yield point of 57.3 ksi were substituted for the intermediate grade steel which was only available in smooth bars. It was considered desirable to use deformed bars where possible. Smooth SWG No. 4 wire with a yield of 35.8 ksi was used for the second layer of steel. These changes affect the ultimate flexural strength (increasing it) but should not affect service load performance.

The instrumented No. 2 bars indicated yield in girders E, H, and K at a load of $5.75(H_{20} + I)$. The steel in girders C, E, H, J, and K had yielded at $6.00(H_{20} + I)$. Yielding then progressed until the steel in all girders yielded by $7.75(H_{20} + I)$. First yield for intermediate grade steel (f_y assumed at 40 ksi) would have occurred at $5.0(H_{20} + I)$ in girders C, H, J and K.

Load continued to increase over the yield load to a maximum of $9.50(H_{20} + I)$. Deflections were large, as may be observed in Fig. 7.61a. The rear wheel position H-4 punched through the structure around the loading pad at $9.5(H_{20} + I)$ (Fig. 7.61b). The model wheel load was 6546 lb., representing 198,000 lb. on the prototype. The wheel was located directly over a girder. Cracking had penetrated well into the slab at this point, leaving only a thin slab depth to carry the load.

* This is the load per truck.

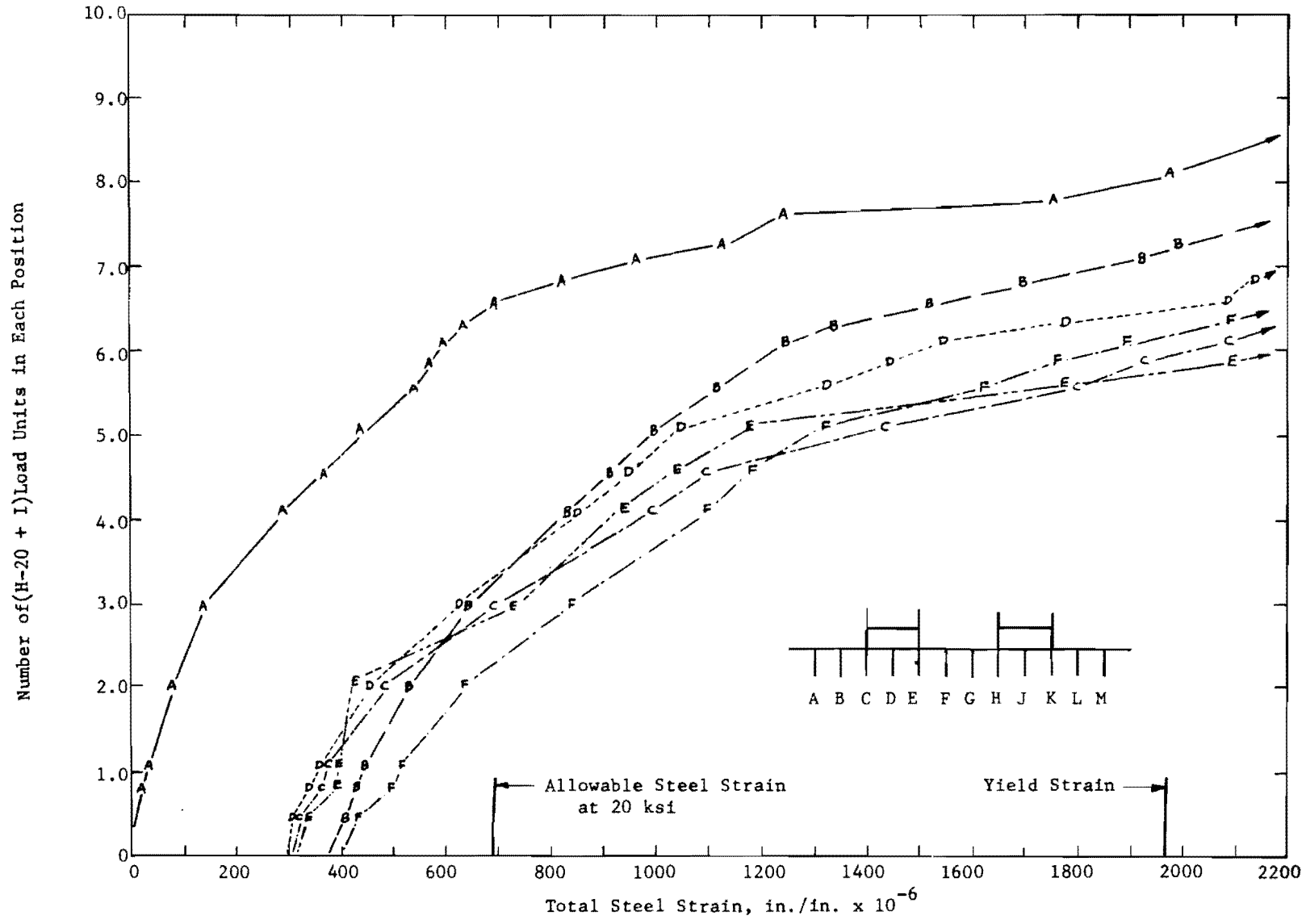


Fig. 7.59a. Midspan Strain on Girders A through F for SG-4 during Ultimate Load Cycle.

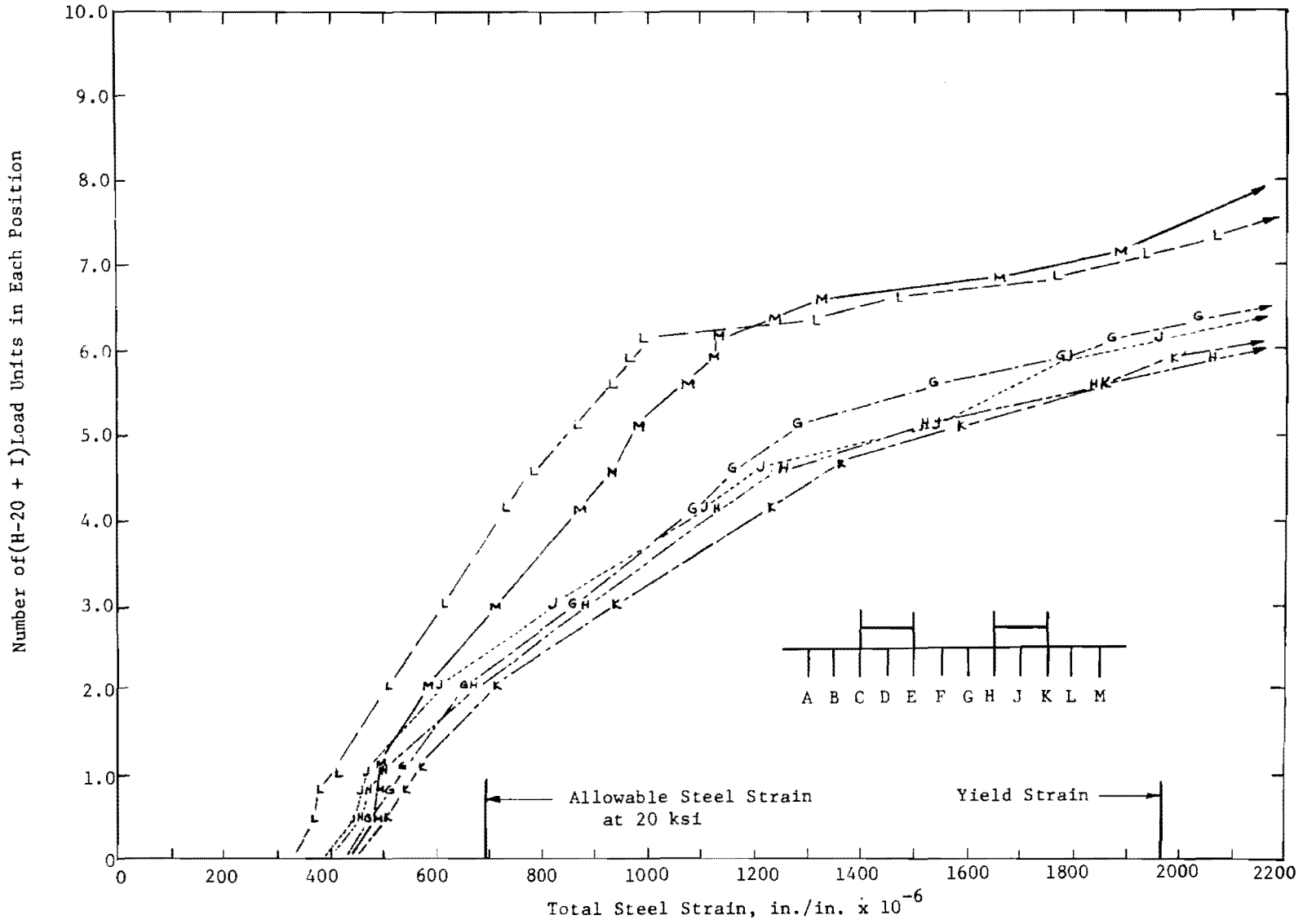


Fig. 7.59b. Midspan Strain on Girders G through M for SG-4 during Ultimate Load Cycle.

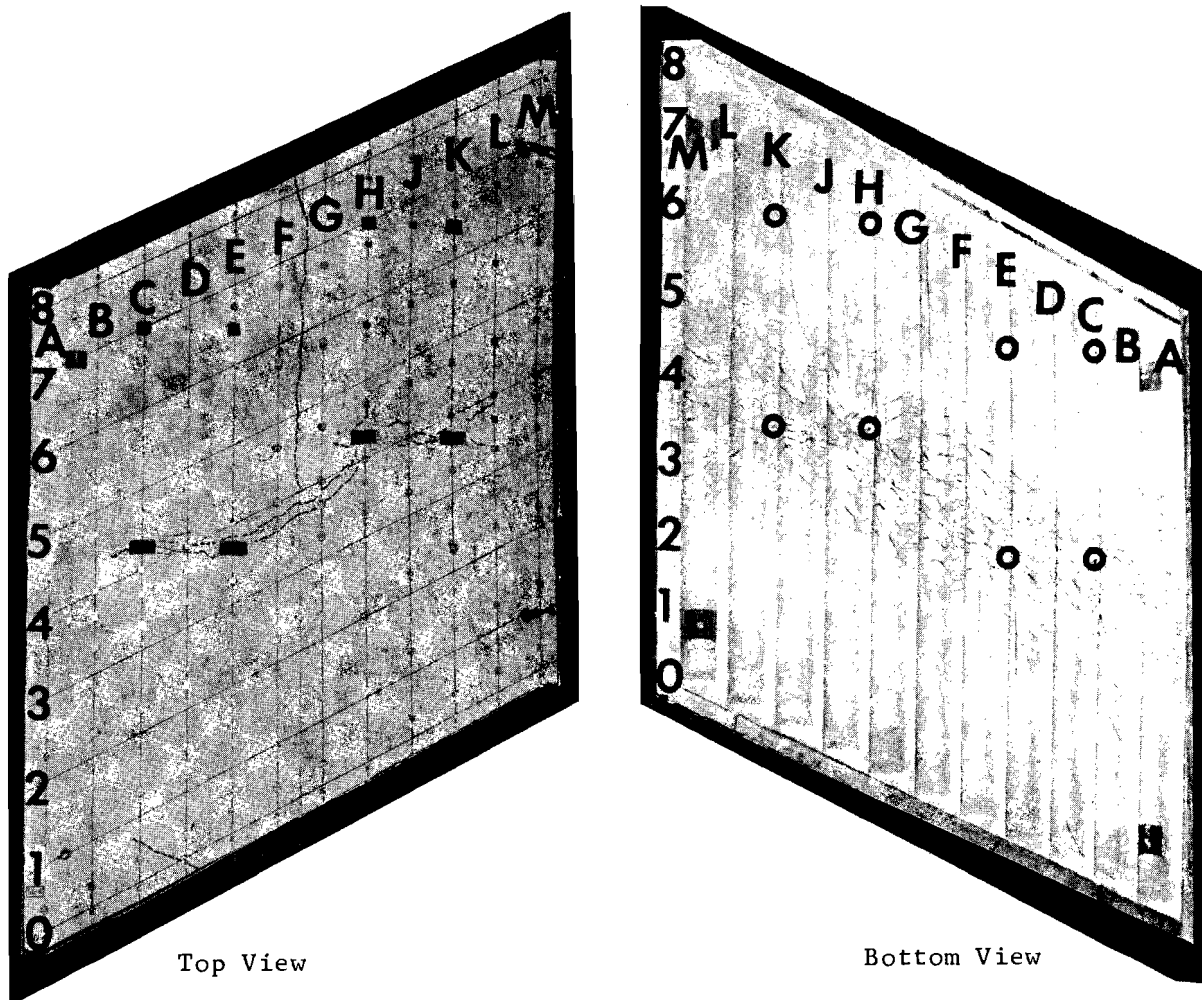
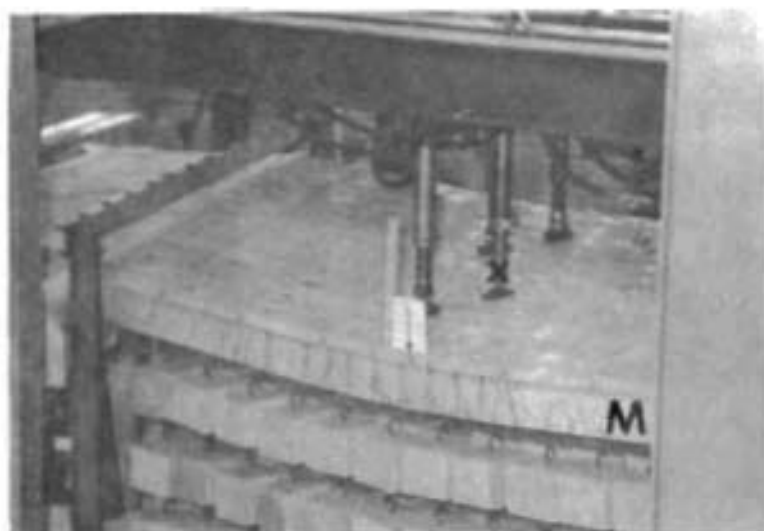
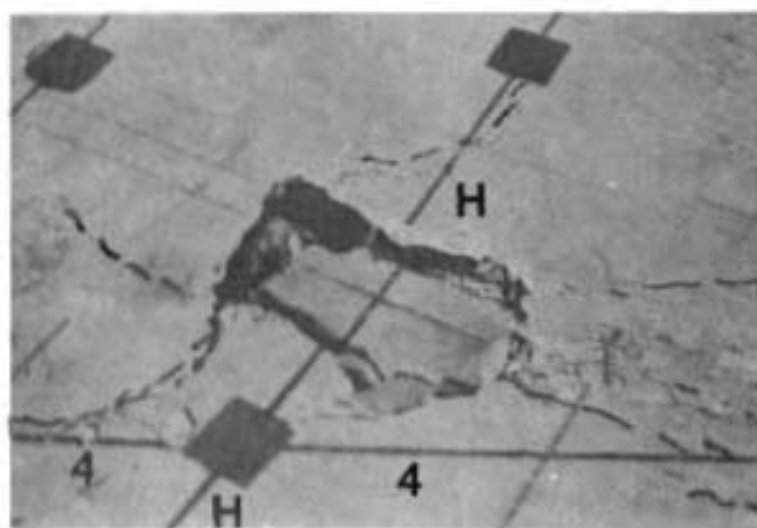


Fig. 7.60. SG-4 Crack Pattern.



(a) General View.



(b) Punching.

Fig. 7.61. SG-4 after Ultimate.

The ultimate flexural capacity, neglecting strain hardening, should be taken as $7.75(H20 + I)$, due to the large deflection increase in going from 7.50 to $7.75(H20 + I)$ (Figs. 7.57 and 7.58).

The total factor of safety for $7.75(H20 + I)$ is 3.50. The total factor of safety for $9.50(H20 + I)$ is 5.16. These large safety factors are due to the steel in the central girders having entered strain hardening when the first girders yielded.

7.6.7 Deterioration of Deflection and Strain Distribution. The experimental distribution of strain and deflection as shown in Fig. 7.39 remained reasonably constant for each bridge until the design stress was exceeded in one or more girders. At this point the ability of the bridge section to transfer load to unloaded girders was altered. This alteration resulted in the most heavily loaded girders carrying a larger percentage of the total load than previously. Thus, the ability of the bridge to transfer load deteriorated. Table 7.6 has been prepared to show that the deterioration of strain and deflection distribution occurred at the same load level which caused the steel to exceed its design stress. These load levels were larger than the usual design service loads and moderate overloads. This observation further justifies the use of AASHTO-type factors in the form of S/C for service loads and moderate overloads.

TABLE 7.6 DISTRIBUTION DETERIORATION

Bridge	Skew	A_s in. ²	f_y ksi	Design Stress ksi	Exceeded Design Stress	Deterioration of Strain and Deflection Distribution
SG-1	0°	0.1920	46.6	20.0	2.0(OL+I)	2.0(OL+I)
SG-2	45°	0.2152	44.9	20.0	2.0(OL+I)	2.0(OL+I)
SG-3	45°	0.1964	57.3	24.0	1.5(OL+I)	1.5(OL+I)
SG-4	26°	0.1782	57.3	20.0	2.0(H20+I)	2.0(H20+I)

7.6.8 Effect of Skew. No well-defined effect of skew was observed at ultimate load levels. Observed data were of the same order of magnitude for the same loads in the skew and no-skew bridges. The 45° skew bridges did appear somewhat more ductile than the no-skew bridge. This ductility

was exhibited in the form of gradual yielding of girders and plentiful warning of the formation of a failure mode. The formation of a failure mode in the case of the no-skew bridge was rapid and occurred shortly after the yield of flexural reinforcement.

7.6.9 Effect of Steel Percentage. As expected, the strains and deflections for the two 45° skew bridges varied, due to different steel percentages. The difference was smaller than at service loads. For instance, at a load level of 5.0(OL + I) the deflection of girder B for SG-3 was 1.1 times the deflection for SG-2. (The ratio of longitudinal steel areas was also 1.1.) This indicates that near ultimate the two bridges were cracked about equally.

7.6.10 Transverse Strains. Transverse strains were small until the bridges were very close to ultimate load. Table 7.7 has been prepared to illustrate this. As shown in Table 7.7, the transverse strains do not exceed their service load design level until at least 80 percent of the ultimate load. However, there is no assurance that the increase in transverse stresses is linear through the ultimate load. These do justify the conclusion that transverse moments are not critical for service loads. It is thought that the transverse moments do not play a critical part in the failure mode. This is felt to be substantiated by the majority of the data in Table 7.7, although the data for SG-4 indicate that transverse moments might be important at ultimate.

TABLE 7.7 TRANSVERSE STRESSES

Bridge	Exceeds Design Stress	Exceeds Yield Stress
SG-1	At ultimate load	No
SG-2	At 95% of ultimate load	No
SG-3	At 80% of ultimate load	No
SG-4	At 80% of ultimate load	At 90% of ultimate load

7.7 Ultimate Load Calculations

7.7.1 Introduction. Ultimate load calculations based on elastic distribution factors may be of little value, due to redistribution of loads

and moments. It is important to be able to assess the ultimate load capacity of a bridge in order to determine the actual factor of safety of the structure under specific loadings.

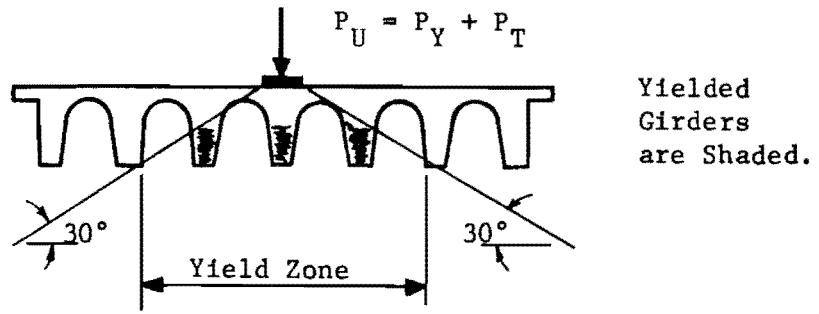
Rowe⁴⁰ suggests dividing a slab and girder type of bridge into a grillage of T-beams interconnected by diaphragms. The ultimate load capacity of the grillage may then be computed using a method described by Reynolds,³³ who has reported a procedure for calculating the ultimate strength of grillages. He uses a procedure similar to the limit analysis of frames. That is, the grillage capacity is computed for various collapse mechanisms consisting of torsion and moment hinges. In this manner he arrives at a collapse mechanism.

Because of the predominance of longitudinal flexural action the procedure suggested by Rowe did not seem applicable to the type of bridge tested. Instead, an ultimate load procedure based on observed failure mechanisms is described in Sec. 7.7.2 and Sec. 7.7.3.

7.7.2 Basis for Hypothesis. A general failure mechanism was observed in the models tested, which suggests an ultimate load calculation procedure. These observations are outlined below:

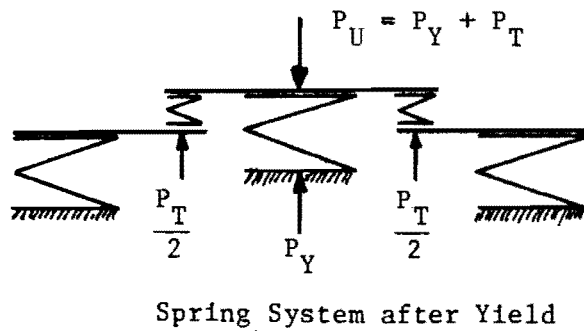
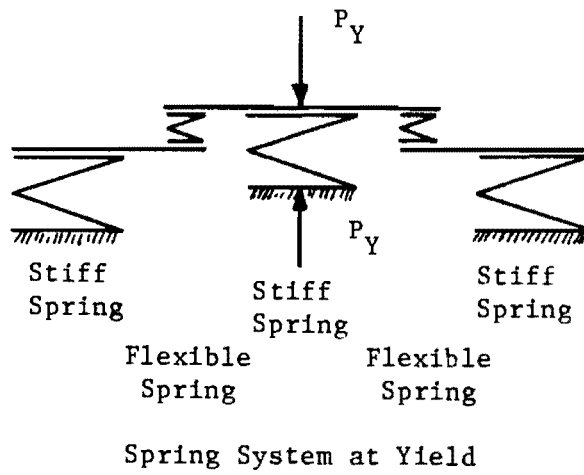
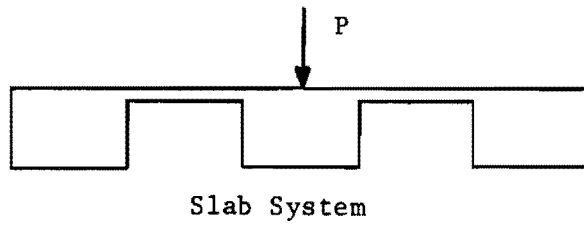
(a) Longitudinal Flexure - The primary mode of failure was by yielding of tensile steel in certain longitudinal girders. Based on detailed observations of the bridges tested in this study, a distribution zone boundary inclined 30° from the horizontal is proposed, as shown in Fig. 7.62a. The main longitudinal tension steel will yield or be very close to yield in all girders in which the tensile steel layers are enclosed within such a 30° cone. This is referred to as the yield zone. The load causing yielding of the girders within the yield zone is referred to as the yield load P_Y . The ultimate load, P_U , is the sum of the yield load, P_Y , plus the load, P_T , which is transferred to girders outside the yield zone. Tests on SG-1, SG-2, and SG-3 indicate that the amount of transferred load is limited by the slab shear capacity in the transverse direction, unless the remaining girders yield before the shear transfer capacity is reached.

(b) Transverse Shear Transfer - Shear diagonal tension failure at the edge of the wheel rather than flexure is the observed mode of transverse



Yielded
Girders
are Shaded.

(a) Yield Zone.



(b) Shear Transfer Mechanism.

Fig. 7.62. Failure Concept.

failure. Consider the system in Fig. 7.62b. In this figure three thick slab sections are connected by thin slab sections. The center thick section is loaded. Consider the thick portions to be replaced by stiff springs and the thin sections to be replaced by flexible springs. The thin sections cannot significantly aid in carrying load, since the loaded thick section is so stiff. Thus the center portion carries essentially all of the applied load. Once the loaded section reaches its yield load at a load P_Y , any additional load must be carried elsewhere unless a collapse mechanism is formed. In this case the weak springs must absorb the increased load while assisting in load transfer. Any increased load, P_T , must be transferred across the weak springs.

In this analogy the stiff springs represent the girders and the weak springs represent the crowns.

Test results indicate that a crown length approximately equal to the load length plus twice the total girder depth is effective in transferring the increased load P_T outside the yield zone. The failure zone and shear transfer length is illustrated in Fig. 7.63. The minimum crown thickness is used as the critical depth in the shear transfer computations.

(c) Transverse Moment - Test results indicate that for these sections transverse bending moment is not critical in transferring load outside the yield zone, hence it will be neglected in this ultimate load procedure.

(d) Punching - Test results indicated that punching of a single wheel is not a design problem, hence it will be neglected in this ultimate load procedure.

7.7.3 Proposed Calculation Procedure. The proposed calculation procedure is an ultimate load method for a given or assumed bridge. As such the AASHTO Specification² does not apply, since it refers only to service loads. The ACI Code³ contains specific ultimate load recommendations. Therefore, the ACI Code is used as the basis for ultimate load procedures.

The ACI Code contains recommendations for basic strength equations. The basic strengths are then reduced by ϕ factors which are intended to account for material variations and uncertainty about the basic strength

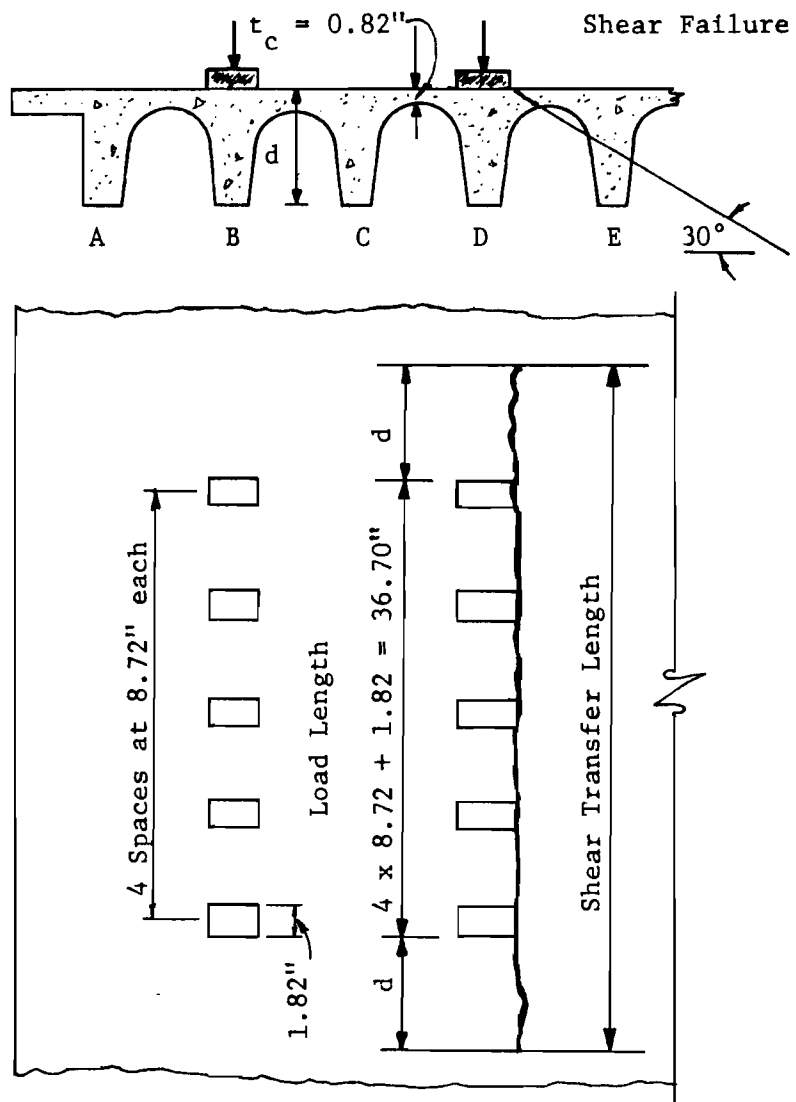


Fig. 7.63. Shear Failure Zone and Shear Transfer Length.

equations. A ϕ factor of 0.9 is presently used for flexure and 0.85 is presently used for shear in the ACI Code. The proposed calculation procedure makes use of flexure and shear equations in the failure model. The ϕ factors are taken as unity, since the material properties are known. In design the ϕ factors should be used along with appropriate load factors. The determination of both ϕ factors and load factors that should be used are beyond the scope of this study.

The Bureau of Public Roads⁴⁶ has recommended load factors of 1.35 and 2.25 for dead live and live load, respectively. The ultimate live load factors from these tests are compared with the Bureau of Public Roads recommendations in Sec. 7.7.6.

The proposed calculation procedure is outlined below:

(a) Divide the structure investigated into a right angle grillage consisting of an appropriate number of longitudinal girders (twelve for the bridges of this investigation).

(b) Estimate the number of girders within the yield zone with a boundary defined by lines inclined 30° with the horizontal from the loaded area.

(c) Compute the service live load, P_S , and service live load moment, M_{SLL} .

(d) Compute the live load capacity per girder, M_{YLL} .

(e) Compute the live load yield capacity of the yield zone, P_Y .

(f) Compute the transferred load, P_T .

(g) Compute the yield load, P_R , of the girders outside the yield zone in (b).

(h) Check to see if the transferred load, P_T , is greater than the load capacity, P_R , of the remaining girders.

(i) If $P_R < P_T$, then the ultimate capacity is simply the product of the number of girders times the live load yield moment.

(j) If $P_R > P_T$, the ultimate load P_U is the sum of P_Y and P_T . The ultimate live load moment is the product of the ratio P_U/P_S times the live load yield moment.

The above steps are summarized in Fig. 7.64.

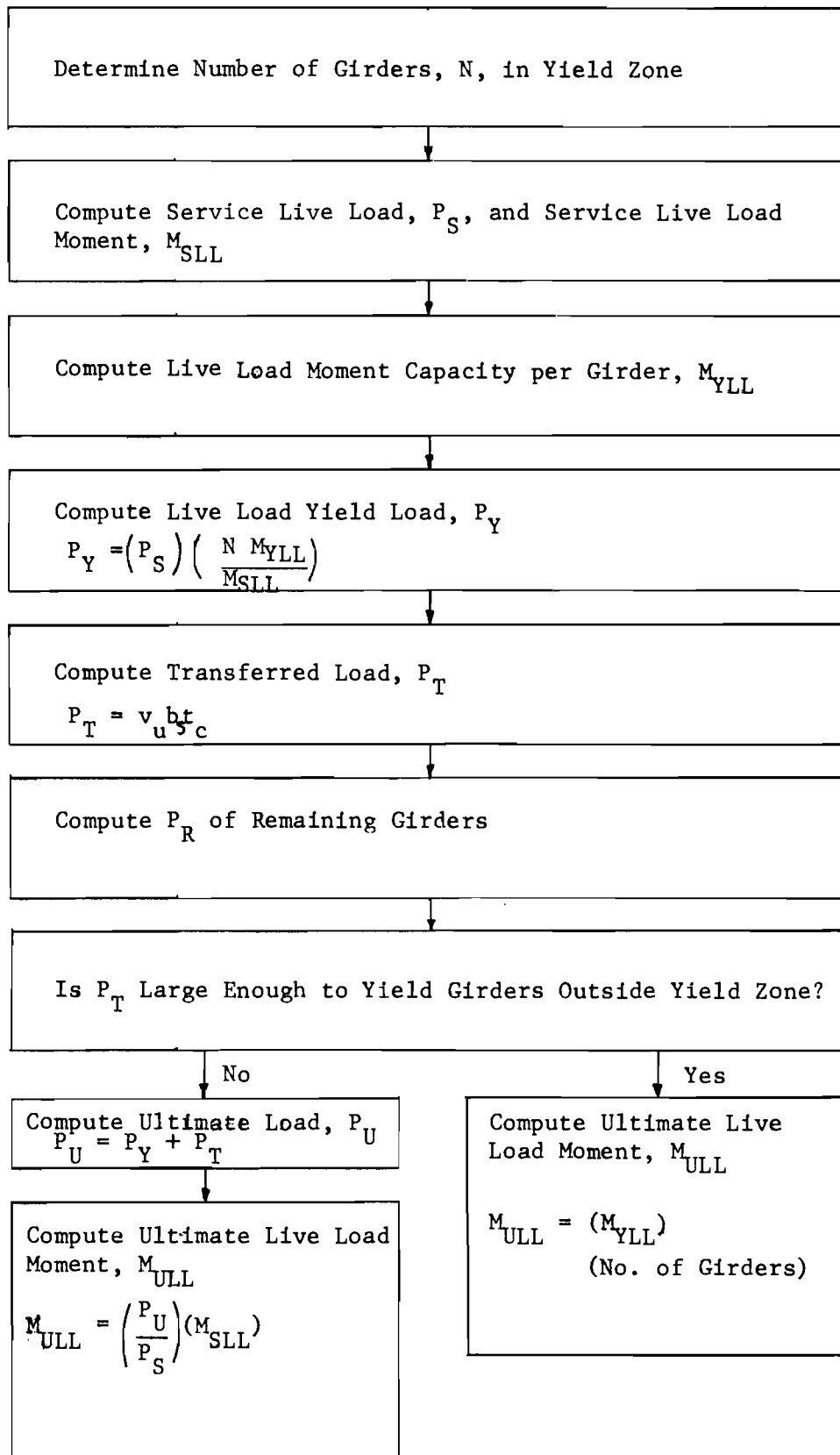


Fig. 7.64. Proposed Calculation Procedure.

7.7.4 Application to this Study. Six ultimate load cases are available for comparing with the failure hypothesis. The quantities needed for ultimate calculations for these six cases are summarized in Table 7.8.

Truck positions are shown in Fig. 7.65 for estimating the girders lying within the yield zone. Shear transfer lengths for the overload truck and the H20 truck are computed in Fig. 7.66.

The six ultimate load cases calculated are:

- (a) Model SG-1 (0° Skew)
- (b) Model SG-2 (45° Skew), Ultimate No. 1
- (c) Model SG-2 (45° Skew), Ultimate No. 2
- (d) Model SG-3 (45° Skew), Ultimate No. 1
- (e) Model SG-3 (45° Skew), Ultimate No. 2
- (f) Model SG-4 (26° Skew)

- (a) Model SG-1 (0° Skew)

Load

Overload Truck Wheel Configuration, Axle 3 at B4-D4

Yield Zone

The yield zone consists of girders A, B, C, D, and E (Fig. 7.65a)

Service Live Load, P_S

The service live load is 1.0 (OL + I).

$$P_S = (10 \text{ wheels})(350 \text{ lb./wheel}) \quad (\text{Table 7.8b})$$

$$P_S = 3500 \text{ lb.}$$

Service Live Load Moment, M_{SLL}

$$M_{SLL} = 4.84 \text{ kip-ft.} \quad (\text{Table 7.8b})$$

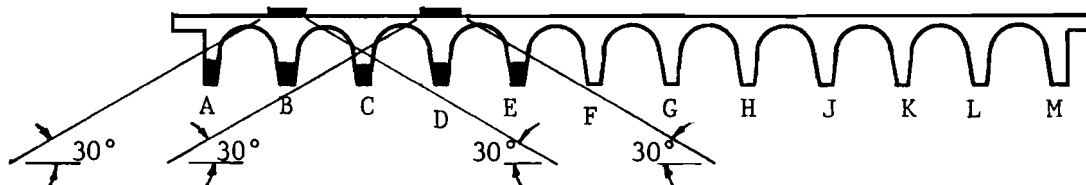
TABLE 7.8 QUANTITIES FOR ULTIMATE LOAD CALCULATIONS

(a) <u>Bridge Properties</u>						
Bridge	Yield Moment		f'_c	$2 \sqrt{f'_c}$		
	kip-ft. girder		psi	psi		
SG-1	3.90		3770	123		
SG-2	4.11		4040	127		
SG-3	4.87		4320	132		
SG-4	3.78		4750	138		

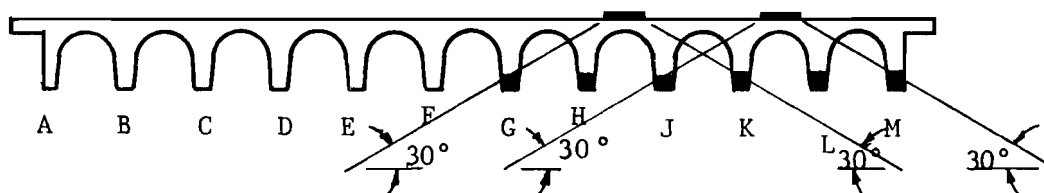
(b) <u>Load Data</u>						
Bridge	Service Live Load Unit	Load Location	Maximum Live Load Moment for One Live Load Unit		Dead Load Moment at Point of Maximum	Ultimate Load No.
			kip-ft.	lb./rear wheel	kip-ft. girder	
SG-1	1 OL + I	B4-D4	4.84	350	0.69	1
SG-2	1 OL + I	B4-D4	5.45	350	0.89	1
	1 OL + I	J-L near support	4.67*	350	0.86**	2
SG-3	1 OL + I	B4-D4	5.45	350	0.89	1
	1 OL + I	HJ4-KL4	5.45	350	0.86	2
SG-4	2 (H20 + I)	C4-E4 H4-K4	5.65	689	0.80	1

*At fourth axle from support.
**At fourth axle.

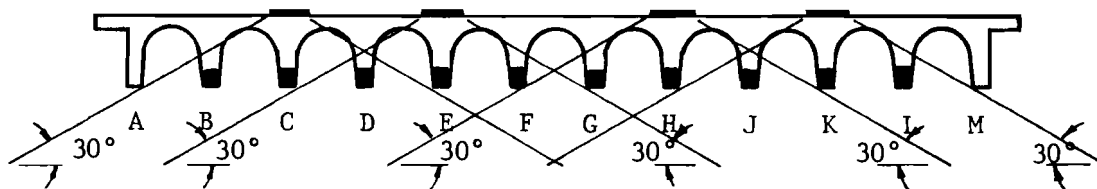
Yielded Girders Are Shaded.



(a) Truck at B4-D4.

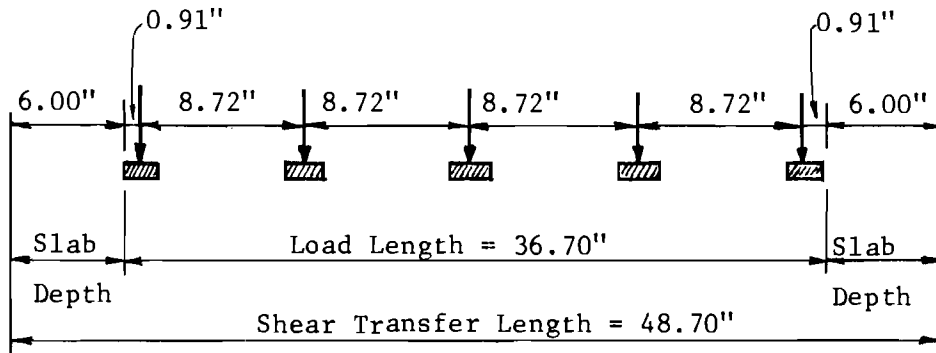


(b) Truck at HJ4-KL4.

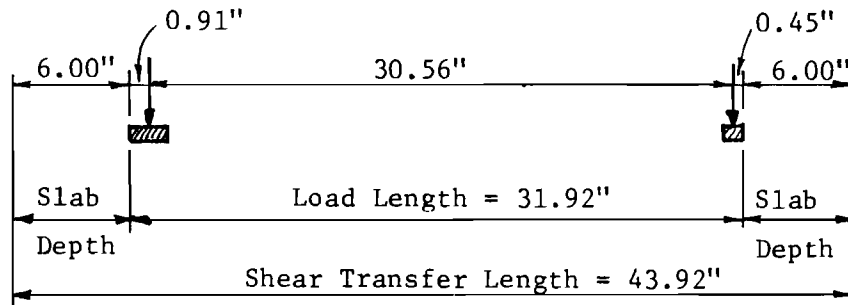


(c) Truck at C4-E4 and H4-K4.

Fig. 7.65. Estimating Girders with Steel Yielding at Ultimate.



(a) Overload Truck.



(b) H20 Truck.

Fig. 7.66. Shear Transfer Lengths.

Live Load Moment Capacity, M_{YLL}

$$\text{Yield Moments, } M_Y \text{ (Table 7.8a)} = 3.90 \text{ kip-ft./girder}$$

$$\text{Dead Load Moment, } M_{DL} \text{ (Table 7.8b)} = \frac{0.69}{M_{YLL}} = 3.21 \text{ kip-ft./girder}$$

Yield Load, P_Y

$$P_Y = (P_S) \left(\frac{N M_{YLL}}{M_{SLL}} \right) = 3500 \times \frac{5 \times 3.21}{4.84}$$

$$P_Y = 11,600 \text{ lb.}$$

Transferred Load, P_T

$$P_T = v_u b_s t_c$$

$$v_u = 123 \text{ psi} \quad (\text{Table 7.8a})$$

$$b_s = 48.70 \text{ in.} \quad (\text{Fig. 7.66a})$$

$$t_c = 0.82 \text{ in.}$$

$$P_T = 123 \times 48.70 \times 0.82$$

$$P_T = 4910 \text{ lb.}$$

Capacity of Girders Outside Yield Zone, P_R

$$\begin{aligned} \text{Live Load Moment Capacity} &= (12-5)(3.21 \text{ kip-ft./ girder}) \\ &= 22.5 \text{ kip-ft.} \end{aligned}$$

$$\begin{aligned} P_R &= 3500 \times \frac{22.5}{4.84} \\ &= 16,250 \text{ lb.} > P_T = 4910 \text{ lb.} \end{aligned}$$

Ultimate Load, P_U

$$P_U = P_Y + P_T = 11,600 + 4910$$

$$P_U = 16,510 \text{ lb.}$$

Ultimate Live Load Moment, M_{ULL}

$$M_{ULL} = \left(\frac{P_U}{P_S} \right) (M_{SLL}) = \left(\frac{16,510}{3,500} \right) (4.84)$$

$$M_{ULL} = 22.8 \text{ kip-ft.}$$

Calculated Factor of Safety, FS_c

$$FS_c = \frac{M_{DL} + M_{ULL}}{M_{DL} + M_{SLL}} = \frac{12(0.69) + 22.8}{12(0.69) + 4.84}$$

$$FS_c = 2.37$$

Measured Factor of Safety, FS_m

$$\text{Maximum Measured Load} = 4.38(QL + I)$$

$$\begin{aligned} \text{Maximum Live Load Moment} &= (4.38)(4.84) \\ &= 21.20 \text{ kip-ft.} \end{aligned}$$

$$FS_m = \frac{12(0.69) + 21.20}{12(0.69) + 4.84}$$

$$FS_m = 2.25$$

$$\text{Ratio } FS_m / FS_c$$

$$\frac{FS_m}{FS_c} = \frac{2.25}{2.37} = 0.95$$

Ratio of Calculated and Measured Live Load Capacity

$$\frac{\text{Measured } M_{ULL}}{\text{Calculated } M_{ULL}} = \frac{21.20}{22.80} = 0.93$$

The difference between calculated and measured live loads is not considered serious in view of the overall factor of safety of the bridge under this particular loading. This is the only ultimate load case for which the calculated load was larger than the measured ultimate load.

(b) Model SG-2 (45° Skew), Ultimate No. 1

Load

Overload Truck Wheel Configuration, Axle 3 at B4-D4.

Yield Zone

The yield zone consists of girders A, B, C, D, and E
(Fig. 7.65a)

Service Load, P_S

The service live load is 1.0 (OL + I)

$$P_S = (10 \text{ wheels})(350 \text{ lb./wheel}) \quad (\text{Table 7.8b})$$

$$P_S = 3500 \text{ lb.}$$

Service Live Load Moment, M_{SLL}

$$M_{SLL} = 5.45 \text{ kip-ft.} \quad (\text{Table 7.8b})$$

Live Load Moment Capacity, M_{YLL}

$$\text{Yield Moment, } M_Y \text{ (Table 7.8a)} = 4.11 \text{ kip-ft./girder}$$

$$\text{Dead Load Moment, } M_{DL} \text{ (Table 7.8b)} = \underline{0.89}$$

$$M_{YLL} = 3.22 \text{ kip-ft./girder}$$

Yield Load, P_Y

$$P_Y = (P_S) \left(\frac{N M_{YLL}}{M_{SLL}} \right) = 3500 \times \frac{5 \times 3.22}{5.45}$$

$$P_Y = 10,350 \text{ lb.}$$

Transferred Load, P_T

$$P_T = v_u b_s t_c$$

$$v_u = 127 \text{ psi} \quad (\text{Table 7.8a})$$

$$b_s = 48.70 \text{ in.} \quad (\text{Fig. 7.66a})$$

$$t_c = 0.82 \text{ in.}$$

$$P_T = 127 \times 48.70 \times 0.82$$

$$P_T = 5,070 \text{ lb.}$$

Capacity of Girders Outside Yield Zone, P_R

$$\begin{aligned} \text{Live Load Moment Capacity} &= (12-5)(3.22 \text{ kip-ft./girder}) \\ &= 22.6 \text{ kip-ft.} \end{aligned}$$

$$P_R = 3500 \times \frac{22.6}{5.45}$$

$$P_R = 14,500 \text{ lb.} > P_T = 5070 \text{ lb.}$$

Ultimate Load, P_U

$$P_U = P_Y + P_T = 10,350 + 5,070$$

$$P_U = 15,420 \text{ lb.}$$

Ultimate Live Load Moment, M_{ULL}

$$M_{ULL} = \left(\frac{P_U}{P_S} \right) (M_{SLL}) = \left(\frac{15,420}{3,500} \right) (5.45)$$

$$M_{ULL} = 24.0 \text{ kip-ft.}$$

Calculated Factor of Safety, FS_c

$$FS_c = \frac{M_{DL} + M_{ULL}}{M_{DL} + M_{SLL}} = \frac{12(0.89) + 24.0}{12(0.89) + 5.42}$$

$$FS_c = 2.15$$

Measured Factor of Safety, FS_m

$$\text{Maximum Measured Load} = 5.25 \text{ (OL + I)}$$

$$\begin{aligned} \text{Maximum Live Load Moment} &= 5.25 \times 5.45 \text{ kip-ft./OL + I} \\ &= 29.6 \text{ kip-ft.} \end{aligned}$$

$$FS_m = \frac{12(0.89) + 29.6}{12(0.89) + 5.45}$$

$$FS_m = 2.42$$

Ratio FS_m/FS_c

$$\frac{FS_m}{FS_c} = \frac{2.42}{2.15} = 1.13$$

Ratio of Calculated and Measured Live Load Capacity

$$\frac{\text{Measured } M_{ULL}}{\text{Calculated } M_{ULL}} = \frac{29.6}{24.0} = 1.23$$

The agreement between the measured and calculated safety factors is quite good.

(c) Model SG-2(45° Skew), Ultimate No. 2

This test was carried out on a relatively undamaged portion of the structure remaining after the first ultimate load test.

Load

Overload Truck Wheel Configuration, near support with wheels over girders J and L

Yield Zone

The yield zone consists of girders H, J, K, L, and M (Fig. 7.65a, mirror image of B-D loading)

Service Load, P_S

The service live load is 1.0 (OL + I)

$$P_S = (10 \text{ wheels})(350 \text{ lb./wheel}) \quad (\text{Table 7.8b})$$

$$P_S = 3500 \text{ lb.}$$

Service Load Moment, M_{SLL}

$$M_{SLL} = 4.67 \text{ kip-ft.} \quad (\text{Table 7.8b})$$

Live Load Moment Capacity, M_{YLL}

$$\text{Yield Moment, } M_Y \text{ (Table 7.8a)} = 4.11 \text{ kip-ft./girder}$$

$$\text{Dead Load Moment, } M_{DL} \text{ (Table 7.8b)} = \underline{0.86}$$

$$M_{YLL} = 3.25 \text{ kip-ft./girder}$$

Yield Load, P_Y

$$P_Y = (P_S) \left(\frac{N M_{YLL}}{M_{SLL}} \right) = 3500 \times \frac{5 \times 3.25}{4.67}$$

$$P_Y = 12,200 \text{ lb.}$$

Transferred Load, P_T

$$P_T = 5,070 \text{ lb.} \quad (\text{From SG-2 Ultimate Load No. 1})$$

Capacity of Girders Outside Yield Zone, P_R

$$\begin{aligned} \text{Live Load Moment Capacity} &= (12-5)(3.25 \text{ kip-ft./girder}) \\ &= 22.80 \text{ kip-ft.} \end{aligned}$$

$$P_R = 3500 \times \frac{22.80}{5.45}$$

$$P_R = 14,600 \text{ lb.} > P_T = 5070 \text{ lb.}$$

Ultimate Load, P_U

$$P_U = P_Y + P_T = 12,200 + 5,070$$

$$P_U = 17,270 \text{ lb.}$$

Ultimate Live Load Moment, M_{ULL}

$$M_{ULL} = \left(\frac{P_U}{P_S} \right) (M_{SLL}) = \left(\frac{17,270}{3,500} \right) (4.67)$$

$$M_{ULL} = 23.0 \text{ kip-ft.}$$

Calculated Factor of Safety, FS_c

$$FS_c = \frac{M_{DL} + M_{ULL}}{M_{DL} + M_{SLL}} = \frac{12(0.86) + 23.0}{12(0.86) + 4.67}$$

$$FS_c = 2.22$$

Measured Factor of Safety, FS_m

$$\text{Maximum Measured Load} = 6.25 \text{ (OL + I)}$$

$$\begin{aligned} \text{Maximum Live Load Moment} &= 6.25 \times 4.67 \text{ kip-ft.} \\ &= 29.2 \text{ kip-ft.} \end{aligned}$$

$$FS_m = \frac{12(0.86) + 29.2}{12(0.86) + 4.67}$$

$$FS_m = 2.63$$

Ratio FS_m / FS_c

$$FS_m / FS_c = 2.63 / 2.22 = 1.19$$

Ratio of Calculated and Measured Live Load Capacity

$$\frac{\text{Measured } M_{ULL}}{\text{Calculated } M_{ULL}} = \frac{29.2}{23.0} = 1.27$$

The calculated and measured capacities do not agree as well as in the case of ultimate load No. 1 (ratio of 1.13). This is believed to be due to the possibility of some steel entering strain hardening. This is not known, however, since strain gages were not actually located at the point of flexural failure.

(d) Model SG-3 (45° Skew), Ultimate No. 1

Load

Overload Truck Wheel Configuration, Axle 3 at B4-D4

Yield Zone

The yield zone consists of girders A, B, C, D, and E (Fig. 7.65a)

Service Load, P_S

The service live load is 1.0 (OL + I)

$$P_S = (10 \text{ wheels})(350 \text{ lb./wheel}) \quad (\text{Table 7.8b})$$

$$P_S = 3500 \text{ lbs.}$$

Service Live Load Moment, M_{SLL}

$$M_{SLL} = 5.45 \text{ kip-ft.} \quad (\text{Table 7.8b})$$

Live Load Moment Capacity, M_{YLL}

$$\text{Yield Moment, } M_Y \text{ (Table 7.8a)} \quad = 4.87 \text{ kip-ft./girder}$$

$$\text{Dead Load Moment, } M_{DL} \text{ (Table 7.8b)} \quad = \frac{0.89}{M_{YLL}} \\ = 3.98 \text{ kip-ft./girder}$$

Yield Load, P_Y

$$P_Y = (P_S) \left(\frac{N M_{YLL}}{M_{SLL}} \right)$$

$$P_Y = 3500 \times \frac{5 \times 3.98}{5.45}$$

$$P_Y = 12,800 \text{ lb.}$$

Transferred Load, P_T

$$P_T = v_u b_s t_c$$

$$v_u = 132 \text{ psi} \quad (\text{Table 7.8a})$$

$$b_s = 48.70 \text{ in.} \quad (\text{Fig. 7.66a})$$

$$t_c = 0.82 \text{ in.}$$

$$P_T = 132 \times 48.70 \times 0.82$$

$$P_T = 5,270 \text{ lb.}$$

Capacity of Girders Outside Yield Zone, P_R

$$\begin{aligned} \text{Live Load Moment Capacity} &= (12.5)(3.98 \text{ kip-ft./girder}) \\ &= 27.8 \text{ kip-ft.} \end{aligned}$$

$$P_R = 3500 \times \frac{27.8}{5.45}$$

$$P_R = 17,850 \text{ lb.} > P_T = 5,270 \text{ lb.}$$

Ultimate Load, P_U

$$P_U = P_Y + P_T = 12,800 + 5,270$$

$$P_U = 18,070 \text{ lb.}$$

Ultimate Live Load Moment, M_{ULL}

$$M_{ULL} = \left(\frac{P_U}{P_S} \right) (M_{SLL}) = \left(\frac{18,070}{3,500} \right) (5.45)$$

$$M_{ULL} = 28.1 \text{ kip-ft.}$$

Calculated Factor of Safety, FS_c

$$FS_c = \frac{M_{DL} + M_{ULL}}{M_{DL} + M_{SLL}} = \frac{12(0.89) + 28.1}{12(0.89) + 5.45}$$

$$FS_c = 2.40$$

Measured Factor of Safety, FS_m

$$\text{Maximum Measured Load} = 6.0 \text{ (OL + I)}$$

$$\begin{aligned} \text{Maximum Live Load Moment} &= 6.0 \times 5.45 \text{ kip-ft./OL + I} \\ &= 32.7 \text{ kip-ft.} \end{aligned}$$

$$FS_m = \frac{12(0.89) + 32.7}{12(0.89) + 5.45}$$

$$FS_m = 2.69$$

$$\text{Ratio } FS_m / FS_c$$

$$FS_m / FS_c = 2.69 / 2.40 = 1.12$$

Ratio of Calculated and Measured Live Load Capacity

$$\frac{\text{Measured } M_{ULL}}{\text{Calculated } M_{ULL}} = \frac{32.7}{28.1} = 1.16$$

(e) Model SG-3 (45° Skew), Ultimate No. 2

This test was carried out on a relatively undamaged portion of the structure remaining after the first ultimate load test.

Load

Overload truck Wheel Configuration, Axle 3 at HJ4-KL4

Yield Zone

The yield zone consists of girders G, H, J, K, L and M (Fig. 7.65b).

Service Load, P_S

The service load is 1.0 (OL + I)

$$P_S = (10 \text{ wheels})(350 \text{ lb./wheel}) \quad (\text{Table 7.8b})$$

$$P_S = 3500 \text{ lb.}$$

Service Live Load Moment, M_{SLL}

$$M_{SLL} = 5.45 \text{ kip-ft.} \quad (\text{Table 7.8b})$$

Live Load Moment Capacity, M_{YLL}

$$\text{Yield Moment, } M_Y \text{ (Table 7.8a)} = 4.87 \text{ kip-ft./girder}$$

$$\text{Dead Load Moment, } M_{DL} \text{ (Table 7.8b)} = \frac{0.89}{M_{YLL}} = \frac{0.89}{3.98 \text{ kip-ft./girder}}$$

Yield Load, P_Y

$$P_Y = (P_S) \left(\frac{N M_{YLL}}{M_{SLL}} \right) = 3500 \times \frac{6 \times 3.98}{5.45}$$

$$P_Y = 15,350 \text{ lb.}$$

Transferred Load, P_T

$$P_T = 5270 \text{ lb.} \quad (\text{SG-3 Ultimate No. 1})$$

Capacity of Girders Outside Yield Zone, P_R

$$\begin{aligned} \text{Live Load Moment Capacity} &= (12-6)(3.98 \text{ kip-ft./girder}) \\ &= 23.9 \text{ kip-ft.} \end{aligned}$$

$$P_R = 3500 \times \frac{23.9}{5.45}$$

$$P_R = 15,300 \text{ lb.} > P_T = 5270 \text{ lb.}$$

Ultimate Load, P_U

$$P_U = P_Y + P_T = 15,350 + 5,270$$

$$P_U = 20,620 \text{ lb.}$$

Ultimate Live Load Moment, M_{ULL}

$$M_{ULL} = \left(\frac{P_U}{P_S} \right) (M_{SLL}) = \left(\frac{20,620}{3,500} \right) (5.45)$$

$$M_{ULL} = 32.1 \text{ kip-ft.}$$

Calculated Factor of Safety, FS_c

$$FS_c = \frac{M_{DL} + M_{ULL}}{M_{DL} + M_{SLL}} = \frac{12(0.89) + 32.1}{12(0.89) + 5.45}$$

$$FS_c = 2.65$$

Measured Factor of Safety, FS_m

$$\text{Maximum Measured Load} = 6.0 \text{ (OL + I)}$$

$$\begin{aligned} \text{Maximum Live Load Moment} &= 6.0 \times 5.45 \text{ kip-ft./OL + I} \\ &= 32.7 \text{ kip-ft.} \end{aligned}$$

$$FS_m = \frac{12(0.89) + 32.7}{12(0.89) + 5.45}$$

$$FS_m = 2.69$$

Ratio FS_m/FS_c

$$FS_m/FS_c = 2.69/2.65 = 1.02$$

Ratio of Calculated and Measured Live Load Capacity

$$\frac{\text{Measured } M_{ULL}}{\text{Calculated } M_{ULL}} = \frac{32.7}{32.1} = 1.02$$

The agreement between calculated and observed values is excellent.

(f) Model SG-4 (26° Skew)

Load

Two H20 Truck Wheel Configurations, Axles 2 at C4-E4 and H4-K4

Yield Zone

The yield zone consists of girders B through L (Fig. 7.65c)

Service Load, P_S

The service live load in each position is 1.0(H20 + I)
(689#/rear wheel, 1/4 x 689#/front wheel)

$$P_S = (2 \times 689 + 2 \times 1/4 \times 689)(2 \text{ trucks})$$

$$P_S = 3444 \text{ lb. for both trucks}$$

Service Live Load Moment, M_{SLL}

$$M_{SLL} = 5.65 \text{ kip-ft. for both trucks} \quad (\text{Table 7.8b})$$

Live Load Moment Capacity, M_{YLL}

$$\text{Yield Moment, } M_Y (\text{Table 7.8a}) = 3.78 \text{ kip-ft./girder}$$

$$\text{Dead Load Moment, } M_{DL} (\text{Table 7.8b}) = \frac{0.80}{M_{YLL}} = 2.98 \text{ kip-ft./girder}$$

Yield Load, P_Y

$$P_Y = (P_S) \left(\frac{N M_{YLL}}{M_{SLL}} \right) = 3444 \times \frac{10 \times 2.98}{5.65}$$

$$P_Y = 18,200 \text{ lb.}$$

Transferred Load, P_T

$$P_T = v_u b_s t_c \times 2 \text{ crowns}$$

$$v_u = 138 \text{ (Table 7.8a)}$$

$$b_s = 43.92 \text{ in. (Fig. 7.66b)}$$

$$t_c = 0.82 \text{ in.}$$

$$P_T = (138 \times 43.92 \times 0.82) \times 2$$

$$P_T = 9,950 \text{ lb.}$$

Capacity of Girders Outside Yield Zone, P_R

$$\text{Live Load Moment Capacity} = (12-10)(2.98 \text{ kip-ft./girder}) \\ = 5.95 \text{ kip-ft.}$$

$$P_R = P_S \times \frac{5.95}{5.65} = 3444 \times \frac{5.95}{5.65}$$

$$P_R = 3630 \text{ lb.} < P_T = 9,950 \text{ lb.}$$

Therefore, girders A and M may be counted as yielding.

Ultimate Live Load Moment, M_{ULL}

$$M_{ULL} = (12 \text{ girders})(2.98 \text{ kip-ft./girder})$$

$$M_{ULL} = 35.8 \text{ kip-ft.}$$

Calculated Factor of Safety, FS_c

$$FS_c = \frac{M_{DL} + M_{ULL}}{M_{DL} + M_{SLL}} = \frac{12(0.80) + 35.8}{12(0.80) + 5.65} = \frac{45.4}{15.25}$$

$$FS_c = 2.98$$

Measured Factor of Safety, FS_m

The measured factor of safety for this bridge should be viewed with judgment. Strain measurements indicate that at least four and possibly six of the interior girders had entered the strain hardening regions before all of the girders reached yield strains. Based on the ultimate load of 9.50(H20 + I) the factor of safety is 5.16, compared to the computed value of 2.98. Deflections at this load were on the order of three inches. Examination of the deflection plots (Figs. 7.43, 7.47, 7.50, 7.52, and 7.55) for previous tests indicate that the deflection over the most heavily loaded girders was on the order of 0.6 to 0.8 inches when failure occurred. Based on these deflections and the fact that all girder steel had yielded at 7.75(H20 + I) (deflections on the order of 0.75 in. under the central girders), the load level of 7.75(H20 + I) is taken as the practical ultimate load. Even at this load the steel in several girders had entered strain hardening.

$$\text{Assumed Ultimate Load Capacity} = 7.75(\text{H20} + \text{I})$$

$$\text{Maximum Live Load Moment} = 7.75 \times 5.65 \text{ kip-ft.}$$

$$= 43.8 \text{ kip-ft.}$$

$$FS_m = \frac{12(0.80) + 43.8}{12(0.80) + 5.65}$$

$$FS_m = 3.50$$

Ratio FS_m/FS_c

$$FS_m/FS_c = 1.17$$

Ratio of Calculated and Measured Live Load Capacity

$$\frac{\text{Measured } M_{ULL}}{\text{Calculated } M_{ULL}} = \frac{43.8}{35.8} = 1.22$$

This is about as accurate as for model SG-3 (ratio of 1.17).

7.7.5 Conclusions on Ultimate Load Calculations. The data obtained from the ultimate load calculations and ultimate load measurements are summarized in Table 7.9. The adequacy of the failure hypothesis may be seen by comparing the ratio of the measured factor of safety to the calculated factor of safety (FS_m/FS_c) and the ratio of the measured to calculated live loads ($\text{Measured } M_{ULL}/\text{Calculated } M_{ULL}$) in the last two columns of Table 7.9. The calculation procedure yields conservative results in five of the six tests. The test on SG-1 is slightly unconservative ($FS_m/FS_c = 0.93$).

The edge loadings, as expected, have the lowest factors of safety but these are still adequate.

The factors of safety in Table 7.9 are for bridges which have been designed in accordance with present AASHO design criteria. These safety factors would change if the design criteria for this type of bridge were revised, based on service load or ultimate load distribution factors.

7.7.6 Live Load Factors. The Bureau of Public Roads⁴⁶ recommends load factors of 1.35 and 2.25 for dead load and live load, respectively. The test live load factors are compared with the Bureau live load factor in Table 7.10. The comparison is made by multiplying the known dead load moments by 1.35 and subtracting the increase from the measured ultimate live load moment. As indicated in Table 7.10, the test results indicate live load factors ranging from 3.78 to 7.15. This indicates that the bridge design based on present AASHO service load distribution factors is overconservative. Test live load factors are 1.68 to 3.18 times as large as the Bureau live load factor. The largest difference occurs for model SG-4, which was loaded to failure using two H20 design truck wheel patterns.

7.7.7 Ultimate Load Distribution Factors. Ultimate load distribution factors should be based on the "yield zone" and the transferred load, P_T , described in Sec. 7.7.2. However, the transferred load is difficult to

TABLE 7.9 ULTIMATE LOAD DATA

Bridge	Skew	$A_s, \text{ in.}^2$	$f_y, \text{ ksi}$	Ultimate Test	Loading Pattern	Load Location	Calculated Factor of Safety, FS_c	Measured Factor of Safety, FS_m	$\frac{FS_m}{FS_c}$	$\frac{\text{Measured } M_{ULL}}{\text{Calculated } M_{ULL}}$
SG-1	0°	0.1920	46.6	1	1 OL+I	B4-D4	2.37	2.25	0.95	0.93
SG-2	45°	0.2152	44.9	1	1 OL+I	B4-D4	2.15	2.42	1.13	1.23
				2	1 OL+I	J-L *	2.22	2.63	1.19	1.27
SG-3	45°	0.1964	57.3	1	1 OL+I	B4-D4	2.40	2.69	1.12	1.16
				2	1 OL+I	HJ4-KL4	2.65	2.69	1.02	1.02
SG-4	26°	0.1782	57.3	1	2H20+I	C4-E4	2.98	3.50	1.17	1.22
						H4-K4				

*Shear Loading

TABLE 7.10 COMPARISON OF BUREAU OF PUBLIC ROADS
AND TEST LIVE LOAD FACTORS

Bridge	Ultimate Test	B.P.R. Live Load Factor	Test Live Load Factor	Test Live Load Factor
				B.P.R. Live Load Factor
SG-1	1	2.25	3.78	1.68
SG-2	1	2.25	4.56	2.03
	2	2.25	5.47	2.43
SG-3	1	2.25	5.32	2.36
	2	2.25	5.32	2.36
SG-4	1	2.25	7.15	3.18

evaluate generally, since it is dependent on load position and loaded length. For simplicity, conservative ultimate load distribution factors may be based on the girders within the yield zone and neglecting any transferred load. Consider the three load positions in Fig. 7.65. A single truck positioned near the edge, as in Fig. 7.65a, has a yield zone consisting of five girders. Each yield zone girder carries 0.4 wheel loads, which is an S/C value of S/7.5. A single truck positioned near the edge, as in Fig. 7.65b, has a yield zone consisting of six girders. Each yield zone girder carries 0.33 wheel loads, which is an S/C value of S/9.0. The double truck loading in Fig. 7.65c has a yield zone of ten girders. Each yield zone girder carries 0.4 wheel loads, which is an S/C value of S/7.5.

The ultimate S/C values range from S/7.5 to S/9.0 for the loadings considered with S/7.5 being critical for design (neglecting P_T).

For comparison, the service load test results for a single truck indicate that a distribution factor of S/5.98 can be used for the first interior girder, S/7.22 for the second interior girder, and S/8.6 for other interior girders. Test results indicate that S/4.5 can be used for the exterior girders. Service load test results indicate that S/6.56 can be used for a double truck loading. Most of the service load values are conservative when compared to the ultimate load distribution factor neglecting transferred load.

It is felt that the most realistic design approach is to consider the general failure mode consisting of the yield zone and transferred load.

For simplicity, conservative ultimate load distribution factors based on the yield zone and neglecting transferred load may be used.

If service load distribution factors are used they should not be smaller than the ultimate load distribution factors, unless a design check based on the general failure mode shows that the service load design is also safe for ultimate loads.

7.8 Secondary Tests

Two secondary test series were performed. The first series was to determine the punching capacity of the slab crown. The second series was to determine the effect of the deck girder system end diaphragm in adding to the bent cap capacity.

7.8.1 Punching Tests. A series of three punching tests was carried out on model SG-3 (45° skew) after completing the two major ultimate load tests. The punching tests were located in an undamaged portion of the slab shown by an "X" in Fig. 7.54. The three tests used different size loading pads. Load response for the third and most severe punching test is shown in Fig. 7.67. The two tests not shown had loading pads 1.82 in. and 3.64 in. wide. The test shown was discontinued after reaching a load level of 17.0 overload wheels plus impact (350 lb. per overload wheel plus impact). This was a final wheel load of 5950 lb. (180,000 lb. on the prototype). If it is assumed the load is distributed along a 45° line, as shown in Fig. 7.67, it can be concluded that the wheel load will not punch through the crown. Instead, several girders must be punched out. Because of this it was felt the test would be influenced by the cracking caused by the previous flexural tests. Hence, the test was discontinued with no sign of distress in the slab crown.

A better idea of the punching capacity of the slab was obtained during the test of model SG-4. The rear wheel located at H-4 in Fig. 7.61 (and 7.60) punched through the slab and girder at a wheel load of 6546 lb. (198,000 lb. on the prototype). This occurred after the steel in all twelve girders had yielded. Flexural cracking had penetrated well into the slab. Some crushing of concrete on the slab surface had occurred. One other wheel at E-4 was also very near punching through.

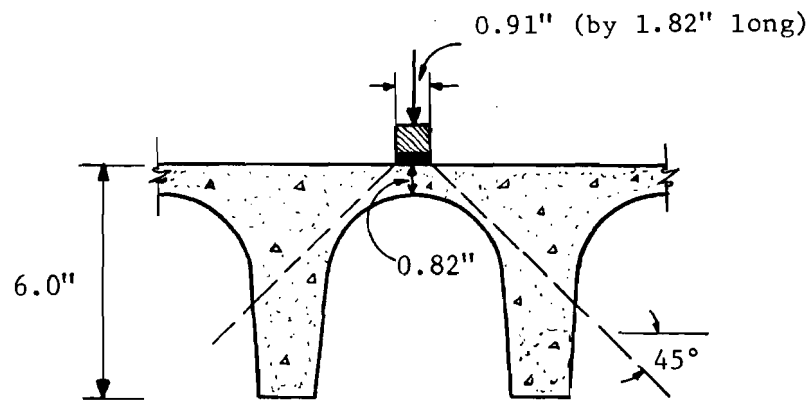
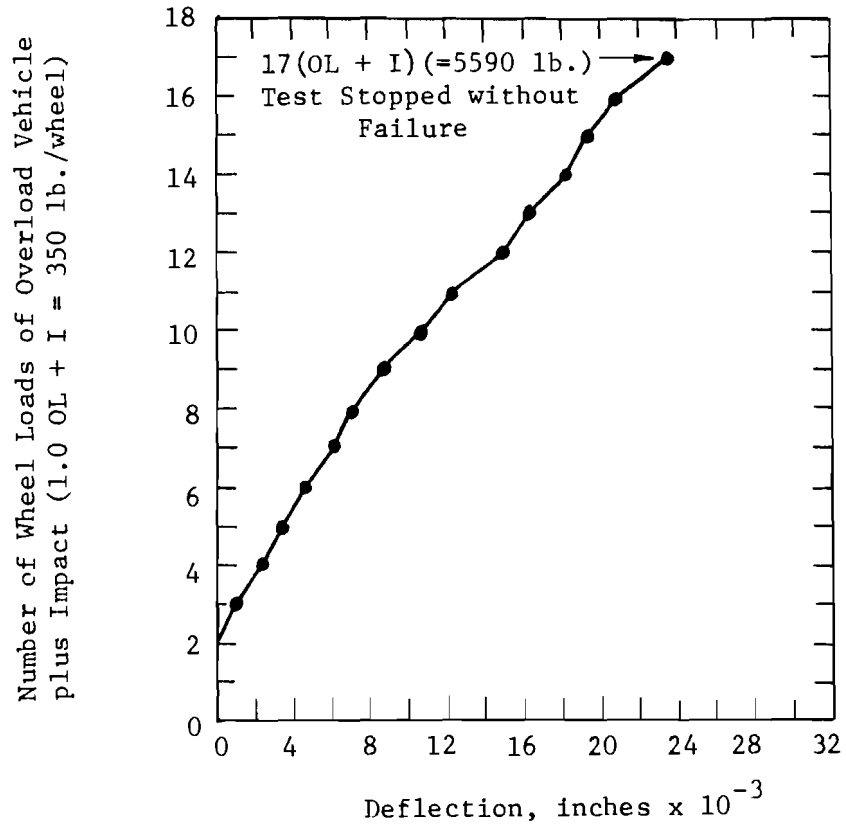
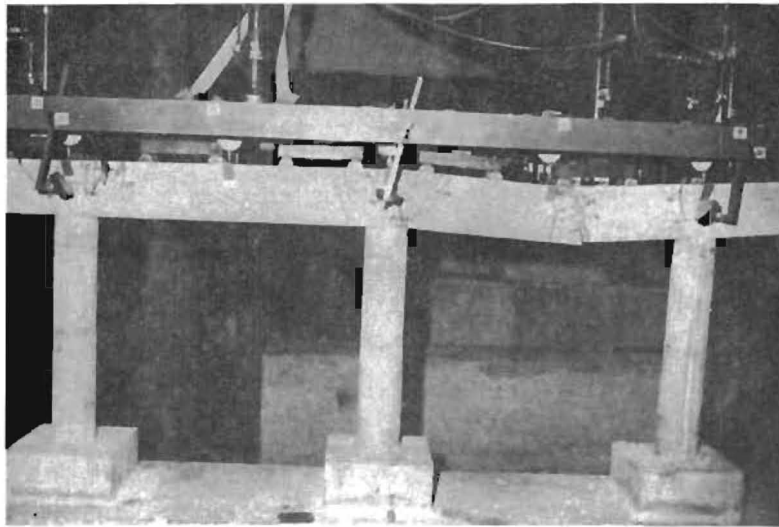


Fig. 7.67. Punching Test.

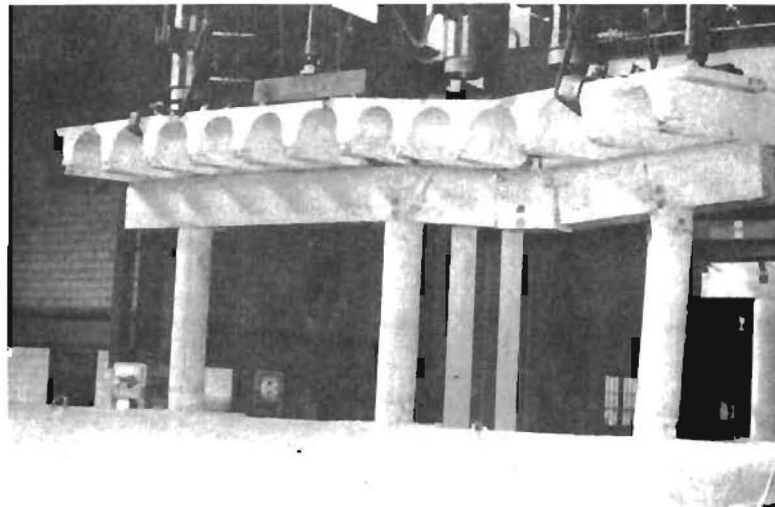
Based on these tests it was concluded that punching is not a problem in the design of this bridge system.

7.8.2 Bent Cap Tests. The substructure for model SG-4 (26° skew) was tested by loading the cap of one bent with a series of concentrated loads (simulating uniform load). The loads were increased until failure occurred. The remaining bent was then loaded to failure by applying the same load configuration through the deck girder system end diaphragms to determine their stiffening effect. The two bents are shown in Fig. 7.68. The end diaphragms were obtained by sawing them from model SG-4. These tests were carried out by Repa³⁴ as a part of the work on another project and are fully described by him. Details of the cap and end diaphragms are given for the prototype structure in Figs. A.6 and A.7. This was a three-column bent with a clear column height of 10.5 ft. on the prototype (1.91 ft. on the model).

The load response for the two cases is shown in Fig. 7.69. The indicated loading produces maximum positive live load moment in span BC. This was determined by Repa to be the critical design load. The failure mechanism for the two specimens was identical. The bent tested with the diaphragms in place carried 2.60 times as much live load as the bent tested without diaphragms. The factor of safety with end diaphragms was 6.8 and the factor of safety without end diaphragms was 3.1. Based upon these tests it was concluded that the end diaphragms should be considered in the design of the bent caps, perhaps considering noncomposite beam action.



(a) Loading of Cap without Diaphragms.



(b) Loading of Cap with Diaphragms.

Fig. 7.68. Bent Cap Tests.

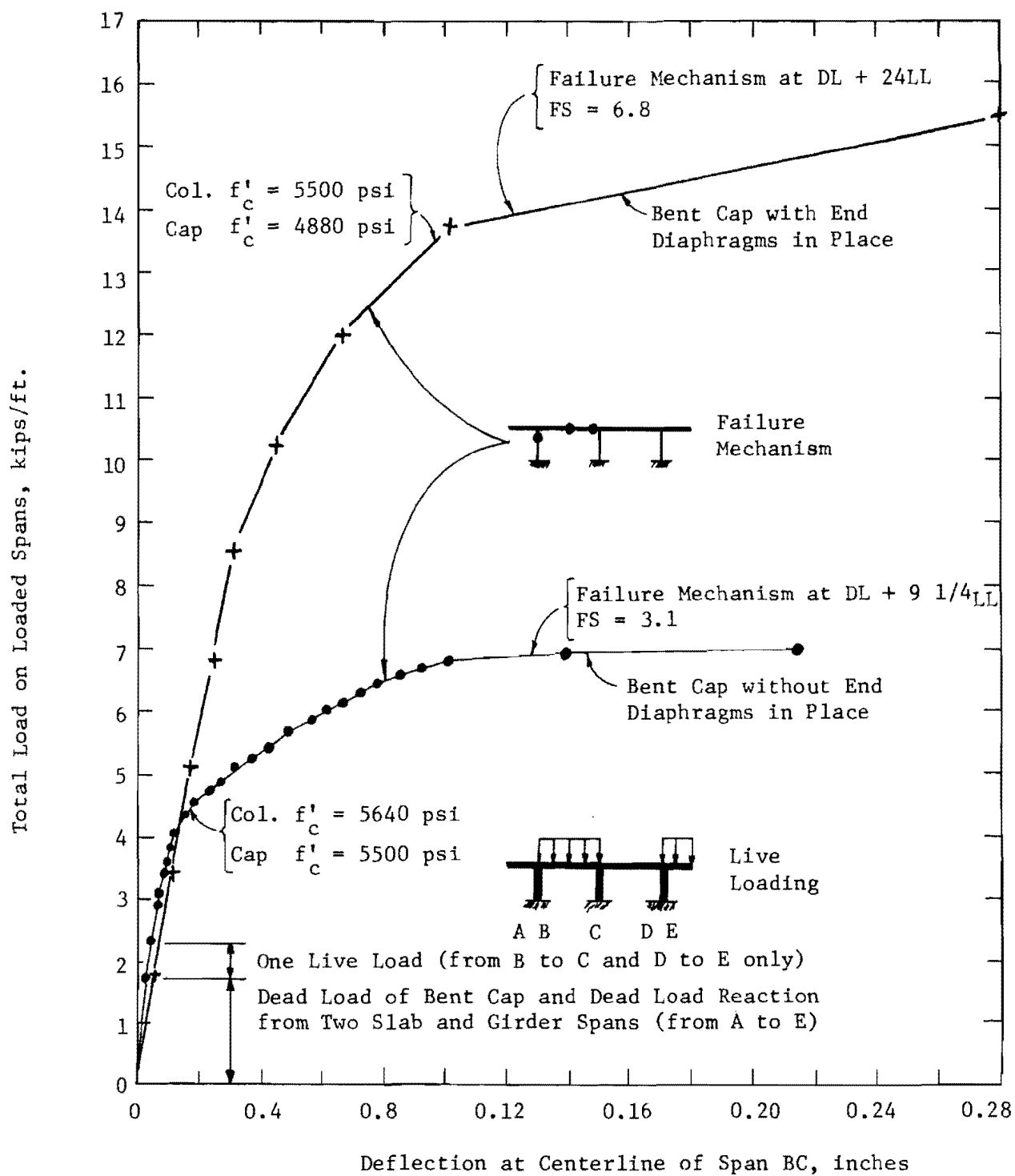


Fig. 7.69. Comparison of Capacity of Bents with and without End Diaphragms in Place.

This page replaces an intentionally blank page in the original.

-- CTR Library Digitization Team

C H A P T E R V I I I

CONCLUSIONS AND RECOMMENDATIONS

8.1 Summary of the Investigation

The research project covered herein is a study of the behavior of pan-formed concrete slab and girder bridges. The technology used to fabricate, test, and interpret results of the primary research tool used, the direct structural model, has been summarized.¹⁶ Four accurate models were tested at service loads, moderate overloads, and ultimate load levels in order to document fully the behavior of the structures for the complete range of load conditions. Patterns of load distribution were obtained using both strain gages and deflection measurements. The main variables in the investigation were angle of skew, load level, and grade and quantity of reinforcement. The model tests were supplemented by full-size testing¹⁵ as well as analytical procedures.

8.2 Conclusions

Although this investigation was restricted to a particular bridge system, the following conclusions are warranted:

(1) The AASHO service load distribution factors are overconservative when compared to the service load test results, which indicated:

- (a) Single Wheel Loads - There are no specific AASHO recommendations for a single wheel load. Test results in Sec. 7.4.3 indicate that a distribution factor of $S/5.5$ can be used for an exterior girder, $S/9.0$ for the first interior girder, and $S/10.0$ for other interior girders.

- (b) Single Truck Loads - The current AASHO specifications use a value of $S/C = S/6.0$ for interior girders for a single truck load. Test results in Sec. 7.4.4 indicate that a distribution factor of $S/5.98$ can be used for the first interior girder, $S/7.22$ for the second interior girder, and $S/8.6$ for other interior girders. AASHO specifies $S/C = S/3.0$ for the exterior girders when the load is directly above. Test results indicate $S/4.5$ may be used.
- (c) Multiple Truck Loads - The current AASHO specifications use a value of $S/C = S/5.0$ for two or more vehicles on the bridge. Test results in Sec. 7.4.6 indicate this factor to be correct for triple truck loads. However, test results in Sec. 7.4.5 indicate that a factor of $S/6.56$ can be used for a double truck loading.

These service load distribution factors are valid regardless of skew angle or percentage of longitudinal steel, within the range of variables included in this study.

Service load distribution factors may not be valid at ultimate load. Design based on service load distribution factors smaller than ultimate load distribution factors should be checked using the general failure mode for safety at ultimate load.

(2) Ultimate load distribution factors should be based on the "yield zone" and the transferred load, P_T . However, the transferred load is difficult to evaluate generally, since it is dependent on load position and loaded length. For simplicity, conservative ultimate load distribution factors may be based on the girders within the yield zone after neglecting any transferred load. Ultimate load distribution factors based only on the girders in the "yield zone" indicate that $S/7.5$ is critical for single and double truck loading.

(3) Test results indicate that the transverse steel rarely exceeded the design stress until failure occurred. At failure the steel usually yielded as a secondary effect.

(4) Under both maximum moment and maximum shear loadings the bridges exhibited a primary mode of failure by yielding of tension steel in the most heavily loaded girders. These girders are defined by a distribution zone boundary extending from the edge of the loaded surface and inclined 30° from the horizontal. The main longitudinal steel will yield or be very close to yield in all girders in which the tensile steel layers are enclosed within such a 30° zone. This is referred to as the yield zone. Increased load will be transferred to the remaining girders. The transferred load is limited by the slab shear capacity in the transverse direction, unless the remaining girders yield before the shear capacity is reached.

(5) A shear test on model SG-2 (45° skew) resulted in the same failure mode described in (4), indicating that girder shear is not a design problem with the percentage of web reinforcement used.

(6) Punching tests directly over the crown indicate that single wheel punching is not a design problem for this section.

(7) Tests on the substructure indicate that the girder end diaphragms double the bent cap live load capacity.

(8) An ultimate load calculation procedure based on the failure mode described in (4) showed good accuracy resulting in the ratios shown in Table 8.1.

TABLE 8.1 ACCURACY OF ULTIMATE LOAD CALCULATIONS

Bridge	Ultimate Test	$\frac{\text{Measured FS}}{\text{Calculated FS}}$	$\frac{\text{Measured } M_{ULL}}{\text{Calculated } M_{ULL}}$
SG-1	1	0.95	0.93
SG-2	1	1.13	1.23
	2	1.19	1.27
SG-3	1	1.12	1.16
	2	1.02	1.02
SG-4	1	1.17	1.22

(9) The overall factors of safety ranged from 2.25 to 3.50. The live load safety factors were rather large, ranging from 4.38 to 7.75.

(10) Using the Bureau of Public Roads⁴⁶ load factor of 1.35 for dead load, the live load factors ranged from 3.78 to 7.15. These latter load factors are 1.68 to 3.18 times as large as the specified live load factor of 2.25.

(11) The use of the present AASHO service load distribution factors results in the excessive live load factors indicated in (10). The use of the ultimate load distribution factor given in (2) as $S/7.5$ is in the direction of reducing the excessive live load factors obtained in this study.

(12) The discrete element mathematical model of an orthotropic slab using gross-transformed section properties is an adequate predictor of service load behavior for a right angle bridge.

8.3 Implementing Research Results into the Texas Highway Department Operations

8.3.1 AASHO Load Distribution Factors. The AASHO service load distribution factors currently used are excessive for this type of bridge in the case of single and double truck loadings.

An ultimate load approach is felt to be the most realistic design method for this type of bridge. It is recommended that design be based on the ultimate load distribution factor (neglecting transferred load) of $S/7.5$ for single and double truck loads, unless a more accurate analysis is made based on the general failure mode.

Recognizing that some engineers may wish to continue to use only service load design, recommendations based on service load tests are also made, although these will not lead to the most realistic design of the bridge system. Service load test results for a single truck load indicate that $S/8.5$ can be used for design of interior girders. This has been changed to $S/7.15$ to be in agreement with the ultimate load criteria.

Test results indicate that the following service load distribution factors may be used for single truck loadings:

- (a) Exterior girder $S/C = S/4.5$
- (b) First interior girder $S/C = S/6.0$
- (c) Second interior girder $S/C = S/7.0$
- (d) Other interior girders $S/C = S/7.5$

Test results indicate that $S/6.5$ may be used for all girders in the case of double truck loads.

8.3.2 Benefit from Implementation of Revised Load Distribution Factors.

- (a) Single Truck Loading - Use of the revised service load distribution factors presented above would reduce the average design load to be carried by the girders by 23 percent, resulting in substantial reinforcement savings, even if present standard cross section dimensions are maintained.
- (b) Double Truck Loading - Use of the revised load distribution factors presented would reduce the average design load to be carried by the girders by 25 percent in service load designs and 33 percent in ultimate load designs. Substantial reinforcement savings would occur even if present standard cross section dimensions are maintained.

8.3.3 Substructure Design. The bent cap should be designed considering its interaction with the end diaphragms as a noncomposite beam. This will significantly decrease bent cap sizes.

This page replaces an intentionally blank page in the original.

-- CTR Library Digitization Team

A P P E N D I X A

PROTOTYPE BRIDGE PLANS

This page replaces an intentionally blank page in the original.

-- CTR Library Digitization Team

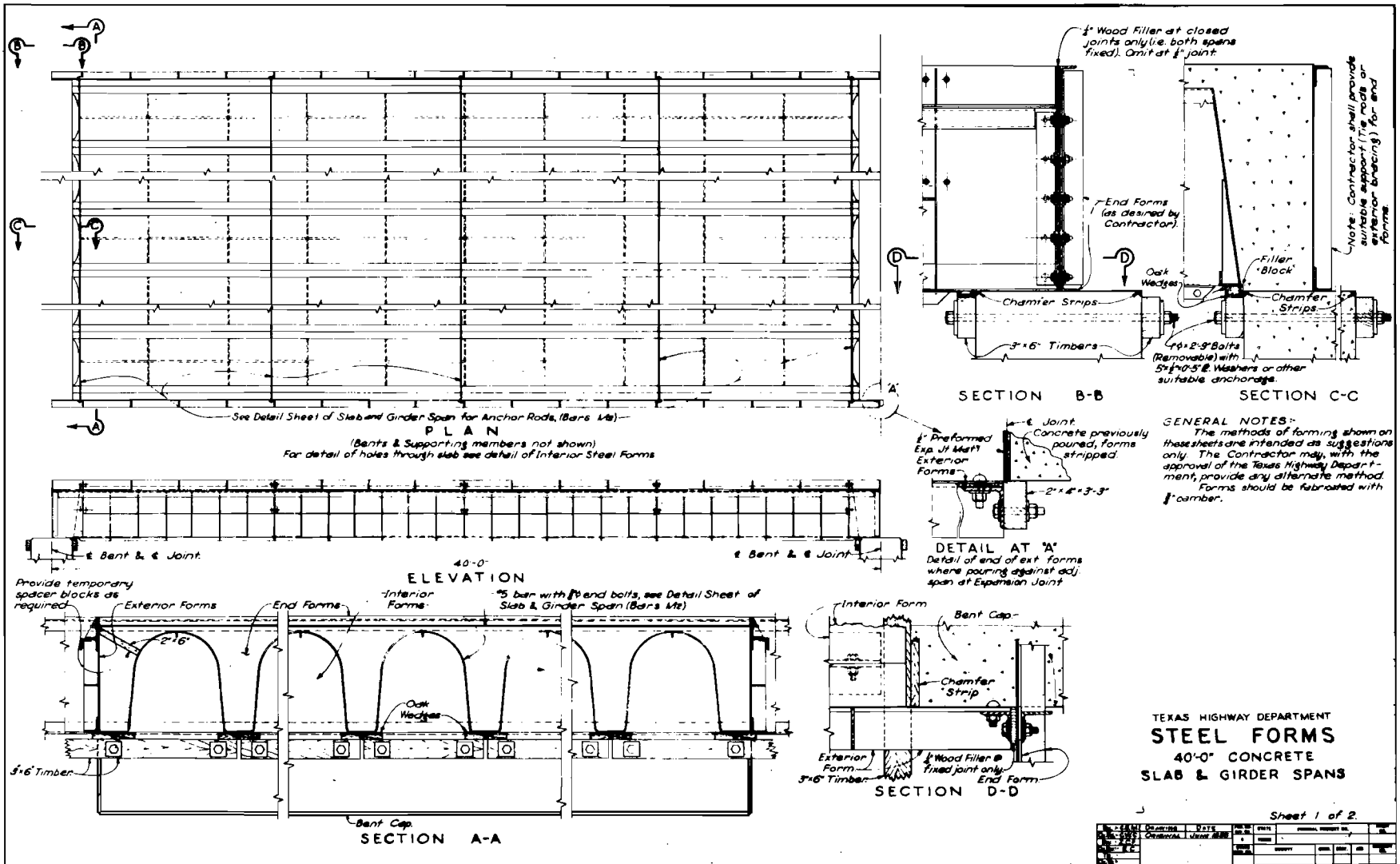


Fig. A.1. Steel Forms for 40'-0" Slab and Girder Spans, Sheet 1 of 2.

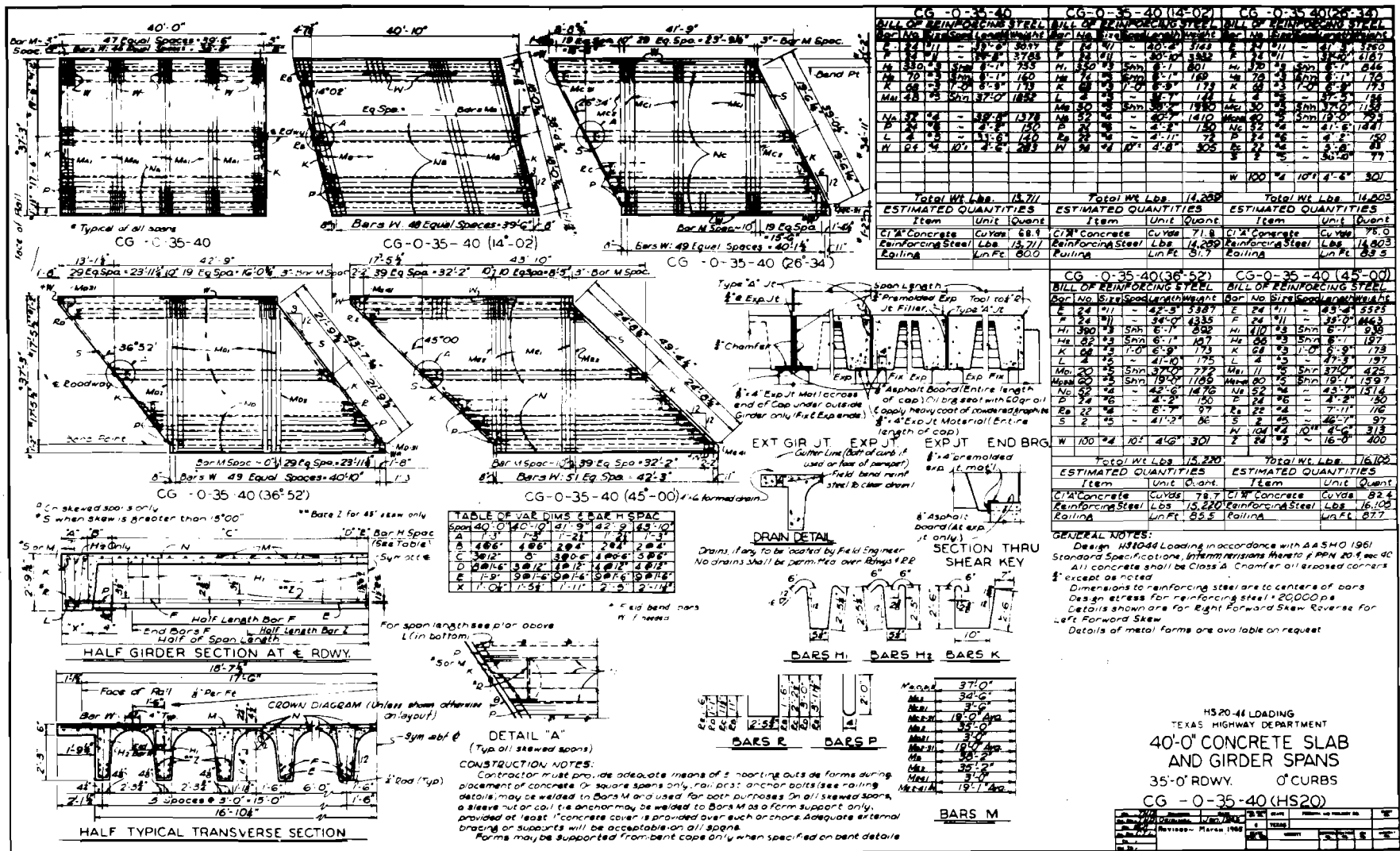
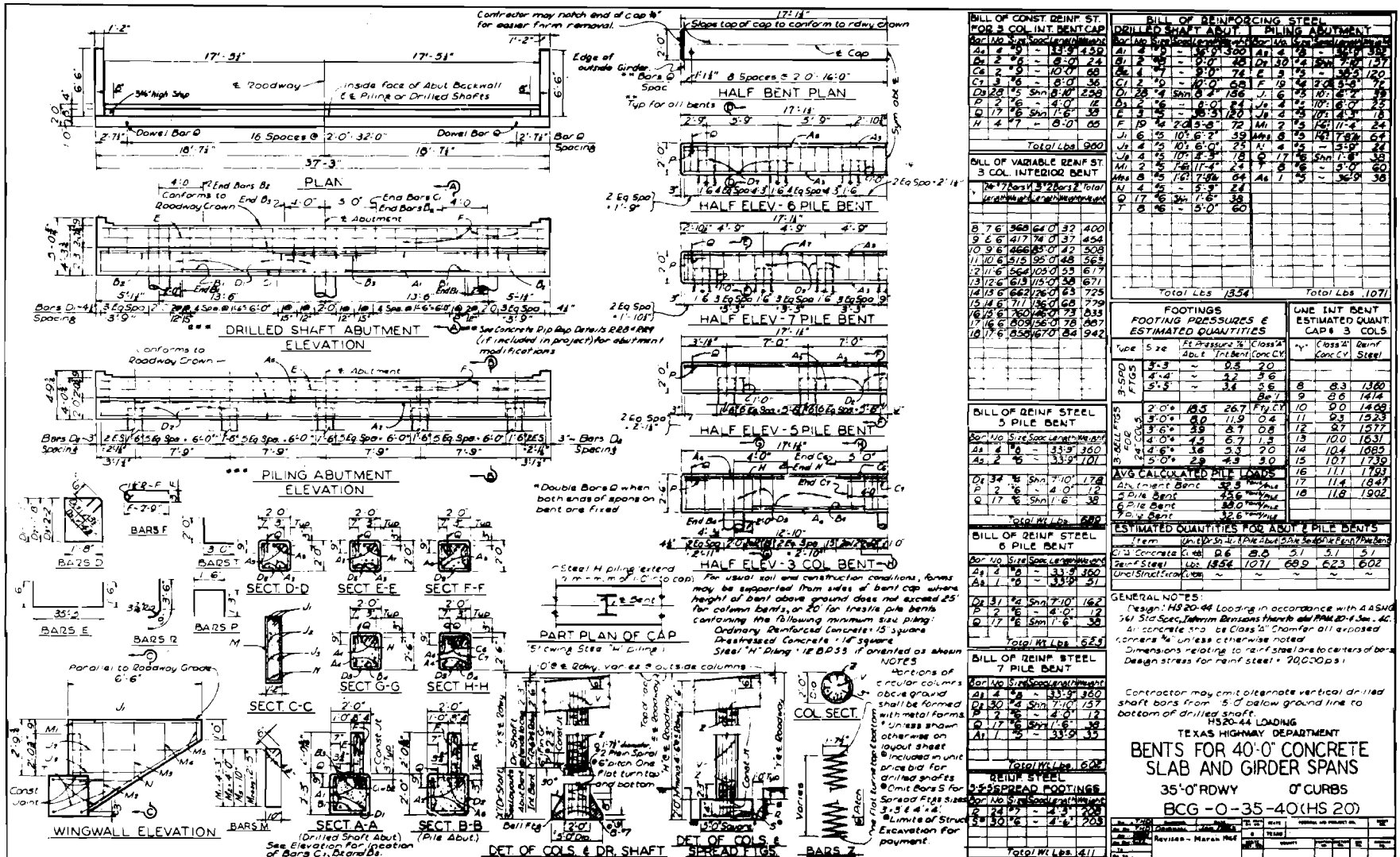


Fig. A.3. Texas Highway Department Plan Sheet, CG-0-35-40.



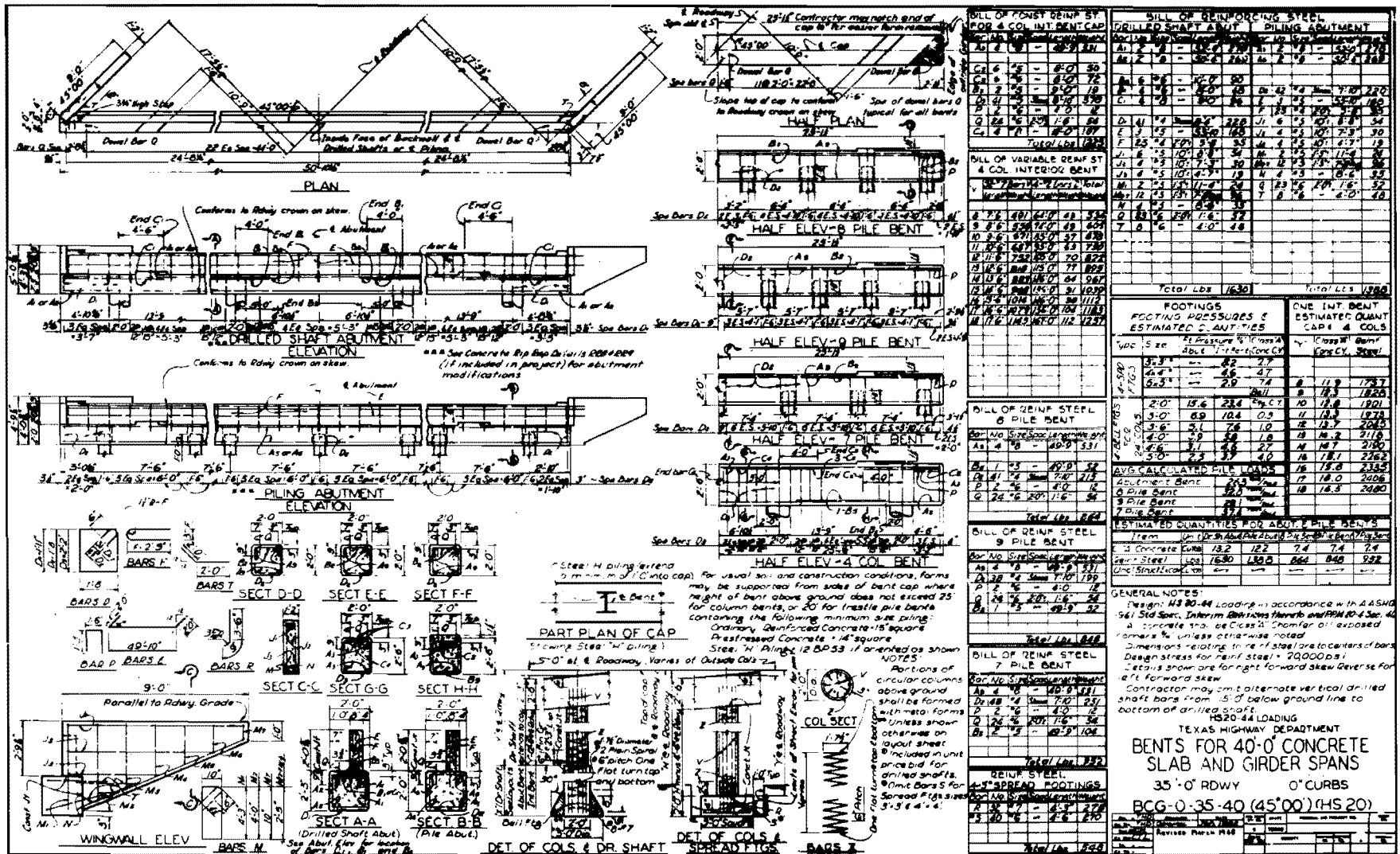


Fig. A.5. Texas Highway Department Plan Sheet, BCG-0-35-40 (45°-00').

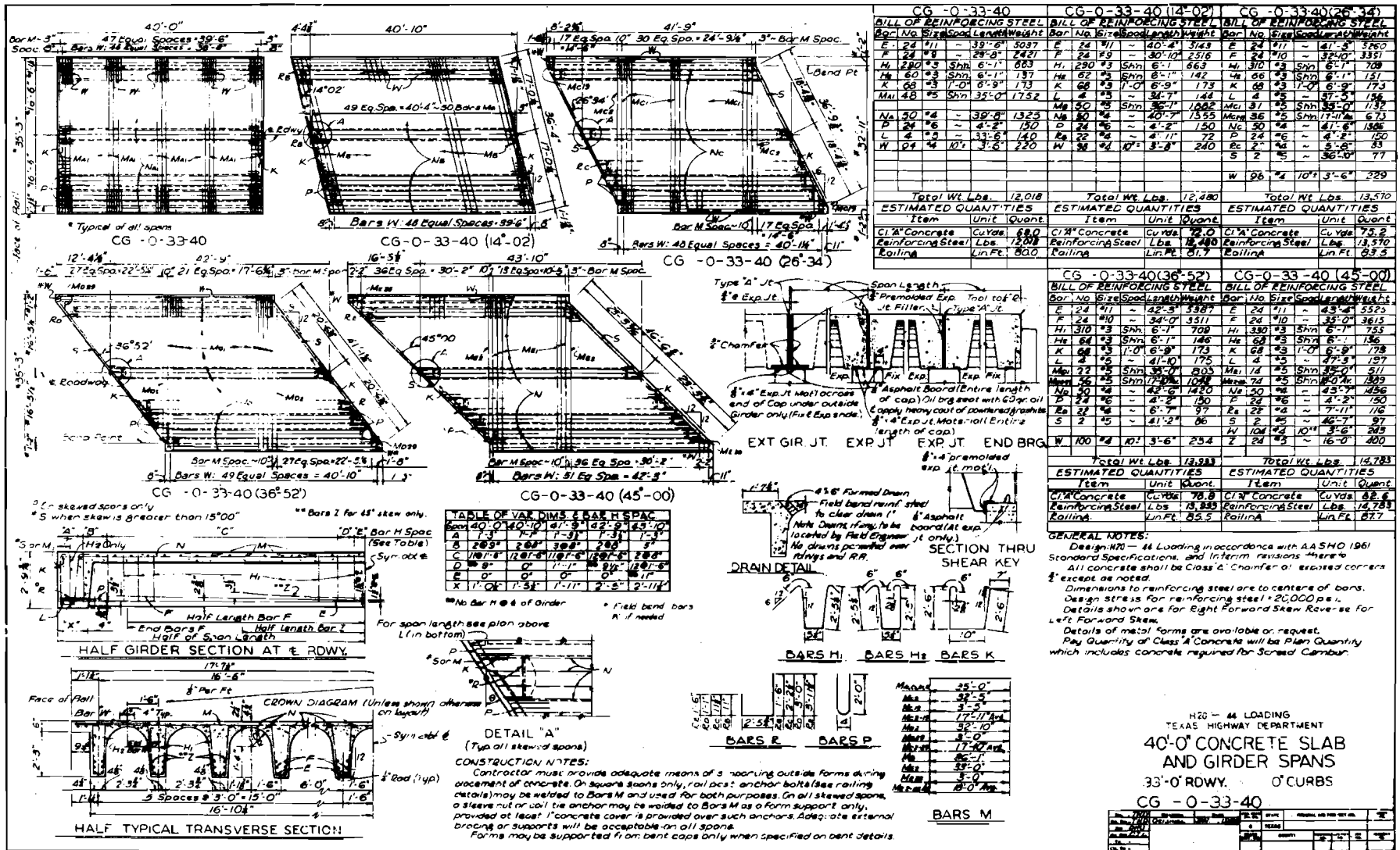


Fig. A.6. Texas Highway Department Plan Sheet, CG-0-33-40.

This page replaces an intentionally blank page in the original --- CTR Library Digitization Team

B I B L I O G R A P H Y

This page replaces an intentionally blank page in the original.

-- CTR Library Digitization Team

B I B L I O G R A P H Y

1. Aldridge, W. W. "Ultimate Strength Tests of Model Reinforced Concrete Folded Plate Structures," unpublished Ph.D. dissertation, The University of Texas, 1966.
2. American Association of State Highway Officials. Standard Specifications for Highway Bridges, Ninth Edition, 1965.
3. American Concrete Institute. Building Code Requirements for Reinforced Concrete (ACI-318), Detroit, Michigan, June 1963.
4. Ang., H. H., and Lopez, L. A. "Flexural Analysis of Elastic Plastic Rectangular Plates," Conference Preprint 478, ASCE Structural Engineering Conference, Seattle, Washington, May 8-12, 1967.
5. Best, B. C., and Rowe, R. E. "Abnormal Loading on Composite Slab Bridges," Cement and Concrete Association, Research Report No. 7, October 1959.
6. Guyon, Y. "Calcul des ponts larges a poutres multiples solidarisees par des entretoises," Annales des Ponts et Chaussees, No. 24, September-October, 1946.
7. Guyon, Y. "Calcul des ponts dalles," Annales des Ponts et Chaussees, Vol. 119, No. 29, 1949.
8. Hendry, A. W., and Jaeger, L. G. The Analysis of Grid Frameworks and Related Structures, Chatto and Windus, London, 1958.
9. Hetenyi, M. "A Method for Calculating Grillage Beams," S. Timoshenko, 60th Anniversary Volume, New York, 1938.
10. Hudson, W. R., and Matlock, H. "Discontinuous Orthotropic Plates and Pavement Slabs," Research Report 56-6, Center for Highway Research, The University of Texas, Austin, May 1966.
11. Hudson, W. R., and Matlock, H. "Discrete-Element Analysis for Discontinuous Plates," Journal of the Structural Division, ASCE, Vol. 94, No. ST10, Proc. Paper 6157, October 1968.
12. Lazarides, T. O. "The Design and Analysis of Openwork Prestressed Concrete Beam Grillages," Civil Engineering and Public Works Review, Vols. 47 and 48, June 1952.

13. Lee, C. E. "A Portable Electronic Scale for Weighing Vehicles in Motion," Paper prepared for presentation at the 45th Annual Meeting of the Highway Research Board, January 17-21, 1966.
14. Leonhardt, E., and Andra, W. Die veremfachte Tragerrost berechnung (The Calculation of Grillage Beams). Julius Hoffman Press, Stuttgart, 1950.
15. Leyendecker, E. V., Armstrong, T. A., and Breen, J. E. "Field Testing of Concrete Slab and Girder Bridges," Research Report 94-2, Center for Highway Research, The University of Texas at Austin, September 1968.
16. Leyendecker, E. V., and Breen, J. E. "Structural Modeling Techniques for Concrete Slab and Girder Bridges," Center for Highway Research, The University of Texas at Austin, August 1968.
17. Lightfoot, E., and Sawko, F. "The Analysis of Grid Frameworks and Floor Systems by Electronic Computer," The Structural Engineer, Vol. 38, No. 3, March 1960.
18. Little, G., and Rowe, R. E. "Load Distribution in Multi-Webbed Bridge Structures from Tests on Plastic Models," Magazine of Concrete Research, Vol. 7, No. 21, November 1955.
19. Matlock, H., and Haliburton, T. A. "A Finite-Element Method of Solution for Linearly Elastic Beam-Columns," Research Report 56-1, Center for Highway Research, The University of Texas, Austin, September 1968.
20. Massonnet, C. "Methode de Calcul des Ponts a poutres multiples tenant compte de leur resistance a la torsion" (Method of Calculation of Bridges with Several Longitudinal Beams, Taking into Consideration Their Torsional Resistance), Surich, International Association for Bridge and Structural Engineering, Publications Vol. 10, 1950.
21. Mattock, A. H., and Kaar, P. H. "Precast-Prestressed Concrete Bridges. 6. Test of Half-Scale Highway Bridge Continuous over Two Spans," Journal of the PCA Research and Development Laboratories, Vol. 3, No. 3, September 1961.
22. Morice, P. B., and Little, G. "Load Distribution in Prestressed Concrete Bridge Systems," The Structural Engineer, Vol. 32, No. 3, March 1954.
23. Morice, P. B., and Little, G. Analysis of Right Bridge Decks Subjected to Abnormal Loading, London, Cement and Concrete Association, July 1956.
24. Morice, P. B., and Little, G. "Load Tests on a Small Prestressed Concrete Highway Bridge," Proceedings of the Conference on the Correlation between Calculated and Observed Stresses and Displacements in Structures. Institution of Civil Engineers. 21st-22nd September 1955.
25. Morice, P. B., Little, G., and Rowe, R. E. Design Curves for the Effects of Concentrated Loads on Concrete Bridge Decks, London, Cement and Concrete Association, July 1956.

26. Newmark, N. M. "A Distribution Procedure for the Analysis of Slabs Continuous over Flexible Beams," Bulletin No. 304, University of Illinois Engineering Experiment Station (1938).
27. Newmark, N. M., and Siess, C. P. "Moments in I-Beam Bridges," Bulletin No. 336, University of Illinois Engineering Experiment Station (1942).
28. Newmark, N. M., and Siess, C. P. "Design of Slab and Stringer Highway Bridges," Public Roads, Vol. 28, No. 7, January-February-March, 1943.
29. Newmark, N. M., Siess, C. P., and Peckham, W. M. "Studies of Slab and Beam Highway Bridges: Part II--Tests of Simple Span Skew I-Beam Bridges," Bulletin No. 375, University of Illinois Engineering Experiment Station (1948).
30. Newmark, N. M., Siess, C. P., and Penman, R. R. "Studies of Slab and Beam Highway Bridges: Part I--Tests of Simple Span Right I-Beam Bridges," Bulletin No. 363, University of Illinois Engineering Experiment Station (1946).
31. Panak, J. J., and Matlock, H. "A Discrete-Element Method of Multiple Loading Analysis for Two-Way Bridge Floor Slabs," Research Report 56-13, Center for Highway Research, The University of Texas at Austin, August 1968.
32. Pippard, A. J. S., and De Waele, J. P. A. "The Loading of Interconnected Bridge Girders," Journal of the Institution of Civil Engineers, Vol. 10, No. 1, November 1938.
33. Reynolds, G. C. "The Strength of Prestressed Concrete Grillage Bridges," Cement and Concrete Association. London. Technical Report TRA/228. June 1957.
34. Repa, J. V. "Flexural Stiffness Redistribution in Typical Highway Bents," M.S. thesis in progress, The University of Texas at Austin, September 1969.
35. Rowe, R. E. "A Load Distribution Theory for Bridge Slabs Allowing for the Effect of Poisson's Ratio," Magazine of Concrete Research, Vol. 7, No. 20, July 1955.
36. Rowe, R. E. "Load Distribution in No-Torsion Bridge Grillages with Various Support Conditions," Cement and Concrete Association, Technical Report TRA/247, March 1957.
37. Rowe, R. E. "Load Distribution in Bridge Slabs (with special reference to transverse bending moments determined from tests on three prestressed concrete slabs)," Magazine of Concrete Research, Vol. 9, No. 27, November 1957.

38. Rowe, R. E. "The Analysis and Testing of a Type of Bridge Suitable for Medium Right Spans Subjected to Abnormal Loading," Cement and Concrete Association, Research Report No. 6, November 1958.
39. Rowe, R. E. "Loading Tests on Two Prestressed Concrete Highway Bridges," Proceedings of the Institution of Civil Engineers, Vol. 13, August 1959.
40. Rowe, R. E. Concrete Bridge Design (Design Curves), John Wiley and Sons, Inc., New York, 1962.
41. Sokolnikoff, I. S., and Sokolnikoff, E. S. Higher Mathematics for Engineers and Physicists, 2nd edition, McGraw-Hill, New York, 1941.
42. Spiegel, M. R. Theory and Problem of Statistics. Schaum's Outline Series. New York: McGraw-Hill Book Company, 1961.
43. Stelzer, C. F., and Hudson, W. R. "A Direct Computer Solution for Plates and Pavement Slabs," Research Report 56-9, Center for Highway Research, The University of Texas at Austin, October 1967.
44. Texas Highway Department. Regulations for Oversize-Overweight Permits. Austin, Texas, Revised September 1, 1965.
45. Timoshenko, S., and Woinowsky-Kreiger, S. Theory of Plates and Shells (Engineering Society Monographs), 2nd edition, McGraw-Hill, New York, 1959.
46. U. S. Department of Commerce, Bureau of Public Roads. Strength and Serviceability Criteria, Reinforced Concrete Members, Ultimate Design, Washington, D.C., August 1966.